Dynamic Liquid Slosh in Moving Containers

Amir Kolaei

A Thesis
In the Department
of
Mechanical and Industrial Engineering

Presented in Partial Fulfillment of the Requirements
For the Degree of
Doctor of Philosophy (Mechanical Engineering) at
Concordia University
Montreal, Quebec, Canada

October 2014

CONCORDIA UNIVERSITY

School of Graduate Studies

This is to certify that the thesis prepared

By: **Amir Kolaei**

Entitled: **Dynamic Liquid Slosh in Moving Containers**

and submitted in partial fulfilment of the requirements for the degree of

DOCTOR OF PHILOSOPHY (Mechanical Engineering)

complies with the regulations of the University and meets the accepted standards with respect to originality and quality.

Signed by the final examining committee:

_____ Chair
Dr. A. A. Kishk

_____ External Examiner
Dr. V. H. Mucino

_____ External to Program
Dr. S. Li

_____ Examiner
Dr. M. Packirisamy

_____ Examiner
Dr. C. Y. Su

_____ Co-supervisor
Dr. S. Rakheja

_____ Co-supervisor
Dr. M. J. Richard

Approved by

_____
Dr. A. Dolatabadi, Graduate Program Director

October 17, 2014

_____
Dr. A. Asif, Dean
Faculty of Engineering & Computer Science

ABSTRACT

Dynamic Liquid Slosh in Moving Containers

Amir Kolaei, PhD

Concordia University, 2014

Liquid sloshing is known to strongly influence the directional dynamics and safety performance of highway tank vehicles in a highly adverse manner. Hydrodynamic forces and moments arising from liquid cargo oscillations in the tank under steering and/or braking maneuvers reduce the stability limit and controllability of the partially filled tank vehicles. While the transient fluid slosh within moving containers has been widely investigated, interactions between the sloshing cargo and the vehicle system dynamics have been addressed in only a few studies due to associated challenges. Furthermore, roll stability of heavy tank vehicles have been extensively studied in the absence of transient slosh-induced forces and moments. This dissertation research aims at exploring the fluid slosh in moving containers through analytical methods and developing efficient models for simulating interactions of fluid slosh and vehicle dynamics. A comprehensive review of relevant studies reporting tank trucks accident data, tank design standards, and analysis methods of liquid sloshing in moving containers is initially performed and briefly summarized. The literature review provides not only the essential knowledge for developing an efficient method of analysis, but also demonstrates the needs for addressing limitations in the current standards so as to include effects of liquid sloshing dynamics in road tankers.

An analytical model of two-dimensional fluid slosh in horizontal cylindrical tanks subject to a lateral excitation is initially formulated assuming potential flows and linearized free-surface boundary. For this purpose, the fluid domain in the Cartesian coordinates is transformed to the bipolar coordinates, where the Laplace equation could be solved using separation of variables. The resulting hydrodynamic pressure, free-surface elevation, and slosh force and roll moment are compared with the reported experimental and numerical results to illustrate the range of applicability and limitations of the linear slosh theory. The results suggest that the linear theory can yield reasonably accurate predictions of non-resonant lateral slosh in liquid transporting vehicles with significantly less computational effort than the CFD models.

A multimodal model of fluid slosh is subsequently developed to study the effect of tank cross-section on transient lateral slosh. Natural frequencies and modes of liquid slosh in tanks of

different cross-sections are obtained using a variational Ritz method, which are implemented into the multimodal model. The effect of transient liquid slosh and tank cross-section on rollover stability limits of a tank vehicle is also investigated by integrating the fluid slosh model into a roll plane model of the suspended tank vehicle. The results are presented for four different tank cross-sections: circular; elliptical; modified-oval; and Reuleaux-triangle. The results show that a tank cross-section with lower overall center of mass and lower critical slosh length could yield enhanced roll stability limit under medium- and high-fill conditions.

The multimodal method is also employed to investigate the effect of partial longitudinal baffles on the transient lateral slosh. Natural slosh frequencies and modes are computed using a boundary integral solution of the Laplace equation. The computational efficiency is significantly improved by reducing the generalized eigenvalue problem to a standard one involving only the velocity potentials of the elements on the half free-surface length. Damping due to the baffles is estimated from the energy dissipation rate. The results are presented for different designs/lengths of longitudinal baffles, namely, top-mounted; bottom-mounted; and center-mounted baffles. It is shown that the multimodal method yields computationally efficient solutions of liquid slosh within moving baffled containers. The results suggest that a baffle is most effective and efficient when it pierces the free-surface and partly submerged in the liquid.

A three-dimensional linear slosh model is further developed to study fluid motions under simultaneously applied lateral and longitudinal excitations, characterizing braking-in-a-turn maneuver, using the multimodal method. Three-dimensional Laplace equation is initially reduced to a two-dimensional Helmholtz equation using separation of variables. A higher order boundary integral solution of the Helmholtz equation is then formulated to compute natural slosh frequencies and modes in a horizontal cylindrical tank of arbitrary cross-section. The results obtained for a circular tank suggested rapid convergence of the natural slosh frequencies and hydrodynamic coefficients. The slosh forces and moments are also computed from the nonlinear analysis of liquid slosh in a tank under various lateral/longitudinal accelerations and fill ratios using the FLUENT software. Comparisons of the results obtained from the linear and nonlinear analyses revealed that the linear slosh theory yields reasonably accurate predictions of the peak slosh forces and moments under lateral/longitudinal accelerations of steady magnitudes of up to 0.3g/0.2g for a tank of aspect ratio of 2.4.

ACKNOWLEDGMENTS

The author wishes to express his sincere appreciation and gratitude to his thesis supervisors, Professor Subhash Rakheja and Professor Marc J. Richard, for their great supports and continued guidance throughout the course of this research.

The author also wishes to acknowledge Concordia University, CONCAVE Research Centre and Laval University for their financial supports provided in the forms of International Tuition Fee Remission, Partial Tuition Fee Remission, Concordia Accelerator Award and Research Assistantship. The cooperation extended by the members of the CONCAVE Research Centre and of the Department of Mechanical and Industrial Engineering is gratefully acknowledged.

Finally, the author would like to express his deepest gratitude to his wife, Najmeh, for her sacrifice and patience during the course of this undertaking.

TABLE OF CONTENTS

CHAPTER 3

EFFECTS OF TANK CROSS-SECTION ON DYNAMIC FLUID SLOSH LOADS AND ROLL STABILITY OF A PARTLY-FILLED TANK TRUCK

CHAPTER 4

A COUPLED MULTIMODAL AND BOUNDARY-ELEMENT METHOD FOR ANALYSIS OF ANTI-SLOSH EFFECTIVENESS OF PARTIAL BAFFLES IN A PARTLY-FILLED CONTAINER

LIST OF FIGURES

LIST OF TABLES

NOMENCLATURE

Symbol	Description
A_0, A_{0y}	Steady-state magnitude of the lateral acceleration
A_{0x}	Steady-state magnitude of the longitudinal acceleration
C_D	Baffle drag coefficient
E	Total energy of the free liquid oscillations in a clean-bore tank
E_k	Kinetic energy of the free liquid oscillations in a clean-bore tank
E_p	Potential energy of the free liquid oscillations in a clean-bore tank
$\overline{\frac{dE}{dt}}$	Mean rate of energy dissipation over the period
$\boldsymbol{F}$	Total hydrodynamic force
F_R, F_{y_R}	Rigid body component of F_y
F_S, F_{y_S}	Sloshing component of F_y
F_x	Longitudinal hydrodynamic force
F_{x_R}	Rigid body component of F_x
F_{x_S}	Sloshing component of F_x
F_y	Lateral hydrodynamic force
F_z	Vertical hydrodynamic force
$\bar{F}_x, \bar{F}_y$	Normalized components of the hydrodynamic forces, $\bar{F}_x = \frac{F_x}{F_{x_R}}$, $\bar{F}_y = \frac{F_y}{F_{y_R}}$
F_{0ss}	Peak steady-state lateral force
U_n	Normal velocity of the tank wall
$[\mathbf{C}]$	Damping matrix
$[\mathbf{G}]$	Boundary element influence matrix
$[\mathbf{H}]$	Boundary element influence matrix
K_0	Modified Bessel function of the second kind and zero
$[\mathbf{K}]$	Stiffness matrix
KC	Keulegan-Carpenter number
L	container of length

L_i	Lagrangian corresponding to mode number i
$\boldsymbol{M}$	Total hydrodynamic moment
$[\mathbf{M}]$	Mass matrix
M_B	Total overturning moment about tank bottom point
M_l	Total sloshing roll moment about the vehicle roll center
M_R	Rigid body component of M_B
M_S	Sloshing component of M_B
M_V	Component of M_B due to vertical forces
M_x	Roll moment
M_{x_R}	Rigid body component of M_x
M_{x_S}	Sloshing component of M_x
M_{x_V}	Component of M_x due to vertical forces
M_y	Pitch moment
M_{y_R}	Rigid body component of M_y
M_{y_S}	Sloshing component of M_y
M_{y_V}	Component of M_y due to vertical forces
$\bar{M}_y, \bar{M}_x$	Normalized components of the hydrodynamic moment, $\bar{M}_y = \frac{M_y}{M_{y_R}}$, $\bar{M}_x = \frac{M_x}{M_{x_R}}$
M_{0ss}	Peak steady-state overturning moment about the tank bottom point
N	Truncation size (chapter 2)
N_f	Number of elements on the half free-surface length
P	Hydrodynamic pressure
R	Tank radius
R_i	Generalized function corresponding to mode number i (chapter 3)
S_b	Submerged surface area of the baffle
S_f	Liquid free-surface (chapters 4,5)
$\hat{\mathrm{S}}_f$	Two-dimensional liquid free-surface (chapter 5)
S_w	Wetted surface area of the tank (chapters 4,5)
$\hat{\mathrm{S}}_w$	Two-dimensional wetted surface area of the tank (chapter 5)

T	Half-track width of the vehicle
T_b	Beat period of fluid slosh, $T_b = \frac{2\pi}{\lvert\sigma_1 - \sigma\rvert}$
$T_i, T_{i,j}$	Period of fluid slosh
V_l	Liquid volume per unit length of the tank
V_0	Amplitude of the tank velocity
W	Total weight of the vehicle including the cargo
W_l	Liquid cargo load
W_s	Sprung weight of the tare tank vehicle
W_u	Unsprung weight of the tare tank vehicle
$\dot{X}, \ddot{X}, \dddot{X}$	Longitudinal velocity, acceleration and time derivative of the longitudinal acceleration
$\dot{Y}, \ddot{Y}, \dddot{Y}$	Lateral velocity, acceleration and time derivative of the lateral acceleration
Z_o	Tank geometric center height
a	Half free-surface length in static condition (chapter 2), or half overall width of the tank (chapter 3)
b	half overall height of the tank
a_y	Lateral acceleration corresponding to wheel lift-off condition in g units
c_f	Force amplification factor, $c_f = \frac{\lvert F_{y,max}\rvert}{mA_0}$
c_m	Overturning moment amplification factor, $c_m = \frac{\lvert M_{B,max}\rvert}{mRA_0}$
c_p	Hydrodynamic pressure coefficient, $c_p = \frac{P}{\frac{1}{2}\rho {V_0}^2}$
h	Liquid fill height measured from the bottom of the tank (chapters 2,4,5) or from the geometric center of the tank (chapter 3)
h_r	Vehicle roll center height
h_s	Center of gravity height of the sprung mass
h_u	Center of gravity height of the unsprung mass
k_s	Equivalent roll stiffness of the vehicle suspension
l	Characteristic dimension of the container

l_b	Total length of the baffle
l_{bs}	Submerged length of the baffle
m	Liquid mass per unit length of the tank (chapters 2-4), or total liquid mass (chapter 5)
m_i	Convective mass corresponding to the i^{th} sloshing mode
$\boldsymbol{n}$	Unit vector normal to the wall
q_i	Normal velocity corresponding to i^{th} natural slosh mode
$\bar{t}$	Normalized time
t_0, t_{0y}	Rise time of the lateral acceleration
$\hat{t}_0, \bar{t}_0$	Normalized rise time of the lateral acceleration
t_{0x}	Rise time of the longitudinal acceleration
u	Normal inflow velocity to the baffle
u_m, u_0	Amplitude of u
v_f	Free surface velocity
y_0	Coordinate of the free-surface at the intersection of the tank wall
z_0	Coordinate of the free-surface at the intersection of the tank wall
z_{cg}	Location of the liquid center of gravity measured from the tank center
Γ	Boundary enclosing the fluid domain
$\hat{\Gamma}$	Boundary enclosing the two-dimensional fluid domain
Σ	Liquid free-surface (chapter 3)
Σ_0	Liquid free-surface of the fitted rectangular tank
$\Delta\Sigma$	Difference between Σ and Σ_0
Φ	Velocity potential function
$\Phi_{i,j}$	Velocity potential corresponding to i^{th} longitudinal and j^{th} transverse mode
Φ_R	Rigid body potential
Φ_S	Sloshing potential
Ω	Fluid domain
Ω_0	Fluid domain of the fitted rectangular tank

$\Delta\Omega$	Difference between Ω and Ω_0
$\widehat{\Omega}$	Two-dimensional fluid domain (chapter 5)
α	Roll angle of the sprung mass about the vehicle roll axis
α_i	Phase angle corresponding to mode number i
α_p	Angle between the tangents at a boundary point
β_i	Generalized function corresponding to i^{th} natural slosh mode (chapters 4,5)
δ	Free-surface elevation
δ_c	Critical amplitude of the free-surface
ζ	Bipolar coordinate
η	Bipolar coordinate
$\kappa_i, \kappa_{i,j}$	Eigenvalue of liquid slosh, $\frac{\sigma_{i,j}^2}{g}$
$\bar{\kappa}_i, \bar{\kappa}_{i,j}$	Normalized eigenvalue
λ_i	Hydrodynamic coefficient corresponding to i^{th} natural slosh mode (chapters 2,4,5), or normalized slosh frequency with respect to the tank characteristic length (chapter 3)
$\bar{\lambda}_i, \bar{\lambda}_{x_{i,j}}, \bar{\lambda}_{y_{i,j}}$	Normalized hydrodynamic coefficient
$\lambda_{x_{i,j}}, \lambda_{y_{i,j}}$	Hydrodynamic coefficient
ξ_i	Damping ratio corresponding to mode number i
ρ	Liquid mass density
$\sigma_i, \sigma_{i,j}$	Circular slosh frequency
τ	Wetted surface area of the tank (chapter 3)
ν	Fluid kinematic viscosity
φ_i	Velocity potential corresponding to i^{th} natural slosh mode
$\{\boldsymbol{\psi}\}$	Vector representing contributions of the external excitation
ω_i	Wave number along the longitudinal axis

CHAPTER 1

LITERATURE REVIEW AND SCOPE OF THE DISSERTATION

1.1 Introduction

Free surface motion of liquid within a partly-filled moving container is known to impose substantial magnitudes of forces and moments to the container structure that affect the stability of the container transport system in a highly adverse manner. The design and analysis of a moving vehicle transporting liquid cargo thus necessitates consideration of the dynamic slosh loads due to the cargo when subjected to excitations arising from the directional maneuvers. General-purpose road tankers are often partially filled due to wide variations in the products' mass density and regulatory axle load limits. Comprehensive magnitudes of hydrodynamic forces and moments together with substantial dynamic load shifts, have been reported for partly-filled tank trucks under braking/acceleration and/or steering inputs, which invariably lead to reduced braking performance and roll stability limits of the vehicle. Analysis of accident data has shown that liquid sloshing has been associated with a large number of tank truck accidents, which pose unreasonable risks to the safety of road, and the environment, particularly when hazardous products are involved (Pape *et al.*, 2007; Woodrooffe, 2000).

The problem of liquid sloshing in moving containers involves the evaluations of potentially destabilizing sloshing forces and moments as well as the natural frequencies of liquid free-surface. Fundamentally, these properties relate to the dynamic fluid slosh and depend on a number of design and operating parameters in a highly nonlinear manner. These include the liquid-fill depth, liquid properties, tank geometry, nature of maneuver and designs of the anti-sloshing devices, when present. Earlier attempts to study the effect of liquid sloshing on directional dynamics of tank vehicles have been performed using quasi-static analysis (Sankar *et al.*, 1986; Rakheja *et al.*, 1988). The Quasi-static method can only predict the mean steady-state position of the liquid mass center assuming a straight line (or a plane in 3D analysis) for the liquid free-surface followed by the mean steady-state responses, while it neglects the important contributions due to dynamic liquid slosh. Furthermore, the quasi-static method is not applicable to tanks with anti-slosh devices such as baffles. Although mean steady-state slosh forces and

moments obtained from the quasi-static analysis can be efficiently integrated to the multi-body vehicle dynamic models, crucial importance of considering the effect of dynamic liquid slosh has been emphasized in a number of studies using the computational fluid dynamics (CFD) methods (e.g., Modaressi-Tehrani, 2004; Yan *et al.,* 2005). These have, invariably, shown that the peak slosh forces and moments in a partially filled tank under longitudinal and/or lateral acceleration excitations are significantly greater than the mean steady-state values. Applications of CFD models for simulations of coupled fluid-vehicle systems, however, have met limited success due to not only high computational demands of the CFD methods, but also due to elaborate data transfer between the CFD and vehicle models (Thomassy *et al.*, 2003; Yan and Rakheja, 2009; Fleissner *et al.*, 2009, 2010).

Alternatively, simulations of tank vehicle dynamics have been attempted using mechanical analogues models of the fluid slosh, which could be efficiently integrated into the multi-body vehicle models. The mechanical analogues models of the fluid slosh, however, require prior evaluations of the model parameters through either experimental measurements or CFD analyses (Ibrahim, 1999; Salem, 2000). Efficient models of liquid slosh thus need to be developed in order to effectively study the directional dynamics and safety performance of tank vehicles with various design and operating conditions. This dissertation research aims at developing efficient models of liquid slosh in terms of the computational demands and ease of integration with the vehicle dynamics models using the concept of linear fluid slosh. The fluid slosh models are developed for the analysis of transient two- and three-dimensional hydrodynamic forces and moments within the moving containers. The transient liquid slosh within a tank equipped with a longitudinal baffle is also analyzed. The forces and moments due to liquid slosh are formulated such that these could be readily incorporated into the multi-body vehicle models. Furthermore, limitations and range of applicability of the models are thoroughly investigated. The validity of the models is examined using the available measured data and the results obtained from analytical benchmark solutions and numerical simulations. Effect of transient slosh forces and moments on the rollover threshold of heavy vehicles carrying liquid cargo is also investigated.

1.2 Literature Review

The reported studies relevant to fluid slosh in road tankers are systematically reviewed to build the essential knowledge and formulate the scope of the dissertation research. The reviewed studies are briefly summarized below, particularly focused on: (i) highway accidents involving tank trucks to demonstrate adverse effect of liquid sloshing on dynamic performance and controllability of tank vehicles; (ii) tank design standards to highlight limitations of current design standards concerning the destabilizing effect of fluid slosh; (iii) methods of analysis of liquid slosh in moving containers; and (iv) methods employed for coupled fluid slosh and vehicle simulations.

1.2.1 Review of tank truck accidents data

The highway safety risks associated with partly filled tank trucks have been widely assessed through reviews of reported accidents data. Although these have suggested substantially higher safety risks of liquid cargo vehicles compared to the rigid cargo vehicles, a definite cause-effect relation between the rollover potential of tank trucks and the fluid slosh has not yet been established. This is partly attributed to limitations of the accident reporting mechanisms, which generally do not report on the fill level, tank design factors and fluid sloshing potential. For instance, an un-tripped rollover in a curve is commonly attributed only to the excessive speed, while the contributions of the substantial lateral load shift in a partly filled tank have been mostly ignored by the accident reporting systems (Winkler and Ervin, 1999; Yan *et al.*, 2005). Some correlation between the fluid sloshing and the rollover of tank trucks, however, could be identified in a qualitative manner from the accident databases reporting somewhat different information related to the vehicle, cargo and the accident situation. For instance, the majority of rollovers involving partly filled tank trucks have been referred to as loss of control in some of the databases, while the reported speeds were not excessive. This suggested contributions of liquid slosh and some degree of correlation between the liquid slosh and rollover of the partly filled tank trucks (Pape *et al.*, 2007).

The reported accidents involving road vehicles have been widely analyzed in many studies in North America. The most important ones reporting the accident data include those by Pape *et al.* (2007), Winkler and Ervin (1999), Woodrooffe (2000) and Rakheja *et al.* (2003). The report of Pape *et al.* (2007) presented an extensive analysis of four accident databases in the

USA, including the Motor Carrier Management Information System (MCMIS), Large Truck Crash Causation Study (LTCCS), Trucks Involved in Fatal Accidents (TIFA) and General Estimates System (GES).

The focus of the accident analyses in most of these studies was to investigate the primary causal factors. The MCMIS database was mostly used for this purpose, in which a sample of 1260 accidents involving cargo tanks in 2002 was selected. Among these, 264 or 21% resulted in rollover. Tank truck rollovers were mainly single vehicle accidents (221 accidents), i.e. about 84% of the 264 rollovers sampled from MCMIS database. Moreover, among the contributing driver-, vehicle-, highway- and environment-related factors, the driver-related factors were identified as the primary reason for the 189 rollover accidents (about 85.5% of 221 single vehicle rollovers).

Table 1.1 summarize the results of accident data analysis reported in Pape *et al.* (2007). The report further characterizes driver error as a "decision error" during an evasive maneuver, a "performance error" or a "non-performance" due to health or fatigue reasons, or a "wrong recognition" error. Among these, the decision error during an evasive maneuver accounted for about 42% of the rollovers. The reported analyses suggest relatively low roll stability limits of tank trucks, which has also been emphasized in many other studies focusing on the fluid cargo-vehicle interactions (e.g., Strandberg 1978, Rakheja and Ranganathan 1993b; Yan *et al.*, 2005). Furthermore, the relatively higher frequency of diver errors, in particular the decision errors during the evasive maneuvers, suggested lower controllability limits of the vehicles.

Table 1.1. Relative frequency of primary causal factors contributing to rollover crashes of tank trucks based on a sample of 264 rollovers reported in MCMIS database (Pape *et al.*, 2007).

Causal Factor	Single Vehicle Rollovers Number (%)	Multiple Vehicle Rollovers Number (%)
Driver Factors	189 (85.5)	11 (25.6)
Vehicle Factors	9 (3.9)	0 (0.0)
Highway Factors	8 (3.7)	0 (0.0)
Weather Factors	0 (0.0)	1 (2.3)
Other Vehicle Induced Factors	12 (5.3)	31 (72.1)
Unknown Factors	3 (1.3)	0 (0.0)
Total	221 (100)	43 (100)

The Pape *et al.* (2007) also analyzed a sample of 482 trucks rollovers from a total of 1,837 tank truck accidents, documented in the TIFA database during 1999 to 2003 with an objective to identify primary causal factors, particularly the driver errors. A set of driver errors considered to contribute significantly to the rollover were identified, which are summarized in Table 1.2. The analyses revealed that most common outcome of a rollover was the "run off road" with almost the same frequency between straight trucks and tractor semitrailer combinations. In almost one third of the accident files considered, the vehicles ran off the road prior to the rollover, while the vehicles were not considered to be travelling too fast. The drowsiness of the driver occurred rarely, while inattentive factors accounted for nearly 6.5% of the rollovers. Moreover, it was not possible to identify causes of nearly 14% of the rollovers. The results also suggested relatively lower controllability limits of tank trucks, which tend to limit the lane keeping ability of the vehicle.

Table 1.2. Relative frequency of driver errors based on a sample of 482 rollover crashes from the TIFA database (Pape *et al.*, 2007).

Driver Factors	Straight Truck Rollovers Number (%)	Tractor Semitrailer Rollovers Number (%)
None	26 (13.7)	87 (14.6)
Physical or Mental Condition		
Inattentive	13 (6.8)	39 (6.5)
Drowsy, Asleep	3 (1.6)	31 (5.2)
Other Physical	1 (0.5)	8 (1.3)
Miscellaneous Driver Errors		
Run Off Road	60 (31.6)	203 (34.0)
Driving too fast	25 (13.2)	102 (17.1)
Erratic/Reckless	8 (4.2)	29 (4.8)
Over Correcting	17 (9.0)	26 (4.3)
Failure to Yield or Obey	9 (4.7)	14 (2.3)
Other Driver Error	7 (3.7)	14 (2.3)
Other		
Avoiding, Swerving, Sliding	11 (5.8)	15 (2.5)
Misc. Non-Driver Causes	2 (1.0)	9 (1.5)
Miscellaneous violation	4 (2.0)	7 (1.1)
Possible Distractions (inside the vehicle)	2 (1.0)	7 (1.1)
Vision Obscured	2 (1.0)	5 (0.8)
Total		
Total	111 (100.0)	371 (100.0)

The study also compared the frequency of tank truck rollovers with that of conventional rigid cargo vehicles (Pape *et al.*, 2007). Percentage of rollovers of tank trucks with respect to the total number of accidents was reported as 26.2% with 482 rollovers in 5 years, while the rollover frequency of conventional freight vehicle was about 10.3%. Table 1.3 shows that straight trucks are more prone to rollover when involved in accidents compared with tractor-semitrailer combinations. The results seem to suggest lower stability characteristics of tank trucks compared with the trucks hauling rigid cargos. The relative lower stability limits of tractor semitrailer combinations have also been reported by Winkler and Ervin (1999).

Table 1.3. Comparison of rollover frequencies of rigid and liquid cargo trucks and tractor-semitrailer combinations identified from accident file sample from TIFA database (Pape *et al.*, 2007).

Configuration	Total Rollovers	Total Crashes	Percent Rollover Crashes	Percent of all rollovers
Conventional rigid cargo vehicles				
Straight Truck	215	1,871	11.5%	20.1%
Tractor-Semitrailer	856	8,525	10.0%	79.9%
Total	1,071	10,396	10.3%	100.0%
Liquid cargo vehicles				
Straight Truck	111	356	31.2%	23.0%
Tractor-Semitrailer	371	1,481	25.1%	77.0%
Total	482	1,837	26.2%	100.%

Table 1.4 presents a correlation between the rollover frequency and the gross combination weight (GCW) at the time of the accident (Pape *et al.*, 2007). In this table, the first row, 0 to 10% refers to the cases with very low cargo load, where the weight of the truck would be dominant compared to cargo weight. The fill volume in this case ranged from 0 to 20% of the total tank volume. The second row, 10 to 50%, represents the partial load condition (20 to 75% of capacity), while the last row, over 50%, represents nearly full load condition (greater than 75% of volume capacity). The study confirmed that the majority of the rollovers occurred among trucks that had partial to full loads, (291 accidents, which correspond to the 71.3% of 394 accidents files considered).

Table 1.4. Correlation between the vehicle load and the rollover frequency based on a sample of 394 rollovers reported in TIFA database (Pape *et al.*, 2007).

Cargo Percentage of GCW	Total Rollovers	Percent of all Rollovers
0 to 10%	32	8.1%
11 to 50%	81	20.6%
>50%	281	71.3%
Total	394	100.0%

Owing to similarities between the transportation systems and the road infrastructures in the US and Canada, one can expect similar results from the accidents reported in Canada. The scenario reported in Canada by Woodrooffe (2000) is similar to the one obtained by Pape *et al.* (2007) for the U.S., even though Rakheja *et al.* (2003) emphasized the difficulty of having data with enough reliability. Woodrooffe (2000) analyzed a total 1,874 road accidents involving dangerous goods from 1990 to 1998. The study showed that 43% of these accidents resulted in a rollover, while tank trucks carrying flammable liquids were involved in 59% of the rollovers, which is likely due to higher population of such vehicles.

1.2.2 Review of tank design standards

The North American (CFR 49, part 178, 2011) and European (ADR, 2011) standards on tank design mainly deal with tanks carrying hazardous materials. There are two main regulations governing design of tanks, namely CFR 49 (Code Federal Regulation) in the United States, which has been adopted in Canada known as CAN/CSA B620 to B622, and the ADR (Agreement Dangerous Road) for the European community. All aspects concerning the transportation of dangerous goods, including classification, consignment procedures (loading, unloading and handling) and packaging are outlined in these regulations. While a review of standards in view of design, classification and consignment procedures falls beyond the scope of the present work, a critical analysis concerning the stability limits of tank vehicles is the primary focus. Recommendations, minimum static rollover threshold, baffle design and layouts for suppressing fluid slosh in partly filled tanks are thus particularly analyzed.

The part 178 of the CFR 49 mainly regulates the thickness and the material of the shell and the bulkheads. The regulation also addresses the use of baffles for circumferential

reinforcement of the tank shell, requiring a baffle or external stiffener spaced every 1.52m span or less. The regulation does not address issues related to lateral or roll stability limits (CFR 49, part 178, 2011; CAN/CSA B620, 1987). The Canadian National regulatory authorities, however, have attempted to consider the adoption of a minimum roll threshold for tank trucks of 0.4g. For this purpose, a comprehensive series of tilt table tests were conducted at the National Research Council of Canada (NCR) to characterize the rollover threshold of tank trucks configurations operating in Canada (Billing and Patten, 2005). A total of 17 vehicle combinations were evaluated which included the principal configurations of tank trucks in service across Canada and between Canada and the US. A total of 7 (41%) vehicle combinations revealed a static rollover threshold under 0.35g, when loaded to their allowable gross weight in Ontario, while 14 (83%) vehicles revealed a rollover threshold under 0.4g. Moreover, the rollover threshold of a combination with liftable axles reduced by 0.01 – 0.03 g, when those axles were raised during a turn. Billing and Patten (2005) have also discussed that reduction of capital cost seems to be of primary importance for Canadian and USA tank manufacturers, while an improvement in roll stability is a priority for the European manufacturers. The use of pneumatic suspension and wide base single tires for trailer's axles could allow the European manufactures to comply easily with the roll stability limit of 0.4g imposed by ADR (2011) for tanks carrying dangerous goods.

Rollover accidents are usually initiated by severe steer inputs performed to avoid obstacles on the roadways or for lane keeping. In such conditions, the stability limits based on static analysis (SRT - static rollover threshold) may be inadequate due to lack of consideration of dynamic responses (Dahlberg, 2000; Dahlberg and Stensson, 2006). It has been suggested that a vehicle may rollover at an acceleration level less than the SRT (Gertsch and Eichelhard, 2003). The Dynamic Rollover Threshold (DRT), defined as the acceleration at which a rollover could occur in a transient maneuver, has been estimated to be about 20% lower for rigid cargo vehicles compared to the SRT (Winkler, 2009; Gertsch and Eichelhard, 2003). The liquid cargo motion within a partially filled tank may further reduce the dynamic rollover threshold. The reported studies have suggested that the worst case sloshing conditions occur when the tank is filled in the 40% to 70% of the tank volume (Winkler *et al.,* 2000). In such load conditions, rollover may occur at an acceleration level equal to half of the SRT (Ervin and Mathew, 1988). The frequency of steering input may also deteriorate the rollover immunity of a vehicle. A steering frequency in the vicinity of 0.5 Hz could cause resonant slosh in partial filled tanks (Ervin and Mathew, 1988;

Winkler and Ervin, 1999). In terms of standards to prevent such phenomenon only the European economic community has adopted one obvious approach in order to avoid stability degradations due to slosh. The ADR (2011) agreement states that the allowable fill volume for a clean-bore tank compartment with the maximum capacity of 7500 liters is more than 80% or less than 20%. Unfortunately, this article is applied only to dangerous loads, and those by nearly half of the tank truck fleet could operate with any fill condition. The regulations in North America, however, do not address such issues related to fluid slosh.

The ADR (2011) agreement addresses the stability of tank vehicles in two stages. The first stage regulates the aspect ratio of the tank in the roll plane, which requires that the maximum width between the outermost contact points must be at least 90% of the center of gravity height of the laden vehicle. The second stage recommends that all tank vehicles with a tank capacity of more than 3 m^3, intended for transportation of dangerous goods in the liquid or molten state, shall comply with the technical requirements of ECE Regulation No. 111 for lateral stability (UN-ECE No. 111, 2000). ECE Regulation 111 requires SRT limits derived from a tilt table test or an alternative estimation method. In case of the tilt table test, the static rollover stability of the vehicle shall be such that the wheels on one side should not lose the contact with the tilt table surface up to angle of 23°. Moreover, the test must be repeated three times for tilting of each side of the vehicle. Furthermore, the tilt table test shall be done under full load condition with at least 70% of the volume being filled. Moreover, the tilt table angle should be increased slowly with an angular speed less than 0.3 °/s. The standard also presents a method for estimating SRT of the vehicle and requires that estimated rollover stability or overturning lateral acceleration of 4 m/s^2. The estimation method also requires considerations of most of the factors influencing the roll stability such as the center of gravity height, the track width and the suspension and tire stiffness.

The ADR (2011) also regulates the use of baffles to prevent damages to the tank shell. For tanks transporting liquid goods, the shell must be equipped with strengthening members comprising partitions, surge plates or external or internal rings, while the distance between two adjacent strengthening elements must not exceed 1.75m. Strengthening elements can be disregarded if the fluid volume between the two adjacent reinforcing elements is less than 7500 liters. Moreover, a surge plate must cover at least 70% of the cross-sectional area of the tank.

As clearly indicated in this section, the tank design standards are quite different in North America and European Community. The North American guidelines lack minimum Static Rollover Threshold (SRT) and requirements on filling conditions, which are addressed in the European community guidelines. It has been suggested that some tank specifications, like US DOT 406 or the Canadian equivalent TC 406, exhibit good quality in terms of SRT, even though there are no requirements about the minimum SRT in the official US Code of Federal Regulation, CFR 49 (Billing and Patten, 2005). Furthermore, the use of lateral baffles is considered neither in European nor in North American standards. Capital cost reductions and difficulty in performing operation of tank cleaning are the main reasons which prohibit the use of baffles, even though, the lateral baffles can significantly limit the hazard due to the liquid sloshing in partly filled tank trucks (Ervin & Mathew 1988).

1.2.3 Liquid sloshing analysis

The liquid sloshing in moving containers has been widely studied since 1960s. Monograph edited by Abramson (1966) presents a comprehensive review of liquid sloshing problems. However, it addresses only issues related to the space vehicle applications based on the experimental and theoretical approaches. Salem *et al.* (1999) also presented a literature review of fluid-container interactions with particular focus on parameters that influence the stability of partly-filled tank trucks under various maneuvers. Furthermore, Ibrahim *et al.* (2001) performed an extensive review of studies on sloshing phenomena in different applications such as liquid natural gas ship carriers, storage tanks, aerospace vehicles and road tankers. The majority of the review publications in the field of liquid sloshing, however, concern aerospace and ocean vehicles as well as ground-supported structures (Ibrahim, 2005; Faltinsen and Timokha, 2009). Fundamentally, the studies reporting fluid sloshing in road containers can be grouped in three categories based on the method of analysis: quasi-static, mechanical analogy and dynamic liquid slosh. These methods of analysis together with their essential features and limitations, in addition to methods employed for coupled fluid slosh and vehicle dynamics, are described in the following subsections.

1.2.4 Quasi-static method

Quasi-static model is a simplified method for prediction of steady-state position of the liquid free-surface in moving containers. It can be shown that the liquid free-surface can be replaced by a straight line, which is related to roll motion and the lateral acceleration imposed in the roll plane or pitch motion and longitudinal acceleration in the pitch plane (Popov, 1991). The steady-state cargo shift is subsequently evaluated to study its effect on directional dynamics performance of the vehicles (Fig. 1.1).

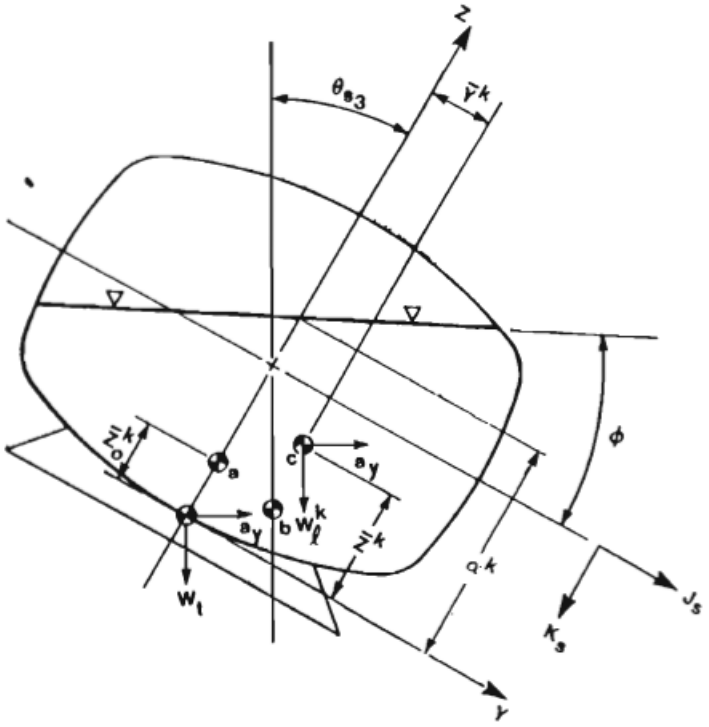

Fig. 1.1. Quasi-static roll plane model of a modified oval tank (Ranganathan *et al*., 1989).

Sankar *et al.* (1986) and Rakheja *et al.* (1988) investigated the rollover immunity levels of articulated vehicles carrying cylindrical cleanbore and compartmented tanks with partial loads during steady turning using quasi-static fluid slosh and a static roll plane model of the vehicle. The study concluded that partially filled cleanbore tank vehicles exhibit lower rollover threshold acceleration compared to the rigid cargo vehicles. Ranganathan *et al.* (1989) and Rakheja *et al.* (1989) developed a quasi-static roll plane model of a partially-filled tank to calculate the forces and moments associated with the cargo load shift. The vertical and lateral translation of center of

mass of liquid bulk was computed during steady turning using an iterative algorithm for four different tank cross-sections; circular, elliptical, modified-oval and modified square. The static roll equilibrium equations were solved for small increments in roll angle until the trailer and tractor tires on a single track lift off the ground. The rollover threshold was determined using the highest lateral acceleration obtained during the computation process. The study concluded that circular tanks reveal greater stability limit with high density liquids, while the modified oval and modified square tanks show higher rollover threshold with low density liquids for the same payload and composite axle loads.

Sankar *et al.* (1989) and Ranganathan *et al.* (1990) developed a three-dimensional vehicle model integrating a quasi-static fluid slosh and roll plane model to study the effects of liquid load shift in tank vehicles under steering inputs assuming a constant forward speed. The study demonstrated significant deviation in the path followed by the tank vehicle due to liquid movement under constant steer maneuver. Ranganathan *et al.* (1993a) further employed this model to analyze directional dynamics of a B-train tank vehicle combination considering partial loads. A simple computer program based on quasi-static analysis was also developed by Southcombe *et al.* (2000) to estimate roll stability of partly-filled tank trailers for various tank geometries under steady state turning maneuvers. Furthermore, Toumi *et al.* (2009) integrated the quasi-static model to a simplified vehicle model consisting of one sprung mass and an unsprung mass with three degrees of freedom for the sprung mass (lateral, yaw and roll). The results obtained from the study revealed considerable lateral load shift in case of liquid cargo compared to the rigid cargo during steady as well as transient steer maneuvers.

Quasi-static model has also been employed for investigation of longitudinal load transfer in the pitch plane. Ranganathan and Yang (1996) studied the effect of steady state liquid load shift occurring within a partially filled cylindrical cleanbore tank on the braking characteristics of the tank vehicle. The vehicle was a five-axle tractor-tank-semitrailer unit represented by three composite axles subjected to constant deceleration and zero steer input. The study showed that the load shift from the rear to the front of the vehicle is relatively large in comparison with an equivalent rigid cargo vehicle, particularly in the range of 40% to 60% fill levels.

Another important application of quasi-static method involved optimization of design parameters of tank vehicles in order to enhance the stability and directional dynamics

performance of such vehicles. For instance, Popov *et al.* (1993c) developed an optimization technique based on the steady state solution of the liquid motion in two-dimensional rectangular tanks under steady cornering maneuvers. The study suggested an optimal tank height, which varied nonlinearly from 0.707 to 0.5 of the tank width, for lateral acceleration from 0 to 1g regardless of the liquid-fill depth. Popov *et al.* (1996) also conducted a numerical analysis to obtain the optimal height/width ratio of an elliptical road container based on the steady-state solution. The Analysis was founded on the minimization of the peak overturning moment under a steady turning maneuver. The result of the study showed that the optimal height/width ratio decreases with increase in the magnitude of lateral acceleration. The study further revealed that elliptical containers are less stable than rectangular or modified rectangular containers of the same capacity.

Another example is the work by Zhanqi *et al.* (1995), which proposed optimal compartment sizing of a partly-filled tank subjected to a constant deceleration maneuver, using the quasi-static fluid slosh. The study suggested that equal length compartments could yield minimal longitudinal load transfer under a straight line braking maneuver. Quasi-static method was also used by Kang *et al.* (1999) to obtain an optimal tank cross-section from a generic tank cross-section including eight symmetrical circular arcs. The optimization was based on minimization of the height of liquid center of mass and lateral movement of liquid bulk for different fill volumes. Two tank geometries were suggested in the study; one for tank vehicles involving large variations in liquid-fill depth and one for tank vehicles operating in nearly full load condition. Similar optimal tank geometries for various fill levels were also suggested by Ziarani *et al.* (2004) who developed a genetic algorithm for optimization of tank geometry based on minimization of the lateral and vertical load shifts.

The above studies have considered only two-dimensional quasi-static fluid movement either in the roll plane or in the pitch plane to study either steady-state turning or braking performances of partly-filled road tankers. Kang *et al.* (2000a) developed a three-dimensional quasi-static fluid slosh model considering simultaneous applications of longitudinal and lateral accelerations, which was integrated to a three-dimensional articulated vehicle model. The model was applied to study the effects of liquid cargo load shift in the roll and pitch planes on dynamic behavior of such vehicles subjected to braking-in-a-turn maneuver. The study confirmed the

adverse effect of roll, pitch and yaw moments arising from the cargo load shift on the dynamic performance of the tank vehicles.

1.2.5 Dynamic liquid slosh analysis

Although quasi-static method makes it possible to accurately compute the steady-state position of liquid center of mass, which contributes to computation of mean dynamic load shifts as well as mean directional responses, the effect of transient liquid sloshing phenomenon is not taken into account by this analysis. Furthermore, the quasi-static method cannot be applied to tanks with baffles. A number of studies have investigated dynamic fluid slosh in partly-filled tanks subject to longitudinal or lateral or longitudinal and lateral accelerations using computational fluid dynamics methods. These studies have invariably shown significant transient slosh and discontinuous free surface under applied acceleration inputs, and have concluded that peak slosh forces and moments are substantially greater than those predicted from a quasi-static model. Modaressi-Tehrani (2004) and Yan *et al.* (2005) analyzed dynamic fluid slosh using FLUENT code and confirmed considerably higher magnitudes of transient fluid slosh suggesting only limited validity of the quasi-static method under transient maneuvers or high magnitude excitations.

In dynamic liquid slosh analyses, the fluid motion within the tank is described by solving the Navier-Stokes equations. Analyses of dynamic fluid slosh can be performed using two different approaches. First approach concerns small amplitude sloshing, assuming an ideal liquid with negligible viscosity as well as incompressible and irrotational flows, where Navier-Stokes equations reduce to potential flow equations with linear boundary conditions on the free surface. This approach is based on the linear slosh theory (Abramson, 1966). In the second approach, high amplitude slosh is simulated through solutions of Navier-Stokes equations using computational methods. A brief review of relevant studies in the context of these approaches is presented below.

1.2.5.1 Linear slosh approach

Ibrahim (2005) suggested that exact solutions for the linear liquid sloshing are limited to regular tank geometries with straight walls, such as rectangular and upright-cylindrical containers. Fluid-free-surface natural frequencies and mode shapes for two- and three-dimensional rectangular tanks have been reported by Abramson (1966) and Ibrahim (2005) using

the method of separation of variables. Owing to difficulties associated with this classical method of separation of variables for analysis of linear slosh in most practical tank geometries (e.g., horizontal cylinders), several other methods have been developed for linear slosh analysis. Conformal mapping is the most frequent and effective method for modeling the linear fluid slosh. In this method, the original tank geometry is transformed into a regular geometry in which the Laplace equation and the wall and free surface boundary conditions are solved explicitly. Budiansky (1960) was the first researcher who used this method to calculate natural frequencies and modes of liquid sloshing in two-dimensional cylindrical and spherical containers as a function of the liquid fill-depth. The fundamental frequency was the lowest for the nearly empty tank and increased monotonically with increase in the liquid fill-depth. The results of the study were confirmed by the experimental data obtained by McCarty and Stephens (1960). Natural frequencies of liquid sloshing in two-dimensional cylindrical tanks with variable liquid depth were also estimated by Kuttler and Sigillito (1984) using a method that provided the lower and upper bounds of the eigenvalues. McIver (1989) also solved the potential flow equation for the free liquid sloshing in two-dimensional cylindrical and spherical containers using the conformal mapping technique and reported the natural frequencies in terms of liquid fill level. The results were in very good agreements with those reported by Budiansky (1960).

Papaspyrou *et al.* (2004a) investigated liquid slosh in two-dimensional circular cylindrical vessels subjected to transverse excitations using an analytical approach. The velocity potential was expressed in terms of a series of spatial and time functions thereby reducing the partial differential equations into a system of linear ordinary differential equations. The proposed method was limited to the half-filled tanks only. Patkas and Karamanos (2007) developed a mathematical model for simulation of linearized liquid sloshing in two-dimensional horizontal cylindrical and spherical containers with arbitrary liquid height under a lateral acceleration using a variational formulation. Natural sloshing frequencies were computed, which were subsequently verified on the basis of those reported by McIver (1989). Faltinsen and Timokha (2010) developed a linear multimodal method to study the two-dimensional liquid slosh in a horizontal cylindrical tank. Based on the linear multimodal approach, the free-surface elevation and velocity potential were expressed by a series of the natural sloshing modes. This reduced the associated linear boundary value problem to a set of ordinary differential equations.

Apart from the circular cross-section, linear analysis has been applied for simulation of liquid sloshing in other tank geometries. Fox and Kuttler (1981) suggested a method for modal analysis and evaluation of slosh frequencies for some general shaped containers based on conformal transformation of rectangles into two families of two-dimensional regions. The proposed technique was employed by Fox and Kuttler (1983) to calculate slosh frequencies of a wide range of two-dimensional containers with various cross-sections including half-filled elliptical with a lip, half-filled elliptical with a bottom-mounted vertical baffle, half-filled elliptical without baffle and half-filled circular tanks. Hasheminejad and Aghabeigi (2009) computed slosh frequencies for a half-filled two-dimensional elliptical container with and without horizontal side baffles mounted at the level of the liquid free-surface. The original cross-section was transformed into an infinite rectangle in the unbaffled case and finite rectangle in the baffled case. The study showed that natural sloshing frequencies for half-filled elliptical tanks increased with decreasing tank aspect ratio, irrespective of the liquid capacity and tank dimensions. The study further discussed that horizontal side baffles are more effective for nearly circular containers compared to the elliptical containers with high aspect ratio.

Analytical modeling of anti-sloshing effect of baffles was limited to a very few studies in which linear sloshing assumption was applied. Goudarzi *et al.* (2010) and Goudarzi & Sabbagh-Yazdi (2012) developed an analytical model based on potential flow and linear sloshing to evaluate the damping effect of horizontal and vertical baffles in rectangular tanks. The damping due to baffles was estimated using the energy-ratio formula and drag coefficient of the baffle plates, which were estimated by the drag coefficient of free flat plates in an oscillating fluid (Keulegan and Carpenter, 1958). The proposed analytical approach was supported by experimental measurements. Faltinsen *et al.* (2010) and Faltinsen and Timokha (2011) also performed an analytical simulation of the linear liquid sloshing in rectangular tanks with a slat screen mounted vertically in middle of the tank. The pressure differential across the plate was estimated by steady state pressure differential and a pressure loss coefficient for the slat screen. Hasheminejad and Mohammadi (2011) employed the conformal mapping technique (Fig. 1.2) to study the effect of surface-touching horizontal side baffles, bottom mounted vertical baffle and surface piercing vertical baffle in cylindrical containers under lateral excitations. The study showed that a long pair of surface-touching horizontal side baffles have considerable effect on the natural sloshing frequencies, while the bottom mounted vertical baffle was not recommended

as an effective anti-sloshing device. A surface-piercing vertical baffle, however, was found to be efficient for controlling the liquid sloshing under high fill levels. The same conclusion was also drawn by Hasheminejad and Aghabeigi (2009, 2011), and Hasheminejad and Aghabeigi (2012), where an elliptical tank with the same baffle configurations was considered.

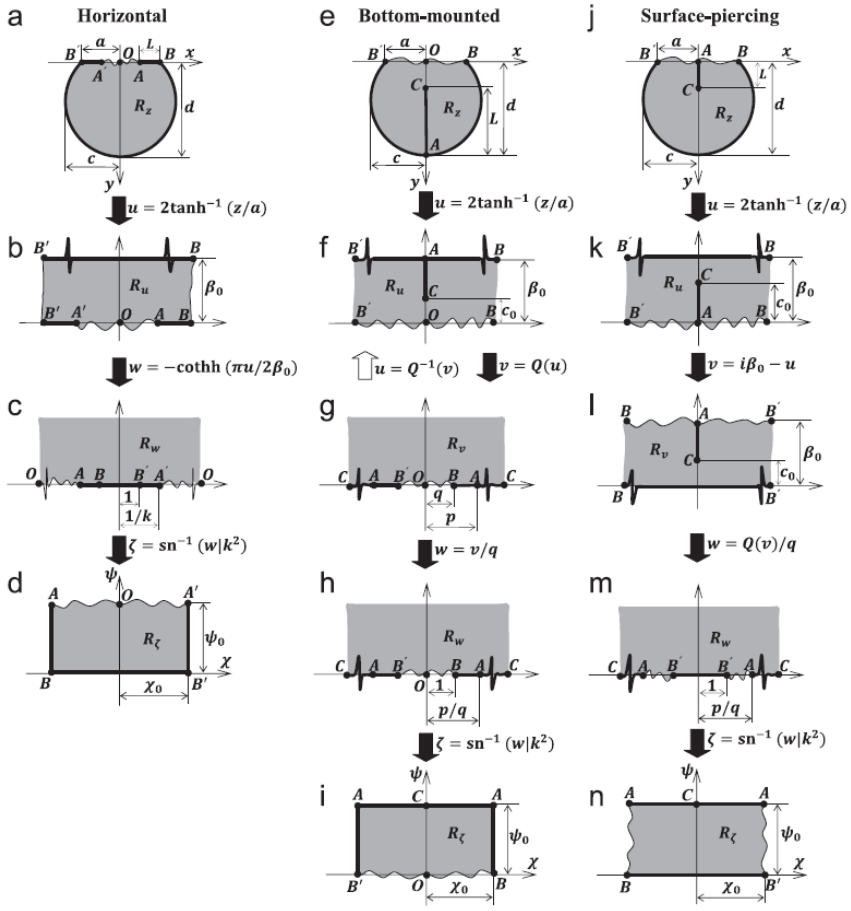

Fig. 1.2. Successive conformal mapping for the baffled cylindrical tank (Hasheminejad and Mohammadi, 2011).

Evaluations of natural frequencies of slosh as well as slosh forces for three-dimensional horizontal cylindrical containers using analytical linear slosh approaches have been addressed in only a few studies. This is mostly attributed to difficulties associated with solution of three-dimensional potential equations and implementation of the free surface boundary condition. Moiseev (1964) and Moiseev and Petrov (1966) developed a variational method for calculation of slosh natural frequencies in various tank geometries including a cylindrical container. Evans

and Linton (1993) derived an expression for the velocity potential as a series of bounded harmonic functions to evaluate slosh frequencies in half-filled two- and three-dimensional cylinder and half-filled spherical containers. Papaspyrou *et al.* (2003, 2004b) also extended the work of Evans and Linton (1993) to analyse the three-dimensional liquid slosh in horizontal cylindrical and spherical vessels. Hydrodynamic forces were evaluated under a longitudinal excitation, while the studies were limited only to half-full vessels.

In addition to the analytical methods, numerical methods have been employed for solutions of the linear boundary value problem of liquid sloshing. Ru-De (1993) presented a finite element analysis of linear liquid slosh in an upright cylindrical tank under a lateral excitation. Cho *et al.* (2005) and Arafa (2007) developed a finite element formulation for linear liquid slosh in two-dimensional baffled rectangular tanks. Mitra *et al.* (2007) employed the finite element method to study motion of the liquid free-surface in two-dimensional horizontal cylindrical, rectangular, trapezoidal and vertical annular cylindrical tanks due to lateral excitation, using the linear theory. The results were presented in terms of hydrodynamic pressure distribution on the tank walls as well as transient free-surface elevation. Karamanos *et al*. (2009) developed a three-dimensional finite element method for calculation of natural frequencies in addition to sloshing forces as a function of the liquid-fill depth for horizontal cylindrical, spherical and conical vessels under a seismic excitation. Teng *et al.* (2006) employed the boundary element method to analyze linear liquid slosh in two-dimensional rectangular tanks. Boundary element method is a numerical method for solving integral equations in which only the boundary of the body is discretized (Katsikadelis, 2002). Dutta and Laha (2000) and Firouz-Abadi *et al.* (2009) developed a boundary element method founded on the linear theory for calculation of natural frequencies as well as slosh forces due to liquid oscillations in arbitrary three-dimensional tanks, including rectangular, upright cylindrical and spherical tanks. Firouz-Abadi *et al.* (2008) and Sygulski (2011) also employed a similar approach to calculate natural frequencies and mode shapes of liquid slosh in three-dimensional baffled tanks with arbitrary geometry. The effect of baffles on the natural sloshing frequencies were also investigated by Gedikli and Erguven (2003) using a variational BEM. Gedikli and Erguven (1999) also reported seismic responses for an upright cylindrical tank with a ring baffle using BEM and superposition of modes. The major contribution of these works was the significant reduction of computational cost compared to other numerical methods such as the finite element method.

1.2.5.2 Nonlinear slosh analysis

Analytical methods for simulation of nonlinear liquid slosh, which utilize the potential flow theory along with the nonlinear free-surface boundary condition, are mostly limited to rectangular and upright cylindrical tanks. Earlier attempts concerning nonlinear phenomena in the slosh flows were documented by Abramson (1966), who discussed three different theories for solving nonlinear oscillations of liquid free surface in rectangular and upright cylindrical tanks under a lateral excitation. These theories were suggested by Moiseev (1958), Penney and Price (1952) and Hutton (1963). Analytical methods for nonlinear liquid slosh in two-dimensional rectangular containers were further developed by Bauer (1967), Kit *et al.* (1987), Lepelletier and Raichlen (1988), Faltinsen *et al.* (2000), Faltinsen and Timokha (2001, 2002), Shankar and Kidambi (2002), Hill and Frandsen (2005), Timokha and Hermann (2006) and Forbes (2010). Moreover, Komatsu (1987), Miles (1984), Yin *et al.* (1999) and Faltinsen *et al.* (2003, 2005a, 2005b, 2006) have analyzed nonlinear liquid slosh within rectangular and vertical cylindrical tanks analytically.

Owning to inherent limitations of the analytical methods, computational methods have been developed for addressing nonlinear fluid slosh problems. A comparative review of recent numerical studies on fluid-structure interaction problems has been presented by Rebouillat and Liksonov (2010). Numerical methods for solving such problems can be classified into four categories: Lagrangian methods, Eulerian methods, Arbitrary Lagrangian-Eulerian methods (ALE) and Smoothed Particle Hydrodynamics methods (SPH).

In Lagrangian methods, mesh moves with the fluid velocity in the entire domain. For discretization purpose, finite element method has been widely used (e.g., Ramaswamy and Kawahara, 1987; Hayashi *et al.,* 1991; Radovitzky and Ortiz, 1998; Staroszczyk, 2009; Cremonesi *et al.*, 2010). Although Lagrangian methods are computationally faster than Eulerian methods and movement of gird nodes with fluid medium results in automatic tracking of the free-surface, large deformation of the free-surface can lead to a highly distorted mesh which can cause an unstable and inaccurate solution. In order to resolve this issue, re-meshing or re-zoning techniques are used, which are generally tedious and very time-consuming. Besides, the fluid medium histories may be lost due to re-zoning (Liu and Liu, 2003). These numerical difficulties associated with Lagrangian methods have contributed to their limited implementation in analysis

of liquid slosh dynamics, which are mostly focused on rectangular tanks (Ramaswamy *et al.,* 1986; Okamoto and Kawahara, 1990; Dogangun *et al.,* 1996; Tang *et al.,* 2008).

Unlike the Lagrangian methods, the Eulerian methods assume that the mesh is fixed on the domain. The free-surface deformation thus does not lead to a change in the shape of the mesh cells, although the free-surface of fluid needs to be tracked using an alternate method such as the volume-of-fluid method (VOF). This method was originally proposed by Hirt and Nichols (1981) and further developed by several researchers such as Rudman (1997), Harvie and Fletcher (2000), Kim and Lee (2003) and Kim *et al.* (2003) on the basis of fractional volumes of liquid in a cell, which can be used to identify the position of the free-surface.

The different discretization approaches have been used with the Eulerian methods for simulation of nonlinear liquid slosh. These include the finite difference method (Popov *et al.,* 1992, 1993b; Kim, 2001; Kim *et al.,* 2004; Liu and Lin, 2008; Wu and Chen, 2009), the finite element method (Nakayama and Washizu, 1980; Aslam, 1981; Wu *et al.,* 1998; Cho and Lee, 2004; Wang and Khoo, 2005), the finite volume method (Modaressi-Tehrani *et al.,* 2006; Ming and Duan, 2010) and boundary element method (Romero and Ingber, 1995; Ortiz and Barhorst, 1998; Chen *et al.,* 2007). While the finite element (FE), finite volume (FV) and finite difference (FD) methods involve longer computational time as well as substantial data storage capacity, the boundary element method (BEM) was found to be quite efficient for this purpose (Nakayama and Washizu, 1981).

Arbitrary Lagrangian-Eulerian methods (ALE) combine the advantages of Lagrangian and Eulerian methods. The concept of coupled Lagrangian and Eulerian method was initially suggested by Noh (1964) and Franck and Lazarus (1964), which was further developed by several other researchers such as Hirt *et al.* (1974) and Hughes *et al.* (1981). In the ALE description, grid nodes may follow the fluid medium (as in the Lagrangian method), or be fixed on the domain (as in the Eulerian approach), or move arbitrarily to give a more advantageous re-zoned mesh. This freedom in moving the computational mesh gives the opportunity to simulate significant deformation of the free-surface effectively. Numerical studies of fluid slosh by ALE, however, have been mostly limited to two- and three-dimensional rectangular tanks, two-dimensional circular tanks and vertical cylinders (Liu and Huang, 1994; Okamoto and Kawahara,

1997; Ushijima, 1998, 2000; Braess and Wriggers, 2000; Souli and Zolesio, 2001; Aquelet and Souli, 2003; BaoZeng, 2008; Zhou *et al.,* 2007).

As an alternative to the conventional grid-based methods, Smoothed Particle Hydrodynamics (SPH) method has been used in fluid slosh problems in a few studies. The Lagrangian nature of the SPH method permits the tracking of the free-surface and the moving interface, which is quite challenging in grid-based methods. The tracking of the free-surface could thus be performed automatically by tracking the particles in the fluid domain, thereby eliminating the need for a free-surface boundary condition (Liu and Liu, 2003). The simulations of fluid slosh using this method have been mostly limited to rectangular tanks (Souto-Iglesias *et al.,* 2006; Delorme *et al.,* 2009; Colagrossi *et al.,* 2010; Rafiee *et al.,* 2011)

As indicated earlier, studies on nonlinear liquid slosh in rectangular as well as vertical cylindrical containers have attracted relatively greater attention. The simulation of nonlinear slosh in typical tank cross-sections used for carrying liquid cargo by heavy vehicles, such as horizontal circular, elliptical and oval tanks, have been addressed in relatively fewer studies. Popov *et al.* (1993a) obtained steady-state and transient solutions for liquid slosh in two-dimensional horizontal cylindrical road containers under steady turn manoeuvres using finite difference method assuming laminar flows. Yan *et al.* (2005) simulated two-dimensional nonlinear liquid slosh in circular and conical cross-section containers under ramp-step lateral acceleration using FLUENT software. Coordinates of center of gravity as well as horizontal and vertical components of the hydrodynamic force were expressed as second-order polynomial regression functions in terms of lateral acceleration for different liquid-fill depths. These functions were integrated into the roll moment equilibrium of an articulated tank vehicle to calculate the rollover threshold limits of the partly-filled tank vehicle. The study confirmed that tank trucks with lower fill volume, despite their lower center of gravity, may exhibit lower rollover threshold for a constant cargo load. The rollover threshold was observed to be significantly lower than that derived from quasi-static analysis. Dai and Xu (2006) investigated transient liquid slosh in a two-dimensional horizontal cylindrical tank subject to acceleration excitations arising from steady-turning, lane-change and double-lane-change maneuvers, based on the potential flows. In order to avoid dealing with complicated free surface boundary condition, the liquid domain was transformed to a rectangle so that the curved free surface became a line in the mapped domain. Finite deference method was then employed for

discretization of transformed governing equations in the mapped domain. A similar approach was also followed by Frandsen and Borthwick (2003), Frandsen (2004), Turnbull *et al.* (2003), and Chen and Nokes (2005). Dai and Xu (2006) also applied the suggested approach for three-dimensional cylindrical containers subject to both lateral and longitudinal excitation to demonstrate the capability of this approach for investigating nonlinear three-dimensional liquid slosh in arbitrary tank geometries.

1.2.6 Mechanical analogy method

An alternative approach for analyzing the liquid slosh in moving containers can be represented by drawing an analogy between the liquid motion and the mechanical systems. The key idea of this method is that the liquid within the container can be treated as two distinct parts: a stationary part with respect to the container and the moving part attributed to the liquid sloshing. The moving part of the liquid is modeled by a series of mass-spring-dashpot systems or a set of simple pendulums assuming linear liquid motion (Fig. 1.3). The parameters of the equivalent mechanical system can be evaluated considering equivalent mass, equivalent oscillation frequencies and moments of inertia, preservation of liquid center of gravity and the resultants slosh forces and moments. In case of the mass-spring-dashpot system, the spring constants can be determined from natural frequencies of liquid sloshing, while in case of pendulum analogy, the length of pendulums are calculated from the natural frequencies. Comprehensive formulations of equivalent mechanical systems for a general-shaped container have been documented by Ibrahim (2005). Early attempts for simulation of liquid slosh using the equivalent mechanical model were reported by Abramson (1966), where the parameters of simple mechanical models (with one sloshing mass) and complex mechanical models (with more than one sloshing mass) were presented for upright cylindrical and rectangular tanks. The equivalent mechanical system parameters were generally obtained from the linear theory or experimental data (e.g., Sumner, 1965; Unruh *et al.*, 1986).

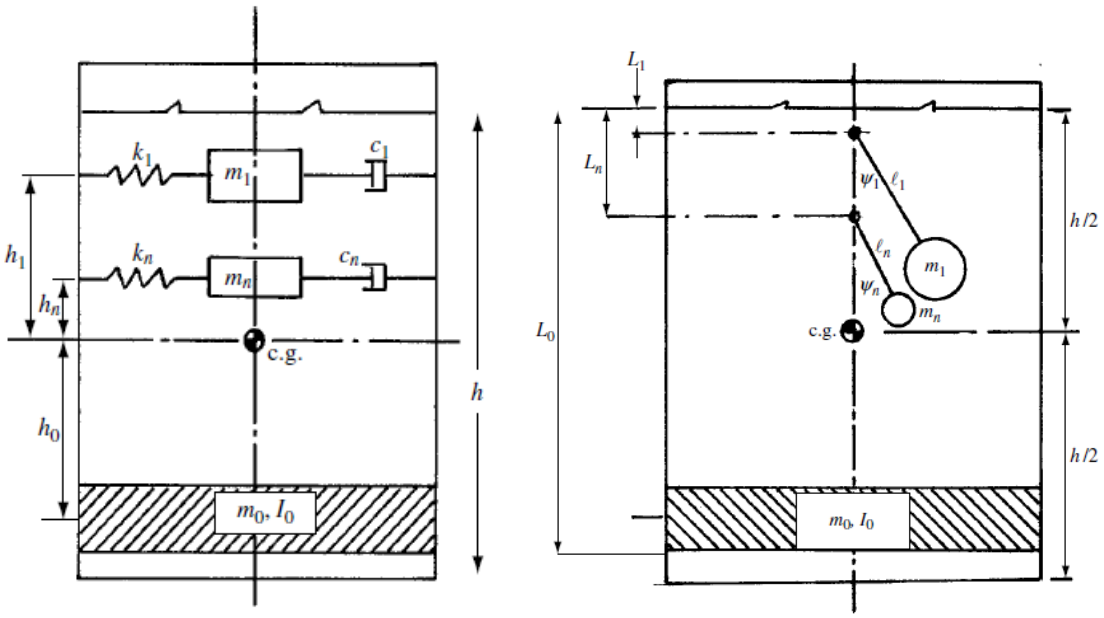

(a) (b)

Fig. 1.3. Mechanical equivalent models: (a) mass-spring-dashpot model; and (b) pendulum model (Ibrahim, 2005).

Unlike the CFD slosh models, the mechanical equivalent models can be conveniently integrated in the overall equations of motion of a road vehicle for directional dynamic analysis of the coupled tank and vehicle system. Bauer (1972, 1973) developed a mechanical model describing the liquid motion in rectangular and upright circular cylindrical containers using a mass-spring-dashpot model to obtain liquid natural frequencies as well as slosh forces and moments exerted upon the vehicle. Slibar and Troger (1975, 1977) employed a similar mechanical model presented by Bauer (1972) to investigate the effect of liquid sloshing on the lateral wheel-load transfer of a tractor-semitrailer-system under periodic steering. Khandelwal and Nigam (1982) employed the pendulum analogy including a fixed mass and an oscillating mass to simulate liquid sloshing in a rectangular railway wagon moving on a random uneven railway track with constant longitudinal acceleration.

Ranganathan *et al.* (1993b) integrated a pendulum model of liquid sloshing in two-dimensional circular tanks to a three-dimensional vehicle model to investigate the directional response of the tank vehicle during steady state maneuvers. Parameters of the pendulum model were determined from the approach proposed by Budiansky (1960). Ranganathan *et al.* (1994)

further developed an equivalent mass-spring system for liquid slosh in a three-dimensional horizontal cylindrical tank using a summation technique to study straight-line braking performance of a tractor-semitrailer tank vehicle. For this purpose, the partially-filled tank was divided into a number of rectangular elements and parameters of equivalent system were calculated for each individual element using the linear theory. Parameters of the equivalent mass-spring system for the entire cylindrical tank were then computed by summation of parameters for each rectangular element. The proposed model was validated in terms of fundamental frequency versus the liquid fill level against the experimental data reported by McCarty (1960). Aquaro *et al.* (1999) conducted roll stability analysis of partially-filled tank trucks using mechanical analogy of the moving cargo. A roll-plane vehicle model was formulated using finite element approach and integrated to a simple pendulum model.

Ibrahim (1999) developed an equivalent pendulum-dashpot model of liquid sloshing in a cylindrical container having a longitudinal slotted partition and integrated it into a roll plane model of a truck with three axles. Damping ratio and damped natural frequency were measured experimentally using a small-scale model tank. Xu *et al.* (2004) investigated the ride quality of a partially-filled compartmented tank truck in presence of the liquid sloshing effect, which was modeled by a linear mass-spring-dashpot system. Acarman and Özgüner (2006) suggested a controller to stabilize and attenuate the sloshing effect in heavy commercial vehicles. The study integrated a vehicle model with six degrees of freedom with an equivalent mechanical model of liquid slosh proposed by Ranganathan *et al.* (1993b, 1994). Salem (2000) simulated lateral fluid slosh in two-dimensional partly-filled elliptical containers using equivalent trammel pendulums. The parameters of equivalent pendulum model including arms of trammel pendulum, fixed and oscillating masses, and the height of fixed mass with respect to the tank base were calculated by matching the pendulum natural frequency, horizontal force component and static moment around the tank base to those calculated from the finite element simulation of the fluid motion. The trammel pendulum model was further integrated into a finite element three-dimensional vehicle model.

The simplicity of integration of mechanical equivalent models into the vehicle dynamics models allows convenient real-time simulation of the coupled fluid-vehicle system. Linear equivalent mechanical models, however, are subjected to the same limitations as the linear sloshing analysis including amplitude and frequency of excitations. Parameters of the linear

equivalent models should be determined from the simulation results for different tank configurations, which are mostly used in liquid-transporting vehicles, since these parameters can only be obtained for upright cylindrical and rectangular containers in the closed forms. Moreover, complexities associated with evaluations of nonlinear mechanical model parameters require equivalent representation of nonlinear phenomena in the free surface through careful experimental measurements or from CFD simulation results. Furthermore, three-dimensional motion of liquid in moving containers, which can significantly affect the simulation results, particularly for complex external loads such as simultaneous lateral and longitudinal excitations, cannot be model by mass-spring and pendulum systems.

1.2.7 Analyses of coupled tank vehicle systems

In order to achieve real-time simulations and investigation of effects of transient liquid slosh forces and moments on the directional dynamic performance of tank trucks, the liquid slosh and vehicle dynamics need to be coupled. Although fluid sloshing within the tank has been widely studied using computational and analytical methods, interactions between the transient liquid sloshing and the vehicle system dynamics have been addressed in only a few studies. As an earlier attempt to address the coupled nonlinear fluid sloshing and vehicle dynamics, Sankar *et al.* (1992) performed simulations of fluid sloshing coupled with the vehicle dynamics to investigate the directional response of tank vehicles for steady and transient steer inputs. The nonlinear two-dimensional fluid slosh model, suggested by Popov *et al.* (1993a) based on finite difference scheme, was coupled with a three-dimensional model of a five-axle tractor-semitrailer, developed by Ranganathan (1990). The vehicle model comprised a tractor and a tare semitrailer, each with five-degrees-of-freedom (lateral, vertical, yaw, roll and pitch), and five unsprung masses due to five axles, each with two-degrees-of-freedom (roll and bounce with respect to associated sprung mass). In order to carry out a real-time simulation, differential equations of vehicle dynamics model were solved using a small time step to calculate lateral and vertical acceleration of the semitrailer sprung mass. These acceleration components were transformed to the non-dimensional accelerations along the tank axes to compute the acceleration components of each fluid cell. The Navier-stokes equations were then solved at the same time step to obtain slosh forces and moments, which were incorporated to the vehicle dynamics model to continue the computational process at the subsequent time step. The responses of the vehicle

obtained under a constant steer input revealed oscillating directional response about the steady-state value obtained from the quasi-static model.

Rumold (2001) also developed a coupled fluid-multibody dynamics model to investigate braking characteristics of a partially filled square cross-section tank vehicle based on two-dimensional analysis. For this purpose, a modular approach was proposed to simulate the coupled liquid slosh model based on the Navier-stokes equations and the multi-body vehicle model. The entire tank vehicle was modeled as a multi-body system comprising two subsystems; the tank vehicle without the fluid cargo and the fluid cargo within the tank. The two components were represented by a rigid body vehicle model and a fluid sloshing model, which was implemented in the software code UG (Bastian *et al.*, 1997). The coupled system responses were obtained through data exchange between the two subsystem models at specific time steps. Rumold (2001) formulated the Navier-Stokes equations in a reference frame fixed to the container assuming no-slip boundary condition on the tank walls and derived an equation for the external force acting on the fluid. Adoption of the non-inertial reference frame gives the opportunity to avoid the treatment of complicated boundary conditions on moving walls. Rumold (2001) used a simple vehicle model with three degrees-of-freedom (DOF) including translation of the car body and rotations of the front and rear axles to simulate longitudinal dynamics of a small straight truck subjected to constant braking torque. The suspension forces were not was not considered, while the tangential tire forces were related to normal forces using the magic tire formula suggested by Pacejka and Bakker (1993). Based on the modular simulation of the two subsystems, Rumold (2001) considered the slosh forces and moments as the input to the rigid body subsystems. In the similar manner, the translational and rotational accelerations along with rotational velocity responses of the rigid body subsystem served as inputs to the fluid subsystem. The vehicle model revealed that an increase in the brake torque resulted in lower mean and amplitude of the oscillatory vehicle acceleration but higher mean and amplitude of the sloshing force. Furthermore, a comparison of the rear tire normal loads of the liquid and equivalent rigid cargo vehicles revealed that liquid slosh contributes to decrease in the rear tires normal loads, which can result in rear wheel lock-up and a loss of vehicle controllability.

Thomassy *et al.* (2003) developed a methodology for simulation of the coupled vehicle dynamics and fluid slosh. For this purpose, a master program, called Glue Code, was developed for managing data transfer between two separate codes; FLOW-3D and MSC.ADAMS, which

simulated independently liquid sloshing and vehicle dynamics. In order to verify the suggested methodology, a small-scale tank mounted on a rigid frame supported by three multi-axis load cells was simulated in MSC.ADAMS software. Simulations of fluid motion within the tank under different maneuvers, including lane change and going over symmetric/asymmetric bumps, were performed in FLOW-3D software. Biglarbegian and Zu (2006) also solved the coupled fluid and vehicle model for a tractor–semitrailer carrying liquid cargo under constant braking torques. Similar to the simulations performed by Rumold (2001), the vehicle model was used to obtain kinematic parameters (angular velocity and acceleration, linear acceleration, and transformation matrices) at each instant, which served as inputs to the liquid slosh model to obtain sloshing forces and moments at a successive instant. A three-DOF (translational, roll, and pitch motion) tractor–semitrailer model with linear suspension was developed to study the liquid sloshing under constant braking torques. The magic tyre formula (Pacejka and Bakker, 1993) was used to obtain longitudinal tire forces. The study revealed that vehicles carrying liquid cargo need considerably greater braking torque compared to the equivalent rigid cargo vehicles to achieve comparable stopping distance.

Wasfy *et al.* (2008) used commercial finite element code DIS developed by Advanced Science and Automation Corp. (2007) to numerically simulate transient response of a heavy vehicle carrying an oval tank with a single orifice baffle under typical maneuvers (turning and lane-change), while traversing a terrain with symmetric or asymmetric bumps. The fluid motion in the partially-filled container was modeled using the Arbitrary Lagrangian-Eulerian (ALE) description of the full Navier-Stokes equations assuming turbulent flows and free-slip boundary condition at the walls. A multi-body model of a heavy tank truck was developed using rigid bodies, flexible bodies, joints and actuators. The computational model was validated through laboratory experiments performed under vertical displacements at the rear axle of the trailer. A similar approach was also used by Wasfy *et al.* (2007) to perform a coupled simulations of a partially-filled small scale tank with oval cross section and equipped with a pair of partial longitudinal and transverse baffles.

Yan and Rakheja (2009) used a coupled fluid-multibody dynamics method to investigate straight-line braking performance of a partially filled tank truck with and without the baffles. The entire tank vehicle was modeled using the multi-body system (MBS) approach. Similar to Rumold (2001), Yan and Rakheja (2009) used the modular simulation of the two subsystems; the

tank vehicle without the fluid cargo and the fluid cargo within the tank. They suggested a three-dimensional liquid sloshing model for a tank geometry, referred to as 'Reuleaux triangle' (Kang, 2001), assuming laminar incompressible flow and no-slip boundary condition on the tank walls, which was implemented into the FLUENT software. The vehicle model was a two-dimensional pitch-plane model with seven-DOF (longitudinal, vertical and pitch motions of the sprung mass, vertical motions of two unsprung masses, and angular motions of the wheels) assuming linear stiffness and damping for the suspension system in addition to a tire model referred to as magic tyre formula (Pacejka and Bakker, 1993) was applied. Similar to the previously mentioned studies, fluid slosh model was solved considering instantaneous vehicle response as the external acceleration imposed on the fluid. Consequently, the resulting transient slosh forces and moments were applied to the vehicle model at the subsequent instant (Fig. 1.4). The process was continued until the vehicle forward velocity diminished. The study evaluated responses to time-varying braking torques using a ramp-step change in the brake treadle pressure, such that wheel lock-up does not occur. The validity of the model was examined by comparison of the slosh natural frequency as well as the slosh forces and moments predicted by the model with those measured from the experiments performed on a scaled tank with different fill levels (30%, 50% and 70%), and with and without baffles under different excitations (Yan, 2008). The transient and steady-state sloshing forces and moments obtained from the simulation model revealed good agreements with the experimental data.

Fleissner *et al.* (2009, 2010) coupled three-dimensional liquid/granulates sloshing model by a transport vehicle model with 17 degrees of freedom. The motion of fluid within the container was simulated by SPH method, which was applied through PASIMODO code developed at the University of Stuttgar, while the tank truck was modeled using the SIMPAC software. Coupled simulations of these two codes were performed through a MATLAB/SIMULINK program. The stability of tank trucks was investigated under different driving maneuvers including braking and a double lane change maneuver. The study considered a cubic tank with one and two compartments as well as a cylindrical tank with three compartments to demonstrate the positive effect of dividing the tank into compartments on the braking stability.

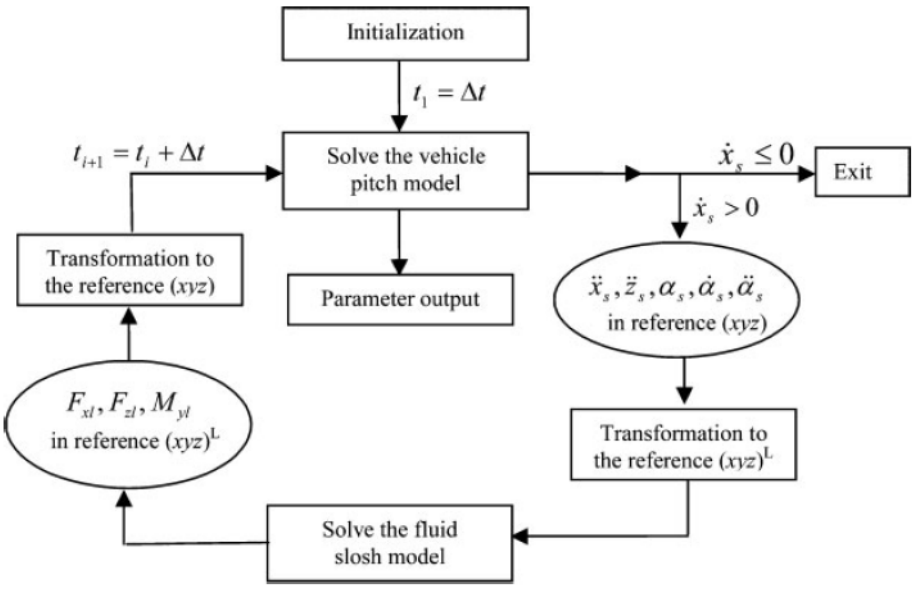

Fig. 1.4. Simulation algorithm employed for analysis of the coupled fluid slosh and vehicle models (Yan and Rakheja, 2009).

1.3 Scope and Objectives of the Dissertation Research

From the review of the literature conducted on directional dynamics of road tank vehicles, it became apparent that analyses of coupled simulation of liquid sloshing and vehicle dynamics have been mostly limited to the quasi-static method, which only accounts for the mean steady-state load shift due to change in position of liquid cargo center of mass. Moreover, this method is not applicable for the analysis of liquid cargo movement within the baffled tanks. Although transient behaviour of liquid sloshing in partially filled containers has been explored in many studies, interactions between the transient motion of liquid and dynamics of the vehicle have been reported in a few studies using CFD fluid slosh models. A few studies have also reported coupled transient liquid sloshing and vehicle dynamics using the equivalent mechanical method, which required prior estimations of model parameters from the CFD simulation results or analytical solutions. The lack of coupled fluid-vehicle studies is mostly attributed to the computational demands of the CFD fluid slosh models in addition to elaborate data transfers between the fluid and the vehicle models. It should also be noted that such CFD simulations are carried out using commercial software codes, which are generally not intended for communication with the open-source codes. Furthermore, in spite of significantly lower rollover

stability of tank trucks, the reported studies have been limited only to static stability analysis, which consider only steady state position of liquid center of mass. While many studies reported a lower dynamic rollover threshold limits of conventional rigid cargo vehicles compared to the static rollover threshold, the transient motion of liquid cargo within the tank is expected to yield even lower dynamic rollover threshold of tank vehicles, which has not yet been reported. The primary objective of the dissertation research is thus formulated to develop efficient fluid slosh models using analytical approaches for efficient analysis of the coupled fluid-vehicle system. The specific goals of the dissertation study are:

- Formulate analytical-based models of two-dimensional transient slosh in partially-filled clean-bore and baffled tanks considering different tank cross-sections using linear slosh theory.
- Develop an analytical-based model of three-dimensional linear slosh in horizontal cylindrical containers.
- Formulate the forces and moments due to the transient linear sloshing for direct integration into the multibody vehicle equations.
- Examine validity of the models using available experimental data and analytical benchmark solutions, and determine the range of applicability of the linear slosh theory for predicting transient slosh in liquid transporting vehicles.
- Investigate roll stability limits of a tank vehicle in the presence of transient cargo slosh as functions of various vehicle operating parameters.

1.4 Organization of the Dissertation-Manuscript Based Format

This "Manuscript-based" dissertation is prepared as per requirements defined in “Thesis Preparation and Thesis Examination Regulation” booklet of the School of graduate Studies at Concordia University. The dissertation is organized into six chapters. Four of these chapters present two published peer-reviewed journal papers and two papers submitted to different journals for peer review, while the content of the chapters are interrelated according to the aforementioned thesis regulation in order to ensure that the thesis is coherent. Some repetitions in the analytical formulations, however, are evident. The first chapter summarizes a comprehensive literature review including the review of accident reports of tank trucks, tank

design standards and different analysis methods of liquid slosh in moving containers. The scope and objectives of the dissertation research is also presented in the first chapter based on the reviewed studies.

Chapter 2 presents the following paper published in the Journal of Sound and Vibration:

Kolaei, A., Rakheja, S. and Richard, M. J. (2014), Range of applicability of the linear fluid slosh theory for predicting transient lateral slosh and roll stability of tank vehicles, *Journal of Sound and Vibration*, Vol. 333, pp. 263–282.

The paper develops an analytical model to study the transient lateral sloshing in horizontal cylindrical containers assuming inviscid, incompressible and irrotational flows. The model is derived by implementing the linearized free-surface boundary condition and bipolar coordinate transformation, resulting in a truncated system of linear ordinary differential equations, which is numerically solved to determine the fluid velocity potentials followed by the hydrodynamic forces and moment. The model results are compared with those obtained from the multimodal solution. The free-surface elevation and hydrodynamic coefficients are also compared with the reported experimental and analytical data as well as numerical simulations to establish validity of the model. The capability of the model for predicting non-resonant slosh is also evaluated using the critical free-surface amplitude. The model validity is further illustrated by comparing the transient liquid slosh responses of a partially filled tank subject to steady lateral acceleration characterizing a vehicle turning maneuver with those obtained from fully nonlinear CFD simulations and pendulum models. The slosh model is subsequently applied to the roll plane model of a suspended tank vehicle to study the effect of dynamic liquid slosh on steady-turning roll stability limit of the vehicle under constant and variable axle load conditions. The ranges of applicability of the linear slosh theory are finally identified considering the range of excitation and fill levels that are encountered in liquid cargo vehicles.

Chapter 3 presents the following paper published in the European Journal of Mechanics B/Fluids:

Kolaei, A., Rakheja, S. and Richard, M. J. (2014), Effects of tank cross-section on dynamic fluid slosh loads and roll stability of a partly-filled tank truck, *European Journal of Mechanics B/Fluids*, Vol. 46, pp. 46–58.

The paper introduces an analytical model of a partly-filled clean-bore tank of arbitrary cross-section for predicting transient lateral slosh force and overturning moment using the linear slosh theory. Slosh frequencies and mode shapes are initially estimated using the variational method, which is applied to the linearized free-surface boundary condition. The resulting truncated system of linear ordinary differential equations is subsequently solved numerically to determine the fluid velocity potentials followed by hydrodynamic force and moment. The validity of the model is examined through comparisons with available analytical solutions and experimental data. The slosh force and roll moment are obtained for four different tank cross-sections, namely, circular, elliptical, modified-oval and Reuleaux-triangle. The slosh model is subsequently integrated to a roll plane model of an articulated tank-semitrailer vehicle to study the effect of dynamic liquid slosh as well as the tank cross-section on the steady-turning roll stability limit of the vehicle under constant and variable cargo load conditions. It is shown that the proposed analytical method is far more efficient and could be easily integrated to the multibody dynamic vehicle models.

Chapter 4 presents the following paper submitted to Computers and Fluids:

Kolaei, A., Rakheja, S. and Richard, M. J., A coupled multimodal and boundary-element method for analysis of antislosh effectiveness of partial baffles in a partly-filled container, *submitted to Computers and Fluids*, Dec. 2013.

The paper analyzes transient lateral slosh in a partially-filled cylindrical tank with different designs of longitudinal partial baffles using a coupled multimodal and boundary-element method. A boundary element method is initially formulated to solve the eigenvalue problem of free liquid slosh, assuming inviscid, incompressible and irrotational flows. Significant improvement in computational time is achieved by reducing the generalized eigenvalue problem to a standard one involving only the velocity potentials on the half free-surface length. The resulting natural slosh frequencies and modes are subsequently implemented in a linear multimodal method to obtain generalized coordinates of the free-surface under a lateral acceleration excitation. Damping due to baffles, estimated from the energy dissipated per cycle, is also implemented into the multimodal equation. The validity of the model is illustrated through comparisons with available analytical solutions. The results are presented for the tank with bottom-mounted, top-mounted and center-mounted partial baffles of different lengths. The

effects of baffle design and length on the natural slosh frequencies/modes, damping ratios and hydrodynamic coefficients are further investigated. The lateral force and overturning moment due to liquid motion within the container are derived in terms of generalized coordinates and the natural slosh modes.

Chapter 5 presents the following paper submitted to the Journal of Sound and Vibration:

Kolaei, A., Rakheja, S. and Richard, M. J., Three-dimensional dynamic liquid slosh in partially-filled horizontal tanks subject to simultaneous longitudinal and lateral excitations, *submitted to Journal of Sound and Vibration*, July 2014.

The paper presents the analysis of three-dimensional liquid slosh in a horizontal cylindrical tank subject to longitudinal and lateral accelerations simultaneously, idealizing braking-in-a turn maneuver, assuming inviscid, incompressible and irrotational flows. The spectral problem of liquid slosh in the partially-filled horizontal tank of arbitrary cross-section and finite length is initially formulated using higher order boundary element method. Using the separation of variables, three-dimensional Laplace equation is reduced to a two-dimensional Helmholtz equation, which significantly reduces the computational cost. A further improvement in computational time is achieved by reducing the generalized eigenvalue problem to a standard one considering only the velocity potential on the half free-surface length. The generalized coordinates of the free-surface oscillations are subsequently obtained by implementing the natural slosh frequencies and modes in a linear multimodal method. Damping due to the liquid viscosity in the boundary layer is also calculated and implemented in the multimodal analysis. The results are only presented for a tank of circular cross-section. The slosh force and moment are formulated in terms of the generalized coordinates and hydrodynamic coefficients. The validity of the model is also illustrated using available analytical solutions and experimental data. Furthermore, the range of applicability of the linear theory for predicting three-dimensional transient slosh is examined by comparing the results with CFD simulations results, which are obtained using the commercial software (FLUENT).

Chapter 6 summarizes the major conclusions of the dissertation research together with a few recommendations and suggestions for future studies in the field.

CHAPTER 2

RANGE OF APPLICABILITY OF THE LINEAR FLUID SLOSH THEORY FOR PREDICTING TRANSIENT LATERAL SLOSH AND ROLL STABILITY OF TANK VEHICLES

2.1 Introduction

Liquid-transporting vehicles are known to constitute higher safety risks due to their low stability characteristics, primarily attributed to high center of mass and interactions of the sloshing cargo with the vehicle. Fluid sloshing in partially filled tanks has been associated with a large number of tank truck accidents, which pose unreasonable risks to the road safety, particularly when hazardous products (hazmat) are involved. Hazmat release occurred in 86% of the rollover accidents involving tank trucks, and 50% of such accidents resulted in fires and explosions (Pape *et al.*, 2007; Woodrooffe *et al.*, 2000). Based on a U.S. Department of Transportation report (U.S. DOT, 2008), 31% of the fatalities associated with rollovers of commercial truck vehicles occurred with tank trucks. Although the number of rollovers account for less than 1% of the total tank trucks fleet in the US (Pape *et al.*, 2007), the associated fatalities and economic losses are considered to be most unreasonable. The destabilizing effects of liquid sloshing also influence the dynamic performance of railway tank cars, ship tankers and aerospace vehicles in a highly adverse manner (Bauer, 1964, 1972). Safety and structural performance of ground and elevated storage tanks under seismic excitations are also significantly affected by the liquid sloshing (Fischer and Rammerstorfer, 1999). These suggest that dynamic liquid sloshing must be considered and accurately modeled in applications involving free-surface flows.

The basic problem of liquid sloshing involves evaluations of sloshing forces and moments as well as natural frequencies of the free liquid surface, which are known to affect the dynamics of the vehicle system. Fundamentally, these depend on a number of design and operating parameters such as liquid-fill depth, liquid properties, tank geometry, nature of excitation and anti-sloshing devices, if present. Fluid slosh in moving containers has been widely investigated using different methods. The study of interactions between the sloshing liquid and

the vehicle system, however, has been mostly limited to the steady-state and mechanical analogy models of the liquid cargo. Quasi-static fluid slosh models have been widely used to predict steady-state position of the liquid free-surface, and the effects on roll stability and directional response characteristics of the vehicles (e.g. Sankar *et al.*, 1986; Rakheja *et al.*, 1988). These have suggested lower rollover threshold accelerations of partially filled tank vehicles compared to the equivalent rigid cargo vehicles.

Alternatively, the liquid slosh in moving containers has been analyzed using mechanical analogous models of the sloshing cargo. The applications of such models, however, necessitate prior estimations of the model parameters, which have been evaluated analytically (Ranganathan *et al.*, 1993b), and through CFD simulations (Salem, 2000) and experimentation (Ibrahim, 1999). The applications of such models in analyses of coupled liquid cargo-vehicle system have been limited due to complexities associated with identification of model parameters.

Although the quasi-static method permits efficient analyses of steady-state load shift and directional responses of the tank trucks, the effect of transient liquid slosh is entirely neglected. A number of studies have investigated dynamic fluid slosh in partly-filled tanks subject to longitudinal and/or lateral accelerations using CFD methods (e.g., Yan *et al.*, 2005; Modaressi-Tehrani *et al.*, 2006). These have invariably shown significant transient slosh under applied acceleration inputs, and that peak slosh forces and moments are substantially greater than those predicted from a quasi-static model, suggesting only limited validity of the quasi-static method under transient maneuvers or high amplitude excitations. The implementations of CFD fluid slosh models in vehicle dynamics simulations have also been limited due to excessive computational demands. Yan and Rakheja (2009), Biglarbegian and Zu (2006) and Thomassy *et al.* (2003) have investigated braking and steering responses of partly filled tank trucks by integrating the CFD fluid slosh model to the vehicle dynamic model. These involved highly inefficient and elaborate data transfers between the vehicle and the fluid slosh models.

Alternatively, linear liquid slosh models offer promising potential for efficient analyses of coupled liquid cargo-vehicle system dynamics. The general equations of motion of the fluid within a rigid container can be simplified assuming an ideal liquid with negligible viscosity effect, and incompressible and irrotational flows. Modaressi-Tehrani *et al.* (2006) has shown negligible viscosity effects on transient slosh forces and moments for a range of liquid cargo

products. Under these conditions, the Navier-Stokes equations can be reduced to potential flow equations. Ibrahim (2005) suggested that exact solutions of potential flow equations are limited to linear liquid sloshing within regular tank geometries with straight walls such as rectangular and upright-cylindrical containers. Conformal mapping technique has been employed for analysis of the linear slosh in other tank geometries, where the original tank geometry is transformed into a regular geometry in which the Laplace equation together with the wall and free surface boundary conditions are solved explicitly. Budiansky (1960) and McIver (1989) used this method to solve the potential flow equation for free liquid sloshing in two-dimensional cylindrical and spherical containers and reported the natural slosh frequencies in terms of the liquid fill level. Hasheminejad and Mohammadi (2011) employed the conformal mapping technique to study the effect of anti-sloshing devices on the two-dimensional free liquid oscillations in horizontal cylindrical containers. The study suggested that a long pair of surface-touching horizontal side baffles have considerable effect on natural slosh frequencies, while the bottom mounted vertical baffles were not effective in limiting the slosh. Similar findings were also reported in Hasheminejad and Aghabeigi (2009, 2012) for half-full elliptical tanks with same baffle configurations. Two-dimensional liquid slosh in half-full horizontal cylindrical vessels subjected to transverse excitations was also investigated by Papaspyrou *et al.* (2004a) using an analytical approach.

Among all the methods employed for simulation of fluid slosh, analytical models seem to be attractive due to the simplicity associated with their integration to the multibody vehicle dynamic models. Only a few studies, however, have reported analytical solutions for transient liquid sloshing in tanks with curved walls, which have been mostly limited to half-filled tanks (Papaspyrou *et al.*, 2004a; Hasheminejad and Aghabeigi, 2009, 2011, 2012). Problem of transient lateral sloshing in horizontal cylindrical containers with arbitrary fill ratios is only addressed using the variational method. Faltinsen & Timokha (2010) suggested a multimodal model for analysis of transient lateral slosh based on a modified Trefftz variational method considering a special set of harmonic functions. Patkas & Karamanos (2007) solved the flow field equations using the variational method based on the Galerkin discretization of the potential function. The applicability of the analytical fluid slosh models in directional analysis of partly filled tank-trucks with varying fill height and curved cross-sections have thus met limited success.

In the present study, the transient liquid slosh in horizontal cylindrical containers subjected to a lateral acceleration excitation is studied using an efficient analytical model based on the linear slosh theory. The validity of the developed model is examined using the available measured data and the results obtained from the analytical and numerical simulations. The range of validity of the linear slosh theory is also investigated considering high amplitude liquid slosh under excitations in the vicinity of the fundamental slosh frequency. Slosh forces and moments developed during turning maneuvers are further analyzed and compared to those obtained from the CFD and pendulum analogy models to demonstrate the overall effectiveness of the present model for simulation of transient liquid slosh in tank trucks. The model is subsequently applied to a simple roll plane model of a partly-filled tank truck to investigate its steady-turning roll stability in the presence of transient fluid slosh.

2.2 Formulations

2.2.1 Basic governing equations of fluid motion

Two-dimensional motion of an ideal liquid in a circular tank is formulated in this section. Geometrical representation of the problem is shown in Fig. 2.1a, where a circular tank with radius R and liquid fill height h is subjected to a lateral motion. The Cartesian coordinate system Oyz with origin at the midpoint of the free-surface of length $2a$ is used with the z-axis directed downwards and y-axis in the plane of the undisturbed free-surface. The liquid fill-level h is measured with respect to the tank bottom 'B', as shown in the figure. The general equations of motion for an ideal fluid in a rigid container with negligible viscosity effect, and incompressible and irrotational flows, can be expressed in the form of Laplace equation of the velocity potential function Φ, i.e.:

$$\nabla^2\Phi = 0 \tag{2.1}$$

The linearized free-surface boundary condition, which has been presented in many reported studies (Abramson, 1966; Ibrahim, 2005; Faltinsen and Timokha, 2009), can be expressed as:

$$\frac{\partial^2\Phi}{\partial t^2} - g\frac{\partial\Phi}{\partial z} = 0; \qquad z = 0 \tag{2.2}$$

The above equation represents the combined dynamic and kinematic boundary conditions at the free-surface based on Euler equation and irrotationality condition, where g is acceleration due to

gravity. Considering negligible effects of viscosity and shear stress on the walls, the free-slip boundary condition on the tank walls yields that the flow velocity perpendicular to the wall is equal to the normal velocity of the wall such that:

$$\boldsymbol{n} \cdot \boldsymbol{\nabla}\Phi = U_n \tag{2.3}$$

where $\boldsymbol{n}$ is the unit normal vector to the wall and U_n is the normal velocity of the tank wall.

The above linear boundary value problem, Eqs. (2.1) to (2.3), is solved considering two components of the velocity potential: the potential Φ_{R} representing rigid body motion of the fluid, which is same as the potential of the container motion; and the potential Φ_{S} representing liquid motion relative to the container, which is potential of the sloshing fluid. The liquid sloshing problem under a lateral excitation can thus be reduced to the following set of equations:

$$\boldsymbol{\nabla}^2\Phi_{\mathrm{S}} = 0 \tag{2.4}$$

$$\frac{\partial^2\Phi_{\mathrm{S}}}{\partial t^2} - g\frac{\partial\Phi_{\mathrm{S}}}{\partial z} = -\ddot{Y}\mathrm{y}; \qquad \mathrm{z} = 0 \tag{2.5}$$

$$\boldsymbol{n} \cdot \boldsymbol{\nabla}\Phi_{\mathrm{S}} = 0 \tag{2.6}$$

$$\frac{\partial\Phi_{\mathrm{R}}}{\partial y} = \dot{Y} \tag{2.7}$$

where $\dot{Y}$ and $\ddot{Y}$ are the lateral velocity and time derivative of the lateral acceleration excitation, respectively.

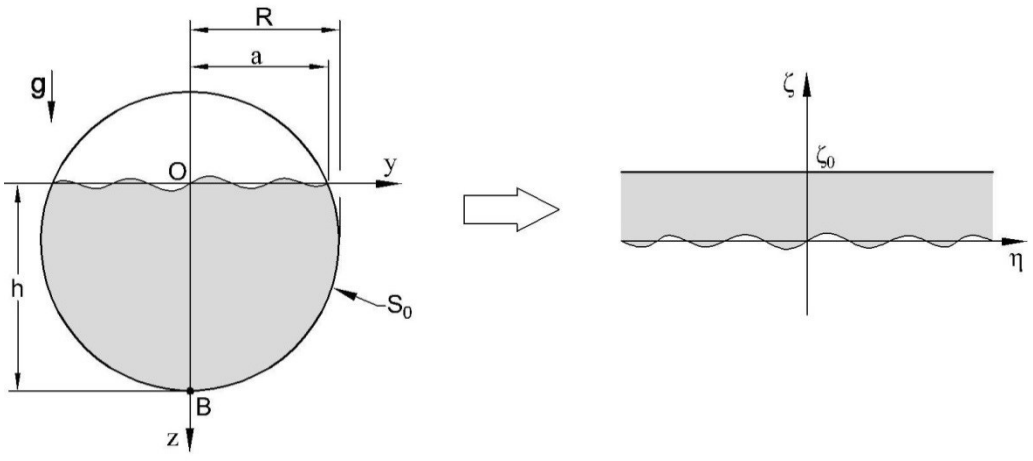

(a) (b)

Fig. 2.1. (a) Two-dimensional fluid motion in a circular cross-section tank. (b) Transformed fluid domain.

2.2.2 Bipolar coordinate transformation

The Laplace equation (2.4) together with the boundary conditions (2.5) and (2.6), associated with the problem illustrated in Fig. 2.1a, may be solved using the bipolar coordinates to transform the fluid domain in the partially-filled circular tank into a semi-infinite strip (Fig. 2.1b). The advantage of using bipolar coordinates for describing the potential fluid field is that the governing Laplace equation can be solved using the method of separation of variables. A system of ordinary differential equations is subsequently obtained from the transformed free-surface boundary condition. Numerical solutions of the system of differential equations yield the potential function Φ_S. The hydrodynamic pressure distribution on the container, and the sloshing forces and moments are subsequently obtained from both the liquid slosh and rigid body potentials. The mathematical formulation of linear liquid slosh in a partly filled circular tank based on the bipolar coordinate transformation of the fluid domain is described below.

The relationship between two-dimensional Cartesian and bipolar coordinates can be described through a complex function (Ibrahim, 2005):

$$y + iz = a \tanh\left(\frac{\eta + i\zeta}{2}\right) \tag{2.8}$$

where y and z can be expressed in terms of transformed coordinates η and ζ (Fig. 2.1) as:

$$\frac{y}{a} = \frac{\sinh \eta}{\cosh \eta + \cos \zeta} \quad , \qquad \frac{z}{a} = \frac{\sin \zeta}{\cosh \eta + \cos \zeta} \tag{2.9}$$

The wetted cylinder surface is transformed to the horizontal line $\zeta = \zeta_0$, where ζ_0 is related to the cylinder radius and fill level, as:

$$\cos \zeta_0 = 1 - \frac{h}{R} \tag{2.10}$$

The intersection of the free-surface with the tank occurs at $\eta = \pm\infty$ and the free-surface coincides with $\zeta = 0$. The transformed Laplace equation and boundary conditions are subsequently given by:

$$\frac{\partial^2 \Phi_S}{\partial \zeta^2} + \frac{\partial^2 \Phi_S}{\partial \eta^2} = 0; \quad -\infty < \eta < +\infty \, , 0 < \zeta < \zeta_0 \tag{2.11}$$

$$\frac{\partial \Phi_S}{\partial \zeta} = 0; \qquad \zeta = \zeta_0 \tag{2.12}$$

$$\frac{\partial^2 \Phi_S}{\partial t^2} - \frac{g}{a}(1+\cosh\eta)\frac{\partial \Phi_S}{\partial \zeta} = -\ddot{Y}\frac{a\sinh\eta}{1+\cosh\eta}; \qquad \zeta = 0 \tag{2.13}$$

Using the method of separation of variables, it can be shown that the anti-symmetric solution of Eq. (2.11) satisfying the boundary condition (2.12) can be written as:

$$\Phi_S = \int_0^\infty \varphi(t,\tau)\frac{\cosh[\tau(\zeta-\zeta_0)]}{\cosh(\tau\zeta_0)}\sin(\tau\eta)d\tau \tag{2.14}$$

Substituting for Φ_S from Eq. (2.14) into the free-surface boundary condition (2.13) yields:

$$\frac{a}{1+\cosh\eta}\int_0^\infty \ddot{\varphi}(t,\tau)\sin(\tau\eta)d\tau + g\int_0^\infty \varphi(t,\tau)\,\tau\tanh(\tau\zeta_0)\sin(\tau\eta)d\tau = -\ddot{Y}f(\eta) \tag{2.15}$$

in which

$$f(\eta) = \frac{a^2\sinh\eta}{(1+\cosh\eta)^2} \tag{2.16}$$

The Fourier sine transform of both sides of the integral equation (2.15) with respect to the variable η yields:

$$a\int_0^\infty \ddot{\varphi}(t,\tau)T(\tau,\tau')d\tau + g\varphi(t,\tau')\tau'\tanh\left(\tau'^{\zeta_0}\right) = -\ddot{Y}\frac{2a^2\tau'^2}{\sinh(\pi\tau')} \tag{2.17}$$

where

$$T(\tau,\tau') = \frac{\tau-\tau'}{\sinh\pi(\tau-\tau')} - \frac{\tau+\tau'}{\sinh\pi(\tau+\tau')} \tag{2.18}$$

and τ' is the Fourier variable. The integral in Eq. (2.17) can readily be expressed into summation using the N-point Gauss-Laguerre quadrature formula (Abramowitz and Stegun, 1972), where the integral of a function $\mathrm{g}(x)$ is expressed by the weighted summation in the following manner:

$$\int_0^\infty \mathrm{g}(x)dx \approx \sum_{i=1}^{N} w_i e^{4\pi x_i}\,\mathrm{g}(x_i) \tag{2.19}$$

in which x_i and w_i $(i = 1,2,\ldots N)$ are scaled abscissas (zeros of Laguerre polynomials) and weighting coefficients, respectively; N is the truncation size and 4π is a scaling factor used to facilitate the convergence rate. Eq. (2.17) is subsequently expressed in the matrix form, as:

$$[\mathbf{M}]\{\ddot{\boldsymbol{\varphi}}\} + [\mathbf{K}]\{\boldsymbol{\varphi}\} = -\ddot{Y}\{\boldsymbol{\psi}\} \tag{2.20}$$

where $\{\ddot{\boldsymbol{\varphi}}\}$ and $\{\boldsymbol{\varphi}\}$ are unknown vectors with components $\ddot{\varphi}(t,\tau_i)$ and $\varphi(t,\tau_i)$, respectively, $[\mathbf{M}]$ is a $N \times N$ square matrix and $[\mathbf{K}]$ is a $N \times N$ diagonal matrix with elements given by:

$$M_{ji} = aw_i e^{4\pi\tau_i}T(\tau_i,\tau_j) \tag{2.21}$$

$$K_{jj} = g\tau_j \tanh(\tau_j \zeta_0) \tag{2.22}$$

where $i, j = 1,2, \ldots N$. In the above formulation, the matrices $[\mathbf{M}]$ and $[\mathbf{K}]$ may be considered as mass and stiffness of the system, and $\{\boldsymbol{\psi}\}$ as the vector representing contributions of the external excitation to a specific mode. The elements of vector $\{\boldsymbol{\psi}\}$ can be expressed as:

$$\psi_j = \frac{2a^2 {\tau_j}^2}{\sinh(\pi\tau_j)} \tag{2.23}$$

Although a few studies have shown negligible effect of viscosity on the resulting slosh forces and moments (e.g., Modaressi-Tehrani *et al.*, 2006), consideration of the viscosity effect is important for achieving a steady solution. The linear theory, however, does not account for the liquid viscosity, since it is based on the potential flow assumption. Faltinsen and Timokha (2009) suggested the use of a viscous damping term in the differential equations derived from the free-surface boundary condition such that:

$$[\mathbf{M}]\{\ddot{\boldsymbol{\varphi}}\} + [\mathbf{C}]\{\dot{\boldsymbol{\varphi}}\} + [\mathbf{K}]\{\boldsymbol{\varphi}\} = -\ddot{Y}\{\boldsymbol{\psi}\} \tag{2.24}$$

where $[\mathbf{C}]$ is a square damping matrix representing the energy dissipation in the fluid boundary layer. Papaspyrou *et al.* (2004a) further suggested that the damping matrix $[\mathbf{C}]$ can be expressed in the form of a Rayleigh damping matrix, as $[\mathbf{C}] = \alpha[\mathbf{M}]$, where α is a coefficient depending on the fill condition, tank diameter and the liquid kinematic viscosity. The coefficient α can be estimated from $\alpha = 2\xi_1\sigma_1$, in which ξ_1 is the damping ratio corresponding to the fundamental slosh mode and σ_1 is the fundamental slosh frequency. The damping ratio for an arbitrary-shaped container can be estimated from the following empirical relationship (Ibrahim, 2005):

$$\xi_1 = C_1 \sqrt{\frac{\nu}{g^{1/2}(2a)^{3/2}}} \tag{2.25}$$

where ν is the fluid kinematic viscosity, $2a$ is the length of the free-surface in static condition (Fig. 2.1a) and C_1 is a coefficient that depends on the tank geometry and fill condition. Although a value of C_1 close to 1 has been suggested in the absence of specific information, $C_1 = \frac{0.8}{(\sigma_1^2 R/g)^{0.5}}$ is used in the present study to account for variation in ξ_1 with the fill ratio. Using Keulegan theory, Faltinsen and Timokha (2010) derived damping ratios corresponding to different slosh modes. For typical fluids involved in bulk transportation, the damping is generally very low. Identical damping ratio ξ_1 is thus assumed for different modes, which provided values

comparable to those computed from the hydrodynamic coefficients presented in Faltinsen and Timokha (2010).

The system of linear ordinary differential equations (2.24) is solved using the Laplace transform so as to obtain the transform of $\dot{\varphi}(t,\tau)$, as:

$$\{\mathcal{L}[\dot{\varphi}(t,\tau)]\} = \{\bar{\varphi}(s,\tau)\} = -s^2\mathcal{L}[\ddot{Y}](s^2[\mathbf{M}] + \mathrm{s}[\mathbf{C}] + [\mathbf{K}])^{-1}\{\boldsymbol{\psi}\} \tag{2.26}$$

Numerical inversion of the Laplace transform based on the Fourier series (Crump, 1976) is then used to calculate the $\dot{\varphi}(t,\tau)$ in the interval $[0,2T_0]$:

$$\dot{\varphi}(t,\tau) = \frac{e^{ct}}{T_0}\left[\frac{1}{2}\mathrm{Re}\{\bar{\varphi}(c,\tau)\} + \sum_{k=1}^{\bar{N}}\left(\mathrm{Re}\left\{\bar{\varphi}(c+\frac{k\pi i}{T_0},\tau)\right\}\cos\left(\frac{k\pi t}{T_0}\right) - \mathrm{Im}\left\{\bar{\varphi}(c+\frac{k\pi i}{T_0},\tau)\right\}\sin\left(\frac{k\pi t}{T_0}\right)\right)\right] \tag{2.27}$$

The free parameter *c* in the above solution is determined based on the desired accuracy such that (Crump, 1976):

$$c = \beta - \frac{Ln(E)}{2T_0} \tag{2.28}$$

where β is a number slightly larger than the real part of the greatest pole of $\bar{\varphi}(s,\tau)$ and *E* is the relative error.

2.2.3 Free-surface elevation, hydrodynamic pressure, and slosh force and moment

The free-surface elevation can be obtained from the dynamic boundary condition on the free-surface in the form:

$$\delta(y,t) = -\frac{1}{g}\frac{\partial(\Phi_{\mathrm{R}} + \Phi_{\mathrm{S}})}{\partial t}; \quad z = 0 \tag{2.29}$$

where $\delta = \delta(y,t)$ is the free-surface elevation. Substituting for Φ_{R} and Φ_{S} from Eqs. (2.7) and (2.14) into Eq. (2.29) yields following equation for the free-surface elevation in the transformed domain:

$$\delta(\eta,t) = -\frac{1}{g}\left(\ddot{Y}y(0,\eta) + \int_0^{\infty}\dot{\varphi}(t,\tau)\sin(\tau\eta)d\tau\right) \tag{2.30}$$

Replacing for $y(0,\eta)$ from the bipolar representation (2.9), and making use of the N-point Gauss-Laguerre quadrature formula (2.19) for evaluating the integral term in the above equation, yields:

$$\delta(\eta,t) = -\frac{1}{g}\left(\ddot{Y}\frac{a\sinh\eta}{\cosh\eta+1} + \sum_{i=1}^{N} w_i e^{4\pi\tau_i}\dot{\varphi}(t,\tau_i)\sin(\tau_i\eta)\right) \tag{2.31}$$

The hydrodynamic pressure distribution, $P(\eta,\zeta_0,t)$, on the container wall is derived upon substituting for Φ_S from integral expression (2.14) into $\Phi = \Phi_R + \Phi_S$ and using the linearized Bernoulli's equation (Abramson, 1966), such that:

$$P(\eta,\zeta_0,t) = -\rho\frac{\partial(\Phi_R+\Phi_S)}{\partial t} = -\rho\left\{\ddot{Y}y(\zeta_0,\eta) + \int_0^{\infty}\frac{\dot{\varphi}(t,\tau)\sin(\tau\eta)}{\cosh(\tau\zeta_0)}d\tau\right\} \tag{2.32}$$

where ρ is the liquid mass density. Substituting for $y(\zeta_0,\eta)$ from Eq. (2.9) and evaluating the integral using Gauss-Laguerre quadrature formula (2.19) leads to an expression for the hydrodynamic pressure distribution on the container wall, as:

$$P(\eta,\zeta_0,t) = -\rho\left\{\frac{a\ddot{Y}\sinh\eta}{\cosh\eta+\cos\zeta_0} + \sum_{i=1}^{N} w_i e^{4\pi\tau_i}\frac{\dot{\varphi}(t,\tau_i)\sin(\tau_i\eta)}{\cosh(\tau_i\zeta_0)}\right\} \tag{2.33}$$

The total lateral force, $F_y(t)$, acting on the container wall, per unit length of the container, is obtained from integration of the hydrodynamic pressure over the tank wetted area, S_0 (Fig. 2.1a), such that:

$$F_y(t) = \int_{S_0} P dz = F_R(t) + F_S(t) \tag{2.34}$$

where F_R and F_S are the components of the lateral force that could be associated with the rigid body and sloshing motions of the liquid, respectively, expressed as:

$$F_R(t) = -\rho\ddot{Y}\int_{S_0} y dz = -m\ddot{Y} \tag{2.35}$$

$$F_S(t) = -\rho\int_{S_0}\dot{\Phi}_S dz \tag{2.36}$$

in which m is the fluid mass per unit length of the tank. Using Green's second identity and noting that $\frac{\partial\dot{\Phi}_S}{\partial n}\Big|_{S_0} = 0$, the above integral can be transformed into an integral over the free-surface in the form:

$$F_S(t) = -\rho \int_{-a}^{a} y \frac{\partial \dot{\Phi}_S}{\partial z} dy\,; \qquad z = 0 \tag{2.37}$$

From bipolar representation (2.9) and the quadrature formula (2.19) it follows that:

$$F_S(t) = -2\rho a \sum_{i=1}^{N} \dot{\varphi}(t,\tau_i)\tau_i w_i e^{4\pi\tau_i} \tanh(\tau_i\zeta_0) \int_0^{\infty} \tanh\left(\frac{\eta}{2}\right) \sin(\tau_i\eta)\, d\eta \tag{2.38}$$

The integral in the above equation represents the Fourier sine transform of $\tanh\left(\frac{\eta}{2}\right)$. The explicit form of $F_S(t)$ in terms of the potential function coefficients $\dot{\varphi}(t,\tau_i)$ is thus expressed as:

$$F_S(t) = -2\rho a\pi \sum_{i=1}^{N} \frac{\dot{\varphi}(t,\tau_i)\tau_i w_i e^{4\pi\tau_i} \tanh(\tau_i\zeta_0)}{\sinh(\pi\tau_i)} \tag{2.39}$$

It should be noted that the vertical component of the net slosh force is zero due to geometric symmetry.

The overturning moment about the container bottom point "*B*", M_B, (Fig. 2.1a), per unit tank length, can be determined by integrating the moments resulting from the horizontal and vertical components of the hydrodynamic forces:

$$M_B(t) = \int_{S_0} P[y dy + (z-h)dz] \tag{2.40}$$

Substituting for the pressure from Eq. (2.32) into the above equation yields the total overturning moment that may be decomposed into three components attributed to the rigid body moment (M_R), dynamic fluid slosh (M_S) and moment due to the vertical forces (M_V):

$$M_B(t) = M_R(t) + M_V(t) + M_S(t) \tag{2.41}$$

After some manipulations, the components of the overturning moment can be expressed as:

$$M_R(t) = -\rho\ddot{Y} \int_{S_0} y(h-z)dz = -mR\left(1 - \frac{4\sin^3(\zeta_0)}{3(2\zeta_0 - \sin(2\zeta_0))}\right)\ddot{Y} \tag{2.42}$$

$$M_V(t) = -\rho\ddot{Y} \int_{S_0} y^2 dy = -\frac{2}{3}\rho a^3 \ddot{Y} \tag{2.43}$$

$$M_S(t) = -2\rho a\pi R \sum_{i=1}^{N} \frac{\dot{\varphi}(t,\tau_i)\tau_i w_i e^{4\pi\tau_i} \tanh(\tau_i\zeta_0)}{\sinh(\pi\tau_i)} \tag{2.44}$$

The expression within the parenthesis in Eq. (2.42) denotes the distance between the liquid mass center from the container bottom point '*B*' for a unit circle in terms of angle ζ_0, which can be obtained from Eq. (2.10). It is not difficult to show that M_V can be regarded as the overturning

moment caused by the lateral shift in the liquid mass center when the container is subjected to a constant lateral acceleration, encountered during steady-turning of the vehicle. The quasi-static overturning moment about 'B' may thus be calculated from Eqs. (2.42) and (2.43), as:

$$M_{B,qs} = M_R + M_V = -mRA_0 \tag{2.45}$$

where A_0 is the constant lateral acceleration magnitude imposed on the container. It can be shown that the quasi-static roll moment about a point below the tank bottom point, such as roll center of a tank vehicle, can also be computed directly from Eq. (2.35). The roll moment attributed to dynamic slosh is also obtained in a similar manner from the dynamic slosh component of the horizontal force from Eq. (2.39).

2.2.4 Rollover threshold analysis of a partly-filled tank truck

It is well known that the fluid slosh and directional dynamics of tank vehicles interact in a complex manner. The steady-turning roll stability limit of a partially-filled tank truck, widely described by the rollover threshold acceleration, can be evaluated by integrating the fluid slosh forces and moments to the roll plane vehicle model. The influence of dynamic fluid slosh on the roll stability limit can thus be conveniently evaluated from roll moment equilibrium of the vehicle in the roll plane (Yan *et al.*, 2005). The slosh forces and moments derived from the analytical slosh model are applied to the roll plane model of a six-axle tractor-semitrailer tank vehicle (Fig. 2.2a) to investigate the influence of dynamic liquid slosh on the vehicle rollover threshold acceleration. The vehicle is characterized in the roll plane by grouping the axles into a single composite axle. Figure 2.2b illustrates a simplified single composite axle representation of the suspended tank vehicle assuming negligible roll motion of the lumped unsprung mass. The simplicity of the vehicle model conforms to the two-dimensional fluid slosh and could provide a reasonable estimate of the rollover threshold acceleration of the partly-filled tank vehicle in the presence of dynamic slosh. The total moment about the vehicle roll axis arises from four components: (i) the primary overturning moment arising from the centrifugal force attributed to lateral acceleration encountered during a steady-turn; (ii) the roll moment caused by lateral displacement of the sprung and cargo weights; (iii) the overturning moment due to fluid motion within the tank; and (iv) the restoring roll moment resulting from the lateral load shift from inner wheel to the outer wheel. A relative rollover is considered to occur when one of the wheels loses contact with the ground as the lateral acceleration increases during a turning maneuver (Liu *et*

al., 1997). The rollover threshold is subsequently obtained as the maximum lateral acceleration that a vehicle can attain before the tires inside the turn lift off the ground. The total vehicle load is consequently sustained by the outer wheels at the relative rollover condition. Assuming small roll angles, the moment equilibrium equation about the roll center can be given by:

$$(W_s h_s + W_u h_u) a_y + M_d \alpha + M_l = WT \tag{2.46}$$

In the above equation, W_s and W_u are the sprung and unsprung weights of the tare tank vehicle, respectively, W is the total weight of the vehicle including the cargo, h_s and h_u are the center of gravity heights of sprung and unsprung masses, respectively, α is the roll angle of the sprung mass about the vehicle roll axis and T is the half-track width (see Fig. 2.2b). In Eq. (2.46), M_l is the total roll moment caused by fluid motion about the roll center, which can be obtained in a similar way as M_B in Eq. (2.41), a_y is the lateral acceleration corresponding to wheel lift-off condition in g units, and M_d is the lateral displacement moment for unit roll angle, given by:

$$M_d = W_s(h_s - h_r) + W_l(Z_o - h_r) \tag{2.47}$$

where W_l is liquid cargo load, h_r is the roll center height and $Z_o$is the tank geometric center height. Furthermore, the rolling resistance moment due to the suspension system is related to the

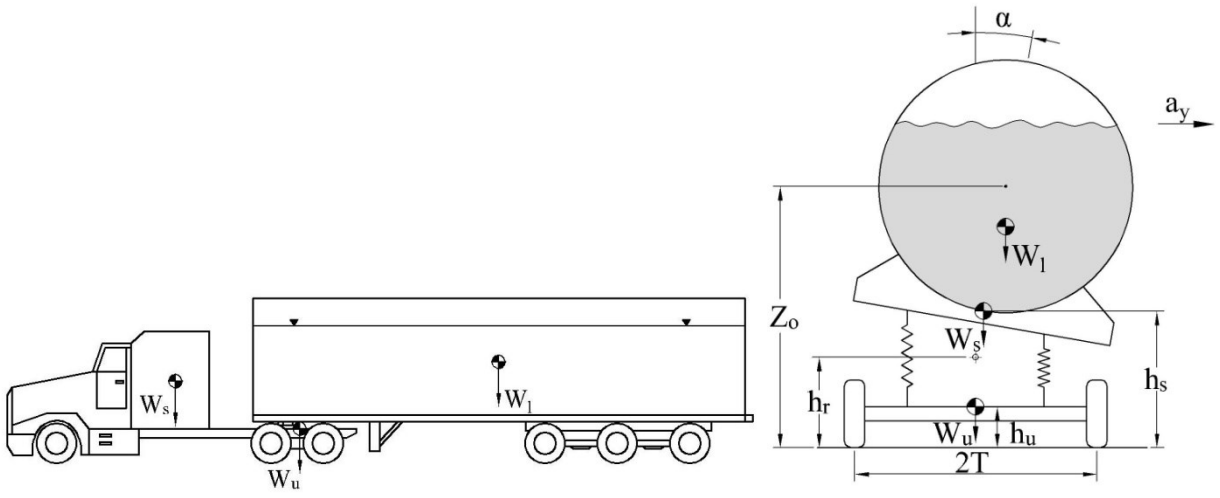

(a) (b)

Fig. 2.2. (a) Schematic of a six-axle tractor-semitrailer tank vehicle. (b) Roll plane model of a suspended tank vehicle.

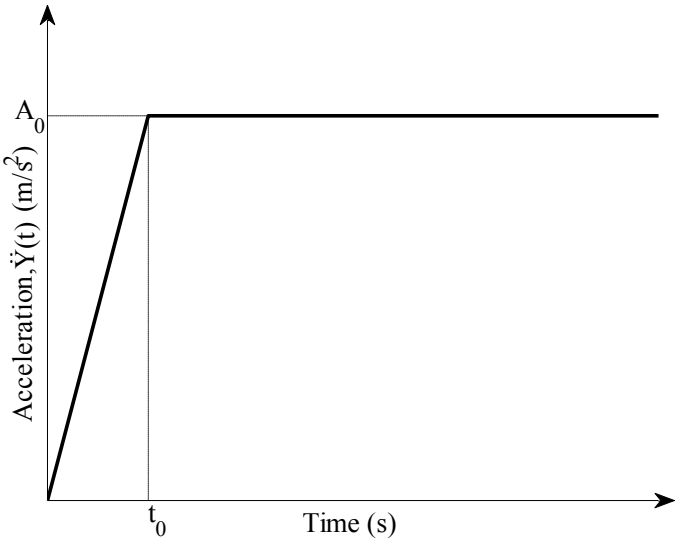

Fig. 2.3. Idealized lateral acceleration during a steady turning maneuver.

restoring moment as:

$$k_s\alpha = WT - Wa_y h_r + W_u a_y (h_r - h_u) \tag{2.48}$$

where k_s is the equivalent roll stiffness of the vehicle suspension. Substituting for α from Eq. (2.48) into Eq. (2.46) yields the following roll moment equilibrium expression:

$$a_y \left[W_s h_s + W_u h_u + \frac{M_d}{k_s} (W_u (h_r - h_u) - W h_r) \right] + M_l = WT \left(1 - \frac{M_d}{k_s} \right) \tag{2.49}$$

The analyses are performed under a ramp-step lateral acceleration input, $\ddot{Y}(t)$, as shown in Fig. 2.3 with $t_0 = 0.5\ s$. The moment M_l is initially obtained from the analytical slosh model, which is subsequently applied to Eq. (2.49) to derive a_y which may not be equal to the steady value of $\ddot{Y}(t)$. The magnitude of $\ddot{Y}(t)$ is gradually increased until a_y approaches steady value of $\ddot{Y}(t)$ satisfying the roll moment equilibrium of the vehicle. The solution are obtained by considering peak values of $M_l(t)$. Eq. (2.49) is also solved to obtain quasi-static rollover threshold limits, by considering the quasi-static components of the roll moment alone.

2.3 Results and Discussion

2.3.1 Comparison with the multimodal solution

The accuracy and efficiency of the proposed model are initially examined by performing modal analysis, as in Faltinsen and Timokha (2010). This approach is also essential to obtain the hydrodynamic coefficients in the subsequent section. The system of ODEs, Eq. (2.20), is represented by a system of uncoupled equations using the change of variable $\{\boldsymbol{\varphi}\} = [\mathbf{B}]\{\mathbf{q}\}$, where $[\mathbf{B}]$ is the modal matrix. The potential function coefficients are subsequently obtained as: $\varphi(t, \tau_i) = B(\tau_i)\cos(\sigma t)$. The uncoupled system of equations can be written as:

$$\{\ddot{\mathbf{q}}\} + [\mathbf{D}]\{\mathbf{q}\} = -\ddot{Y}\{\boldsymbol{\lambda}\} \tag{2.50}$$

where $[\mathbf{D}]$ is a diagonal matrix of natural frequencies σ_j^2, and $\{\boldsymbol{\lambda}\}$ is given by:

$$\{\boldsymbol{\lambda}\} = [\mathbf{D}][\mathbf{B}]^{-1}[\mathbf{K}]^{-1}\{\boldsymbol{\psi}\} \tag{2.51}$$

The above system of equations is solved using the Runge-Kutta scheme to obtain the normalized hydrodynamic force $\frac{|F_y|}{mA_0}$ for different fill ratios in a manner similar to that described in Faltinsen and Timokha (2010). The explicit form of the slosh force, Eq. (2.39), is also used to obtain the normalized force under a ramp-step input (t_0=0.5 s) considering different truncation sizes and fill ratios. The force responses at different instants are summarized in Table 2.1 for different fill ratios (h/R) and compared with those obtained from the above-described multi-model solution. The results are in very good agreement. The comparisons suggested that only 4 modes are required to calculate the normalized force up to three decimal places. A truncation size N=50, however, is needed for calculating the corresponding eigenvalues and eigenvectors. The solution based on the coupled system of equations, on the other hand, needed a truncation size N=15 with $\bar{N}$=300 for the numerical inversion of the Laplace transformation, Eq. (2.27). The relatively larger deviation at t_0=0.5 s is attributable to discontinuities in the ramp-step excitation and the multimodal solution. We further noted nearly identical computing times for both the methods. The numerical values of amplification factor, $c_f = \frac{|F_{y,max}|}{mA_0}$, obtained from the multi-modal and the proposed methods are also identical for the fill ratios considered (Table 2.2). The proposed method for calculating slosh force is thus considered to be accurate and efficient, and unlike the multi-modal approach it does not require prior solutions of the eigenvalue problem.

Table 2.1. Normalized force response as a function of truncation size ($\bar{N}$) for different fill ratios.

				h/R=0.6			
$\bar{N}$	*t*=0.25 s	*t*=0.5 s	*t*=0.75 s	*t*=1 s	*t*=2 s	*t*=5 s	*t*=10 s
100	0.164	0.596	1.085	1.538	0.380	1.621	0.972
150	0.165	0.579	1.085	1.542	0.378	1.623	0.967
200	0.165	0.576	1.081	1.542	0.378	1.623	0.968
250	0.165	0.573	1.084	1.542	0.377	1.623	0.966
300	0.165	0.570	1.085	1.542	0.377	1.623	0.967
Multimodal solution	0.165	0.560	1.084	1.542	0.377	1.623	0.967
				h/R=1.0			
100	0.247	0.728	1.134	1.445	0.504	0.970	1.282
150	0.247	0.715	1.135	1.449	0.503	0.971	1.278
200	0.247	0.712	1.132	1.448	0.503	0.972	1.279
250	0.247	0.710	1.134	1.448	0.502	0.971	1.277
300	0.247	0.708	1.134	1.449	0.502	0.971	1.278
Multimodal solution	0.247	0.700	1.134	1.448	0.502	0.971	1.278
				h/R=1.6			
100	0.391	0.931	1.142	1.190	1.024	1.193	0.815
150	0.391	0.925	1.142	1.192	1.023	1.193	0.813
200	0.391	0.923	1.141	1.192	1.023	1.193	0.813
250	0.391	0.922	1.142	1.192	1.023	1.193	0.812
300	0.391	0.921	1.142	1.192	1.023	1.193	0.813
Multimodal solution	0.391	0.918	1.142	1.192	1.023	1.194	0.813

Table 2.2. Comparisons of force amplification factors obtained from the multimodal method and the current study corresponding to different fill ratios.

h/R	c_f	
	Multi-modal	Proposed model
0.6	1.658	1.658
1.0	1.484	1.484
1.6	1.202	1.202

The validity of the empirical relation used for estimating the damping ratio, Eq. (2.25), is also examined considering water as the fluid. The use of damping is primarily intended for achieving convergence to a steady-state solution, while the damping ratio is estimated from the empirical relation considering only the fundamental mode. Since the viscous damping effect of typical liquids in bulk transportation is very small due to low viscosity and large size tanks

(Modaressi-Tehrani *et al.*, 2006), it would be reasonable to consider very light damping for all the modes. Damping factors corresponding to first five anti-symmetric modes ($2\xi_i\sigma_i; i = 1,..,5$) are obtained from the hydrodynamic coefficients reported in Faltinsen and Timokha (2010), and compared with the fundamental mode damping factors ($2\xi_1\sigma_1$) for different fill ratios. From the comparison shown in Table 2.3, it can be seen that the variations in damping factors corresponding to different modes are quite small for fill height above 25% of the diameter. The assumption of constant damping ratio for all the modes is thus considered reasonable, particularly for practical ranges of fill ratios encountered in partially-filled tank vehicles.

Table 2.3. Comparisons of damping factors obtained from hydrodynamic coefficients in Faltinsen and Timokha (2010) with the fundamental mode damping factor (Ibrahim, 2005) for different fill levels.

		Faltinsen and Timokha (2010)				
h/R	$2\xi_1\sigma_1$	$2\xi_1\sigma_1$	$2\xi_2\sigma_2$	$2\xi_3\sigma_3$	$2\xi_4\sigma_4$	$2\xi_5\sigma_5$
0.1	0.03	0.18	0.56	0.82	0.93	0.98
0.2	0.02	0.09	0.23	0.28	0.29	0.31
0.3	0.02	0.06	0.13	0.14	0.15	0.16
0.4	0.02	0.04	0.08	0.09	0.09	0.10
0.5	0.02	0.03	0.06	0.06	0.07	0.07
0.6	0.02	0.03	0.04	0.05	0.05	0.05
0.7	0.02	0.02	0.03	0.04	0.04	0.04
0.8	0.02	0.02	0.03	0.03	0.03	0.03
0.9	0.02	0.02	0.02	0.02	0.03	0.03
1.0	0.02	0.01	0.02	0.02	0.02	0.02
1.1	0.02	0.01	0.02	0.02	0.02	0.02
1.2	0.02	0.01	0.02	0.02	0.02	0.02
1.3	0.02	0.01	0.01	0.02	0.02	0.02
1.4	0.02	0.01	0.01	0.01	0.02	0.02
1.5	0.02	0.01	0.01	0.01	0.02	0.02
1.6	0.02	0.01	0.01	0.01	0.02	0.02
1.7	0.02	0.01	0.01	0.02	0.02	0.02
1.8	0.02	0.01	0.02	0.02	0.02	0.02
1.9	0.03	0.02	0.02	0.02	0.03	0.03
1.95	0.04	0.02	0.03	0.03	0.04	0.04

The numerical values of anti-symmetric eigenvalues, $\bar{\kappa}_j$ $(j = 1,2,3,4)$, are also obtained for different fill ratios and truncation sizes. The results are shown in Table 2.4 together with those reported in Faltinsen and Timokha (2010), for the sake of validity of our approach. As seen from the table, the results are identical with those reported in Faltinsen and Timokha (2010). The convergence rate is fast and uniform for all the fill ratios considered. Although the convergence rate for calculating eigenvalues in Faltinsen and Timokha (2010) is faster (see supplementary materials appended in Faltinsen and Timokha, 2010), it involves elaborate calculations for determining the set of trial functions and numerical integrations for computing the matrices of the spectral problem. For the sake of completeness, the first anti-symmetric natural sloshing modes for six different fill ratios are also presented in Fig. 2.4. The normalized wave profiles were observed to be in complete agreement with those reported in Faltinsen and Timokha (2010).

2.3.2 Hydrodynamic coefficients and free surface elevation

The validity of the analytical fluid slosh model is examined on the basis of the reported measured data, and analytical and numerical simulation results. The range of applicability of the linear slosh theory is also examined using the concept of critical free-surface amplitude (Liu and Huang, 1994). Hydrodynamic coefficients introduced by Faltinsen and Timokha (2010) are calculated to examine the accuracy of the proposed method. Table 2.5 summarizes normalized hydrodynamic coefficients $\bar{\lambda}_j$ $(j = 1,2,3,4,5)$ corresponding to different fill ratios, which are obtained from:

$$\bar{\lambda}_j = \frac{1}{R^2}\int_{-a}^{a} y\Phi_j dy\,; \qquad z = 0 \tag{2.52}$$

where Φ_j are the normalized eigenfunctions of the free liquid sloshing such that $\int_{-a}^{a}\left|\Phi_j\right|^2 dy = 1$ on the free-surface. Using the conformal transformation and the quadrature formula, $\bar{\lambda}_j$ can be obtained as:

$$\bar{\lambda}_j = \frac{\pi}{R^2}\sum_{i=1}^{N} w_i e^{4\pi\tau_i} B_j(\tau_i)\psi_i \tag{2.53}$$

where $B_j(\tau_i)$ is eigenvector corresponding to the j^{th} natural sloshing mode and is calculated from Eq. (2.20) by letting $\ddot{Y} = 0$ and $\varphi(t,\tau_i) = B(\tau_i)\cos(\sigma t)$ (McIver, 1989). The

Table 2.4. Anti-symmetric eigenvalues, $\bar{\kappa}_j$ $(j = 1, 2, 3, 4)$, obtained for different fill ratios and truncation sizes.

N	$\bar{\kappa}_1$	$\bar{\kappa}_2$	$\bar{\kappa}_3$	$\bar{\kappa}_4$
		h/R=0.4		
10	1.09698	4.96319	10.4375	24.9768
20	1.09698	4.93704	9.00672	13.0062
30	1.09698	4.93704	9.00748	12.9829
40	1.09698	4.93704	9.00749	12.9835
45	1.09698	4.93704	9.00749	12.9835
Faltinsen & Timokha (2010)	1.09698	4.93704	9.00749	12.9835
		h/R=0.8		
10	1.24606	4.65528	9.54954	23.5000
20	1.24606	4.60669	7.85271	11.1145
30	1.24606	4.60670	7.85372	11.0732
40	1.24606	4.60670	7.85373	11.0740
45	1.24606	4.60670	7.85373	11.0741
50	1.24606	4.60670	7.85373	11.0741
Faltinsen & Timokha (2010)	1.24606	4.60670	7.85373	11.0741
		h/R=1.0		
10	1.35574	4.70950	9.64492	23.9340
20	1.35573	4.65105	7.81875	11.0192
30	1.35573	4.65105	7.81985	10.9708
40	1.35573	4.65105	7.81986	10.9717
45	1.35573	4.65105	7.81986	10.9718
50	1.35573	4.65105	7.81986	10.9718
Faltinsen & Timokha (2010)	1.35573	4.65105	7.81986	10.9718
		h/R=1.2		
10	1.50753	4.92032	10.0775	25.1728
20	1.50751	4.85090	8.07711	11.3485
30	1.50751	4.85091	8.07832	11.2920
40	1.50751	4.85091	8.07833	11.2931
45	1.50751	4.85091	8.07834	11.2931
48	1.50751	4.85091	8.07834	11.2932
50	1.50751	4.85091	8.07834	11.2932
Faltinsen & Timokha (2010)	1.50751	4.85091	8.07834	11.2932
		h/R=1.6		
10	2.12376	6.24630	12.8093	32.3233
20	2.12372	6.13930	10.0791	14.0965
30	2.12372	6.13932	10.0807	14.0122
40	2.12372	6.13932	10.0807	14.0138
45	2.12372	6.13932	10.0807	14.0138
Faltinsen & Timokha (2010)	2.12372	6.13932	10.0807	14.0138
		h/R=1.8		
10	3.02150	8.47268	17.3836	44.0564
20	3.02140	8.31385	13.5572	18.9205
30	3.02140	8.31388	13.5595	18.7973
40	3.02140	8.31388	13.5596	18.7996
45	3.02140	8.31388	13.5596	18.7997
50	3.02140	8.31388	13.5596	18.7997
Faltinsen & Timokha (2010)	3.02140	8.31388	13.5596	18.7997

convergence is ensured after stabilizing the sixth decimal place using several values of truncation size *N*, up to a maximum of 50. Only a maximum of 15 truncated terms, however, are needed for calculating the hydrodynamic coefficients for the fundamental mode, $\bar{\lambda}_1$. The convergence rate was observed to be faster under low fill ratios but decreased under intermediate to high fill ratios. The first five hydrodynamic coefficients, presented in Table 2.5, were identical to those obtained by Faltinsen and Timokha (2010) using the modified Trefftz variational method. The convergence rate of the hydrodynamic coefficients, $\bar{\lambda}_j$, were not discussed in Faltinsen and Timokha (2010).

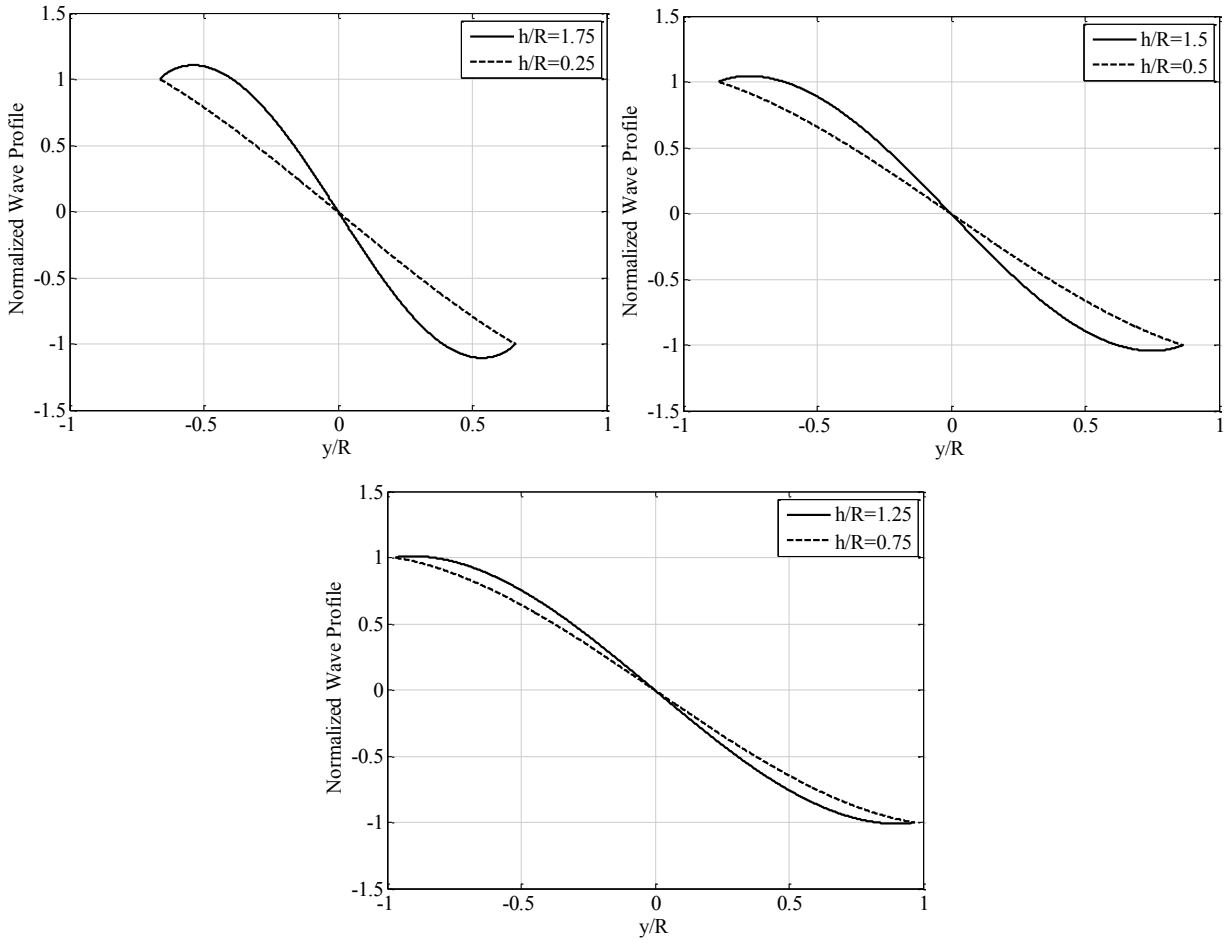

Fig. 2.4. Free-surface profiles of the first anti-symmetric natural sloshing modes for different fill ratios.

Table 2.5. The first five normalized hydrodynamic coefficients $\bar{\lambda}_j$ for various fill ratios.

$\frac{h}{R}$	$\bar{\lambda}_1$	$\bar{\lambda}_2$	$\bar{\lambda}_3$	$\bar{\lambda}_4$	$\bar{\lambda}_5$
0.1	0.155126	0.001617	0.000127	0.000024	0.000007
0.2	0.293875	0.006068	0.000864	0.000256	0.000107
0.4	0.522105	0.021049	0.004950	0.002014	0.001041
0.6	0.684522	0.040456	0.011994	0.005534	0.003116
0.8	0.781124	0.060439	0.020443	0.010132	0.006003
1.0	0.812062	0.077529	0.028538	0.014844	0.009107
1.2	0.777645	0.088423	0.034552	0.018629	0.011734
1.4	0.678346	0.089857	0.036771	0.020403	0.013128
1.6	0.514833	0.078467	0.033394	0.018993	0.012447
1.8	0.288084	0.050477	0.022312	0.012994	0.008667
1.9	0.151479	0.028703	0.012964	0.007651	0.005153
1.95	0.077529	0.015411	0.007055	0.004198	0.002845

The hydrodynamic coefficients associated with estimation of damping ratios are also obtained based on the tangential velocity at the wall surface as:

$$\bar{\gamma}_j = \int_{S_0} \left(\frac{\partial \Phi_j}{\partial s} \right)^2 ds \tag{2.54}$$

The hydrodynamic coefficients $\bar{\gamma}_j$ are computed in the physical plane through a numerical integration considering the relations between the physical and transformed plane, as described in Eq. (2.9). Table 2.6 summarizes numerical values of $\bar{\gamma}_j$ $(j = 1,2,3,4,5)$ for various fill ratios considering the anti-symmetric modes only. Number of truncated terms required to obtain a convergent numerical integration was two to three times more than that used for calculating $\bar{\lambda}_j$. The results are in full agreement with those reported in Faltinsen and Timokha (2010) except for the higher modes of fill ratios *h/R*>1. The peak discrepancy was observed in $\bar{\gamma}_5$ in the order of 2% for extreme fill ratio *h/R*=1.95.

The effectiveness of the present model for predicting the hydrodynamic force is also investigated in terms of the sloshing mass ratio given by Patkas and Karamanos (2007):

$$\chi_j = \frac{m_j}{m} \tag{2.55}$$

where m_j is regarded as the convective mass corresponding to the j^{th} sloshing mode. Using Eq. (2.39), the modal mass ratio can be calculated as:

$$\chi_j = \frac{2\rho a \pi R^2}{m} \sum_{i=1}^{N} \frac{B_j(\tau_i)\tau_i w_i e^{4\pi\tau_i} \tanh(\tau_i \zeta_0)}{\sinh(\pi\tau_i)} \bar{\lambda}_j \tag{2.56}$$

The sloshing mass ratio corresponding to first four modes, χ_j ($j = 1,2,3,4$), and four different fill ratios are summarized in Table 2.7 considering different truncation sizes, ranging from 10 to 45. The results suggest rapid convergence of the solutions, particularly for lower liquid-fill depths. The results are in very good agreement with those obtained by Patkas and Karamanos (2007) using the variational method based on Galerkin's dicretization.

Table 2.6. The first five normalized hydrodynamic coefficients $\bar{\gamma}_j$ considering only anti-symmetric modes for various fill ratios.

$\frac{h}{R}$	$\bar{\gamma}_1$	$\bar{\gamma}_2$	$\bar{\gamma}_3$	$\bar{\gamma}_4$	$\bar{\gamma}_5$
0.1	6.444	71.08	187.2	302.1	403.5
0.2	4.379	38.67	78.83	112.5	145.5
0.4	2.864	17.31	28.94	40.36	51.98
0.6	2.171	9.859	15.99	22.31	28.68
0.8	1.757	6.508	10.63	14.84	19.06
1.0	1.484	4.785	7.887	11.02	14.15
1.2	1.302	3.837	6.348	8.870	11.39
1.4	1.194	3.332	5.504	7.682	9.864
1.6	1.175	3.171	5.209	7.254	9.302
1.8	1.353	3.555	5.785	8.020	10.26
1.9	1.738	4.480	7.236	9.997	12.76
1.95	2.349	5.958	9.571	13.19	16.80

The slosh responses attained from the analytical model are also compared with the finite element solutions of the linear liquid slosh model, reported in Mitra *et al.* (2008). The study reported distribution of instantaneous hydrodynamic pressure on the container wall for a half-filled tank of radius $R = 0.5\,m$ under a harmonic displacement excitation $Y(t) = Y_0 \sin \sigma t$ ($Y_0 = -0.01\,m$; $\sigma = 5\,rad/s$). Figure 2.5a illustrates comparisons of the analytical results in terms of hydrodynamic pressure coefficient $c_p = \frac{P}{\frac{1}{2}\rho {V_0}^2}$ (V_0 being the amplitude of the tank velocity) with the reported results at instants t = 1, 4, 6 and 10s, and different angular positions θ of the wetted surface, measured along the clockwise direction from the positive y-axis. Time histories of the normalized free-surface elevation δ/R at the intersection of the

container wall is also presented in Fig. 2.5b against normalized time t/T_b, where $T_b = \frac{2\pi}{|\sigma_1 - \sigma|}$ is the beat period of fluid slosh. The results are in good agreement with those reported in Mitra *et al.* (2008), which is further shown in Fig. 2.5c over ¼ of the oscillation cycle. The presence of the beating has also been reported in a few experimental and simulation-based studies, when the excitation frequency is close to the fundamental natural frequency of liquid slosh (Yan *et al.*, 2009, 2010).

Table 2.7. The first four modal sloshing mass ratios $\boldsymbol{\chi_j}$ for various fill ratios and truncation sizes.

	$\frac{h}{R} = 0.6$				$\frac{h}{R} = 1.0$			
N	χ_1	χ_2	χ_3	χ_4	χ_1	χ_2	χ_3	χ_4
10	0.749901	0.010909	0.001942	0.000290	0.569171	0.018741	0.005348	0.001276
20	0.749894	0.010585	0.001623	0.000510	0.569156	0.017797	0.004052	0.001625
30	0.749894	0.010585	0.001623	0.000491	0.569156	0.017797	0.004054	0.001538
40	0.749894	0.010585	0.001623	0.000491	0.569156	0.017797	0.004054	0.001539
45	0.749894	0.010585	0.001623	0.000491	0.569156	0.017797	0.004054	0.001539
Patkas and Karamanos (2007)	0.74989	0.010585	0.001623	0.000496	0.56916	0.017797	0.004054	0.001539
	$\frac{h}{R} = 1.4$				$\frac{h}{R} = 1.8$			
10	0.370792	0.021176	0.007745	0.002457	0.140351	0.012878	0.005675	0.002260
20	0.370768	0.019790	0.005475	0.002510	0.140332	0.011855	0.003776	0.001917
30	0.370768	0.019791	0.005478	0.002348	0.140332	0.011855	0.003778	0.001774
40	0.370768	0.019791	0.005478	0.002351	0.140332	0.011855	0.003778	0.001776
45	0.370768	0.019791	0.005478	0.002351	0.140332	0.011855	0.003778	0.001776
Patkas and Karamanos (2007)	0.37077	0.019790	0.005477	0.002350	0.14032	0.011849	0.003770	0.001767

The model validity and applicability is also examined by comparing the slosh responses with the measured data for a partly-filled cylindrical tank (R=132.5 mm; length=950 mm) reported in Bogomaz and Sirota (2002). The study reported the steady-state (maximum and minimum) elevations of the free-surface at a distance of 80 mm from the center of the tank under a harmonic lateral displacement excitation $Y(t) = Y_0 \sin(\sigma t)$ with amplitude Y_0=2.7 mm at different frequencies. The analytical slosh model was used to derive the steady-state elevation of the free-surface by expressing the potential function coefficient $\varphi(t, \tau)$ in terms of a harmonic function, $\varphi(t, \tau) = \mathrm{B}(\tau)\cos(\sigma t)$. Substituting for $Y(t)$ and $\varphi(t, \tau)$ in Eq. (2.20) resulted in an expression for the unknown coefficients, $B(\tau) = Y_0 \sigma^3 [\mathbf{K} - \sigma^2 \mathbf{M}]^{-1} [\boldsymbol{\psi}]$, and the steady-state position of the free-surface is subsequently evaluated from Eq. (2.31).

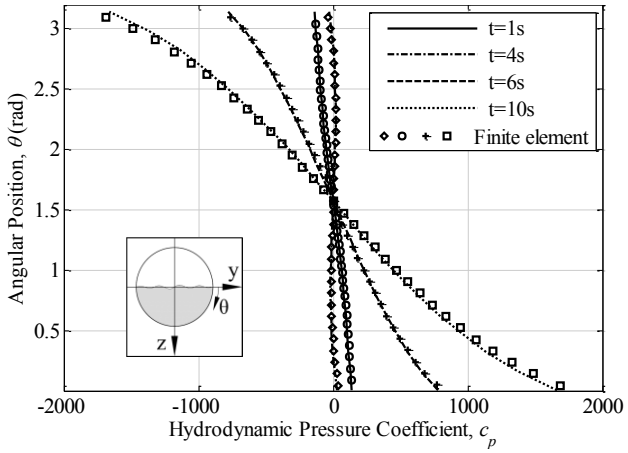

(a)

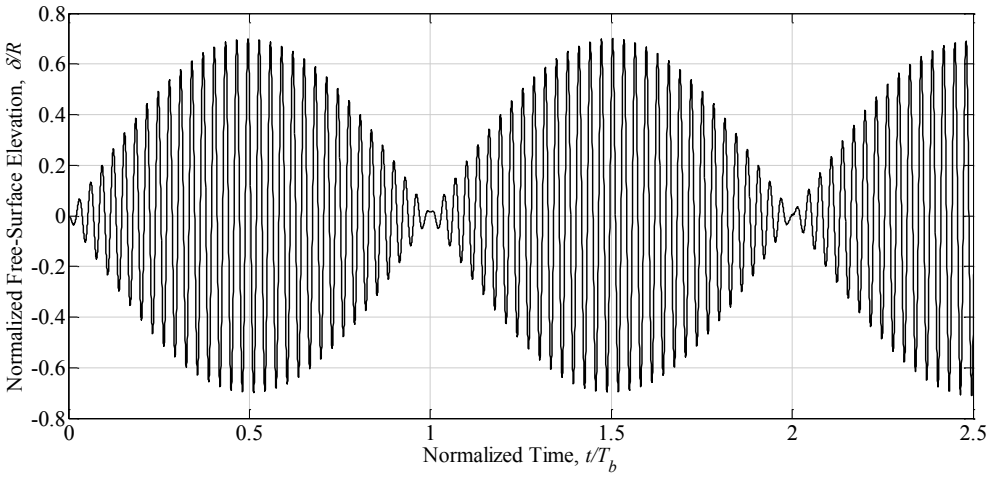

(b)

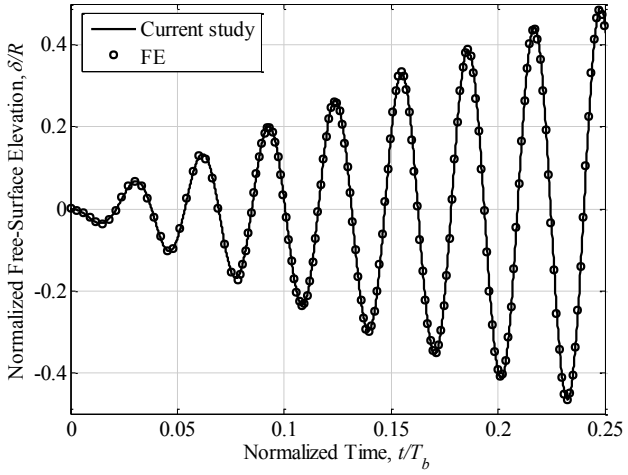

(c)

Fig. 2.5. Comparisons of fluid slosh responses obtained from the analytical model with the finite element results reported in Mitra *et al.* (2008): (a) Distribution of hydrodynamic pressure coefficient $\boldsymbol{c_p}$ on the wetted container surface at different instants; (b) Time history of the normalized free-surface elevation at the left wall of the container showing the beating phenomenon; (c) Comparison of the free-surface elevation over ¼ oscillation cycle.

Figure 2.6 shows comparisons of the free surface elevation responses normalized with respect to tank radius (δ/R) with the reported measured data for different liquid fill-depths, ranging from h/R=1.1 to h/R=1.66, as a function of the excitation frequency. The excitation frequency is normalized with respect to the fundamental slosh frequency σ_1. The comparisons suggest reasonably good agreements between the model results and the measured data in most of the frequency range for all the fill conditions considered, except near the fundamental slosh frequency. The wave elevations from the linear analysis are substantially higher than the measured data around the fundamental slosh frequency. The deviations around the resonance frequency were observed to be greater with higher fill ratio, and are attributable to nonlinear fluid slosh and flow separation, which cannot be predicted by the linear theory (Faltinsen and Timokha, 2009).

The range of applicability of the linear slosh model is further examined in terms of ranges of excitation frequencies, where the effects of nonlinearities may be considered small. For this purpose, the critical amplitude of the free-surface, δ_c, are evaluated under different excitation conditions, defined as (Liu and Huang, 1994):

$$\frac{\delta_c}{R} = \frac{\epsilon}{\bar{\kappa}_1} \tag{2.57}$$

where $\bar{\kappa}_1 = \frac{R{\sigma_1}^2}{g}$ is the lowest eigenvalue describing free oscillations of the liquid, and $\epsilon < \left|v_f\right|^2/\delta g$ is a small dimensionless parameter, where v_f is the free surface velocity. It has been shown that a linear equation for the dynamic boundary condition on the free-surface can be obtained, when the free-surface amplitude is less than the critical amplitude ($\delta < \delta_c$) (Liu and Huang, 1994). The shaded regions in Fig. 2.6 satisfy this condition where the free-surface amplitude ratio δ/R is less than the critical amplitude ratio, δ_c/R, for $\epsilon = 0.25$. The results suggest that the linear slosh model would yield considerable errors under excitations in the frequency range $0.95 \lesssim \frac{\sigma}{\sigma_1} \lesssim 1.05$ for intermediate fill levels, and $0.9 \lesssim \frac{\sigma}{\sigma_1} \lesssim 1.1$ for higher fill levels. The results also suggest greater contributions of the nonlinear slosh around the resonance frequency with increasing fill level.

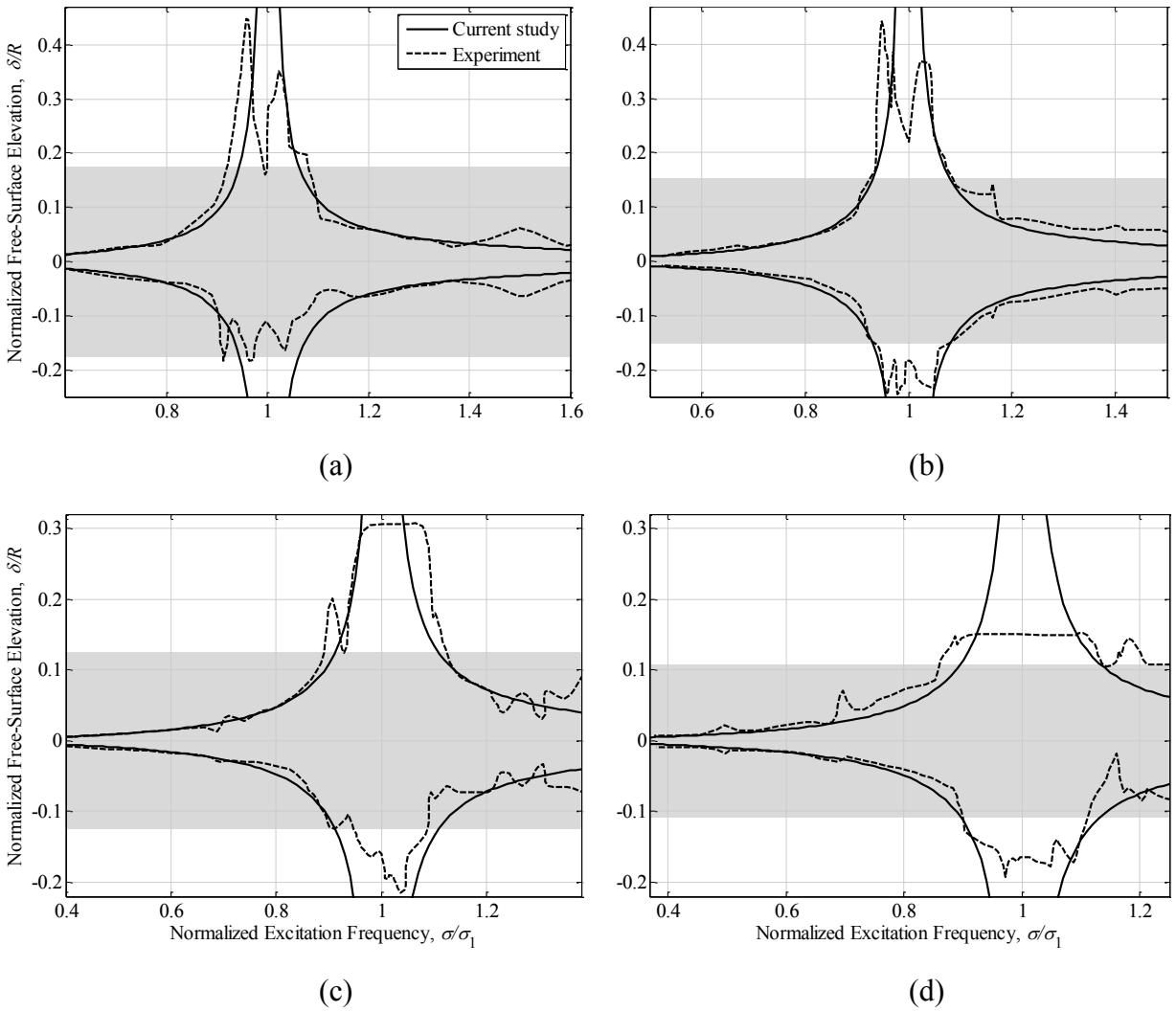

Fig. 2.6. Comparisons of normalized steady-state (maximum and minimum) elevation of the free-surface (80 mm from the tank center) predicated from the analytical model with the experimental data reported in Bogomaz and Sirota (2002) for different fill ratios: (a) h/R=1.1; (b) h/R=1.32; (c) h/R=1.55; and (d) h/R=1.66.

2.3.3 Responses to a lateral acceleration excitation

In the context of directional stability of partly-filled tank trucks, the dynamic lateral force and roll moment responses to lateral acceleration excitations are of greater interest. The steady-turning roll stability of the tank trucks are evaluated under a steady lateral acceleration idealized by a ramp-step function shown in Fig. 2.3. The magnitude A_0 is the steady-state lateral acceleration following the time lapse t_0. The analytical solutions in terms of the dynamic lateral force and overturning moment responses obtained under a lateral excitation idealizing a steady-

turn maneuver of a tank truck are compared with those reported from nonlinear CFD analysis and pendulum models for simulation of lateral slosh.

Modaressi-Tehrani (2004) reported transient lateral force and overturning moment responses due to fluid slosh in a partially filled cylindrical tank (R=1.016 m) subject to different levels of ramp-step acceleration inputs with rise time, t_0=0.5s (Fig. 2.3). The two-dimensional nonlinear fluid slosh analysis was performed using a CFD software (FLUENT), considering laminar flows, and incompressible form of Navier-Stokes and continuity equations that were discretized using the finite volume method. Free-surface tracking was achieved using the volume-of-fluid method (VOF). The fluid in the tank was assumed to be a fuel oil with density and dynamic viscosity of 850 kg/m^3 and 0.0867 kg/ms, respectively. Figures 2.7a and 2.7b compare the lateral force and overturning moment responses derived from the analytical model for the 40%-filled tank with those reported by Modaressi-Tehrani (2004) corresponding to different magnitudes of lateral acceleration excitations. The lateral force and overturning moment are normalized with respect to the respective quasi-static values, mA_0 and mRA_0. In the figures, the time is normalized with respect to the fundamental slosh period T_1. It should be noted that the normalized slosh force and overturning moment derived from the linear model are independent of the lateral acceleration amplitude. Furthermore, the normalized slosh force and overturning moment are identical, as seen in Eqs. (2.35), (2.39) and (2.41) to (2.44). Practically, a truncation size N=15 and $\bar{N}$=300 in numerical inversion of the Laplace transformation (Eq. 2.27) are needed to calculate the normalized force with the accuracy of 0.1%. The computing time is thus substantially smaller compared to the nonlinear CFD simulations that require discretization of the fluid domain.

The comparisons suggest that the force and moment responses obtained from the analytical model are in good agreement with those obtained from the CFD simulations under 0.1g and 0.2g lateral acceleration excitation. Notable deviations in the lateral force, however, are evident under the higher excitation of 0.4g. The analytical solution, however, exhibits better agreement with the CFD results during the first oscillation cycle under the higher excitation amplitude. The maximum deviation in the normalized slosh force predicted by the linear and nonlinear analyses during the first period is in the order of 6% under A_0= 0.4g. The results suggest that fluid slosh predominantly occurs near the fundamental slosh mode, while the nonlinear analyses show contributions of the higher modes under 0.4g excitation.

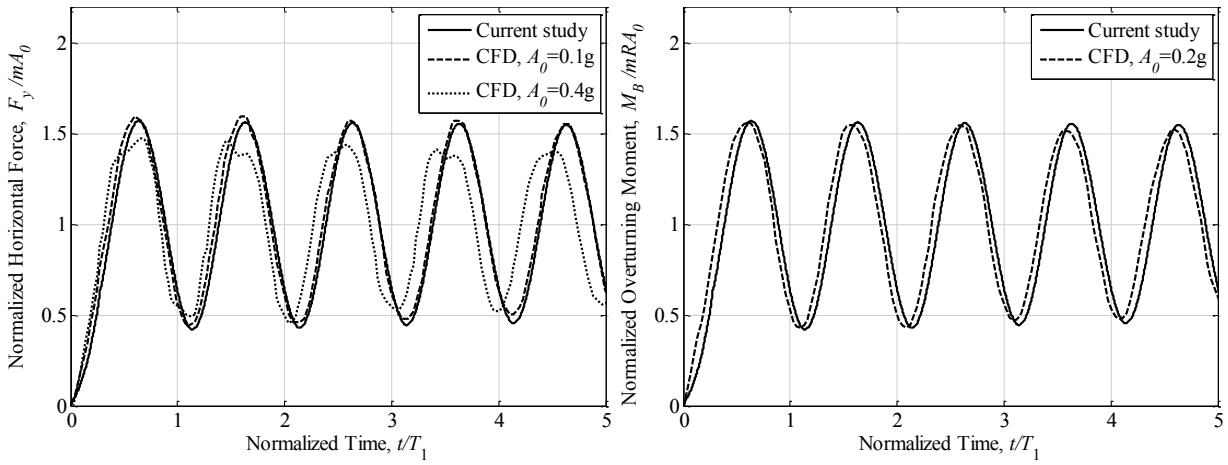

(a) (b)

Fig. 2.7. Comparisons of normalized (a) lateral force and (b) overturning moment response obtained from the analytical model with those reported from nonlinear CFD simulations in Modaressi-Tehrani (2004) under different levels of lateral acceleration.

The normalized force responses of the model corresponding to different fill ratios are also compared with those obtained from a simple pendulum model. Aliabadi *et al.* (2003) reported the horizontal slosh forces in a partially filled circular tank (R=0.5m; h/R = 0.3 to 0.9) under the lateral excitation (A_0=0.0408g; t_0=0s) using a pendulum model and a CFD model. In the simple pendulum approach, the mass of the liquid within the tank was assumed to be a point mass suspended from the tank center. The time histories of normalized lateral force responses obtained using the linear model are compared with those reported by Aliabadi *et al.* (2003) using the pendulum and CFD models in Fig. 2.8. The results suggest substantial deviations between the responses of the pendulum and the CFD models for all the fill ratios considered in the analyses, while a better agreement is evident between the analytical and the CFD models for the fill conditions considered. The deviations between the pendulum and the CFD models are significantly higher with higher fill ratios. The difference in the peak force responses of the two models approaches 21% for h/R=0.9, while the deviation in the peak responses obtained from the analytical and CFD models is only about 5%. The results suggest that the analytical model yields far more accurate predictions of the transient slosh responses than the simple pendulum model, while it provides reasonable good agreements with the CFD model. Furthermore, the analytical model is substantially more computationally efficient than the CFD model, which makes it well-

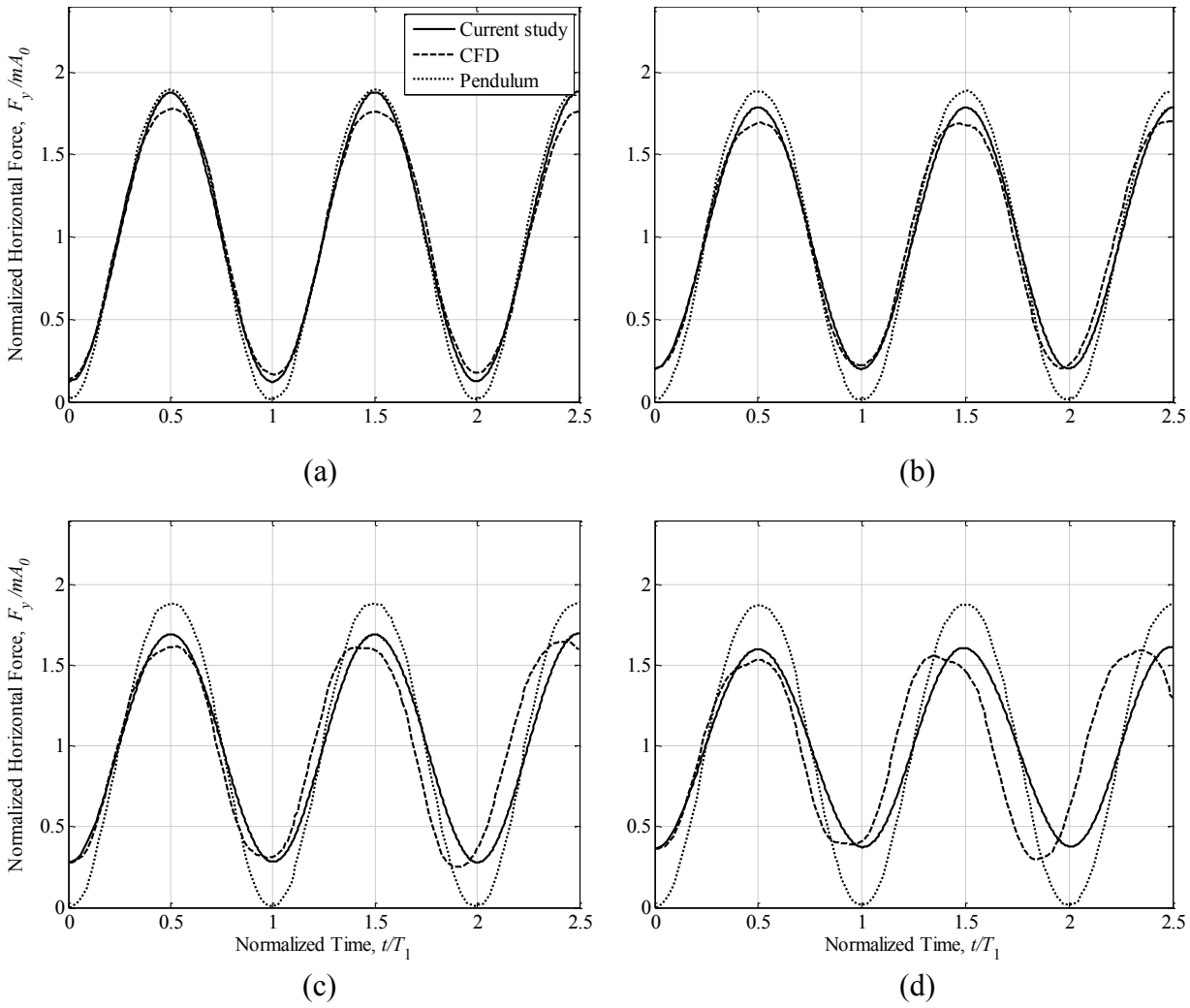

Fig. 2.8. Comparisons of normalized force response of the analytical model with those obtained from a simple pendulum model and the nonlinear CFD simulations, reported in Aliabadi *et al.* (2003) for different fill levels: (a) *h/R*=0.3; (b) *h/R*=0.5; (c) *h/R*=0.7; (d) *h/R*=0.9.

suited for integration to the multi-body vehicle dynamics models for evaluations of directional performance characteristics of the partly-filled liquid cargo vehicles.

The applicability of the analytical model for predicting slosh force and moment under intermediate and high liquid fill levels is also evaluated by comparing the responses with those reported from a nonlinear trammel pendulum model by Salem (2000). Figure 2.9 compares the overturning moment amplification factors ($c_m = \frac{|M_{B,max}|}{mRA_0}$ Popov *et al.*, 1993a) derived from the analytical model corresponding to different fill ratios with those obtained from the trammel

pendulum model. The parameters of the nonlinear pendulum model including the arms lengths, fixed and oscillating masses, and height of the fixed mass with respect to the tank base were estimated by matching the pendulum natural frequency, horizontal force component and the static moment around the tank base to those obtained from the finite element simulations of the fluid motion using the LSDyna-3D software (Salem, 2000). The figure also presents the reported amplification factors derived from the finite element analysis. The results in each case are obtained for a circular container (R=0.8552m) partially filled with water and subjected to a constant lateral acceleration, A_0 = 0.0875g.

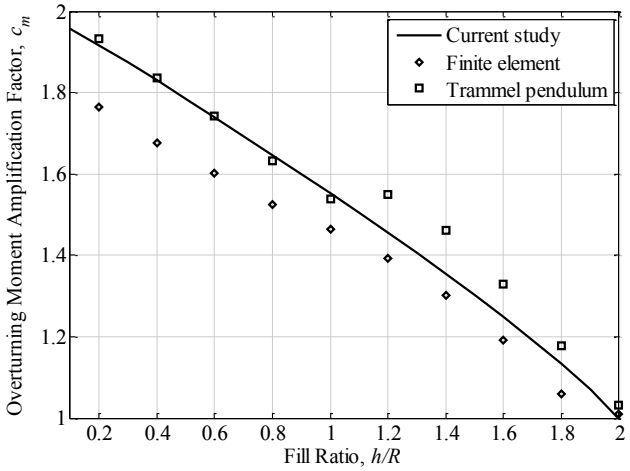

Fig. 2.9. Comparisons of Overturning amplification factor obtained from the analytical model with those reported from the nonlinear trammel pendulum model and nonlinear finite element simulations, reported in Salem (2000) for different fill levels.

The results show that the amplification factor could be as high as 2 under low fill conditions, and implies that the roll moment associated with transient slosh could be of critical importance for preserving the roll stability of a partly-filled tank vehicle. The amplification factor decreases with increasing fill level in a nearly linear manner. This suggests that the contribution of slosh component of the overturning moment (M_S) decreases with increase in the fill level. A higher fill ratio yields relatively greater non-sloshing mass of the liquid, which together with the constraints of the circular cross section container wall contributes to less intensive slosh motion. Such trends have also been reported in a few studies (Popov *et al.*, 1993a). Given that the validity of the analytical model under low amplitude excitations has been

proven, the FE model is considered to underestimate the slosh response over the entire fill range. The deviations between the FE and analytical model results are believed to be caused by two factors. Firstly, the reported FE model results showed a diverging trend over the initial few cycles, particularly under higher fill levels. Secondly, the amplification factor is based upon the peak response during the first oscillation cycle alone, where the peak magnitude is substantially smaller than those observed from the subsequent cycle. Furthermore, the analytical model response agrees very well with that of the trammel pendulum model for fill up to 50%, $h/R \leq 1.0$. The overturning moment amplification predicted by the trammel pendulum, however, shows considerable deviations from analytical model response for fills exceeding 50%.

2.3.4 Effect of dynamic liquid slosh on roll stability of tank trucks

The roll moment equilibrium equation, Eq. (2.49), integrating with the moment due to dynamic fluid slosh is solved to determine the rollover threshold acceleration of a partly-filled six-axle tractor-tank-semitrailer vehicle. The simulations are performed considering R=1.016m, and constant as well as variable cargo load for different fill ratios. The cargo load is varied from 0 to 338 kN with the fill ratio, $0 \leq h/R \leq 2$, for a fuel oil (ρ = 850 kg/m^3; ν=1.02×10^{-4}m^2/s), which represents partial fill conditions encountered on a local delivery route. The constant cargo load of 338 kN, is realized considering liquid cargo of different density in the fill range, $1 \leq h/R \leq 2$, which represents the general-purpose liquid bulk transportation, where the maximum cargo load is limited by the regulatory axle load limits. The parameters of the vehicle are summarized in Table 2.8. The rollover threshold limits of the vehicle model derived considering dynamic fluid slosh are compared with those obtained for quasi-static analysis in Fig 2.10. The limits are also compared with those of the equivalent rigid cargo vehicle.

The results suggest that rollover limits of the partly-filled vehicle, derived from the quasi-static analysis are substantially lower than those of the equivalent rigid cargo vehicles, for both the loading conditions. These results are in close agreement with those reported in Rakheja *et al.* (1988). Consideration of overturning moment due to dynamic fluid slosh, derived from the analytical model, yields even lower threshold limits for both the loading conditions, irrespective of the fill level. The threshold limits obtained from both the quasi-static and dynamic slosh analysis, corresponding to h/R =0 and h/R =2, however, are identical to those of the equivalent rigid vehicle, where the fluid slosh is absent. In the variable cargo load case, increasing the fill

height yields higher cargo load and higher mass center height, which causes substantially greater reduction in the rollover threshold acceleration for both the rigid and liquid cargo vehicles, as seen in Fig. 2.10a. The decrease, however, is significantly larger for the intermediate fill ranges, when overturning moment due to dynamic slosh is considered. The effect of dynamic fluid slosh tends to diminish under higher fills ($h/R \geq 1.4$), which is attributed to relatively lower free surface motion, as it is also seen in Fig. 2.9. For the equivalent rigid cargo vehicle with constant cargo load, lower fill ratio causes lower mass center height and thus the higher rollover acceleration limit. The acceleration limit obtained from the quasi-static analysis tends to be constant over the entire fill range, as seen in Fig. 2.10b, since the overturning moment is directly related to the cargo mass, as seen in Eq. (2.45). This suggests that the additional overturning moment attributed to quasi-static slosh counterbalances the gain due to lower mass center height. The additional moment associated with dynamic fluid slosh further deteriorates the stability limits, the greatest effect is seen for the 50% fill condition (h/R=1).

Table 2.8. Simulation parameters of the six-axle tractor-tank-semitrailer vehicle model.

Sprung Weight (empty tank), W_s	120900 N
Unsprung Weight, W_u	47596 N
Center of gravity height of the sprung mass, h_s	1.12 m
Center of gravity height of the unsprung mass, h_u	0.536 m
Roll center height, h_r	0.725 m
Tank center height, Z_o	2.116 m
Tank length	12.5 m
Half track width, T	0.813 m
Roll stiffness, k_s	1110 kNm/rad

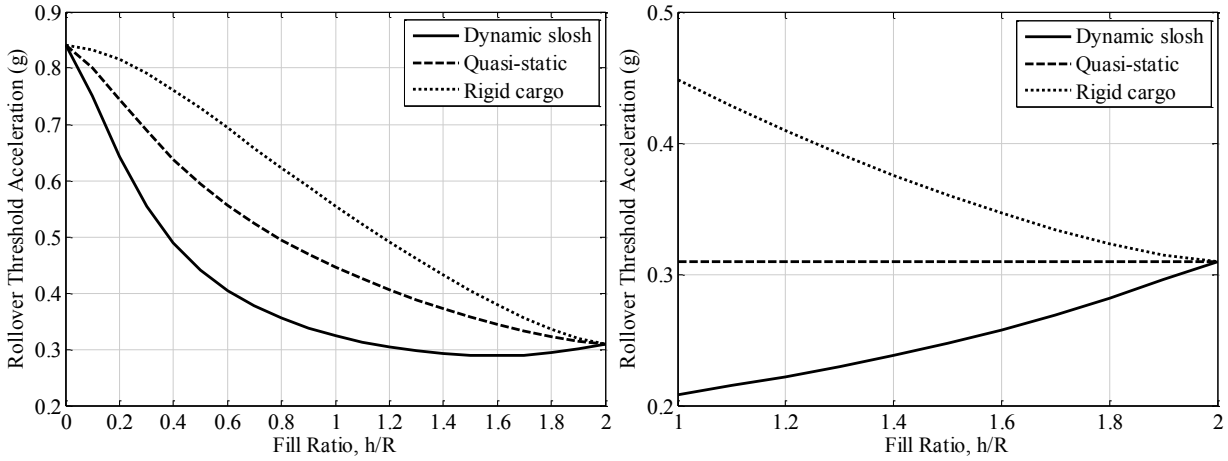

Fig. 2.10. Effect of transient sloshing on rollover threshold acceleration of a heavy tank vehicle for two different loading conditions: (a) Variable axle load; (b) Constant axle load.

2.4 Conclusions

A mathematical model, based on linear slosh theory, was developed for analysis of transient liquid sloshing in laterally excited partly-filled cylindrical containers used in bulk liquid cargo transportation. Rapid convergence of the solution was ensured using the scaled quadrature formula. Furthermore, simple integral form of the potential function enabled straightforward calculations of the system matrices. The proposed model is thus expected to be more efficient and simpler than the previously suggested models based on the variational method. The explicit expressions obtained for slosh force and overturning moment further permit efficient integration of the fluid slosh dynamics to the vehicle model for analyses of directional properties of partly filled tank vehicles.

Comparisons of the model responses with the reported experimental and simulation results suggest that the linear slosh theory can yield reasonably good predictions of free surface elevation, slosh force and slosh moment responses under lateral excitations idealizing steady-turning of the vehicle, irrespective of the fill height. The linear slosh theory, however, yields substantial error when the excitation occurs in the vicinity of the fundamental slosh frequency, which is attributable to nonlinear slosh and flow separation. Relatively greater errors were observed under higher fill levels. Notable differences with respect to the reported CFD simulation results were also evident under high magnitude excitation of 0.4g, which represents the upper limit of lateral acceleration for vast majority of tank truck configurations. The linear theory, however, provided more accurate slosh responses than the simple and trammel pendulum models, which generally impose complex challenges in identifying the model parameters, particularly under varying fill levels. The significantly superior computational efficiency of the linear model compared to the CFD models, coupled with its reasonably accurate prediction of slosh response under vehicular excitations, makes it attractive for integration in the multi-body vehicle dynamic models for assessing directional stability limits of partly-filled tank trucks.

It was shown that the overturning amplification factor could reach up to 2 in low fill levels, suggesting the significance of considering the effect of transient motion of the liquid in the stability analysis of partially-filled tank vehicles. In case of the varying cargo load and thereby the varying axle loads, the consideration of dynamic slosh could yield 20% to 28% lower rollover threshold in the 20% to 70% fill range. For the constant cargo load case, the rollover

threshold obtained from the dynamic slosh could be up to 33% lower compared to the quasi-static value near 50% fill level. The threshold values obtained in the study, however, represent the lower limit since the moment equilibrium is based on the peak slosh moment.

CHAPTER 3

EFFECTS OF TANK CROSS-SECTION ON DYNAMIC FLUID SLOSH LOADS AND ROLL STABILITY OF A PARTLY-FILLED TANK TRUCK

3.1 Introduction

The directional responses of heavy vehicles carrying liquid cargo are known to be strongly affected by liquid slosh caused by road- or maneuver-induced disturbances. The forces and moments caused by fluid slosh under steering and/or braking maneuvers have been associated with reduced stability limits and poor directional performance of partly-filled tank trucks (Rumold, 2001; Yan *et al.*, 2005). Directional responses and roll stability of partially-filled tank trucks have been mostly evaluated using quasi-static fluid slosh theory, which neglects the contributions due to dynamic sloshing. The steady-turning rollover immunity levels of articulated vehicles with partly-filled cleanbore and compartmented cylindrical tanks have been evaluated using a static roll plane model of the vehicle integrating forces and moments arising from the quasi-static fluid slosh (Rakheja *et al.*, 1988). The study concluded that partially filled cleanbore tank vehicles exhibit lower rollover threshold acceleration compared to the rigid cargo vehicles. The quasi-static fluid slosh models have also been employed to obtain directional responses of partly-filled tractor-tank-semitrailer combinations under steering or braking inputs (Ranganathan et al., 1989; Ranganathan and Yang, 1996). Southcombe *et al.* (2000) developed a simple numerical model for estimating the steady-turning roll stability limits of partly-filled tank vehicles with various tank geometries using quasi-static fluid slosh analysis.

The quasi-static method permits analyses of mean steady-state directional responses of the coupled cargo-vehicle system in a highly efficient manner through computations of mean dynamic load shifts, mean slosh forces and moments. The method, however, cannot account for the effects of dynamic liquid slosh. Studies reporting dynamic fluid slosh in partly-filled containers using computational fluid dynamics (CFD) codes have invariably concluded that peak slosh forces and moments are substantially greater than those predicted from a quasi-static model (Yan *et al.*, 2005; Popov *et al.*, 1993a; Modaressi-Tehrani, 2006). These suggest only limited

validity of the quasi-static method for predicting directional responses of the vehicles, particularly under transient directional maneuvers or moderate to high amplitude steering or braking inputs. It has thus been widely suggested that considerations of transient fluid slosh could yield lower stability limits of partly-filled tank trucks compared to those estimated from the quasi-static analyses. Moreover, the quasi-static approach cannot be applied to study fluid slosh in baffled tanks.

The applications of CFD slosh models to vehicle models for braking and steering dynamic analysis, however, have been limited due to extreme computational demands, and complexities involving elaborate data transfers and coordinate transformations between the vehicle and the CFD fluid slosh models. A few studies have attempted analyses of coupled tank-vehicle system dynamics through continuous updating of the vehicle state on the basis of transient fluid slosh forces and moments derived from a CFD fluid slosh model, in an off-line manner (Rumold, 2001; Biglarbegian and Zu, 2006; Yan and Rakheja, 2009). Thomassy *et al.* (2003) developed a master program, called Glue Code, for managing data transfer between the CFD (FLOW-3D) and multi-body dynamic (MSC.ADAMS) codes, which simulated the liquid slosh and vehicle dynamics, respectively, in an independent manner. Such methods, however, are considered highly inefficient due to excessive computing demands (Biglarbegian and Zu, 2006; Yan and Rakheja, 2009; Thomassy *et al.* 2003).

Alternatively, the dynamic fluid slosh in moving containers under lateral and longitudinal accelerations may be characterized through mechanical analogous models. Such models can be easily integrated to the vehicle model for directional response analyses in a highly efficient manner. In the mechanical analogous modeling approach, dynamic motion of liquid within a container is represented by a series of mass-spring-dashpot systems or a set of simple pendulums (Bauer, 1972; Khandelwal and Nigam, 1982). While the simplicity of the mechanical equivalent models could permit even real-time simulations of directional responses of a partly-filled tank vehicle, the identification of equivalent mechanical model parameters poses certain complexities. The model parameters are generally estimated from experimental data (Ibrahim, 1999) or slosh responses obtained through CFD simulations (Salem *et al.*, 2009).

Analytical models of liquid slosh, based on the potential flow equations and linearized free-surface boundary condition, are known to be efficient in terms of their computational

demand and ease of integration to vehicle dynamic models. Ibrahim (2005) suggested that exact solutions of linear liquid slosh are limited to tank geometries with straight walls, such as rectangular and upright-cylindrical containers. Analytical solutions of fluid slosh in tanks with curved walls have also been attempted in a few studies using a conformal mapping technique. Budiansky (1960) and McIver (1989) used this method to calculate natural sloshing modes and frequencies of liquid sloshing in two-dimensional cylindrical and spherical containers as a function of liquid fill-depth. Hasheminejad and Aghabeigi (2009, 2012) computed natural frequencies and modes of two-dimensional slosh in a half-filled elliptical container with vertical or horizontal side baffles. For lateral liquid slosh in containers with curved walls, analytical solutions have been mostly limited to half-full condition. Papaspyrou *et al.* (2004a) investigated liquid sloshing in half-full cylindrical vessels subjected to transverse excitations considering the velocity potential as a series of spatial and time functions. Hasheminejad and Aghabeigi (2011, 2012) employed the conformal mapping technique to obtain slosh force and overturning moment in half-filled elliptical containers equipped with vertical or horizontal side baffles under a lateral acceleration excitation. The ranges of applicability and limitations of the linear slosh theory have been presented in a recent study (Kolaei *et al.*, 2014). It was shown that the linear slosh theory can provide accurate predictions of transient lateral slosh, when the free-surface elevation is less than the critical free-surface elevation. Comparisons with the nonlinear CFD simulations also suggested reasonably good predictions of slosh force and moment responses under lateral acceleration magnitude up to 0.4g, which represents the upper limit of the rollover threshold acceleration for vast majority of tank truck configurations.

The primary motivation of this study arises from the desire to develop an efficient tool for real-time simulations of fluid slosh in partly filled tanks of different cross-sections and to investigate the effect of dynamic fluid slosh on the directional performance of partly-filled tank vehicles. An analytical model is proposed to characterize dynamic fluid slosh in moving containers of different cross-sections using modal analysis technique. The eigenvalues and eigenvectors of free liquid slosh in a partially filled tank of arbitrary cross-section are initially obtained using the variational method. The estimated eigenvalues and eigenvectors are subsequently incorporated into a multimodal representation of lateral liquid slosh to compute the velocity potential followed by the hydrodynamic pressure, slosh force and moment. The results are presented for the partly-filled circular, elliptical, modified-oval, and Reuleaux-triangle (Kang

et al., 2000b) cross-section tanks. The validity of the model is also illustrated using the reported measured data and analytical benchmarks. The effect of tank cross-section on the lateral slosh force and overturning moment is also investigated. Moreover, a simple roll plane model of a tank vehicle is used to illustrate the effect of dynamic liquid slosh and tank cross-section on the rollover threshold acceleration of the partly-filled tank vehicle.

3.2 Formulations

An analytical model of fluid slosh within a tank of arbitrary cross-section is formulated to facilitate its integration to the multi-body vehicle dynamic models. The model is developed using linear modal theory, which can describe velocity potential of the sloshing liquid through various slosh modes. The proposed multi-modal approach is supported by the fact that natural modes of liquid slosh satisfy the Laplace equation as well as the zero-Neumann boundary condition on the tank walls. The analytical model of lateral liquid slosh in an arbitrary tank cross-section involves determination of slosh frequencies and modes, and their summation to derive the velocity potential and thus the slosh force and moment.

3.2.1. Natural sloshing modes and frequencies

Consider a partly-filled arbitrary cross-section tank of overall width *2a* and height *2b* fitted within an open rectangular tank, as shown in Fig. 3.1. The Cartesian coordinate system *Oyz*, located at the center of the tank, is used with the *z*-axis directed upward, and the liquid fill-level *h* is measured from the *y*-axis. Since the eigenfunctions of free-liquid slosh can be derived analytically for the rectangular tank, these functions are used for a problem with more complex geometry. Assuming inviscid, incompressible and irrotational flows, the problem of free linear slosh in partially-filled tanks can be expressed in the form (Abramson, 1966; Ibrahim, 2005):

$$\nabla^2 \varphi_i = 0 \qquad \text{in } \Omega \tag{3.1}$$

$$\frac{\partial \varphi_i}{\partial n} = 0 \qquad \text{on } \tau \tag{3.2}$$

$$\frac{\partial \varphi_i}{\partial z} = \kappa_i \varphi_i \qquad \text{on } \Sigma \tag{3.3}$$

Here φ_i represents the velocity potential corresponding to i^{th} natural mode, $\frac{\partial}{\partial n}$ denotes the derivative along the normal to the container wall and $\kappa_i = \frac{\sigma_i^2}{g}$ is related to the circular frequency

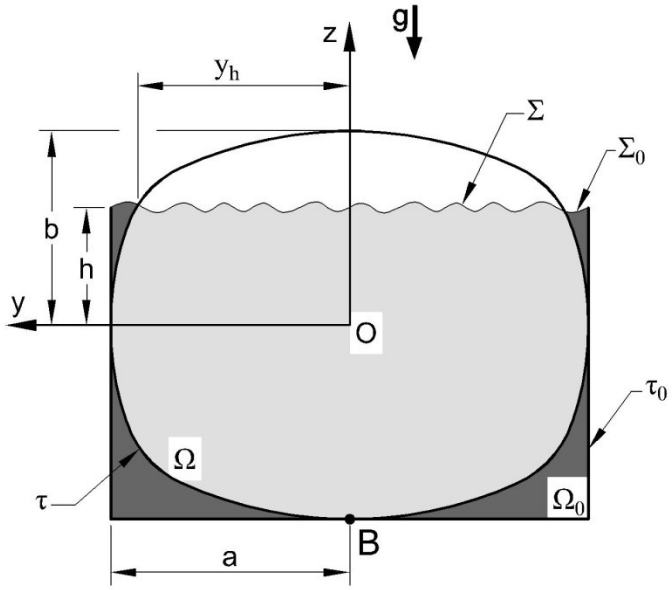

Fig. 3.1. Arbitrary tank geometry fitted within a rectangular tank.

σ_i of the liquid oscillations. In above equations, Ω and Σ represent the fluid domain and the liquid free-surface, respectively, and τ is the wetted surface area of the tank (Fig. 3.1).

The variational method (Ibrahim, 2005; Faltinsen and Timokha, 2009) is adopted in this study to compute the fundamental frequencies and modes of fluid slosh in a tank of arbitrary cross-section. The variational principle, also termed as Hamilton's principle, implies that the Lagrangian has to be extremum for a stationary solution. Determination of the natural oscillations of the liquid can be expressed as a variational problem involving kinetic and potential energy functions for the liquid within the container, and assuming harmonic functions for the free-surface height and velocity potential at the free-surface. The variational problem thus reduces to determination of a set of velocity potential functions, which minimize the Lagrangian L_i, given by (Moiseev, 1964):

$$L_i = \int_{\Omega} |\nabla \varphi_i|^2 d\Omega - \kappa_i \int_{\Sigma} {\varphi_i}^2 dS \tag{3.4}$$

The solution of the variational problem could be conveniently obtained using the Ritz method (Faltinsen and Timokha, 2009), which describes the velocity potential by a linear combination of coordinate functions ψ_j such that:

$$\varphi_i = \sum_{j=0}^{N} a_{ij}\psi_j \tag{3.5}$$

where a_{ij} are the unknown coefficients of eigenvectors. Substituting for φ_i in Eq. (3.4) and letting $\frac{\partial L_i}{\partial a_{ij}} = 0$ yields the following set of linear algebraic equations in a_{ij}:

$$\sum_{j=0}^{N} a_{ij}\left(A_{ij} - \kappa_i B_{ij}\right) = 0, \qquad (i = 0,1,2,\dots N) \tag{3.6}$$

where

$$A_{ij} = \int_{\Omega} \boldsymbol{\nabla}\psi_i \cdot \boldsymbol{\nabla}\psi_j d\Omega, \quad B_{ij} = \int_{\Sigma} \psi_i \psi_j dS \tag{3.7}$$

The determinant of coefficients a_{ij} in Eq. (3.6) must vanish for the existence of a nontrivial solution, i.e.:

$$\left|A_{ij} - \kappa_i B_{ij}\right| = 0 \tag{3.8}$$

The solutions of the above equation yield the natural slosh frequencies, while the slosh modes are obtained from Eq. (3.5).

The eigenfunctions ψ_j in Eq. (3.7) can be estimated from the eigenfunctions associated with the free sloshing of liquid in the rectangular tank containing the arbitrary cross-section tank (Fig. 3.1) (Moiseev, 1964; Ibrahim, 2005; Faltinsen and Timokha, 2009). The anti-symmetric eigenfunctions of free sloshing in rectangular tanks, reported in many studies (e.g., Faltinsen and Timokha, 2009), can be expressed as:

$$\psi_j = \sin\left(\beta_j y\right)\frac{\cosh\left[\beta_j(z+b)\right]}{\cosh\left[\beta_j(h+b)\right]} \tag{3.9}$$

where *h* represents the liquid fill height as shown in Fig. 3.1, and

$$\beta_j = \frac{(2j+1)\pi}{2a} \tag{3.10}$$

It should be noted that only anti-symmetric modes are considered in the analysis, since the symmetric modes are not generated in lateral motion of the container (Ibrahim, 2005). Coefficients A_{ij} and B_{ij} in Eq. (3.7) can thus be expressed as (Moiseev and Petrov, 1966):

$$A_{ij} = \int_{\Omega_0} \boldsymbol{\nabla}\psi_i \cdot \boldsymbol{\nabla}\psi_j d\Omega - \int_{\Delta\Omega} \boldsymbol{\nabla}\psi_i \cdot \boldsymbol{\nabla}\psi_j d\Omega, \qquad B_{ij} = \int_{\Sigma_0} \psi_i \psi_j dS - \int_{\Delta\Sigma} \psi_i \psi_j dS \tag{3.11}$$

in which Ω_0 and Σ_0 represent the fluid domain and the liquid free-surface in the rectangular tank, respectively; $\Delta\Omega$ denotes difference between Ω and Ω_0; and $\Delta\Sigma$ is the difference between Σ and Σ_0 (Fig. 3.1). Moiseev & Petrov (1966) have shown that A_{ij} in Eq. (3.11) can be expressed in a more convenient form as:

$$A_{ij} = \mu_i B_{ij} + \int_{\tau} \psi_j \frac{\partial \psi_i}{\partial n} dS \tag{3.12}$$

where $\frac{\partial \psi_i}{\partial n}$ is the derivative of eigenfunctions in the normal direction to the wall and μ_i are the eigenvalues of free liquid sloshing in the rectangular tank, given by (Abramson, 1966; Ibrahim, 2005;):

$$\mu_i = \beta_i \tanh[\beta_i(h+b)] \tag{3.13}$$

Substituting for ψ_j from Eq. (3.9) in Eq. (3.11), coefficients B_{ij} can be obtained from:

$$B_{ij} = \begin{cases} y_h - \dfrac{\sin(2\beta_i y_h)}{2\beta_i}, & i = j \\ \dfrac{a \sin\left(\dfrac{(i-j)\pi y_h}{a}\right)}{(i-j)\pi} - \dfrac{a \sin\left(\dfrac{(i+j+1)\pi y_h}{a}\right)}{(i+j+1)\pi}, & i \neq j \end{cases} \tag{3.14}$$

where y_h is the half-length of the free surface (Fig. 3.1). The determination of coefficients A_{ij} form Eq. (3.12) depends on the tank geometry, and could be obtained through numerical integration techniques. The natural frequencies and modes of lateral liquid slosh calculated from the above analysis are then incorporated into the multimodal solution to compute the velocity potentials in the fluid domain.

3.2.2 Multimodal solution

The general equation of linearized free-surface boundary condition for an ideal fluid in a rigid container (Fig. 3.1) can be written as (Abramson, 1966):

$$\frac{\partial^2 \Phi}{\partial t^2} + g \frac{\partial \Phi}{\partial z} = 0, \qquad \text{on } \Sigma \tag{3.15}$$

One may decompose the velocity potential Φ in the above equation into two parts; the potential Φ_R representing the rigid body motion of the fluid, which is the same as the potential of the container motion, and the potential Φ_S representing the liquid motion relative to the container, which is the potential of sloshing fluid. Therefore, substitution $\Phi = \Phi_R + \Phi_S$ into Eq. (3.15) yields:

$$\frac{\partial^2 \Phi_S}{\partial^2 t} + g\frac{\partial \Phi_S}{\partial z} = -\frac{\partial^2 \Phi_R}{\partial^2 t}, \qquad \text{on } \Sigma \tag{3.16}$$

Based on the multimodal approach, the sloshing potential is evaluated as a series of natural slosh modes and generalized functions R_i as:

$$\Phi_S = \sum_{i=0}^{N} R_i(t)\varphi_i \tag{3.17}$$

In case of lateral motion, the rigid body potential is represented by $\Phi_R = \dot{Y}y$, where $\dot{Y}$ is the lateral velocity of the container. Substituting for Φ_R and Φ_S into the Eq. (3.16), and considering Eq. (3.3), yields:

$$\sum_{i=0}^{N} \ddot{R}_i(t)\varphi_i + g\kappa_i \sum_{i=0}^{N} R_i(t)\varphi_i = -\ddot{Y}y, \qquad \text{on } \Sigma \tag{3.18}$$

Multiplying both sides of the above equation by φ_k, integrating over the free-surface and using the orthogonality condition $\int_\Sigma \varphi_i \varphi_k dS = 0, (i \neq k)$ (Luab, 2005) results in a uncoupled system of equations as:

$$\ddot{R}_i + \sigma_i^2 R_i = -\ddot{Y}\gamma_i \tag{3.19}$$

where

$$\gamma_i = \frac{\int_\Sigma y\varphi_i dS}{\int_\Sigma (\varphi_i)^2 dS} = \frac{2\sum_{j=0}^{N} a_{ij}\left[\frac{\sin(\beta_j y_h)}{{\beta_j}^2} - \frac{y_h \cos(\beta_j y_h)}{\beta_j}\right]}{\sum_{j=0}^{N}\sum_{p=0}^{N} a_{ij}a_{ip}B_{jp}} \tag{3.20}$$

The above set of ordinary differential equations is numerically solved to obtain generalized functions R_i, and thereby, the slosh potential Φ_S from Eq. (3.17).

To account for the effect of damping due to the viscous energy dissipation in the boundary layer, Eq. (3.19) may be written as:

$$\ddot{R}_i + 2\xi_i\sigma_i\dot{R}_i + \sigma_i^2 R_i = -\ddot{Y}\gamma_i \tag{3.21}$$

in which ξ_i is the damping ratio which can be estimated from the following empirical relationship for a general-shaped container [16]:

$$\xi_i = C_i\sqrt{\frac{\nu}{g^{1/2}(l)^{3/2}}} \tag{3.22}$$

where ν is the fluid kinematic viscosity, l is the characteristic dimension of the container and C_i is a coefficient that primarily depends on the tank geometry and fill condition. Faltinsen and Timokha (2010) calculated the coefficients C_i for liquid slosh in circular containers as:

$$C_i = \frac{l^{-1/4}\kappa_i^{-5/4}}{2\sqrt{2}} \int_S \left(\frac{\partial \varphi_i}{\partial s}\right)^2 dS \tag{3.23}$$

where $\frac{\partial \varphi_i}{\partial s}$ represents the tangential velocity at the wetted walls. Taking $l = \sqrt{ab}$ as the characteristic dimension of the tank, the damping ratio for two-dimensional slosh can be estimated from the following expression:

$$\xi_i = \frac{g}{2\sqrt{2ab}} \nu^{1/2} \sigma_i^{-5/2} \int_S \left(\frac{\partial \varphi_i}{\partial s}\right)^2 dS \tag{3.24}$$

3.2.3 Hydrodynamic pressure, sloshing force and moment

Once the sloshing potential Φ_S is calculated, the other quantities of practical interest such as hydrodynamic pressure as well as slosh force and moment can be computed in terms of time and spatial coordinates. The hydrodynamic pressure distribution, $P(y, z, t)$, on the container wall is derived upon substituting for φ_i from Eq. (3.5) into Eq. (3.17) and using the linearized Bernoulli's equation (Abramson, 1966), such that:

$$P(y, z, t) = -\rho \frac{\partial(\Phi_R + \Phi_S)}{\partial t} = -\rho \left\{ \ddot{Y} y + \sum_{i=0}^{N} \sum_{j=0}^{N} \dot{R}_i(t) a_{ij} \psi_j \right\}, \qquad \text{on } \tau \tag{3.25}$$

where ρ is the fluid density, ψ_j are the eigenfunctions of liquid slosh in the rectangular tank shown in Fig. 1 and is given by Eq. (3.9), and a_{ij} are the elements of the eigenvectors, obtained from Eq. (3.6).

The total lateral force, $F_y(t)$, acting on the container wall, per unit length of the container, is obtained from integration of hydrodynamic pressure over the tank wetted area, τ, such that:

$$F_y(t) = \int_\tau P dz = F_R(t) + F_S(t) \tag{3.26}$$

where F_R and F_S are the components of the lateral force that could be associated with the rigid body and sloshing motions of the liquid, respectively, expressed as:

$$F_R(t) = -\rho\ddot{Y}\int_\tau ydz = -m\ddot{Y} \tag{3.27}$$

$$F_S(t) = -\rho\sum_{i=0}^{N}\sum_{j=0}^{N}\dot{R}_i(\mathrm{t})a_{ij}I_j \tag{3.28}$$

in which m is the fluid mass per unit length of the tank and

$$I_j = \int_\tau \psi_j dz \tag{3.29}$$

The integral in the above equation can be computed using numerical techniques. It should be noted that the vertical component of the net slosh force is zero due to geometric symmetry.

The peak steady-state slosh force under a harmonic acceleration excitation $\ddot{Y}(t) = A_0\sin(\sigma t)$, where σ is the excitation frequency, can be obtained by representing the generalized coordinates R_i in terms of a harmonic functions of the form $R_i(t) = R_{0i}\cos(\sigma t + \alpha_i)$ with α_i being the phase angle. Substituting for $\ddot{Y}(t)$ and $R_i(t)$ in differential Eq. (3.21) leads to solutions for the unknown coefficients R_{0i} and phase angle α_i:

$$R_{0i} = \frac{-A_0\sigma\gamma_i}{\sqrt{({\sigma_i}^2-\sigma^2)^2+(2\zeta_i\sigma_i\sigma)^2}}\ , \quad \tan\alpha_i = \frac{2\zeta_i\sigma_i\sigma}{{\sigma_i}^2-\sigma^2} \tag{3.30}$$

The peak steady-state lateral force F_{0ss} from Eqs. (3.27) and (3.28) can thus be expressed as:

$$F_{0ss} = \left[\left(\rho\sigma\sum_{i=0}^{N}\sum_{j=0}^{N}R_{0i}a_{ij}I_j\cos\alpha_i - mA_0\right)^2 + \left(\rho\sigma\sum_{i=0}^{N}\sum_{j=0}^{N}R_{0i}a_{ij}I_j\sin\alpha_i\right)^2\right]^{\frac{1}{2}} \tag{3.31}$$

The overturning moment about the container bottom point *"B"*, M_B, (Fig. 3.1), per unit tank length, can be determined by integrating the moments resulting from the horizontal and vertical components of hydrodynamic forces:

$$M_B(t) = \int_\tau P[-ydy - (b+z)dz] \tag{3.32}$$

Substituting for pressure from Eq. (3.25) into the above equation yields the total overturning moment that may be decomposed into three components attributed to the rigid body moment (M_R), moment due to the vertical forces (M_V), and the moment resulted from the sloshing effect (M_S), i.e.:

$$M_B(t) = M_R(t) + M_V(t) + M_S(t) \tag{3.33}$$

It can be shown that the components of the overturning moment can be expressed in the following forms:

$$M_R(t) = \rho\ddot{Y}\int_\tau y(b+z)dz = m(b+z_{cg})\ddot{Y} \tag{3.34}$$

$$M_V(t) = \rho\ddot{Y}\int_\tau y^2 dy = \frac{2}{3}\rho {y_h}^3\ddot{Y} \tag{3.35}$$

$$M_S(t) = \rho\sum_{i=0}^{N}\sum_{j=0}^{N}\dot{R}_i(\mathrm{t})a_{ij}\,I_j^{'} \tag{3.36}$$

where z_{cg} in Eq. (3.34) denotes the location of the liquid center of gravity measured from the tank center (origin *O* in Fig. 3.1) and

$$I_j^{'} = \int_\tau y\psi_j dy + (b+z)\psi_j dz \tag{3.37}$$

M_V in Eq. (3.35) can be regarded as the overturning moment caused by the lateral shift in the liquid center of gravity, when the container is subjected to a constant lateral acceleration encountered during steady-turning of the vehicle. The quasi-static overturning moment may thus be calculated from Eqs. (3.34) and (3.35) as:

$$M_{B,qs} = \left(m\left(b+z_{cg}\right) + \frac{2}{3}\rho {y_h}^3\right)A_0 \tag{3.38}$$

where A_0 is the steady-state amplitude of the input lateral acceleration.

The peak steady-state overturning moment about the point *"B"*, M_{0ss}, can be obtained using Eqs. (3.30), (3.36) and (3.38), such that

$$M_{0ss} = \left[\left(\rho\sigma\sum_{i=0}^{N}\sum_{j=0}^{N}R_{0i}a_{ij}I_j^{'}\cos\alpha_i - M_{B,qs}\right)^2 + \left(\rho\sigma\sum_{i=0}^{N}\sum_{j=0}^{N}R_{0i}a_{ij}I_j^{'}\sin\alpha_i\right)^2\right]^{\frac{1}{2}} \tag{3.39}$$

3.2.4 Rollover threshold analysis of a partly-filled tank truck

The roll moment due to fluid slosh within a partly-filled tank, derived from the analytical model can be easily integrated to roll plane model of the vehicle to study the effect of dynamic fluid slosh on roll stability limits of the vehicle. For this purpose, a roll plane model of a six-axle tractor-semitrailer tank vehicle (Fig. 3.2a) is developed considering a single composite axle and

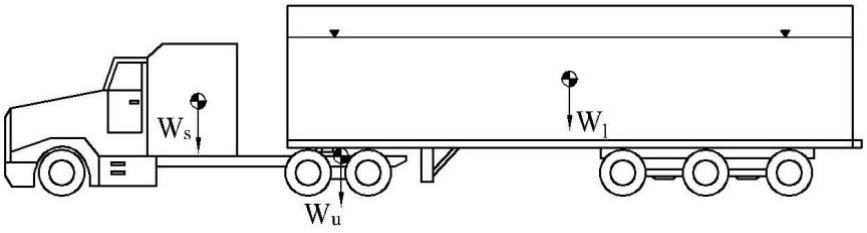

(a)

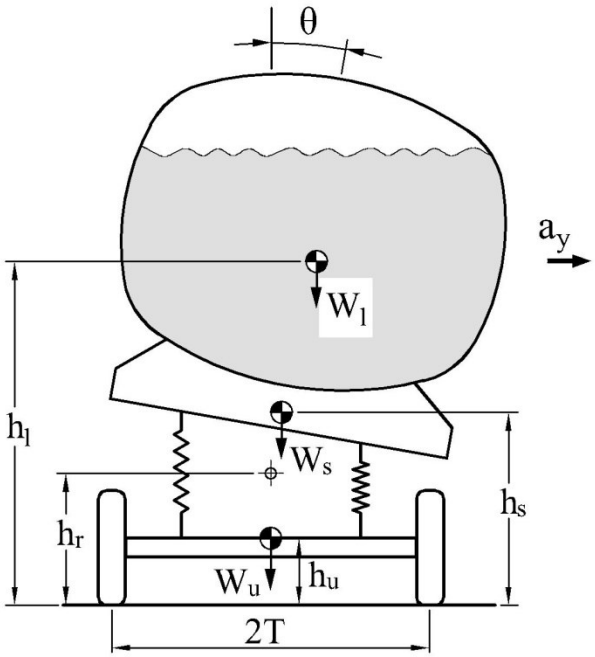

(b)

Fig. 3.2. (a) Schematic of a six-axle tractor-semitrailer tank vehicle. (b) Roll plane model of a suspended tank vehicle.

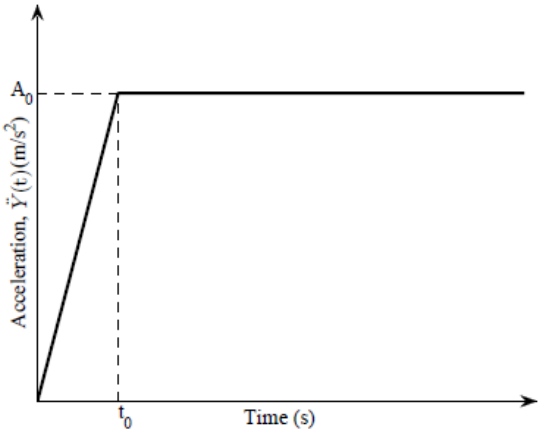

Fig. 3.3. Idealized lateral acceleration during a steady turning maneuver.

using the moment equilibrium equation (Yan *et al.*, 2005). Figure 3.2b shows a simplified roll plane model of the suspended tank vehicle assuming negligible roll motion of the unsprung mass. The total moment about the vehicle roll axis can be decomposed into four components; (i) primary overturning moment arising from the lateral acceleration, (ii) the roll moment caused by the lateral displacement of the sprung and cargo weights, (iii) the roll moment due to liquid motion in the tank, and (iv) the restoring roll moment resulted from the lateral load shift from inside wheels to the outside wheels. The rollover threshold is estimated as the maximum lateral acceleration that the vehicle can attain before the tires inside the turn lift off the ground. The total vehicle load is consequently sustained by the outer wheels at this relative rollover condition. Assuming small roll angles, the moment equilibrium equation about the roll center can be given by:

$$(W_s h_s + W_u h_u) a_y + M_d \theta + M_l = WT \tag{3.40}$$

In the above equation, W_s and W_u are the sprung and unsprung weights of the tank vehicle, respectively, W is the total weight of the vehicle including the cargo, h_s and h_u are the center of gravity heights of sprung and unsprung masses, respectively, θ is the sprung mass roll angle about the vehicle roll axis and T is half-track width (Fig. 3.2). In Eq. (3.40), M_l and a_y represent the total roll moment caused by the fluid motion about the roll center and the lateral acceleration corresponding to the wheel lift-off condition in g units, respectively, and M_d is the lateral displacement moment for unit roll angle, given by:

$$M_d = W_s(h_s - h_r) + W_l\left(h_l - h_r + \frac{2}{3}\frac{{y_h}^3}{V_l}\right) \tag{3.41}$$

where W_l is liquid cargo load, h_r is roll center height, h_l is center of gravity height of the liquid cargo within the tank, and V_l is liquid cargo volume per unit length of the tank. Furthermore, the rolling resistance moment due to the suspension system is related to the restoring moment as:

$$k_s \theta = WT - W a_y h_r + W_u a_y (h_r - h_u) \tag{3.42}$$

where k_s is equivalent roll stiffness due to suspension. Substituting for θ from Eq. (3.42) into Eq. (3.40) and some manipulations lead to the following moment equilibrium expression:

$$a_y\left[W_s h_s + W_u h_u + \frac{M_d}{k_s}(W_u(h_r - h_u) - W h_r)\right] + M_l = WT\left(1 - \frac{M_d}{k_s}\right) \tag{3.43}$$

The analyses are performed under a ramp-step lateral acceleration input, $\ddot{Y}(t)$, as shown in Fig. 3.3 with $t_0 = 0.5\ s$. The moment due to moving liquid cargo, M_l, is initially obtained from the

analytical slosh model, which is subsequently applied to Eq. (3.43) to derive a_y which may not be equal to the steady value of $\ddot{Y}(t)$. The magnitude of $\ddot{Y}(t)$ is gradually increased until a_y approaches steady value of $\ddot{Y}(t)$ satisfying the roll moment equilibrium of the vehicle. The solution are obtained by considering the first peak value of $M_l(t)$. Such a solution, however, would yield an extreme value of the rollover threshold since it assumes sustained level of the peak moment. The above equation is also solved to obtain quasi-static rollover threshold limits by considering the quasi-static components of the roll moment alone.

3.3 Results and discussion

The analytical model of liquid sloshing, presented in section 3.2, is employed to solve the problem of lateral liquid sloshing in four different tank cross-sections: circular, elliptical, modified-oval and Reuleaux-triangle, as shown in Fig. 3.4. The modified-oval tank cross-section consists of eight circular arcs, symmetric about the vertical and horizontal axes. The Reuleaux-triangle tank cross-section also comprises eight circular arcs but it is symmetric only about the vertical axis. The dimensions of the four tanks are selected so as to achieve identical volume per

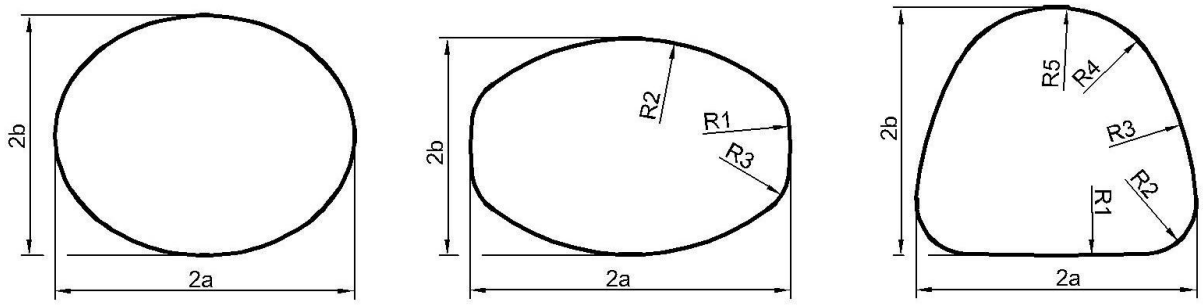

Fig. 3.4. (a) Elliptical (or circular when a=b); (b) modified-oval; and (c) Reuleaux-triangle tank geometries.

Table 3.1. Normalized dimensions of tank geometries.

	Modified-oval	Reuleaux-triangle	Circular	Elliptic
b/a	0.676	0.881	1.0	0.8
R_1/a	1.459	1.591		
R_2/a	1.459	0.749		
R_3/a	0.320	2.437		
R_4/a	-----	0.365		
R_5/a	-----	23.383		

unit length. The dimensions normalized with respect to the tank width are presented in Table 3.1. For the Reuleaux-triangle and modified-oval cross-sections, the intersection between the mean free surface and the tank wall is calculated as a function of fill height to determine the limits of integrations on the tank wall and the free-surface length. The liquid slosh responses are obtained for different fill heights and compared with the reported measured data and those obtained from the available analytical solutions in order to illustrate validity of the multi-modal approach. Considering the same cargo load, the effect of fill volume and tank cross-section on the slosh force and overturning moment are further evaluated and discussed. The roll plane vehicle model developed in section 3.2.4 is subsequently used to investigate the effect of dynamic slosh on roll stability limits of a heavy vehicle with different cross-section tanks.

3.3.1 Validations

In the first verification stage, the normalized natural frequencies of fluid slosh ($\lambda = \sigma^2\sqrt{ab}/g$; a=b) for circular tanks are compared with those reported in McIver (1989). Table 3.2 presents the first three anti-symmetric natural slosh frequencies for two different fill levels (40% and 80%). The fill level is expressed as ratio of the fill height to overall tank height ($2b$). The first three normalized natural frequencies with respect to the fill level are also compared with those reported by McIver (1989) in Fig. 3.5. The results are in very good agreement with the reported values, irrespective of the fill level considered. Fundamental slosh frequencies for three different fill volumes of the Reuleaux-triangle tank are also compared with the experimental data and those from the CFD analysis (Yan, 2008; Yan *et al.*, 2009) in Table 3.3. The experimental measurements have were performed with a scaled tank (cross-section area =0.426 m^2; length =1.85 m). The width of the tank was 774.45 mm, which is approximately $^1/_3$ of a typical full scale tank. The results show good agreements for the all compared fill volumes. Similar to the circular tank, fundamental frequency increases monotonically with the fill volume.

Table 3.2. Comparisons of normalized natural slosh frequencies, $\boldsymbol{\lambda = \sigma^2\sqrt{ab}/g}$, of slosh within partly filled circular tanks (a=b) with the analytical solutions of McIver (1989).

	Fill level=40%			Fill level=80%		
	λ_1	λ_2	λ_3	λ_1	λ_2	λ_3
Present study	1.2612	4.6327	7.8814	2.1266	6.1404	10.0813
McIver (1989)	1.2461	4.6067	7.8537	2.1237	6.1393	10.0807

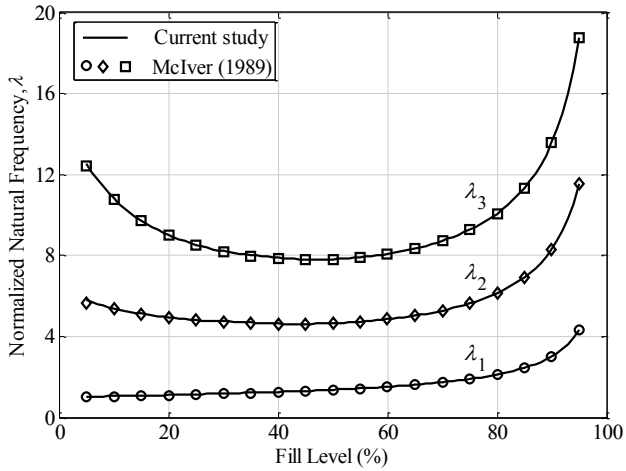

Fig. 3.5. Comparison of first three normalized natural frequencies of liquid slosh in a partly-filled circular tank as a function of fill level with those reported by McIver (1989).

Table 3.3. Comparison of fundamental frequency of liquid slosh (Hz) in a Reuleaux-triangle tank with reported experimental and CFD results.

Fill volume (%)	Present study	Experiment (Yan *et al.*, 2009)	CFD (Yan, 2008)
30	0.793	0.813	0.78
50	0.961	1.000	0.96
70	1.101	1.125	1.08

The range of validity of the linear slosh model is also examined by comparing the slosh force and overturning moment responses with the reported experimental data in Figs. 3.6a and 3.6b. The peak steady-state lateral force responses, normalized with respect to mA_0, are compared with those measured by Strandberg (1978) for half-full circular and elliptical tanks containing fuel oil (ρ=920 kg/m^3, υ=9×10^{-4} m^2/s) under harmonic lateral excitations (amplitude, A_0≈0.214g) at different frequencies, σ. The tank dimensions used in the experimental study were a=b=0.95 m for the circular tank (Fig 3.6a) and a=1.13 m, b=0.735 m for the elliptical tank (Fig. 3.6b). The excitation frequency σ is normalized with respect to the first natural sloshing frequency σ_1. The steady-state lateral forces obtained from the linear fluid slosh model are in good agreement with the measured data except near the fundamental slosh frequency, where analytical predictions yield considerably higher values than the measurements. The observed discrepancies near the resonant frequencies can be attributed to strongly nonlinear free-surface deformations, which cannot be predicted by the linear models.

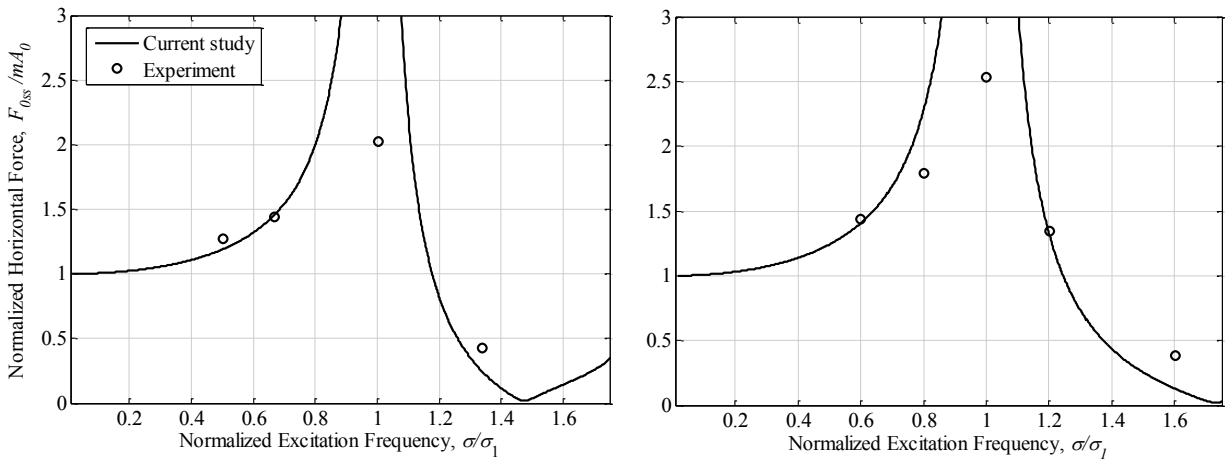

Fig. 3.6. Comparisons of normalized peak steady-state lateral force due to fluid slosh under harmonic excitations with the experimental data reported in Strandberg (1978): (a) circular tank, a=b=0.95 m; and (b) elliptical tank, a=1.13 m, b=0.735 m.

Normalized peak steady-state lateral force and overturning moments due to the liquid sloshing in a partially filled Reuleaux-triangle tank are also compared with the experimental measurements reported by Yan (2008) in Fig. 3.7. The experimental study was conducted for a water-filled scale tank (width = 774.45 *mm;* length = 1.85 m) with three different fill volumes; 30% (Figs. 7a,b), 50% (Figs. 3.7c,d) and 70% (Figs. 3.7e,f). The results are compared for three different amplitudes of harmonic lateral acceleration excitations (A_0= 0.051g, 0.102g and 0.204g). It should be noted that normalized slosh force and overturning moment obtained from the linear analysis are independent of the lateral acceleration amplitude, since these are linear functions of the imposed acceleration, as seen in Eqs. (3.27), (3.28) and (3.34)-(3.36). As seen in Fig. 3.7, the analytical results are in satisfactory agreement with the experimental data for the fill conditions considered, while notable discrepancies are observed near the fundamental slosh frequency. Furthermore, the differences between the analytical and measured results near the resonant frequency increase with increase in the fill volume as well as the excitation amplitude. Indeed, the effect of nonlinearities in the free-surface is much stronger near the resonant frequency, which tends to be higher under higher excitation amplitude and fill level. These suggest strong dependence of the slosh force and moment responses on the excitation amplitude and frequency, which is also evident from the experimental data in Fig. 3.7. The free-surface motion also depends on the fill volume. A higher fill volume leads to higher free surface velocity (Faltinsen and Timokha, 2010) and thus relatively greater deviations from the experimental data,

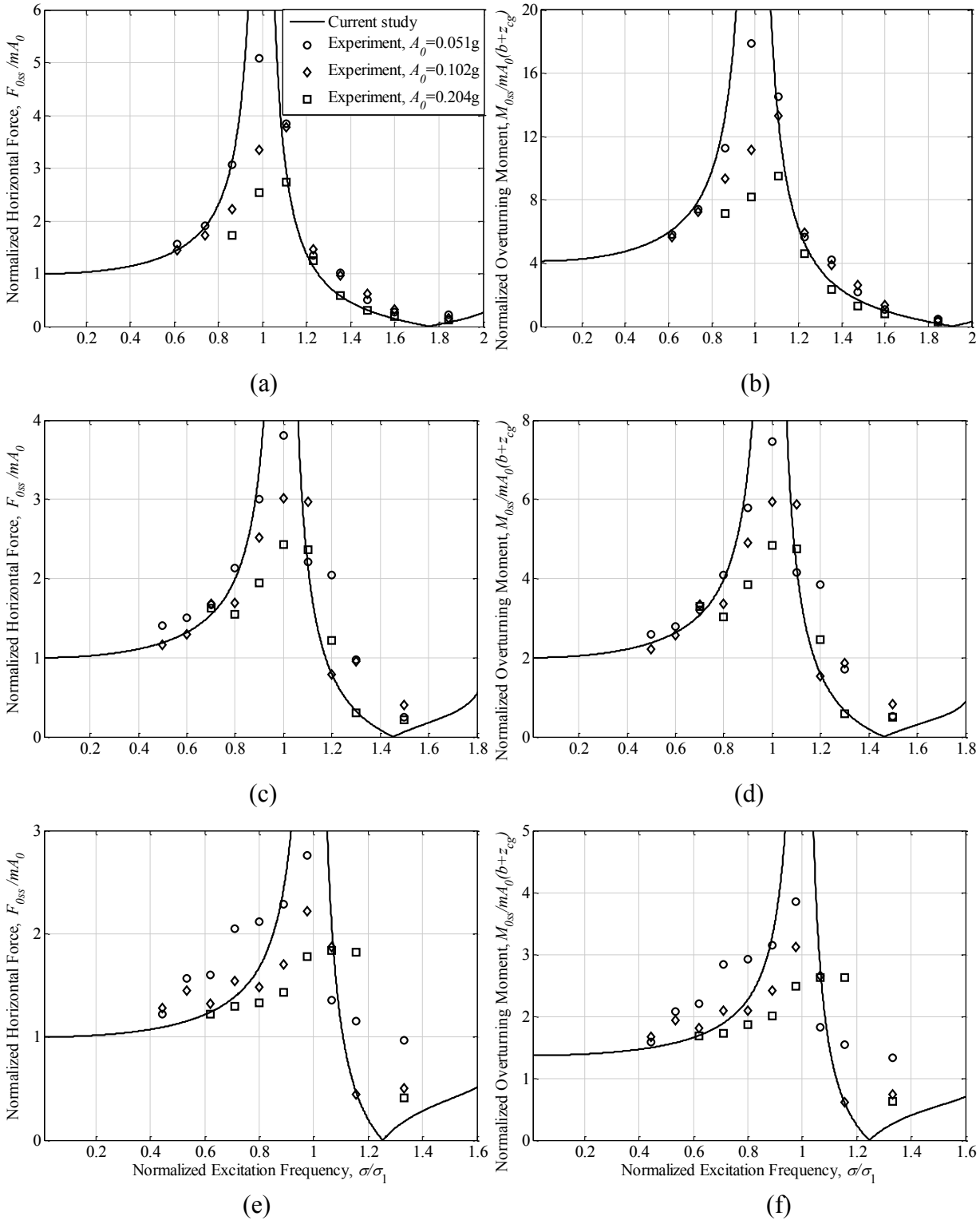

Fig. 3.7. Comparison of normalized peak steady-state lateral slosh force and overturning moment responses for partly-filled Reuleaux-triangle tank with the experimental results reported in Yan (2008): (a,b) 30%; (c,d) 50%; and (e,f) 70% fill volume.

as seen in Figs. 3.7e and 3.7f. Moreover, the normalized slosh force and moment decrease with increasing fill volume, which demonstrates that the relative contribution of the slosh components F_S and M_S in the total lateral force and overturning moment decrease under higher fill volumes. This is attributable to the relatively limited motion of the free surface in such a tank under high fill volumes or reduced critical slosh length.

3.3.2 Comparison of liquid slosh in different cross-section tanks

The effect of tank cross-section on the lateral force and roll moment due to liquid movement are evaluated under harmonic lateral acceleration excitations. The responses for the selected water-filled tanks with identical cross-section area (3.24 m^2) and cargo load are compared in Fig. 3.8. The figures show normalized peak steady-state lateral force and overturning moment responses of the four tank geometries (Table 3.1) with four different fill volumes: 30% (Fig. 3.8a,b), 50% (Fig. 3.8c,d), 70% (Fig. 3.8e,f) and 90% (Fig. 3.8g,h). In order to obtain appropriate factors for comparing the responses of different cross-section tanks with identical volume, the peak steady-state lateral force and overturning moment about the tank bottom *"B"* are normalized in the form, $\frac{F_{0ss}}{mA_0}$ and $\frac{M_{0ss}}{mA_0\sqrt{V_l}}$, respectively, where V_l is liquid volume per unit length of the tank. Although the responses are evaluated for the 3.24m^2 area tanks, the normalized responses are equally applicable for tanks with different volumes considering negligible effect of fluid viscosity. Moreover, the steady-state responses in Fig. 3.8 are presented as function of frequency normalized with respect to fundamental slosh frequency of each tank, $\frac{\sigma}{\sigma_1}$.

It can be seen from Fig. 3.8 that magnitudes of normalized steady-state lateral slosh force and overturning moment decrease with increasing fill volume for all frequency ratios, irrespective of the tank geometry. This suggests relatively limited slosh motion under higher fill volumes. The normalized lateral slosh forces are almost identical in all tank cross-sections up to the frequency ratio $\frac{\sigma}{\sigma_1} = 0.4$, while above this frequency ratio, the Reuleaux-triangle tank exhibits the lowest lateral slosh force under all fill volumes, as shown in Figs. 3.8a,c,e,g. The steady-state lateral force responses of the circular tank are also comparable with those of the Reuleaux-triangle tank under low and intermediate fill volumes. The highest lateral force is

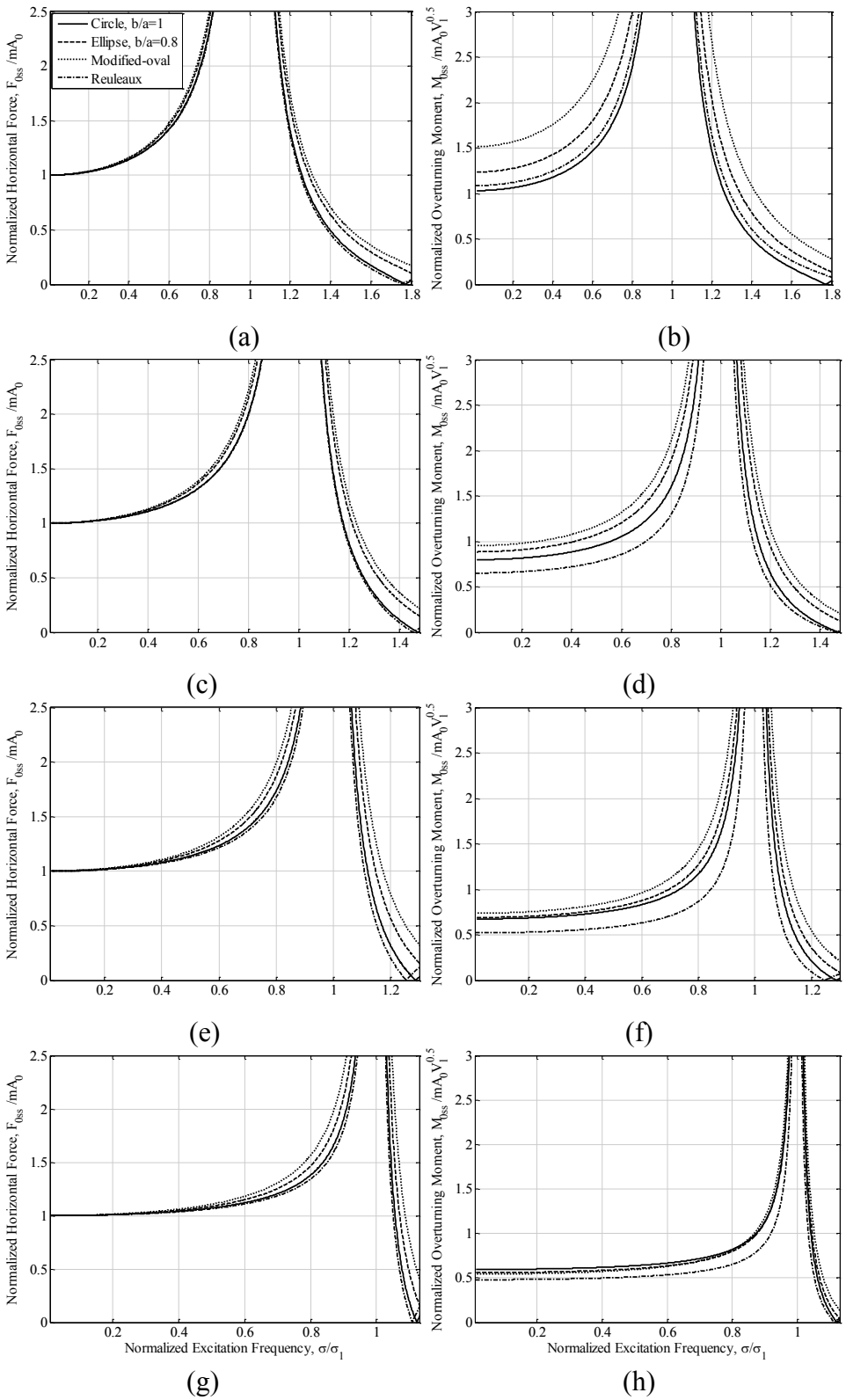

Fig. 3.8. Normalized peak steady-state lateral force and overturning moment responses due to fluid motion within different cross-section tanks subject to lateral harmonic excitations: (a,b) 30%; (c,d) 50%; (e,f) 70% ; and (g,h) 90% fill volume.

observed in the modified-oval tank, irrespective of fill volume. In the Reuleaux-triangle tank, the free surface length is decreases with increasing fill volume, which helps limit the lateral liquid slosh and thereby yields the lowest normalized lateral slosh force, particularly under high fill volumes. The modified-oval and elliptical tank geometries, on the other hand, exhibit relatively greater free-surface length compared to the Reuleaux and circular tanks, and thus result in higher liquid motion and greater lateral slosh force.

The lowest normalized steady-state overturning moment is observed for the circular tank under 30% fill volume, the Reuleaux tank yields lowest moment under higher fill volumes in the entire frequency range, as shown in Figs. 3.8b,d,f and h. The highest normalized overturning moment occurs for the modified-oval tank for all the fill volumes considered, except for 90%. The overturning moment due to sloshing liquid load is dependent upon the lateral force and the lateral load shift and thus the magnitude of liquid slosh. Considering that the modified-oval and elliptic tanks yield higher magnitudes of lateral force and higher liquid slosh, these tanks generally cause higher overturning moment magnitudes. This is attributable to the relatively higher free-surface length in these tanks, which not only causes greater liquid load shift but also contributes to higher amplitude slosh motion of the liquid. This is despite the fact that the cargo center of gravity height in these tanks is lower compared to the circular tank with same fill volume, as shown in Fig. 3.9. The Reuleaux-triangle tank with lower cargo center of gravity height together with limited free-surface length results in the lowest normalized overturning moment under intermediate to high fill volumes. Whereas Kang *et al.* (2000b) proposed Reuleaux-triangle cross-section tank as the optimal tank geometry on the basis of quasi-static liquid motion (mean-steady state response), the present analysis further confirms that the Reuleaux cross-section can also be regarded as favourable in the presence of dynamic liquid slosh under intermediate and high fill volumes.

The analytical liquid slosh model is also used to study the relative performance of different tanks subject to a lateral acceleration excitation idealizing a steady-turning maneuver (Fig. 3.3). For this purpose, the selected tank cross-sections with identical total volume of 3.24 m^3/m water are considered to evaluate maximum lateral slosh force and overturning moment encountered under the same excitation. The results are obtained over a normalized time interval $\hat{t}_0 = 1.57/\sqrt{g/\sqrt{ab}}$. Figure 3.10 shows variations in the peak normalized lateral force $\frac{F_{y,max}}{mA_0}$ and

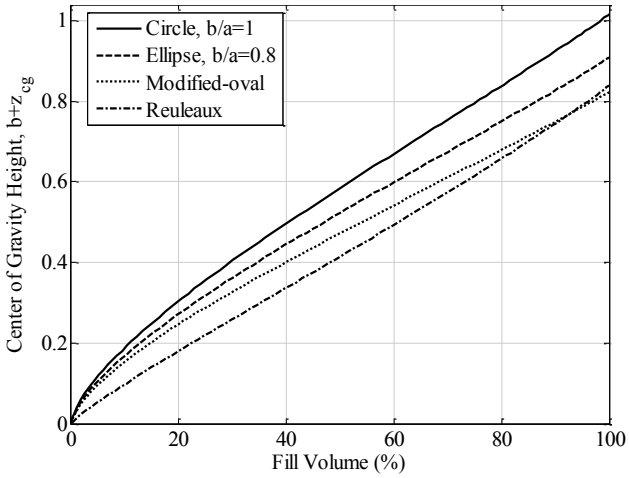

Fig. 3.9. Center of gravity height from the tank bottom point for different cross-sections.

overturning moment $\frac{M_{B,max}}{mA_0\sqrt{V_l}}$ developed due to liquid slosh in the selected four tank cross-sections as a function of the fill volume. As stated earlier, the normalized responses can be considered independent of the tank volume due to negligible viscosity effect. The results from Fig. 3.10a suggest that, regardless of the tank geometry, the normalized lateral force reduces with the fill volume in a nearly linear manner. Indeed, an increase in the fill volume would result in greater proportion of non-sloshing mass together with reduced free surface length and thus relatively less intensive slosh motion under high fill volumes. The lowest normalized lateral slosh force is obtained for the Reuleaux tank in the entire fill range, while the highest peak forces occur for elliptical and modified-oval tanks under all fill volumes, which implies that the slosh is more limited in the Reuleaux-triangle tank than other cross-section tanks. The maximum difference between the normalized lateral slosh forces for different tanks corresponds to 70 to 80% fill volumes, where the peak forces in modified-oval and circular tanks are about 15% and 8%, respectively, greater than those obtained for the Reuleaux-triangle tank.

As it can be seen from Fig. 3.10b, the normalized peak overturning moment initially decreases sharply with increase in fill volume and then reduces lightly with increasing fill volumes for all the cross-sections considered in the study. The circular tank yields lowest normalized overturning moment for fill volumes up to 32%, while above this fill volume the lowest values are associated with the Reuleaux-triangle tank. Although the cargo center of gravity height in partially-filled modified-oval and elliptical tanks are lower than that in the circular tank with same fill volume (Fig. 3.9), the overturning moments for the modified-oval

and elliptical tanks are greater up to fill volumes 86 and 83%, respectively. This is attributed to the greater liquid load shift in addition to the higher amplitude slosh motion in relatively wider elliptic and modified-oval tank geometries. Under very high fill volumes, where the effect of liquid slosh is insignificant, the higher center of gravity in the circular tank causes greater overturning moment compared to other cross-sections. For the Reuleaux tank, the lower center of gravity height in addition to the relatively limited slosh motion in intermediate and high fill volumes results in lowest overturning moment in the 32 to 97% fill volume range.

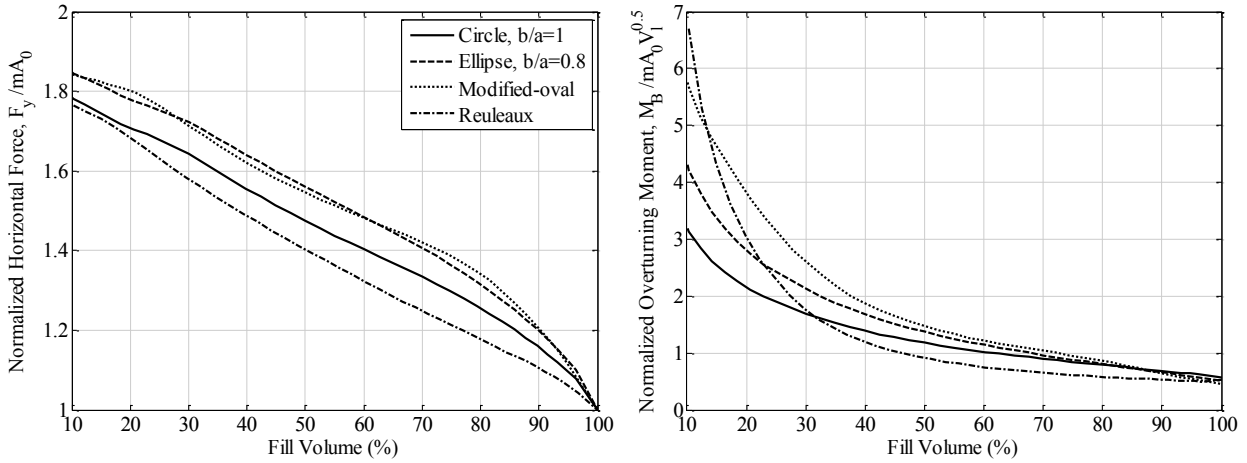

Fig. 3.10. Comparisons of peak (a) normalized lateral force and (b) overturning moment developed due to lateral slosh in partly-filled different cross-section tanks subject to lateral acceleration excitation idealizing a steady-turning maneuver.

3.3.3 Effect of dynamic liquid slosh on roll stability of tank trucks

The roll moment equilibrium equation for the roll-plane vehicle model (section 3.2.4) is solved to investigate the relative static roll stability limits of the vehicle with selected tank cross-sections. The candidate vehicle is a six-axle tractor-semitrailer tank vehicle whose parameters are summarized in Table 3.4. The analysis is performed considering the tanks with total volume of 3.24 m^3/m. The steady-turning rollover threshold limits are evaluated considering two different loading conditions: (i) constant cargo load irrespective of the fill level, a condition encountered in general purpose fleets transporting liquid products of varying mass density; and (ii) varying cargo load under different fill levels, a condition occurring in vehicles during delivery routes. In the latter case, the cargo load is varied from 0 to 338 kN with fill level

ranging from 0 to 100%, for a fuel oil (ρ = 850 kg/m^3; ν=1.02×10^{-4} m^2/s). For the constant cargo load analysis (338 kN), liquid cargos with different mass density are considered, while the fill level is permitted to vary from 50 to 100%.which represents the general-purpose liquid bulk transportation, where the maximum cargo load is limited by the regulatory axle load limits.

Table 3.4. Simulation parameters of the six-axle tractor-tank-semitrailer vehicle model.

Sprung Weight (empty tank), W_s	120900 N
Unsprung Weight, W_u	47596 N
Center of gravity height of the sprung mass, h_s	1.12 m
Center of gravity height of the unsprung mass, h_u	0.536 m
Roll center height, h_r	0.725 m
Tank bottom height	1.1m
Tank length	12.5 m
Half track width, T	0.813 m
Roll stiffness, k_s	1110 kNm/rad

The rollover threshold limits of the vehicle with different tank cross-sections considering dynamic fluid slosh are compared with those obtained from the quasi-static analysis in Figs. 3.11a,c,e and g for the variable cargo load and in Figs. 3.11b,d,f and h for the constant cargo load. The limits are also compared with those derived for an equivalent rigid cargo vehicle. The results suggest that rollover threshold acceleration limits of the partially-filled tank vehicle derived from the quasi-static analysis are substantially lower than those of the equivalent rigid cargo vehicle, irrespective of the tank cross-section and loading condition considered. These results are in close agreement with those reported in Rakheja *et al.* (1988).

Consideration of overturning moment due to dynamic fluid slosh, derived from the analytical model, yields even lower threshold limits for both the loading conditions, irrespective of the fill level and tank cross-section. In the variable cargo load case, increasing the fill volume yields higher cargo load and higher center of gravity height, which causes substantially greater reduction in the rollover limits for both the rigid and liquid cargo vehicles, as shown in Figs. 3.11a,c,e and g. The decrease, however, is significantly larger under intermediate fill ranges, when overturning moment due to dynamic slosh is considered. With higher fill levels, where the effect of dynamic fluid slosh tends to diminish, the rollover limits increase gradually with the fill level and approach those of the equivalent rigid cargo vehicle. For the variable cargo load

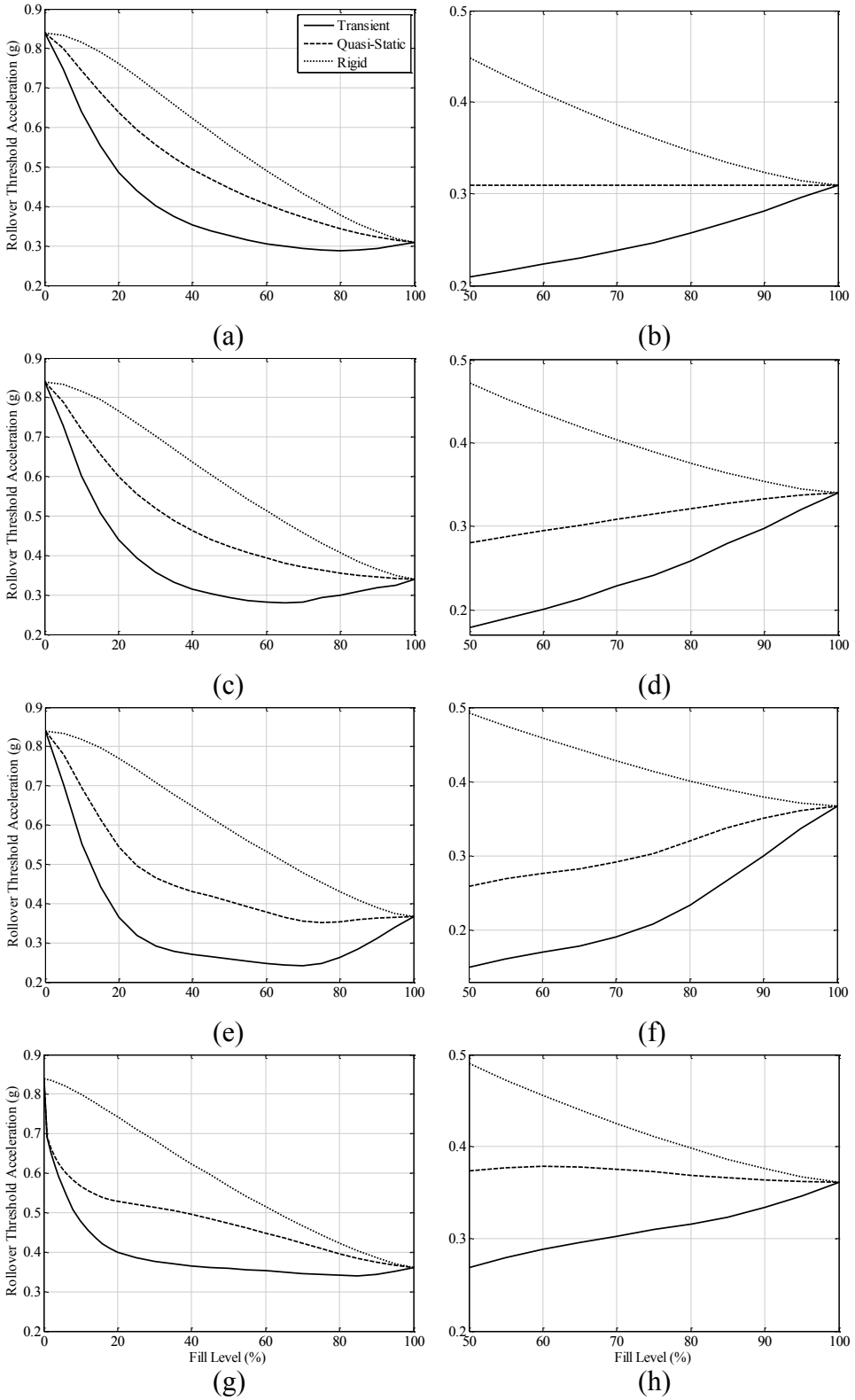

Fig. 3.11. Comparisons of roll stability limits of the equivalent rigid and liquid cargo vehicles with different cross-section tanks considering quasi-static and dynamic liquid slosh, and variable and constant cargo load conditions:(a,b) circular; (c,d) elliptical; (e,f) modified-oval; and Reuleaux-triangle tank cross-section.

condition, the lowest rollover limits of the vehicle with the circular, elliptical, modified-oval and Reuleaux tanks are obtained as 0.29g (fill level=86%), 0.28g (fill level=68%), 0.24g (fill level=74%) and 0.34g (fill level=92%), respectively.

For the equivalent rigid cargo vehicle with constant cargo load, higher fill levels cause higher center of gravity height and thus lower rollover acceleration limits, irrespective of tank geometry, as shown in Figs. 3.11b,d,f and h. The acceleration limits obtained from the quasi-static analysis for the elliptical and modified-oval tanks increase with fill levels, despite the increase in cargo center of gravity height. This is attributable to lower additional overturning moment under higher fill levels due to lower liquid load shift. For the circular tanks, however, the reduction in the overturning moment is balanced by the center of gravity height, which causes the quasi-static rollover limits to remain constant over the entire fill range. The quasi-static rollover limit also tends to be almost constant for the Reuleaux tank over the entire fill range. The additional moment associated with dynamic fluid slosh, however, further deteriorates the roll stability limits. Lower fill conditions yield a lower center of gravity, which would be expected to result in enhanced stability limits. The greater magnitudes of additional overturning moments, however, cause lower roll stability limits because the slosh motion and quasi-static cargo load shift exceed the gains attributed to lower center of gravity height. This clearly indicates the adverse effect of dynamic liquid motion on the rollover limits under partial fill conditions.

Figure 3.12 compares the rollover threshold accelerations of the vehicle with different tank cross-sections considering dynamic fluid slosh as a function of the liquid fill volume for variable as well as constant load conditions. For the variable cargo load, the highest rollover limits are obtained for the vehicle with a circular tank up to the fill volume of 29%, while above this fill volume the highest values are achieved with the Reuleaux-triangle tank, as shown in Fig. 3.12a. The lowest values of rollover threshold accelerations are achieved for the vehicle with the modified-oval tank in the 5% to 91% fill volume range. The relative advantages of the low center of gravity height elliptical and modified-oval tanks over the circular tank could be seen under very high volumes (>79% for elliptical tank and >91% for modified-oval), as seen in Fig. 3.12a.

For the constant cargo load, the rollover limits for the vehicle carrying the Reuleaux tank show the highest roll stability limits over nearly entire fill volume range, as seen in Fig. 3.12b.

The greatest differences among the roll stability limits are observed around the intermediate fill volumes, where the rollover limits of the vehicle with the Reuleaux tank are about 25%, 40% and 60% higher than those of the vehicle with the circular, elliptic and modified-oval tanks. Similar to the variable cargo load, lower center of gravity heights of elliptical and modified-oval tanks compared to the circular tank result in relatively higher rollover limits of the vehicle with these tanks under high fill volumes. These limits, however, are lower than those of the vehicle with the Reuleaux tank.

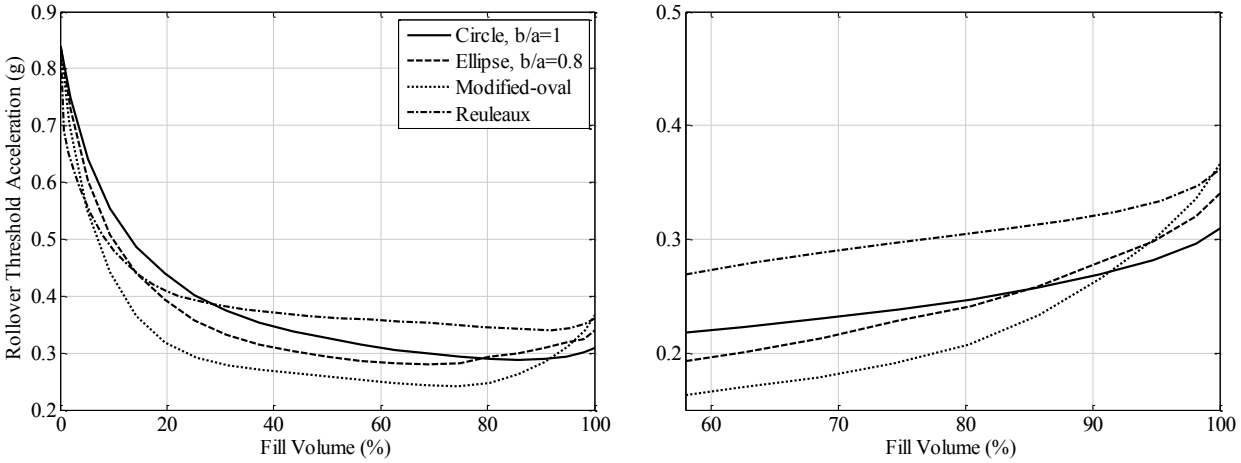

(a) (b)

Fig. 3.12. Comparison of rollover threshold acceleration obtained using the analytical fluid slosh model for a heavy tank vehicle of different cross-sections under (a) variable; and (b) constant cargo load conditions.

3.4 Conclusions

A mathematical model, based on linear multi-modal method, was developed for analysis of transient liquid sloshing in laterally excited containers of different cross-sections and partially filled to an arbitrary depth. The method resulted in accurate estimations of the hydrodynamic loads by considering only a few lower natural modes for implementations in the potential flow equations, since the higher modes are strongly damped and their contributions are negligible. The multimodal approach is thus substantially more efficient compared with direct numerical solutions, which require a boundary-value problem to be solved at each time step. Unlike the CFD based dynamic slosh models, the proposed model could be easily integrated to multi-body

vehicle dynamics programs to investigate the direction response characteristics of partly-filled tank trucks and tank-semitrailer combinations, in a highly efficient manner. Comparisons with the experimental results revealed relatively good agreements except in the vicinity of the fundamental natural slosh frequency, where the linear theory cannot predict slosh motions of the liquid.

The results also demonstrated the overall effectiveness of the Reuleaux-triangle cross-section tank in suppressing the liquid slosh under intermediate to high fill volumes. This was mostly attributable to the lower free surface length and center of gravity height of the Reuleaux-triangle cross-section. Analysis of a vehicle roll plane model integrating the dynamic roll moment due to the fluid slosh clearly showed substantially lower steady-turning rollover threshold of the partly-filled vehicle compared to those obtained from the widely-used quasi-static analysis. This was attributed to transient motion of the liquid within the tank. The highest rollover threshold accelerations were obtained for the vehicle with the Reuleaux-triangle tank, particularly under intermediate and high fill volumes under both variable and constant cargo load conditions. The threshold values obtained in the study, however, represent the lower limit since the moment equilibrium is based on the peak slosh moment. The dynamic roll stability and directional performance characteristics of partly-filled tank vehicles could be evaluated through dynamic simulation of the vehicle model integrating the multi-modal fluid slosh model proposed in this study.

CHAPTER 4

A COUPLED MULTIMODAL AND BOUNDARY-ELEMENT METHOD FOR ANALYSIS OF ANTI-SLOSH EFFECTIVENESS OF PARTIAL BAFFLES IN A PARTLY-FILLED CONTAINER

4.1 Introduction

It is known that liquid oscillations in partially filled tank vehicles subject to excitations during braking and/or steering cause undesirable hydrodynamic forces and moments of significant magnitude. Such forces and moments adversely affect the direction dynamics and stability of the partly-filled vehicle and may impose higher stresses on the container structure. Anti-slosh devices such as transverse baffles are widely used in order to limit the adverse liquid slosh effect on directional performance and stability of the tank vehicles. While the effects of ring and radial baffles on liquid slosh suppression in missiles and storage tanks has been extensively studied (e.g., Abramson, 1966; Ibrahim, 2005), the role of baffles in limiting fluid slosh in tank trucks has been addressed in relatively fewer studies. Furthermore, the regulations governing design of tanks recommend the use of baffles only for circumferential reinforcement of the tank shell with little or no consideration of fluid slosh effects on lateral or roll stability limits of tank vehicles (CFR 49, part 178, 2011; CAN/CSA B620, 1987). Capital cost reductions and difficulty associated with cleaning of the tank in a general-purpose road tanker fleet are the main reasons that prohibit the use of baffles.

The effects of fluid movement within the tank on directional performance and roll stability of partly-filled tank trucks and tractor-tank-trailer combinations have been investigated using widely different methods. The vast majority of these have provided vehicle steering and braking responses considering steady-state fluid slosh (e.g., Ranganathan *et al.*, 1990; Kang *et al.,* 2000a). This approach, however, cannot provide the transient slosh forces and moments, whose magnitudes are known to be substantially greater than the corresponding steady state values. Analogous mechanical-equivalent and pendulum models have also been proposed to study the transient fluid slosh effects on vehicle responses (e.g., Ranganathan *et al.*, 1993b,

1994). Both the steady-state and mechanical analogous models cannot be applied to analyses of fluid slosh within tanks with baffles, which are known to provide substantial slosh damping.

A few studies have employed linear slosh theory for analysis of anti-slosh effects of baffles. Goudarzi and Sabbagh-Yazdi (2012) developed an analytical model based on potential flow and linear slosh to evaluate damping effects of horizontal and vertical baffles in rectangular tanks. Faltinsen *et al.* (2010) and Faltinsen and Timokha (2011) presented analytical solutions for free liquid slosh in rectangular tanks with a slat screen mounted vertically in middle of the tank. The effect of solidity ratio of the baffle on lateral sloshing was also investigated using a multimodal approach. Hasheminejad and Mohammadi (2011) obtained natural slosh frequencies and pressure modes of free liquid sloshing in a circular tank with surface-touching horizontal baffles, bottom-mounted and surface-piercing vertical baffles using successive conformal transformations of the fluid domain. A similar method has also been used to obtain slosh force and overturning moment in half-filled elliptical containers equipped with vertical or horizontal side baffles under a lateral acceleration excitation (Hasheminejad and Aghabeigi, 2011, 2012). The damping effect of the baffles was neglected, while the method involved elaborate successive transformations of the fluid domain using special functions.

Apart from the analytical models, computational fluid dynamics (CFD) techniques have been widely applied for simulation of liquid slosh in baffled tanks. Modaressi-Tehrani *et al.* (2007) developed a three-dimensional model of a partly-filled cylindrical tank with three conventional baffles with a centrally-located single-orifice to obtain transient slosh forces and moments under longitudinal and combined lateral/longitudinal accelerations idealizing braking and turning excitations. Yan *et al.* (2008, 2010) simulated three-dimensional liquid slosh in a 'Reuleaux triangle' cross-section tank with different transverse baffles designs under similar lateral and/or longitudinal acceleration excitations. The results showed that conventional transverse baffles offer significant suppression of longitudinal slosh force and pitch moment, but offer only little resistance to fluid slosh under lateral excitations arising from the steering maneuvers.

The applications of CFD methods for assessing the fluid slosh effects on braking and steering dynamics of partly-filled tank trucks, however, have been limited to a very few studies. This is likely due to extreme computational demands, and complexities involving elaborate data

transfers and coordinate transformations between the vehicle and the dynamic fluid slosh models (Rumold, 2001; Biglarbegian and Zu, 2006; Yan and Rakheja, 2009). In an attempt to develop computationally efficient coupled vehicle-fluid slosh dynamic models, a few studies have characterized the dynamic fluid slosh in moving containers under lateral and longitudinal accelerations through mechanical analogous models. While the simplicity of the mechanical equivalent models could permit real-time simulations of directional responses of a partly-filled tank vehicle, the identification of equivalent mechanical model parameters poses certain complexities. The model parameters are generally estimated from experimental data (Ibrahim, 1999) or slosh responses obtained through CFD simulations (Salem *et al.*, 2009). Such models, however, have been mostly limited to clean-bore tanks with only one exception (Ibrahim, 1999).

Among the different methods employed for simulation of dynamic fluid slosh, the methods based on linear slosh theory could yield reasonably accurate predictions of slosh forces and moments over the ranges of typical vehicle maneuvers in a highly efficient manner (Kolaei *et al.*, 2014). The multimodal models integrating linear slosh theory seem to be beneficial and practical due to the simplicity associated with their integration to the vehicle dynamic models. The multimodal studies of liquid slosh in tanks used in liquid transporting vehicles, however, have been mostly limited to the clean-bore tanks (e.g., Faltinsen and Timokha, 2010). Multimodal models, in general, require estimation of natural slosh frequencies and modes, which can be obtained using numerical techniques. For baffled tanks, the natural slosh modes may be obtained efficiently using the boundary element method (BEM). In the BEM, the fluid flow in a baffled container is evaluated considering the distribution of singularities along the surfaces enclosing the liquid domain. The resulting boundary integral equations are then solved by discretizing the fluid boundaries, which is far more efficient than the finite element method (FEM), where the entire fluid domain has to be discretized (Katsikadelis, 2002).

Although BEM has been used in many studies, the applications of the method for modal analysis of liquid slosh in baffled tanks have been limited to only a few, particularly for the horizontal baffled tanks used in transportation of liquid products. Firouz-Abadi *et al.* (2009) employed BEM together with a zoning method to enhance the computational efficiency to study the effects of baffles on natural frequencies of slosh in rectangular and spherical tanks. Natural frequencies of liquid oscillations in a rectangular tank with a vertical baffle and upright cylindrical tank with a ring baffle were obtained by Sygulski (2011) using the BEM considering

baffles as double layers immersed in the liquid. The effect of ring baffles on the natural sloshing frequencies were also investigated by Gedikli and Erguven (2003) using a variational BEM. Gedikli and Erguven (1999) also reported responses of an upright cylindrical tank with a ring baffle subject to a seismic excitation using the BEM and superposition of modes.

The primary motivation of this study arises from the desire for developing an efficient tool for real-time simulations of fluid slosh in baffled tanks and its effect on directional performance of partly-filled tank vehicles. In the present study, a multimodal model, based on the linear slosh theory, is presented to characterize dynamic fluid slosh in a partially filled circular tank with three different longitudinal baffles: bottom-mounted; top-mounted and center-mounted. Eigenvalues and eigenvectors of free liquid slosh are initially obtained using BEM. For this purpose, the fluid boundaries are discretized using linear elements. The general eigenvalue problem is then reduced by considering only the elements on the half-length of the free-surface, which significantly reduces the computational time. The resulting eigenvalues and eigenvectors are subsequently incorporated into a multimodal representation of lateral liquid slosh to compute the velocity potential followed by the hydrodynamic pressure, slosh force and roll moment. Furthermore, the slosh damping due to baffles is estimated from the mean energy dissipation rate, and implemented into the multimodal analysis. The validity of the model is illustrated using the available analytical benchmarks. The effects of different baffle designs/lengths on the slosh frequencies, modes, hydrodynamic coefficients and damping ratio are further illustrated together with those on the slosh force and overturning moment imposed on the tank structure.

4.2 Formulations

4.2.1 Natural sloshing modes and frequencies

Consider a horizontal cylindrical container of radius R with a typical baffle in the mid-longitudinal plane, as shown in Fig. 4.1a. The Cartesian coordinate system Oyz, located at the center of the tank, is used with the z-axis directed upward, and the liquid fill-level h is measured with respect to the tank bottom *"B"*, while the z_0 and y_0 denote the coordinates of the free-surface at the intersection of the tank wall. The free surface slosh modes for the baffled tank can be obtained using the boundary element method (BEM). The method is initially formulated for deriving free liquid slosh modes in a clean-bore tank and is subsequently applied for the tank

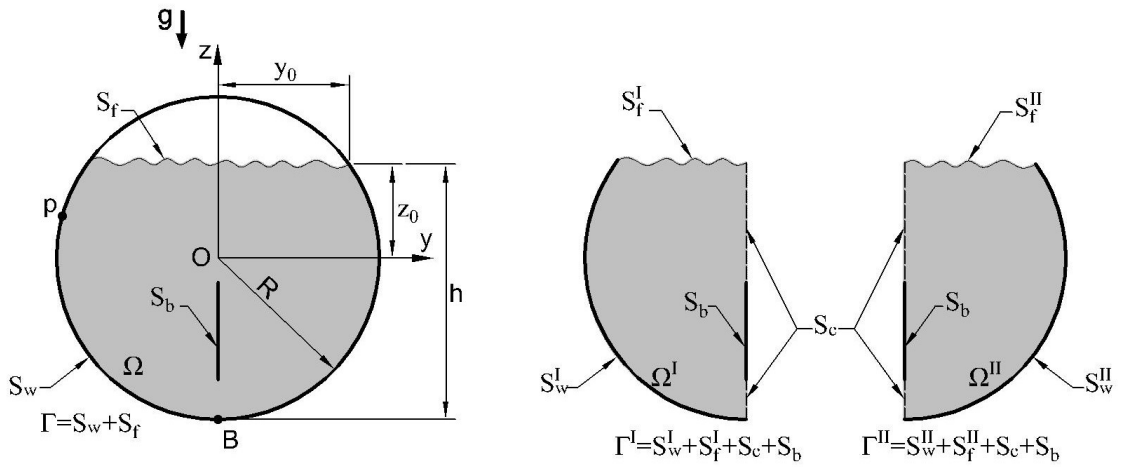

(a) (b)

Fig. 4.1. (a) Two-dimensional fluid motion in a circular cross-section tank with a partial baffle in the mid-longitudinal plane; and (b) Separated fluid domains.

with a typical baffle in the mid-longitudinal plane of the container using the zoning method. Assuming inviscid, incompressible and irrotational flows, the problem of free linear slosh in partially-filled tanks can be expressed in the following form (Abramson, 1966; Ibrahim, 2005):

$$\nabla^2 \varphi_i = 0 \qquad \text{in } \Omega \tag{4.1}$$

$$\frac{\partial \varphi_i}{\partial n} = 0 \qquad \text{on } S_w \tag{4.2}$$

$$\frac{\partial \varphi_i}{\partial z} = \kappa_i \varphi_i \qquad \text{on } S_f \tag{4.3}$$

Here φ_i represents the velocity potential corresponding to i^{th} natural mode, $\frac{\partial}{\partial n}$ denotes the derivative along the normal to the surface and $\kappa_i = \frac{\sigma_i^2}{g}$ is related to the circular frequency σ_i of the liquid oscillations. In the above equations, Ω and S_f represent the fluid domain and the liquid free-surface, respectively, and S_w is the wetted surface area of the tank (Fig. 4.1a).

The boundary integral representation of the solution for the Laplace Eq. (4.1) at a boundary point *"p"* for a clean-bore tank can be expressed as (Katsikadelis, 2002):

$$\frac{\alpha_p}{2\pi}\varphi_i(p) = -\int_\Gamma \left(\psi \frac{\partial \varphi_i}{\partial n} - \varphi_i \frac{\partial \psi}{\partial n}\right) dS \tag{4.4}$$

where $\Gamma = S_w + S_f$ is the boundary enclosing the fluid domain (Fig. 4.1a). In the above equation, α_p is π when point p is located on a smooth boundary, or the angle between the tangents of the boundary at p, when p is a corner point and ψ is given by (Katsikadelis, 2002):

$$\psi(y,z;y_p,z_p)=\ln\sqrt{(y-y_p)^2+(z-z_p)^2} \tag{4.5}$$

Dividing the fluid boundary into two-node linear elements, one can obtain a matrix equation from Eq. (4.4) for each mode of the free liquid oscillations in a clean-bore tank as:

$$[\mathbf{H}]\{\boldsymbol{\varphi}\}=[\mathbf{G}]\{\mathbf{q}\} \tag{4.6}$$

where $\{\boldsymbol{\varphi}\}$ and $\{\mathbf{q}\}$ are the unknown vectors of velocity potential φ_i and $q_i=\frac{\partial\varphi_i}{\partial n}$ on each node; and $[\mathbf{H}]$ and $[\mathbf{G}]$ are influence matrices, which are obtained from Eq. (4.4) using linear interpolating functions to evaluate φ_i and q_i on each element. The conditions of continuous velocity potential φ_i and discontinuous normal velocity q_i are considered at points where the type of boundary conditions change. Furthermore, the boundary integrals, Eq. (4.4), including the singular and non-singular integrals can be solved analytically, which can substantially reduce the computational time.

For a baffled tank, neglecting the thickness of the baffle plate, the fluid domain is divided such that the baffle is a part of the fluid boundaries. For this purpose, the fluid domain in the tank with a longitudinal baffle in the mid-section is divided into two parts, Ω^I and Ω^{II}, as shown in Fig. 4.1b. The matrix Eq. (4.6) for the two fluid domains can be obtained as:

$$\begin{bmatrix}
\mathbf{H}^I_{ff} & \mathbf{H}^I_{fc} & \mathbf{H}^I_{fb} & \mathbf{H}^I_{fw} & & & & \\
\mathbf{H}^I_{cf} & \mathbf{H}^I_{cc} & \mathbf{H}^I_{cb} & \mathbf{H}^I_{cw} & & & & \\
\mathbf{H}^I_{bf} & \mathbf{H}^I_{bc} & \mathbf{H}^I_{bb} & \mathbf{H}^I_{bw} & & & & \\
\mathbf{H}^I_{wf} & \mathbf{H}^I_{wc} & \mathbf{H}^I_{wb} & \mathbf{H}^I_{ww} & & & & \\
 & & & & \mathbf{H}^{II}_{ff} & \mathbf{H}^{II}_{fc} & \mathbf{H}^{II}_{fb} & \mathbf{H}^{II}_{fw} \\
 & & & & \mathbf{H}^{II}_{cf} & \mathbf{H}^{II}_{cc} & \mathbf{H}^{II}_{cb} & \mathbf{H}^{II}_{cw} \\
 & & & & \mathbf{H}^{II}_{bf} & \mathbf{H}^{II}_{bc} & \mathbf{H}^{II}_{bb} & \mathbf{H}^{II}_{bw} \\
 & & & & \mathbf{H}^{II}_{wf} & \mathbf{H}^{II}_{wc} & \mathbf{H}^{II}_{wb} & \mathbf{H}^{II}_{ww}
\end{bmatrix}
\begin{Bmatrix}
\boldsymbol{\varphi}^I_f \\ \boldsymbol{\varphi}^I_c \\ \boldsymbol{\varphi}^I_b \\ \boldsymbol{\varphi}^I_w \\ \boldsymbol{\varphi}^{II}_f \\ \boldsymbol{\varphi}^{II}_c \\ \boldsymbol{\varphi}^{II}_b \\ \boldsymbol{\varphi}^{II}_w
\end{Bmatrix}$$

$$=\begin{bmatrix}
\mathbf{G}^I_{ff} & \mathbf{G}^I_{fc} & \mathbf{G}^I_{fb} & \mathbf{G}^I_{fw} & & & & \\
\mathbf{G}^I_{cf} & \mathbf{G}^I_{cc} & \mathbf{G}^I_{cb} & \mathbf{G}^I_{cw} & & & & \\
\mathbf{G}^I_{bf} & \mathbf{G}^I_{bc} & \mathbf{G}^I_{bb} & \mathbf{G}^I_{bw} & & & & \\
\mathbf{G}^I_{wf} & \mathbf{G}^I_{wc} & \mathbf{G}^I_{wb} & \mathbf{G}^I_{ww} & & & & \\
 & & & & \mathbf{G}^{II}_{ff} & \mathbf{G}^{II}_{fc} & \mathbf{G}^{II}_{fb} & \mathbf{G}^{II}_{fw} \\
 & & & & \mathbf{G}^{II}_{cf} & \mathbf{G}^{II}_{cc} & \mathbf{G}^{II}_{cb} & \mathbf{G}^{II}_{cw} \\
 & & & & \mathbf{G}^{II}_{bf} & \mathbf{G}^{II}_{bc} & \mathbf{G}^{II}_{bb} & \mathbf{G}^{II}_{bw} \\
 & & & & \mathbf{G}^{II}_{wf} & \mathbf{G}^{II}_{wc} & \mathbf{G}^{II}_{wb} & \mathbf{G}^{II}_{ww}
\end{bmatrix}
\begin{Bmatrix}
\mathbf{q}^I_f \\ \mathbf{q}^I_c \\ \mathbf{q}^I_b \\ \mathbf{q}^I_w \\ \mathbf{q}^{II}_f \\ \mathbf{q}^{II}_c \\ \mathbf{q}^{II}_b \\ \mathbf{q}^{II}_w
\end{Bmatrix} \tag{4.7}$$

where the subscripts *f, c, b* and *w* refer to the free-surface, interface of the two flow domains, and baffle and wall boundaries, respectively. The first subscript of submatrices $\mathbf{H}^I$, $\mathbf{H}^{II}$, $\mathbf{G}^I$ and $\mathbf{G}^{II}$ denotes the location of the source point (point *"p"* in Eq. (4.4)) and the second subscript refers to the element location on which the boundary integration is performed. Since the fluid domains Ω^I and Ω^{II} are symmetric, the influence submatrices $\mathbf{H}^I$, $\mathbf{H}^{II}$ and $\mathbf{G}^I$, $\mathbf{G}^{II}$ are identical. The zero-Neumann boundary condition on the tank wall and baffles implies that $\mathbf{q}_b^I = \mathbf{q}_w^I = \mathbf{q}_b^{II} = \mathbf{q}_w^{II} = 0$. The free-surface boundary condition (Eq. 4.3) also implies that $\mathbf{q}_f^I = \kappa_i \boldsymbol{\varphi}_f^I$ and $\mathbf{q}_f^{II} = \kappa_i \boldsymbol{\varphi}_f^{II}$ for each mode. Moreover, the continuity of the potentials and the flux on each side of the fluid interface results in $\boldsymbol{\varphi}_c^I = \boldsymbol{\varphi}_c^{II}$, $\mathbf{q}_c^I = -\mathbf{q}_c^{II}$. Noting that $\boldsymbol{\varphi}_f^I = \boldsymbol{\varphi}_f^{II}$ and $\mathbf{q}_c^{\boldsymbol{I}} = \mathbf{q}_c^{\boldsymbol{II}} = 0$ for the symmetric modes, and $\boldsymbol{\varphi}_f^I = -\boldsymbol{\varphi}_f^{II}$ and $\boldsymbol{\varphi}_c^I = \boldsymbol{\varphi}_c^{II} = 0$ for the antisymmetric modes, Eq. (4.7) can be reduced to the following matrix equations for the symmetric and antisymmetric modes as:

$$\mathbf{A}\boldsymbol{\varphi}_f^I = \kappa_{2i}\boldsymbol{\varphi}_f^I \,, \qquad \mathbf{B}\boldsymbol{\varphi}_f^I = \kappa_{2i-1}\boldsymbol{\varphi}_f^I \tag{4.8}$$

where $\mathbf{A}$ and $\mathbf{B}$ are square matrices with size of N_f+1 (where N_f is number of elements on half of the free-surface), which depend on submatrices $\mathbf{H}^I$ and $\mathbf{G}^I$. The above eigenvalue problems are solved to determine the natural slosh frequencies and modes. The proposed BEM is used for modal analysis of liquid sloshing in a circular tank with bottom-mounted, top-mounted and center-mounted baffles in the mid-longitudinal plane of the tank.

4.2.2 Multimodal solution

The linearized form of the kinematic and dynamic boundary conditions on the free-surface for an ideal fluid in a rigid container (Fig. 4.1a) can be written as (Abramson, 1966):

$$\frac{\partial \delta}{\partial t} = \frac{\partial \Phi}{\partial z} \,, \qquad \frac{\partial \Phi}{\partial t} = -g\delta \qquad \text{on } S_f \tag{4.9}$$

where δ is the free-surface elevation. One may decompose the velocity potential Φ in the above equation into two components, Φ_R and Φ_S, associated with rigid body motion of fluid and fluid slosh potential, respectively. The potential Φ_R denotes the rigid body motion of the fluid which is identical to that of the container motion, while potential Φ_S represents the liquid motion relative to the container. Under a lateral motion of the tank caused by a steering maneuver of the tank vehicle, the rigid body potential is given by $\Phi_R = \dot{Y}y$, where $\dot{Y}$ is the lateral velocity of the container. Based on the multimodal approach (Faltinsen and Timokha, 2009), the sloshing

potential, $\Phi_S(y,z,t)$, and free-surface elevation, $\delta(y,t)$, can be expressed as a summation of the natural slosh modes and generalized functions γ_i and β_i as:

$$\Phi_S(y,z,t) = \sum_{i=1}^{\infty} \gamma_i(t)\varphi_i(y,z), \qquad \delta(y,t) = z_0 + \sum_{i=1}^{\infty} \beta_i(t)\varphi_i(y,z_0) \tag{4.10}$$

Substituting for $\Phi = \Phi_R + \Phi_S$ and δ into the free-surface boundary conditions (Eq. 4.9) together with orthogonality of the sloshing modes on the free-surface and considering Eq. (4.3) results in the following ordinary differential equations in terms of the generalized functions β_i:

$$\ddot{\beta}_i + \sigma_i^2 \beta_i = -\kappa_i \lambda_i \ddot{Y} \tag{4.11}$$

where $\ddot{Y}$ is the lateral acceleration excitation imposed on the container and λ_i may be regarded as hydrodynamic coefficients given by:

$$\lambda_i = \int_{S_f} y\varphi_i(y,z_0)dS \tag{4.12}$$

It is obvious that $\lambda_i = 0$ for the symmetric modes; only antisymmetric modes are thus excited due to lateral motion of the container. Moreover, the generalized functions γ_i and β_i are related as $\dot{\beta}_i = \kappa_i \gamma_i$. It should be noted that the natural modes φ_i obtained from the BEM are normalized such that $\int_{S_f} |\varphi_i|^2 \, dS = 1$.

Since the multi-modal method based on the potential flow assumptions does not consider energy dissipation, an artificial damping term needs to be introduced in Eq. (4.11) to account for the damping effect of the baffles (Faltinsen and Timokha, 2009). Equation (4.11) is thus expressed as:

$$\ddot{\beta}_i + 2\xi_i \sigma_i \dot{\beta}_i + \sigma^2 \beta_i = -\kappa_i \lambda_i \ddot{Y} \tag{4.13}$$

where ξ_i represents the damping ratio, which is estimated from the mean rate of energy dissipation (Abramson, 1966):

$$\xi_i = \frac{\overline{\frac{dE}{dt}}}{2\sigma_i E} \tag{4.14}$$

where $\overline{\frac{dE}{dt}}$ is the mean rate of energy dissipation over the period $T_i = \frac{2\pi}{\sigma_i}$ and E is the total energy of the liquid motion. The total energy E of the free liquid oscillations in a clean-bore tank in addition to the mean dissipation rate $\overline{\frac{dE}{dt}}$ due to baffles are calculated and implemented in Eq.

(4.14) to evaluate the damping ratio. Under free oscillations of the liquid, generalized functions $\beta_i(t)$ and $\gamma_i(t)$ may be expressed by harmonic functions as:

$$\beta_i(t) = \beta_{0i}\sin(\sigma_i t)\ , \quad \gamma_i(t) = \frac{\beta_{0i}g}{\sigma_i}\cos(\sigma_i t) \tag{4.15}$$

The velocity potential and the free-surface elevation corresponding to each mode can thus be expressed in the following forms:

$$\Phi_i(y,z,t) = \frac{\beta_{0i}g}{\sigma_i}\varphi_i(y,z)\cos(\sigma_i t)\,, \qquad \delta_i(y,t) = z_0 + \beta_{0i}\varphi_i(y,z_0)\sin(\sigma_i t) \tag{4.16}$$

The potential and kinetic flow energies per unit length of the container are given by (Ibrahim, 2005):

$$E_p = \frac{1}{2}\rho g\int_{S_f}(\delta_i - z_0)^2 dS\ , \qquad E_k = \frac{1}{2}\rho\int_{\Omega}|\boldsymbol{\nabla}\Phi_i|^2 d\Omega \tag{4.17}$$

where ρ is the fluid density. Substituting for Φ_i and δ_i from Eq. (4.16) into Eq. (4.17) leads to the following expression for the potential energy:

$$E_p = \frac{1}{2}\rho g\beta_{0i}^2\sin^2(\sigma_i t) \tag{4.18}$$

The kinetic energy is obtained by transforming the integral in Eq. (4.17) to an integral over the free-surface using the Divergence theorem and by letting $\Phi_i\boldsymbol{\nabla}\Phi_i$ as the differentiable vector, such that:

$$E_k = \frac{1}{2}\rho\int_{S_f}\Phi_i(\boldsymbol{\nabla}\Phi_i\cdot\boldsymbol{n})dS = \frac{1}{2}\rho g\beta_{0i}^2\cos^2(\sigma_i t) \tag{4.19}$$

The total energy is subsequently derived as:

$$E = E_p + E_k = \frac{1}{2}\rho g\beta_{0i}^2 \tag{4.20}$$

The mean rate of energy dissipation for a vertical baffle is estimated from the drag force caused by pressure distributed over the wetted baffle surface. The drag force acting on the baffle, per unit length of the tank, is obtained using the Morison's equation (Faltinsen and Timokha, 2009):

$$dF_D = \frac{1}{2}\rho C_D u|u|dz \tag{4.21}$$

where u is the horizontal inflow velocity to the baffle and C_D is the drag coefficient. The inflow velocity to the centrally mounted baffle may be obtained from:

$$u = \frac{\partial \Phi_i}{\partial y}\bigg|_{y=0} = \frac{\beta_{0i} g}{\sigma_i} q_i(0,z)\cos(\sigma_i t) \tag{4.22}$$

For a clean-bore tank, $q_i(0,z)$ represents the modal velocity normal to mid-longitudinal plane of the tank, which is obtained from vectors $\mathbf{q}_c^I$ for each mode using back substitution of the eigenvectors $\boldsymbol{\varphi}_f^I$ in Eq. (4.7) and eliminating the other unknowns in the velocity and potential vectors. The mean dissipation rate can thus be obtained using the work done during one period of oscillation as:

$$\frac{\overline{dE}}{dt} = \frac{1}{T_i}\int_0^{T_i}\int_{S_b} |u| dF_D dt = \frac{2}{3\pi}\rho\left|\frac{\beta_{0i} g}{\sigma_i}\right|^3 \int_{S_b} C_D |q_i(0,z)|^3 dz \tag{4.23}$$

where S_b is the submerged surface area of the baffle. Substituting for E and $\frac{\overline{dE}}{dt}$ from Eqs. (4.20) and (4.23) into Eq. (4.14) yields the damping ratio as:

$$\xi_i = \frac{2}{3\pi\sigma_i^4} g^2 |\beta_{0i}| \int_{S_b} C_D |q_i(0,z)|^3 dz \tag{4.24}$$

In the above equation, the drag coefficient C_D is estimated using an empirical relation given in Faltinsen and Timokha (2009), based on the Keulegan-Carpenter number *KC*, in the form:

$$C_D = 8KC^{-1/3} = 8\left(\frac{u_m T_i}{l_{bs}}\right)^{-1/3} \tag{4.25}$$

where l_{bs} is the submerged length of the baffle and u_m is the velocity amplitude from Eq. (4.22). It should be noted that the effect of the tank wall on the drag coefficient is neglected in the above equation. When the tank is subjected to a constant lateral acceleration of magnitude A_0, the values of β_{0i} in Eq. (4.24) can be obtained from the steady-state response, such that:

$$\beta_{0i} = -\frac{\lambda_i A_0}{g} \tag{4.26}$$

It should be noted that the damping ratios in Eq. (4.24) are functions of the excitation amplitude for a container subjected to a constant lateral acceleration. Dependence of the damping ratio due to baffles on the excitation amplitude was also confirmed by Dodge (2000) and Faltinsen and Timokha (2009).

4.2.3 Hydrodynamic pressure, slosh force and overturning moment

The hydrodynamic pressure as well as slosh force and moment are of prime interest to study the effect of fluid slosh on the transporting vehicle directional characteristics and stability.

The dynamic slosh responses in terms of time and spatial coordinates are obtained following the solutions of Eq. (4.13) for β_i. The hydrodynamic pressure distribution, $P(y,z,t)$, on the container wall and baffles is derived using the linearized Bernoulli's equation (Abramson, 1966), such that:

$$P(y,z,t) = -\rho \frac{\partial(\Phi_R + \Phi_S)}{\partial t} = -\rho \left\{ \ddot{Y} y + \sum_{i=1}^{\infty} \frac{\ddot{\beta}_i(t)}{\kappa_i} \varphi_i(y,z) \right\} \qquad \text{on } S_w \text{ \& } S_b \tag{4.27}$$

The total lateral force, $F_y(t)$, acting on the container wall and baffles, per unit length of the container, is obtained from integration of the hydrodynamic pressure over the wetted areas of the tank wall and the baffle, S_w and S_b, such that:

$$F_y(t) = \int_{S_w+S_b} P dz = F_R(t) + F_S(t) \tag{4.28}$$

where F_R and F_S are the components of the lateral force that could be associated with the rigid body and slosh motions of the liquid, respectively, expressed as:

$$F_R(t) = -\rho \ddot{Y} \int_{S_w+S_b} y dz = -m\ddot{Y} \tag{4.29}$$

$$F_S(t) = -\rho \sum_{i=1}^{\infty} \frac{\ddot{\beta}_i(t)}{\kappa_i} \int_{S_w+S_b} \varphi_i(y,z) dz \tag{4.30}$$

in which m is the fluid mass per unit length of the tank. Using Green's second identity and Eqs. (4.2), (4.3) and (4.12), and noting that φ_i on the fluid interface S_c are zero for antisymmetric modes, the dynamic slosh force $F_S(t)$ is obtained from the hydrodynamic coefficients λ_i, as:

$$F_S(t) = -\rho \sum_{i=1}^{\infty} \ddot{\beta}_i(t) \lambda_i \tag{4.31}$$

It should be noted that the vertical component of the net slosh force is zero due to geometric symmetry.

The overturning moment about the container bottom point *"B"*, M_B, (Fig. 4.1a), per unit tank length, can be determined by integrating the moments resulting from the horizontal and vertical components of hydrodynamic forces:

$$M_B(t) = \int_{S_w+S_b} P[-y dy - (R+z) dz] \tag{4.32}$$

Substituting for the pressure from Eq. (4.27) into the above equation yields the total overturning moment that may be decomposed into three components attributed to the rigid body moment (M_R), moment due to the vertical forces (M_V), and the moment resulting from the dynamic fluid slosh effect (M_S), i.e.:

$$M_B(t) = M_R(t) + M_V(t) + M_S(t) \tag{4.33}$$

The above moment components can be expressed as:

$$M_R(t) = \rho\ddot{Y}\int_{S_w+S_b} y(R+z)dz = m(R+z_{cg})\ddot{Y} \tag{4.34}$$

$$M_V(t) = \rho\ddot{Y}\int_{S_w+S_b} y^2 dy = \frac{2}{3}\rho y_0^3\ddot{Y} \tag{4.35}$$

$$M_S(t) = \rho\sum_{i=1}^{\infty}\frac{\ddot{\beta}_i(\mathrm{t})}{\kappa_i}\int_{S_w+S_b}\varphi_i(y,z)[ydy + (z+R)dz] = \rho\sum_{i=1}^{\infty}\ddot{\beta}_i(\mathrm{t})\left(R\lambda_i + \frac{2\chi_i}{\kappa_i}\right) \tag{4.36}$$

where z_{cg} in Eq. (4.34) is the location of the liquid center of gravity measured from the tank center (origin *O* in Fig. 4.1a) and χ_i is given by:

$$\chi_i = \int_{S_b} z\varphi_i(y,z)dz \tag{4.37}$$

4.3 Results and discussion

The boundary element model, presented in section 4.2.1, is employed to solve the spectral problem of liquid oscillations in a circular tank with three different longitudinal baffles. These are the bottom-mounted, top-mounted and center mounted baffles, as shown in shown in Fig. 4.2, where l_b and l_{bs} are total and submerged lengths of the baffles, respectively. It should be noted that the mid-point of the center-mounted baffle coincides with the tank geometric center. The boundaries are discretized using isoparametric linear elements of equal lengths. The results are obtained in terms of normalized slosh frequencies and free-surface profiles for different baffle lengths, which are subsequently applied to compute the lateral slosh force and moment caused by a lateral acceleration excitation of the container. The convergence is ensured by increasing the number of elements to stabilize to the fourth decimal value of the normalized frequencies. The effect of the baffles on hydrodynamic coefficients, damping ratios, and slosh

load responses are evaluated and discussed. The results are also compared with the available analytical solutions to examine the accuracy of the model.

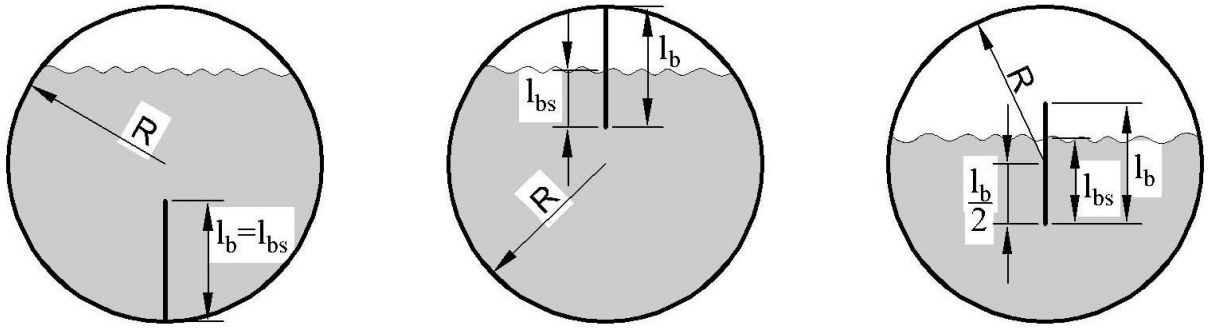

(a) (b) (c)

Fig. 4.2. Baffle configurations: (a) bottom-mounted; (b) top-mounted; and (c) center-mounted.

4.3.1 Natural slosh frequencies and modes

In the first stage, the normalized natural slosh frequencies, $\bar{\kappa}_i = \kappa_i R$, obtained for a clean-bore tank are compared with those reported by Faltinsen and Timokha (2010) in Table 4.1. The table compares the first five antisymmetric and first four symmetric slosh frequencies, excluding the zero frequency corresponding to the rigid body mode, for three different fill ratios *h/R*=0.5, 1.0 and 1.5. The results are identical to those reported from the analytical solutions in Faltinsen and Timokha (2010). It was observed that maximum of 2000 elements over half the free surface length were required to stabilize the fourth decimal value of the normalized slosh frequencies in Table 4.1. Only a maximum of 80 elements on the half-length of the free-surface, however, were needed to obtain the results with peak discrepancy of merely 0.26% corresponding to the fifth antisymmetric mode frequency for fill ratio *h/R*=1.5, while the first antisymmetric frequencies were identical to the analytical results.

The normalized symmetric and antisymmetric natural slosh frequencies for the tank with bottom-mounted, top-mounted and center-mounted baffles of different normalized lengths l_b/R are presented in Tables 4.2 to 4.4 for the three fill ratios (*h/R*=0.5, 1.0 and 1.5), respectively. The results are also compared with those reported in Hasheminejad and Mohammadi (2011) for a few of the modes and fill heights, which were obtained using the conformal mapping technique with

Table 4.1. Comparison of the calculated normalized frequencies, $\bar{\kappa}_i = \kappa_i R$, of slosh in a clean-bore cylindrical tank with those reported in Faltinsen and Timokha (2010).

	$\bar{\kappa}_1$	$\bar{\kappa}_3$	$\bar{\kappa}_5$	$\bar{\kappa}_7$	$\bar{\kappa}_9$	$\bar{\kappa}_2$	$\bar{\kappa}_4$	$\bar{\kappa}_6$	$\bar{\kappa}_8$
	Antisymmetric modes					Symmetric modes			
$h/R = 0.5$									
	1.1280	4.7980	8.5271	12.1862	15.8285	2.8849	6.6787	10.3602	14.0085
Faltinsen and Timokha (2010)	1.1280	4.7980	8.5271	12.1862	15.8285	2.8849	6.6787	10.3602	14.0084
$h/R = 1.0$									
	1.3557	4.6511	7.8199	10.9718	14.1189	3.0331	6.2392	9.3967	12.5457
Faltinsen and Timokha (2010)	1.3557	4.6511	7.8199	10.9718	14.1189	3.0331	6.2392	9.3967	12.5457
$h/R = 1.5$									
	1.8989	5.6284	9.2720	12.9063	16.5377	3.7877	7.4480	11.0868	14.7200
Faltinsen and Timokha (2010)	1.8989	5.6284	9.2720	12.9063	16.5377	3.7877	7.4480	11.0868	14.7200

Table 4.2. Normalized frequencies, $\bar{\kappa}_i = \kappa_i R$, of fluid slosh in a cylindrical tank with a bottom-mounted baffle of different lengths.

l_b/R		$\bar{\kappa}_1$	$\bar{\kappa}_3$	$\bar{\kappa}_5$	$\bar{\kappa}_7$	$\bar{\kappa}_9$	$\bar{\kappa}_2$	$\bar{\kappa}_4$	$\bar{\kappa}_6$	$\bar{\kappa}_8$
		Antisymmetric modes					Symmetric modes			
$h/R = 0.5$										
0.25		1.0039	4.6699	8.5098	12.1829	15.8282	2.8849	6.6787	10.3602	14.0085
0.25	Hasheminejad and Mohammadi (2011)	1.0119	4.7597	8.7312			2.8903	6.8503		
$h/R = 1$										
0.25		1.3290	4.6489	7.8199	10.9718	14.1189	3.0331	6.2392	9.3967	12.5457
0.5		1.2172	4.6340	7.8197	10.9717	14.1189	3.0331	6.2392	9.3967	12.5457
0.5	Hasheminejad and Mohammadi (2011)	1.2171	4.6341	7.8200			3.0334	6.2414		
0.75		0.9555	4.5398	7.8029	10.9674	14.1182	3.0331	6.2392	9.3967	12.5457
$h/R = 1.5$										
0.25		1.8917	5.6283	9.2719	12.9063	16.5376	3.7877	7.4480	11.0868	14.7200
0.5		1.8605	5.6278	9.2716	12.9061	16.5375	3.7877	7.4480	11.0868	14.7200
0.75		1.7797	5.6274	9.2708	12.9056	16.5371	3.7877	7.4480	11.0868	14.7200
0.75	Hasheminejad and Mohammadi (2011)	1.7799	5.6300	9.2792			3.7877	7.4480		
1.0		1.5985	5.6266	9.2689	12.9049	16.5366	3.7877	7.4480	11.0868	14.7200
1.25		1.2283	5.5821	9.2523	12.9040	16.5351	3.7877	7.4480	11.0868	14.7200

Table 4.3. Normalized frequencies, $\bar{\kappa}_i = \kappa_i R$, of fluid slosh in a cylindrical tank with a top-mounted baffle of different lengths.

l_b/R		$h/R = 0.5$								
		Antisymmetric modes					Symmetric modes			
		$\bar{\kappa}_1$	$\bar{\kappa}_3$	$\bar{\kappa}_5$	$\bar{\kappa}_7$	$\bar{\kappa}_9$	$\bar{\kappa}_2$	$\bar{\kappa}_4$	$\bar{\kappa}_6$	$\bar{\kappa}_8$
1.75		0.8878	3.5415	6.7430	10.3695	14.0096	2.8849	6.6787	10.3602	14.0085
1.75	Hasheminejad and Mohammadi (2011)	0.8941	3.5801	6.8676			2.8901	6.8508		
		$h/R = 1$								
1.25		1.1647	3.5230	6.3122	9.4099	12.5481	3.0331	6.2392	9.3967	12.5457
1.5		0.8511	3.1362	6.2411	9.3969	12.5457	3.0331	6.2392	9.3967	12.5457
1.5	Hasheminejad and Mohammadi (2011)	0.8511	3.1370	6.2431			3.0339	6.2416		
1.75		0.5885	3.0684	6.2393	9.3968	12.5457	3.0331	6.2392	9.3967	12.5457
		$h/R = 1.5$								
0.75		1.5699	4.1294	7.4985	11.0950	14.7234	3.7877	7.4480	11.0868	14.7200
1.0		1.1514	3.8215	7.4540	11.0896	14.7222	3.7877	7.4480	11.0868	14.7200
1.25		0.8805	3.7921	7.4522	11.0894	14.7220	3.7877	7.4480	11.0868	14.7200
1.25	Hasheminejad and Mohammadi (2011)	0.8805	3.7935	7.4570			3.7882	7.4489		
1.5		0.6875	3.7903	7.4514	11.0891	14.7217	3.7877	7.4480	11.0868	14.7200
1.75		0.5209	3.7901	7.4507	11.0886	14.7214	3.7877	7.4480	11.0868	14.7200

Table 4.4. Normalized frequencies, $\bar{\kappa}_i = \kappa_i R$, of fluid slosh in a cylindrical tank with a center-mounted baffle of different lengths.

l_b/R	$h/R = 1.5$								
	Antisymmetric modes					Symmetric modes			
	$\bar{\kappa}_1$	$\bar{\kappa}_3$	$\bar{\kappa}_5$	$\bar{\kappa}_7$	$\bar{\kappa}_9$	$\bar{\kappa}_2$	$\bar{\kappa}_4$	$\bar{\kappa}_6$	$\bar{\kappa}_8$
0.25	1.8627	5.6222	9.2708	12.9063	16.5376	3.7877	7.4480	11.0868	14.7200
0.5	1.7474	5.5858	9.2602	12.9053	16.5370	3.7877	7.4480	11.0868	14.7200
0.75	1.5277	5.4290	9.1741	12.8709	16.5197	3.7877	7.4480	11.0868	14.7200

baffle length limited to half the fill height. The comparisons suggest very good agreements in frequencies corresponding to the reported modes and fill heights. Since the condition $\frac{\partial \varphi_i}{\partial y}\Big|_{y=0} = 0$ is satisfied for the symmetric modes, the presence of a baffle in the mid-longitudinal plane has no influence on the symmetric mode frequencies. As can be seen from Tables 4.2 to 4.4, the slosh frequencies corresponding to the symmetric modes are identical to those obtained for the clean-bore tank (Table 4.1), irrespective of the fill height and baffle configuration, which further confirms the validity of the present model. The symmetric mode frequencies reported in

Hasheminejad and Mohammadi (2011), however, are slightly different from those of the clean-bore tank obtained in this study and the benchmark solutions presented in Faltinsen and Timokha (2010). This seems to suggest that the method of conformal mapping may yield slight errors, apart from involving elaborate series of coordinate transformations.

The results in Table 4.2 suggest that extending the length of the bottom-mounted baffle up to close to the free surface affects the first antisymmetric mode substantially, with negligible effect on the higher modes. Increasing the length of the top-mounted baffle closer to the free surface such that it is partly submerged, on the other hand, substantially affects lower two antisymmetric mode frequencies (Table 4.3). The observed frequencies are substantially lower than those of the clean-bore tank. The greatest influence is observed in the first antisymmetric mode frequencies, irrespective of the fill height considered. Furthermore, increasing the baffle length causes the antisymmetric frequencies to approach the symmetric ones. For instance, $\bar{\kappa}_1$ approaches towards zero and $\bar{\kappa}_3$ approaches $\bar{\kappa}_2$ as the baffle length is increased. When the fluid in the container is completely divided into two flow domains by the baffle (i.e., $\frac{l_b}{R} \geq \frac{h}{R}$ for the bottom-mounted baffle; and $\frac{l_b}{R} = 2$ for the top-mounted baffle), the antisymmetric modes completely merge with the symmetric modes since the zero-Neumann boundary condition on the baffle is inherently satisfied in symmetric modes.

The normalized slosh frequencies of the tank with the center-mounted baffle are presented in Table 4.4. The results are only shown for the fill ratio h/R=1.5, since the normalized frequencies are identical to those of the tank with top-mounted baffle for the two lower fill ratios, h/R=0.5 and 1. Similar to the bottom-mounted baffle, the center-mounted baffle influences the first antisymmetric mode frequency substantially, with only little effect on the high mode frequencies. The effect is more pronounced as the baffle length approaches the free-surface. Similar to the clean-bore tank, a maximum of 2000 elements over half the free-surface length in the baffled tanks were used to obtain the normalized slosh frequencies with four decimal place convergence. It was also observed that a coarse mesh of only 150 elements would yield peak discrepancy in the order of 0.2% in $\bar{\kappa}_1$ for the tank with top-mounted baffle corresponding to $\frac{h}{R} = 0.5$ and $\frac{l_b}{R} = 1.75$. The peak error was lower for the tank with other baffle configurations and lengths.

The effect of the baffle extension on the antisymmetric modes slosh frequencies $\bar{\kappa}_i$ $(i = 1,3,5,7)$ of the tank with a bottom-mounted baffle is depicted in Fig. 4.3a as a function of the fill height. The results are presented only for $\frac{l_b}{R} < \frac{h}{R}$. It should be noted that when the fill height is less than or equal to the baffle length ($\frac{l_b}{R} \geq \frac{h}{R}$), the antisymmetric mode are not generated and the resulting modes are identical to the symmetric mode of the clean-bore tank. The first antisymmetric frequency increases monotonically with the fill ratio, irrespective of the baffle length, as shown in Fig. 4.3a. Extending the baffle length causes the first antisymmetric frequency to decrease, particularly when the baffle tip is close to the free-surface. The normalized frequencies of the baffled tank rapidly approach those of the clean bore-tank as the fill ratio is increased. As can be seen from Fig. 4.3a, the bottom-mounted baffle yields lower antisymmetric slosh frequencies of the higher modes only when the fill height is very close to the baffle length. Above this fill height, the frequencies converge to those of the clean-bore tank. The decrease in the natural slosh frequencies due to these baffles can be attributed to changes in the fluid flux between the fluid domains, Ω^I and Ω^{II} (Fig. 4.1b), resulting in a higher oscillation period of the liquid. The decrease in natural slosh frequencies due to baffles can also be observed in reported studies on rectangular tanks with vertical baffles (e.g., Evans and McIver, 1987; Faltinsen and Timokha, 2009, 2011; Wu *et al.*, 2012).

Normalized antisymmetric modes slosh frequencies of the tank with top-mounted and center-mounted baffles of different lengths ($\frac{l_b}{R} = 0, 0.5, 1, 1.5$) are also shown in Figs. 4.3b and 4.3c, respectively. As it would be expected, the slosh frequencies of the tank with top-mounted baffle are identical to those of the clean-bore tank for lower fill heights with free surface below the baffle, $\frac{h}{R} \leq 2 - \frac{l_b}{R}$. The antisymmetric slosh frequencies of the baffled tank, however, deviate from those of the clean-bore tank, when the baffle tip pierces the free surface, as shown in Fig. 4.3b. The antisymmetric mode frequencies tend to decrease with only slight increase in the fill height leading to greater submersion of the baffle. Further increase in the fill height, however, yields monotonic increase in the frequency, although substantially lower than those of the clean-bore tank. The results also show that the higher mode frequencies rapidly approach the symmetric mode frequencies with only slight increase in the fill height above the baffle tip, which correspond to those of a compartmented tank ($\frac{l_b}{R} = 2$). Unlike the bottom-mounted baffle,

the top-mounted baffle affects the mainstream fluid flow directly below the free surface, $\frac{h}{R} > 2 - \frac{l_b}{R}$, which significantly influences the fluid flux between the two fluid domains, Ω^I and Ω^{II}.

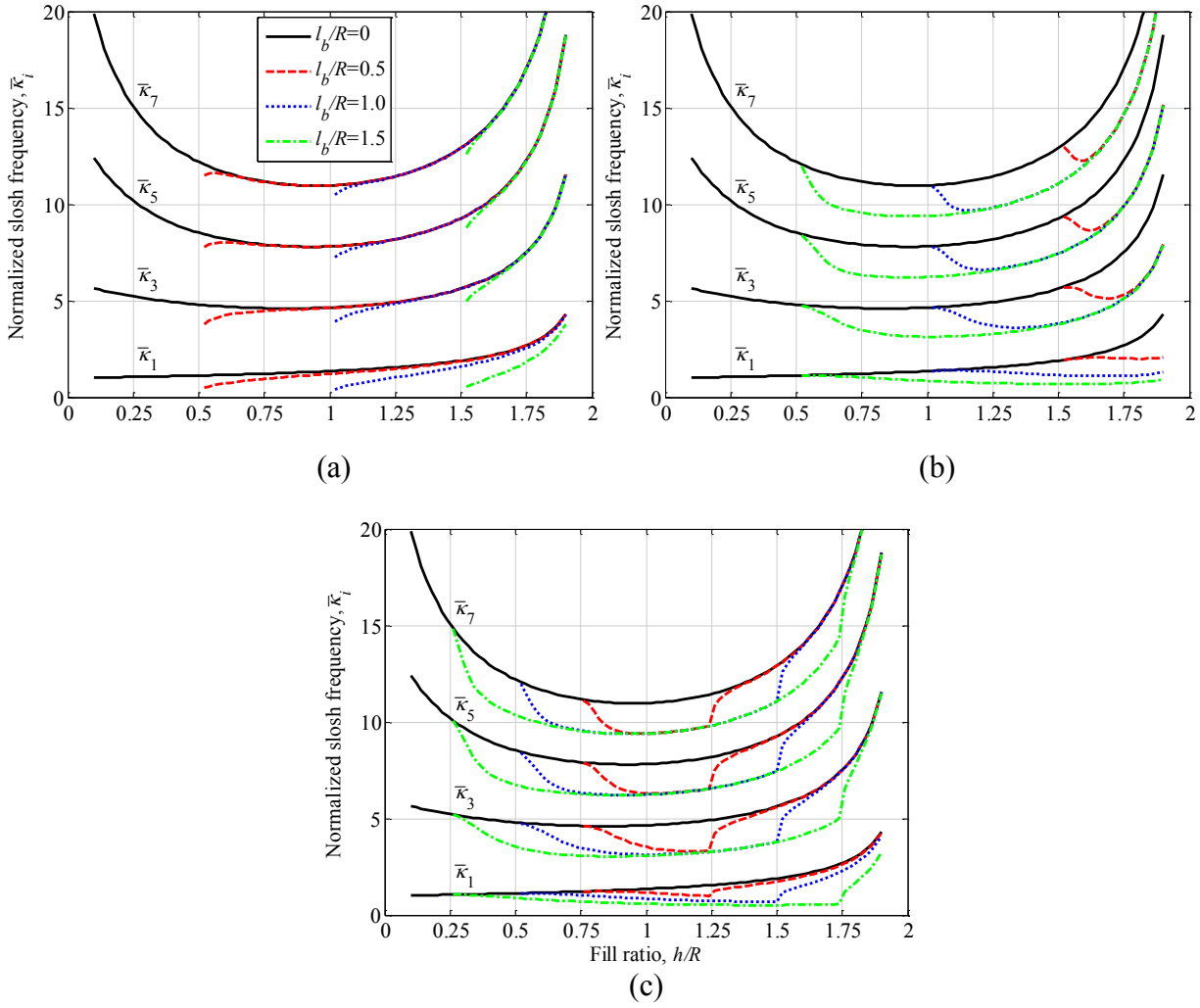

Fig. 4.3. Normalized slosh frequencies associated with the first four antisymmetric modes of the partly-filled tank with varying lengths of the (a) bottom-mounted, (b) top-mounted and (c) center-mounted baffle.

In case of the center-mounted baffle, the antisymmetric slosh frequencies deviate from those of the clean-bore tank when the free surface lies above the lower baffle tip, $\frac{h}{R} > 1 - \frac{l_b}{2R}$, as shown in Fig. 4.3c. The frequencies then rapidly approach the symmetric mode frequencies as the free surface height increases up to the upper baffle edge, $\frac{h}{R} < 1 + \frac{l_b}{2}$, as observed for the top-

mounted baffle. Above this fill ratio, the antisymmetric mode frequencies rapidly approach those of the clean-bore tank, although the first mode exhibits a gradual increase in the frequency.

The natural sloshing modes are further investigated for the tank with the three baffle designs. The free-surface profiles associated with the first three symmetric modes under two fill ratios, h/R=1.25, 1.75, of the clean-bore and baffled tanks are shown in Fig 4.4. The lowest symmetric mode was observed to be identical to that depicted in Faltinsen and Timokha (2010) for both the fill heights. The mode shapes were evaluated for the first three antisymmetric free-surface profiles with the bottom-mounted, top- mounted and center-mounted baffles of different normalized lengths (l_b/R=0.5, 1) considering two different fill ratios (h/R=1.25, 1.75). Figures 4.5 to 4.7 illustrate the natural slosh modes for the three baffle configurations together with those for the clean-bore tank (l_b/R=0). The free-surface profiles associated with the lowest antisymmetric mode in the clean-bore tank were in complete agreement with those reported in Faltinsen and Timokha (2010). As can be seen from Fig. 4.5, the bottom-mounted baffle with l_b/R=0.5 yields negligible effect on the free-surface profiles for the two fill ratios considered. The baffle length

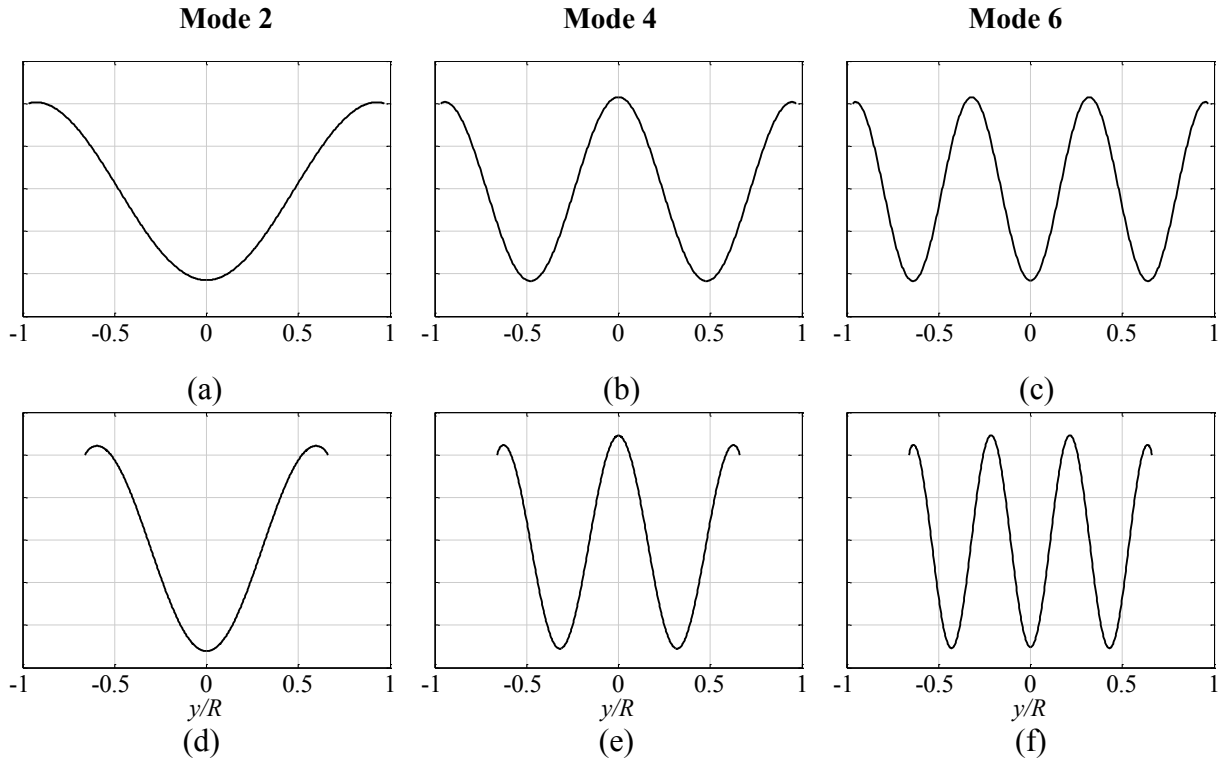

Fig. 4.4. The first three symmetric modes of the free surface in the baffled and clean-bore tanks: (a to c) h/R=1.25; and (d to f) h/R=1.75.

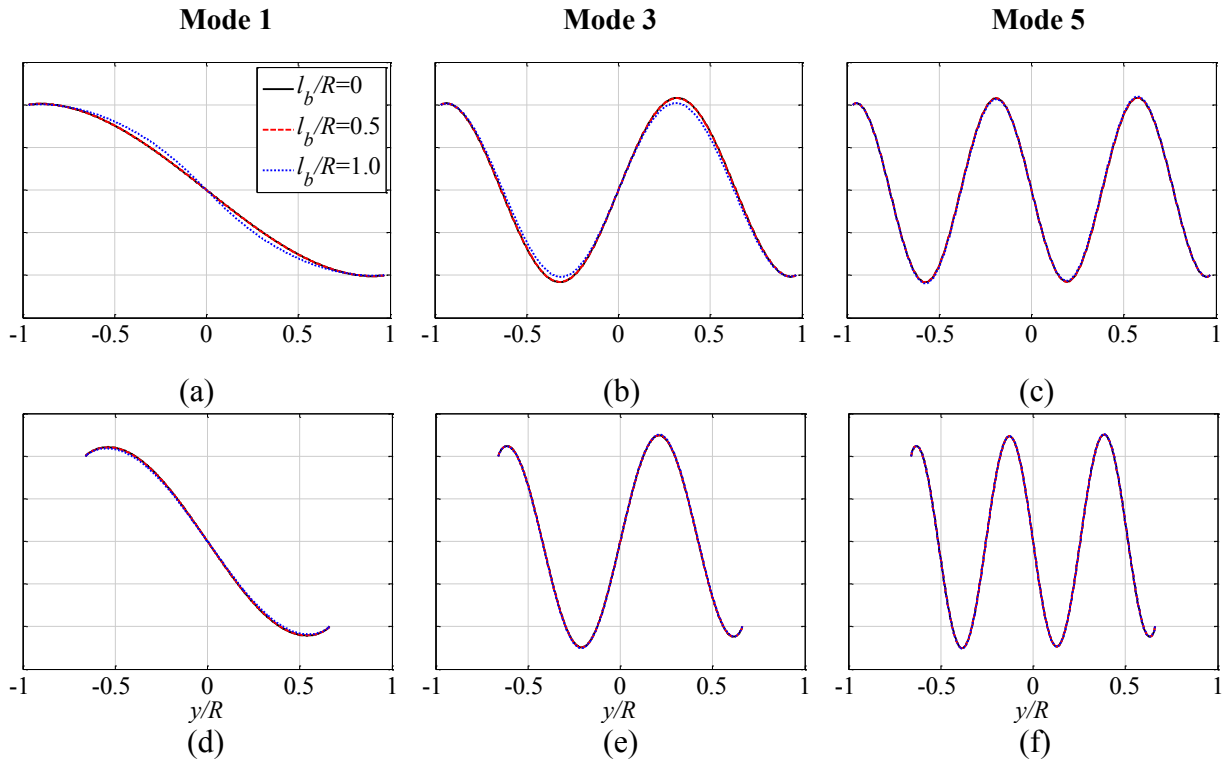

Fig. 4.5. The effect of length of bottom-mounted baffle on first three antisymmetric free-surface modes for two different fill heights: (a to c) h/R=1.25; and (d to f) h/R=1.75.

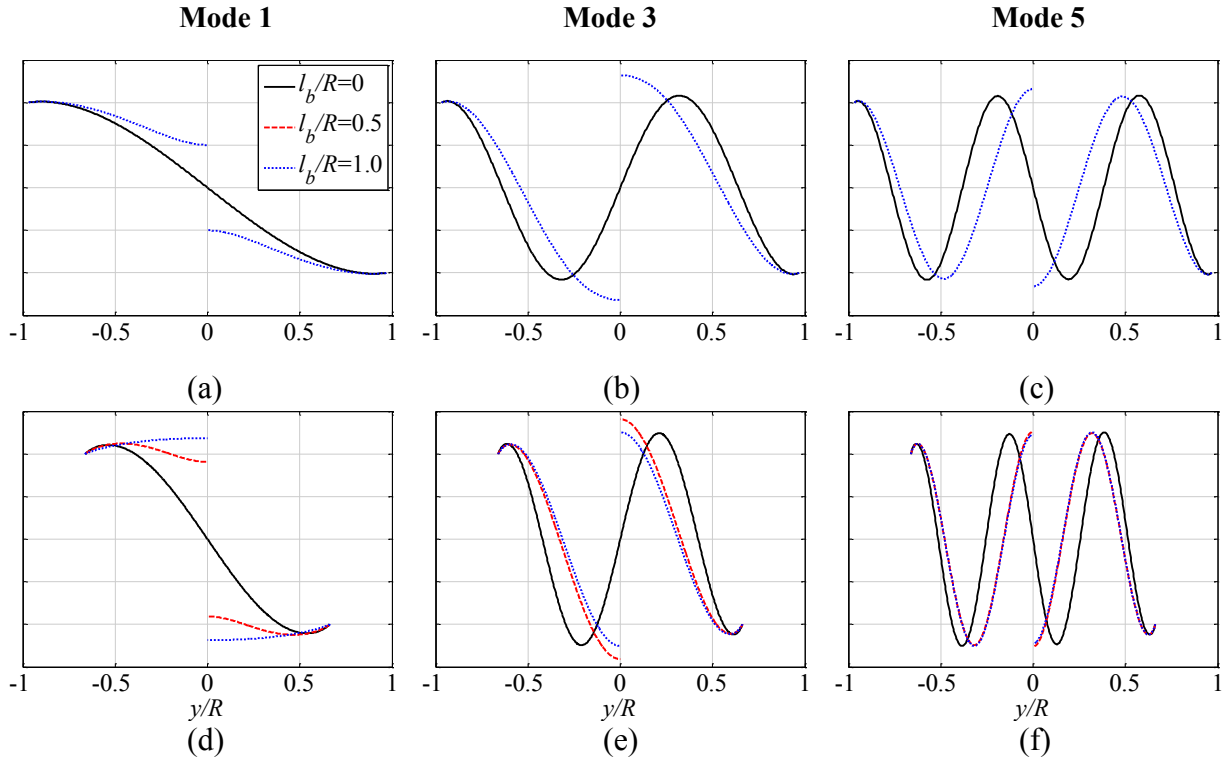

Fig. 4.6. The effect of length of top-mounted baffle on first three antisymmetric free-surface modes for two different fill heights: (a to c) h/R=1.25; and (d to f) h/R=1.75.

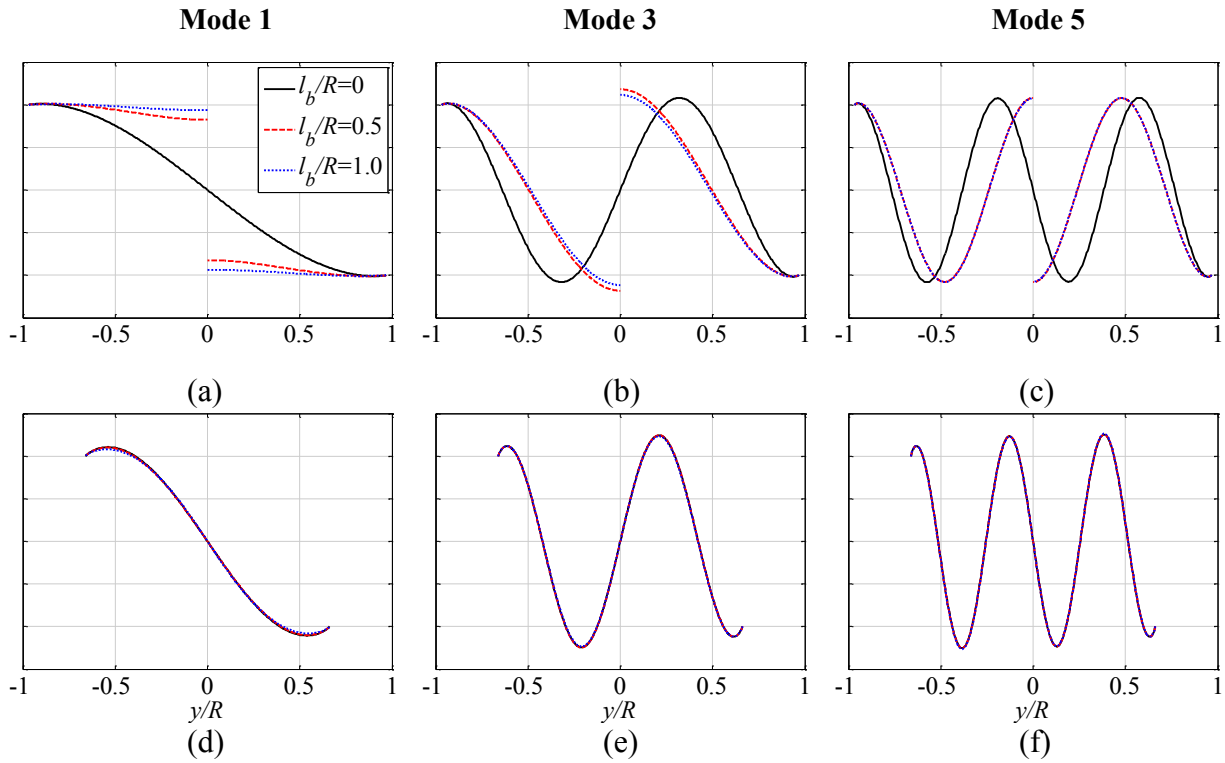

Fig. 4.7. The effect of length of center-mounted baffle on first three antisymmetric free-surface modes for two different fill heights: (a to c) h/R=1.25; and (d to f) h/R=1.75.

l_b/R=1 affects the first and the second antisymmetric modes only slightly for the fill ratio h/R=1.25, while it has almost no effect for the higher fill ratio, h/R=1.75. These suggest that a bottom-mounted partial baffle ($l_b/R \leq 1$) would not offer resistance to fluid slosh in most practical situations where the fill ratio is in excess of 50% (h/R>1). The top-mounted baffle, however, substantially affects the free surface profile only when the baffle is partly-submerged in the fluid mainstream, as seen in Fig. 4.6. A shorter baffle (l_b/R=0.5) thus has no effect on the free surface under the lower fill ratio (h/R=1.25) but strongly alters the free surface under the higher fill ratio (h/R=1.75). A longer baffle, l_b/R=1, however affects the free-surface profiles under both the fill ratios. It is further seen that the effect of length of the top-mounted baffle on the higher modes is nearly negligible for the higher fill ratio, h/R=1.75. The figures show discontinuity in the free surface near y=0, when the baffle is partly immersed in the fluid.

Similar to the top-mounted baffles, the center-mounted baffles cause nearly flat free-surface profiles associated with the lowest antisymmetric mode for the fill ratio h/R=1.25, when the fill height is equal to or below the upper edge of the baffle (l_b/R=0.5 and 1), as shown in Fig. 4.7a. In this case, the free surfaces corresponding to the three modes exhibit a discontinuity near

y=0. The center-mounted baffles, however, do not affect the slosh mode when the free surface lies above the baffles (*h/R*=1.75), as seen in Figs. 4.7d-f. Consequently, the center-mounted baffle could help suppress fluid slosh only under intermediate fill heights.

4.3.2 Hydrodynamic coefficients and damping ratios

Normalized hydrodynamic coefficients $\bar{\lambda}_i = \frac{\lambda_i\sqrt{y_0}}{R^2}$ $(i = 1,3,5,7,9)$ for liquid slosh in a clean-bore tank with three different fill ratios, *h/R*=0.5, 1 and 1.5, are initially obtained and compared with those reported by Faltinsen and Timokha (2010) in Table 4.5. The results were obtained with the accuracy of five decimal places using a maximum of 450 elements on the half-length of the free-surface. The results in Table 4.5 are identical to those reported in Faltinsen and Timokha (2010). Normalized hydrodynamic coefficients, $\bar{\lambda}_i$, obtained for the three baffle configurations for the same fill ratios are presented in Tables 4.6 to 4.8, respectively. The hydrodynamic coefficients associated with the first antisymmetric slosh mode for the bottom-mounted baffled tank are almost identical to those of the clean-bore tank, irrespective of the baffle lengths considered (Table 4.6). The effect of bottom-mounted baffles on the hydrodynamic coefficients associated with the higher modes is also negligible, when the baffle tip is sufficiently far from the free-surface. The results show the hydrodynamic coefficients for the higher modes are affected by the baffle, only in cases when the free flow domain, between the baffle tip and the free surface, is near 0.25*R*. Considering that the first mode is the dominant mode in linear slosh analysis, the reduction in the slosh force due to a bottom-mounted baffle would be expected to be insignificant when the baffle is smaller than the free surface height. As

Table 4.5. Comparison of the normalized hydrodynamic coefficients, $\bar{\boldsymbol{\lambda}}_{\boldsymbol{i}} = \frac{\boldsymbol{\lambda_i\sqrt{y_0}}}{\boldsymbol{R^2}}$, for the clean-bore tank with those reported in Faltinsen and Timokha (2010).

	$h/R = 0.5$				
	$\bar{\lambda}_1$	$\bar{\lambda}_3$	$\bar{\lambda}_5$	$\bar{\lambda}_7$	$\bar{\lambda}_9$
	0.61154	0.03045	0.00819	0.00359	0.00195
Faltinsen and Timokha (2010)	0.61154	0.03045	0.00819	0.00359	0.00195
	$h/R = 1$				
	0.81206	0.07753	0.02854	0.01484	0.00911
Faltinsen and Timokha (2010)	0.81206	0.07753	0.02854	0.01484	0.00911
	$h/R = 1.5$				
	0.60457	0.08599	0.03590	0.02018	0.01310
Faltinsen and Timokha (2010)	0.60457	0.08599	0.03590	0.02018	0.01311

Table 4.6. Normalized hydrodynamic coefficients, $\bar{\lambda}_i = \frac{\lambda_i \sqrt{y_0}}{R^2}$, for the tank with a bottom-mounted baffle of different lengths.

	$h/R = 0.5$				
l_b/R	$\bar{\lambda}_1$	$\bar{\lambda}_3$	$\bar{\lambda}_5$	$\bar{\lambda}_7$	$\bar{\lambda}_9$
0.25	0.61017	0.05135	0.00498	0.00454	0.00175
			$h/R = 1$		
0.25	0.81188	0.07939	0.02855	0.01487	0.00912
0.5	0.81088	0.08914	0.02808	0.01507	0.00915
0.75	0.80635	0.12454	0.02209	0.01720	0.00858
			$h/R = 1.5$		
0.25	0.60459	0.08583	0.03584	0.02014	0.01308
0.5	0.60470	0.08525	0.03556	0.01999	0.01299
0.75	0.60489	0.08436	0.03490	0.01964	0.01276
1.0	0.60483	0.08565	0.03347	0.01903	0.01234
1.25	0.60245	0.10268	0.02848	0.01919	0.01150

Table 4.7. Normalized hydrodynamic coefficients, $\bar{\lambda}_i = \frac{\lambda_i \sqrt{y_0}}{R^2}$, for the tank with a top-mounted baffle of different lengths.

	$h/R = 0.5$				
l_b/R	$\bar{\lambda}_1$	$\bar{\lambda}_3$	$\bar{\lambda}_5$	$\bar{\lambda}_7$	$\bar{\lambda}_9$
1.75	0.59401	0.14472	0.02345	0.02236	0.00722
			$h/R = 1$		
1.25	0.78720	0.21215	0.00094	0.04030	0.00061
1.5	0.74668	0.32702	0.00519	0.04249	0.00121
1.75	0.72738	0.36790	0.00661	0.04282	0.00120
			$h/R = 1.5$		
0.75	0.57121	0.21460	0.02066	0.04137	0.00709
1.0	0.53731	0.28931	0.01715	0.04233	0.00671
1.25	0.52817	0.30579	0.01594	0.04209	0.00649
1.5	0.52654	0.30871	0.01510	0.04168	0.00622
1.75	0.52701	0.30804	0.01421	0.04121	0.00592

Table 4.8. Normalized hydrodynamic coefficients, $\bar{\lambda}_i = \frac{\lambda_i \sqrt{y_0}}{R^2}$, for the tank with a center-mounted baffle of different lengths.

	$h/R = 1.5$				
l_b/R	$\bar{\lambda}_1$	$\bar{\lambda}_3$	$\bar{\lambda}_5$	$\bar{\lambda}_7$	$\bar{\lambda}_9$
0.25	0.60426	0.08832	0.03544	0.02017	0.01304
0.5	0.60293	0.09774	0.03331	0.02051	0.01275
0.75	0.59847	0.12332	0.02672	0.02350	0.01114

the baffle tip approaches within 0.25 R from the free surface, it yields relatively lower coefficient $\bar{\lambda}_1$ and thus the lateral slosh force.

The normalized hydrodynamic coefficients for the tank with top-mounted baffles of different lengths are presented in Table 4.7. Comparison of the coefficients with those of the clean-bore tank (Table 4.5) suggests that the coefficient $\bar{\lambda}_1$ of the tank with a top-mounted baffle is relatively smaller than that of the clean-bore tank, irrespective of the baffle length and the fill ratio. The coefficients $\bar{\lambda}_3$, however, are substantially higher than those of the clean-bore tank for the baffle length and fill ratios considered. The top-mounted baffle also yields higher coefficients $\bar{\lambda}_7$ and lower values of $\bar{\lambda}_9$ compared to the clean-bore tank. The coefficients $\bar{\lambda}_5$ for the baffled tank are also considerably lower, except for the very low fill height (h/R=0.5). Further, the numerical values of these higher modes coefficients are significantly smaller than $\bar{\lambda}_1$ and $\bar{\lambda}_3$. In this case, the first two antisymmetric modes may be considered as the dominant modes. It is further seen that hydrodynamic coefficient $\bar{\lambda}_1$ decreases while $\bar{\lambda}_3$ increases with increase in baffle length, while the change diminishes gradually with further increase in the length. This suggests that the contribution of the second antisymmetric mode to the slosh force would be higher for longer baffles, while that of the first mode would be smaller.

Table 4.8 shows the normalized hydrodynamic coefficients for the tank with center mounted-baffles of different lengths. The results are presented only for the fill ratio of h/R=1.5, since the coefficients for other fill heights are identical to those for the top mounted baffle, when piercing the free surface, or those of the clean-bore tank. The results show trends similar to those observed for the tank with bottom-mounted baffle with increase in the baffle length since the baffle remains fully submerged for the lengths considered in the study. The results for the baffled tanks in Tables 4.6-4.8 were obtained with the accuracy of five decimal places using a maximum of 2000 elements on the half-length of the free-surface. A peak discrepancy in the order of 0.6% was observed when 150 elements on the half-length of the free-surface were used.

Variations in the damping ratios, $\bar{\xi}_i = \xi_i \left(\frac{g}{A_0}\right)^{\frac{2}{3}} (i = 1,3,5,7)$, of different baffled tanks and fill ratios are also evaluated and presented in Fig. 4.8. The results were obtained for 1 m radius tank with bottom-, top-, and center-mounted baffles of lengths l_b =0.5 and 1.0m. The bottom-mounted baffle yield substantially higher damping in the first antisymmetric mode

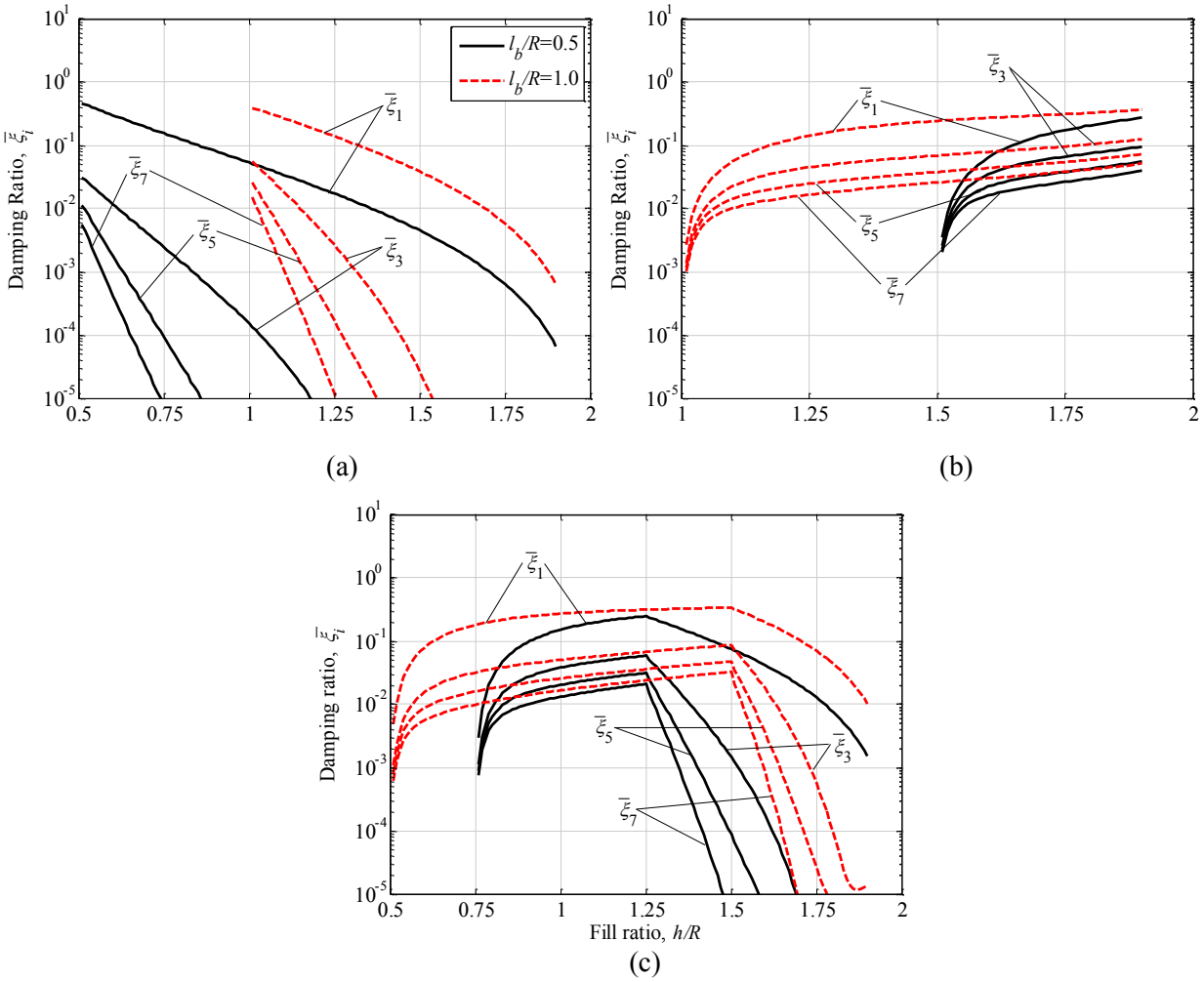

Fig. 4.8. Damping ratios corresponding to first four antisymmetric free surface modes of the tank with a: (a) bottom-mounted; (b) top-mounted; and (c) center-mounted baffle of different lengths (R= 1 m)

compared to the other modes, irrespective of the fill height and baffle length considered, as shown in Fig. 4.8a. The damping ratios in the higher modes also tend to diminish rapidly with increasing fill ratio compared to the first mode damping. Increasing the baffle length yields higher damping in all the modes. For the tank with the top-mounted baffle, the differences in the damping ratios corresponding to the considered modes are relatively small compared to the bottom-mounted baffle, as shown in Fig. 4.8b. Comparison of results in Figs. 4.8a and 4.8b suggest that the top-mounted baffles are more beneficial for suppressing liquid slosh under higher fill ratios, while the bottom-mounted baffle is more effective under lower fill heights. The damping ratios of the tank with the center-mounted baffle are similar to those of the tank with a

top-mounted baffle, when the center-mounted baffle is partly submerged. The damping ratios in all the modes diminish rapidly when the free surface lies above the baffle.

4.3.3 Slosh force and overturning moment

The effect of baffles on the lateral force due to the liquid slosh is evaluated under a turning maneuver idealized by a ramp-step lateral acceleration, as shown in Fig. 4.9, where A_0 is the steady-state lateral acceleration and t_0 is denoted as the rise time. Hasheminejad and Aghabeigi (2011) evaluated the lateral force and roll moment caused by fluid slosh in a cylindrical tank with bottom- (l_b/R=0.25, 0.5, 0.75) and top-mounted baffles (l_b/R=1.25, 1.5, 1.75) using conformal mapping. The study was limited to half-full tanks, while the damping effect of the baffle was neglected. For the purpose of validation, simulations were performed for 50%-filled tank and identical baffle lengths, while suppressing damping due to baffles. Variations in the normalized lateral force, $\bar{F}_y = \frac{F_y}{mA_0}$, versus the normalized time, $\bar{t} = t\sqrt{g/R}$, for the half-full tank under the lateral excitation with different normalized rise times, $\bar{t}_0$, ranging from 0.01 to 5s, are shown in Figs. 4.10 and 4.11, for the bottom- and top-mounted baffles, respectively. The results were in total agreement with those reported in Hasheminejad and Aghabeigi (2011).

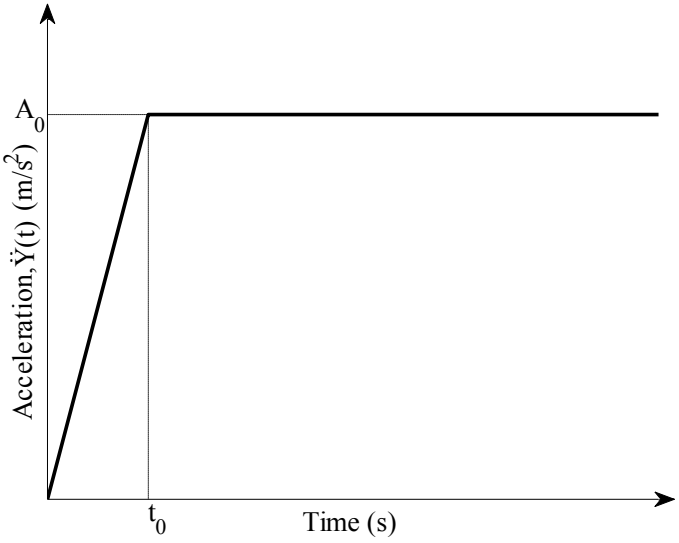

Fig. 4.9. Lateral acceleration input idealizing a steady turning maneuver.

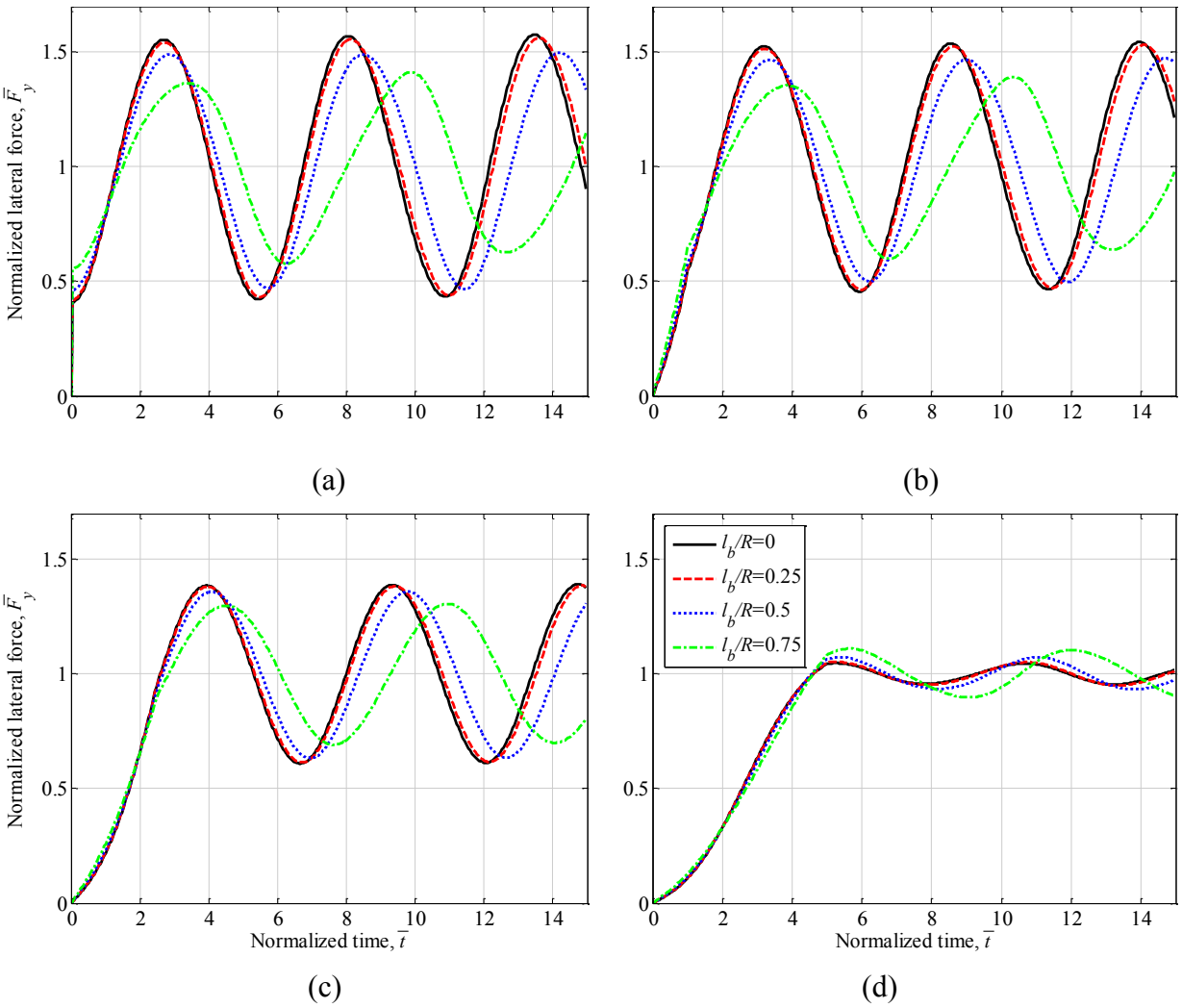

Fig. 4.10. Effect of rise time of the ramp-step lateral acceleration on the normalized lateral slosh force developed in the half-full tank with a bottom-mounted baffle of different lengths: (a) $\bar{t}_0 = 0.01$; (b) $\bar{t}_0 = 1$; (c) $\bar{t}_0 = 2.5$; and (d) $\bar{t}_0 = 5$.

As it can be seen in Fig. 4.10, a short bottom-mounted baffle (l_b/R=0.25) yields negligible effect on the lateral force response, irrespective of the rise-time of the input. A baffle with length l_b/R=0.75 yields lowest peak response, except for $\bar{t}_0 = 5$. The results clearly show the significant effect of the rise time on the lateral slosh force. A shorter rise time of the disturbance causes higher magnitude of the lateral force, which is attributed to higher rate of change of the input. The results generally show lower magnitudes of slosh force with increasing baffle length, except for the slowly increasing input ($\bar{t}_0 = 5$). Similar to the bottom-mounted baffle tank, extending the length of the top-mounted baffle also yields greater suppression of the lateral force, as shown

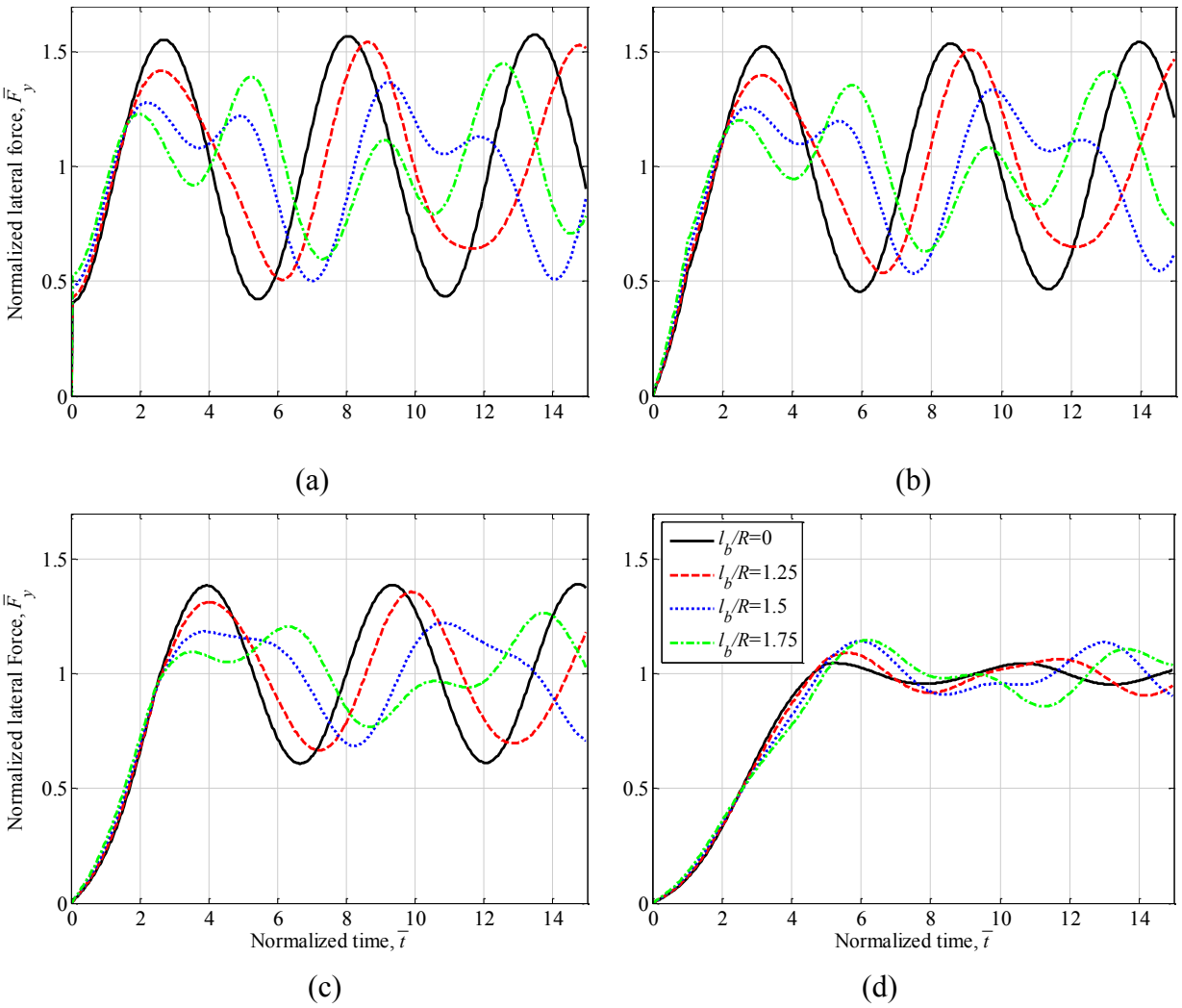

Fig. 4.11. Effect of rise time of the ramp-step lateral acceleration on the normalized lateral slosh force developed in the half-full tank with a top-mounted baffle of different lengths: (a) $\bar{t}_0 = 0.01$; (b) $\bar{t}_0 = 1$; (c) $\bar{t}_0 = 2.5$; and (d) $\bar{t}_0 = 5$.

in Fig. 4.11. Further, the results clearly show the contribution of the second antisymmetric mode, particularly for l_b/R=1.5 and 1.75, as it was observed from the hydrodynamic coefficients (Table 4.7).

The results in Figs. 4.10 and 4.11 were obtained upon neglecting the damping due to baffles in order to validate the methodology using the reported results. The results thus showed continued undamped system oscillations even after the input approached its steady-value. It has been shown that baffle damping together with the fluid viscosity cause gradual decay in the amplitudes of slosh force oscillations (Modaressi-Tehrani *et al.*, 2007). Subsequent simulations

are thus performed considering the damping effect of baffles on the slosh force and moment, as described in Eq. (4.24) and Fig. 4.8, although the fluid viscosity effect could not be incorporated.

Figures 4.12 to 4.14 illustrate the normalized lateral force responses of the bottom-, top- and center-mounted baffle tanks, respectively, for two baffle lengths (l_b/R=0.5 ,1) and two fill heights (h/R=1.5, 1.75) considering A_0=0.3g and $\bar{t}_0 = 1$. The results are also compared with those of the clean-bore tank, where the damping effect is not present. The lateral force response of the tank with a bottom-mounted baffle with smaller length l_b/R=0.5 is similar to that of the clean-bore tank, which is in-part attributed to its negligible damping effect. The longer baffle (l_b/R=1), however, yields lower peak lateral force for h/R=1.5 (a reduction of about 5% in the first peak). A greater reduction in the peak lateral force, however, is evident for top-mounted baffle (Fig. 4.13), provided that the baffle extends into the flow. For h/R=1.5 (Fig. 4.13a), the top-mounted baffle (l_b/R=1) yields about 10% reduction in the peak force compared to that of the clean-bore tank. The corresponding reductions for h/R=1.75 are nearly 5% and 7% with l_b/R=0.5 and 1, respectively. The center mounted baffle yields notable reductions in the peak lateral force for ratio h/R=1.5, as seen in Fig. 4.14. The first peak values are 4% and 13% lower than that of the clean-bore tank for l_b/R=0.5 and 1, respectively. The relative reductions for the higher fill ratio h/R=1.75, however, are very small.

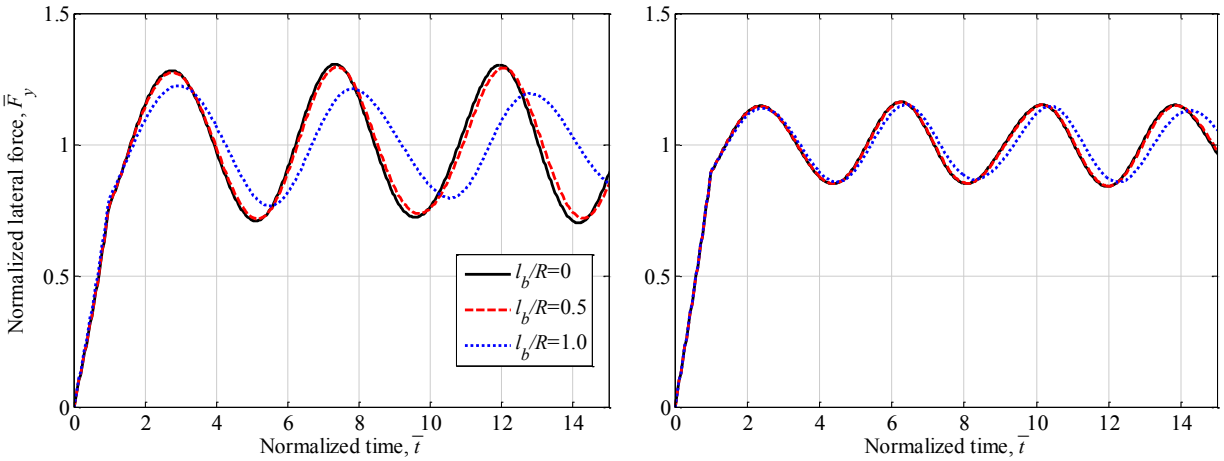

Fig. 4.12. Effect of length of a bottom-mounted baffle on the normalized lateral slosh force developed under a ramp-step lateral acceleration: (a) h/R=1.5; and (b) h/R=1.75 (R=1.0m, A_0=0.3g and $\bar{t}_0 = 1$).

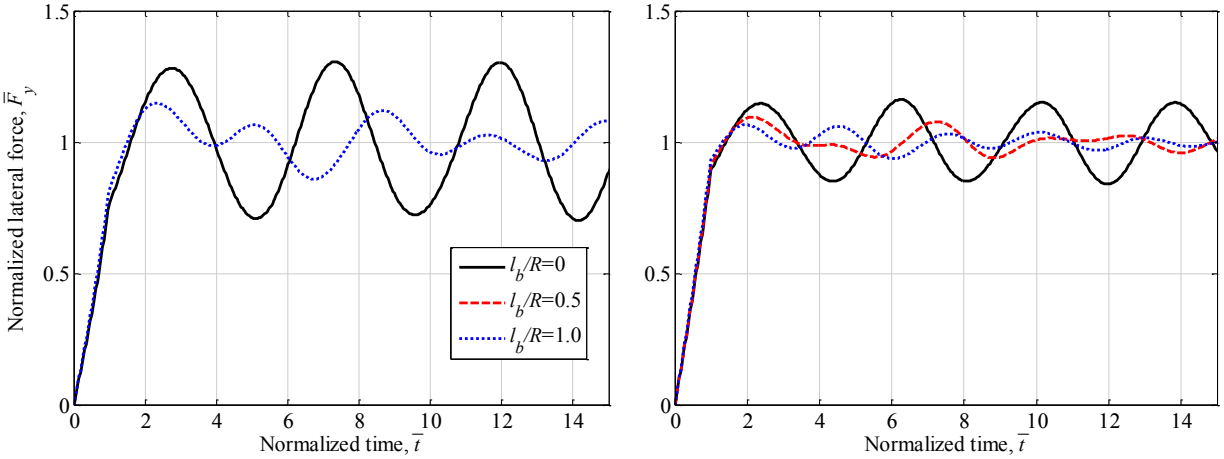

Fig. 4.13. Effect of length of a top-mounted baffle on the normalized lateral slosh force developed under a ramp-step lateral acceleration: (a) h/R=1.5; and (b) h/R=1.75 (R=1.0m, A_0=0.3g and $\bar{t}_0 = 1$).

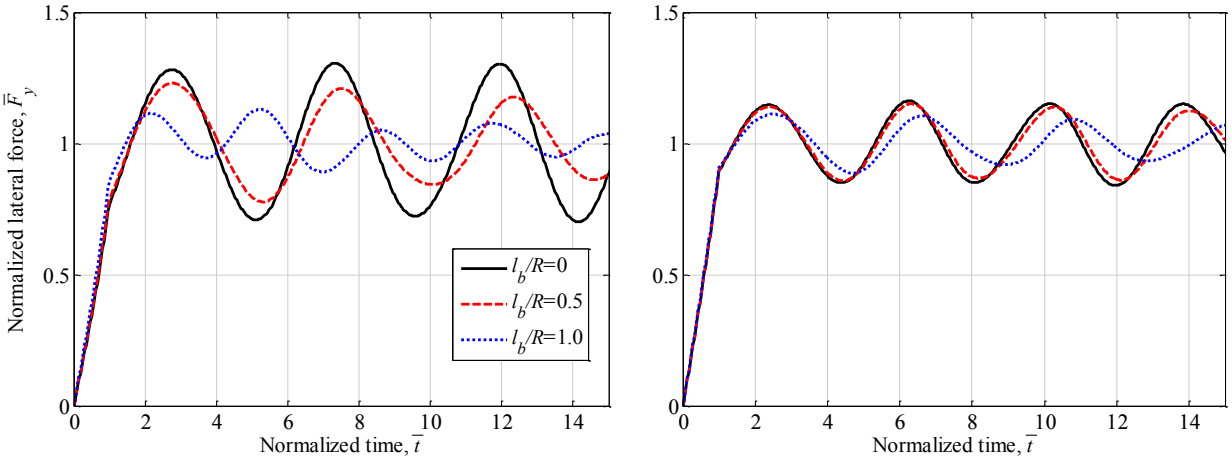

Fig. 4.14. Effect of length of a center-mounted baffle on the normalized lateral slosh force developed under a ramp-step lateral acceleration: (a) h/R=1.5; and (b) h/R=1.75 (R=1.0m, A_0=0.3g and $\bar{t}_0 = 1$).

Time histories of normalized overturning moment due to fluid motion about the tank bottom, $\bar{M}_B = \frac{M_B}{mA_0(R+z_{cg})}$, are presented in Figs. 4.15 to 4.17 for the three baffle designs, two fill heights (h/R=1.5,1.75) and two baffle lengths l_b/R=0.5,1. Similar to the lateral force response, only a longer bottom-mounted baffle (l_b/R=1) helps reduce the peak overturning moment for the

lower fill ratio, (nearly 12% and 4% reduction in the first peak for fill ratios h/R=1.5 and h/R=1.75, respectively), as shown in Fig 4.15. The top-mounted baffle of the same length also resulted in nearly 10% and 8% reductions in the peak overturning moment for the fill ratios h/R=1.5 and h/R=1.75, respectively. The relatively lower reduction in the first peak response of the tank (h/R=1.5; l_b/R=1) with a top-mounted baffle compared to that with a bottom mounted baffle may be attributed to the higher mean pressure acting on the baffle and greater distance between the pressure center and the tank bottom point for the tank with the top-mounted baffle. The higher damping effect of the top-mounted baffle (Fig. 4.8), however, would cause greater rate of decay in the overturning moment response, as shown in Fig. 4.16. A longer baffle may also lead to a higher bending moment about its support due to greater wetted area and thus the slosh force, and larger distance between the center of pressure and the baffle mounting. The center-mounted baffle of length l_b/R=1 exhibits largest reduction (14%) in the peak moment for h/R=1.5, while it offers only 3% reduction for h/R=1.75 (Fig. 4.17).

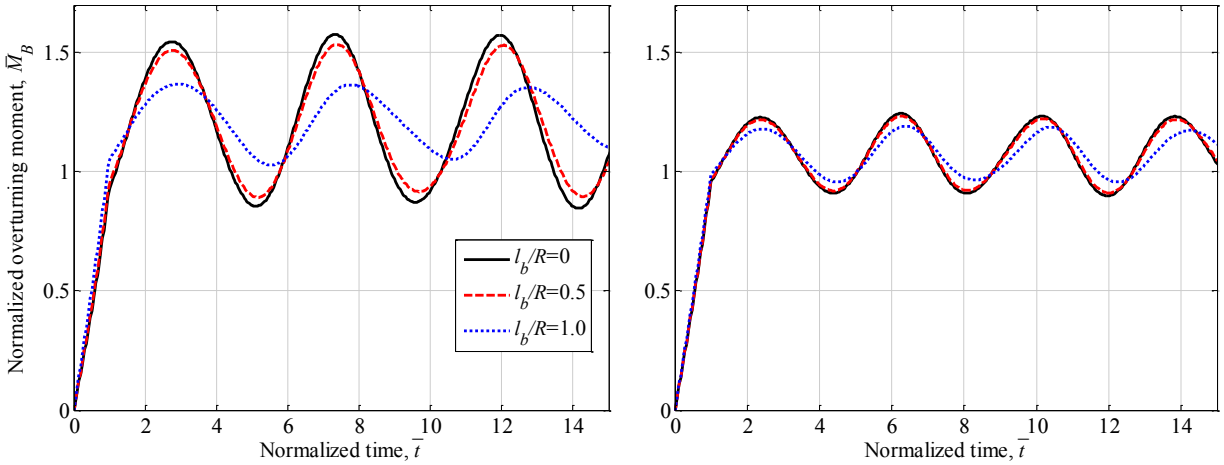

Fig. 4.15. Effect of length of a bottom-mounted baffle on the normalized overturning moment developed under a ramp-step lateral acceleration: (a) h/R=1.5; and (b) h/R=1.75 (R=1.0m, A_0=0.3g and $\bar{\boldsymbol{t}}_{\boldsymbol{0}} = \mathbf{1}$).

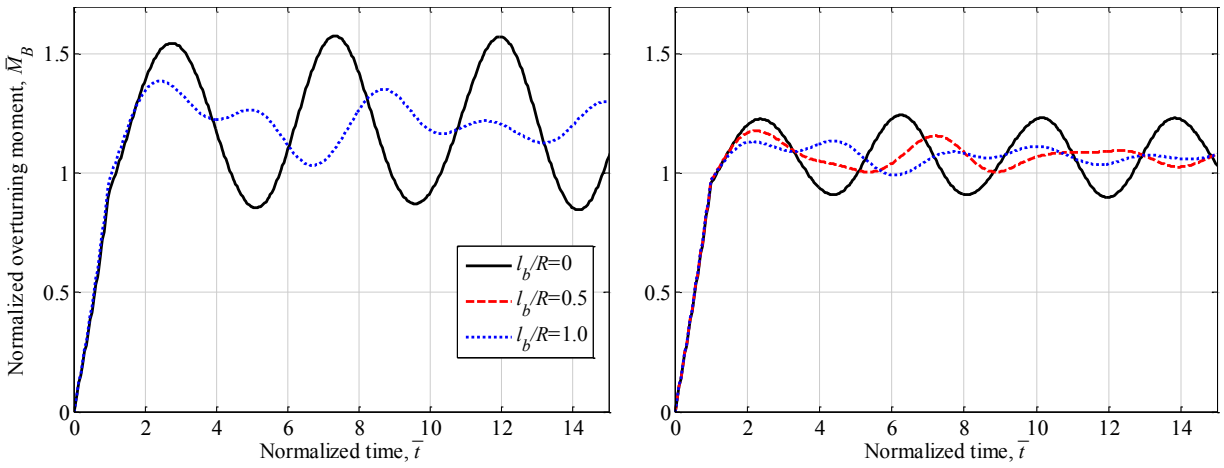

Fig. 4.16. Effect of length of a top-mounted baffle on the normalized overturning moment developed under a ramp-step lateral acceleration: (a) h/R=1.5; and (b) h/R=1.75 (R=1.0m, A_0=0.3g and $\bar{\boldsymbol{t}}_{\boldsymbol{0}} = \mathbf{1}$).

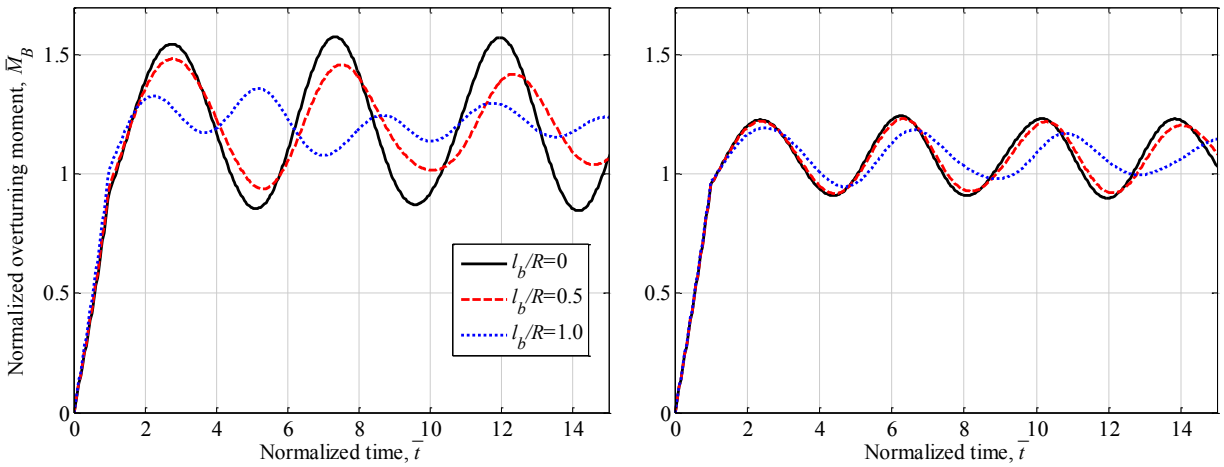

Fig. 4.17. Effect of length of a center-mounted baffle on the normalized overturning moment developed under a ramp-step lateral acceleration: (a) h/R=1.5; and (b) h/R=1.75 (R=1.0m, A_0=0.3g and $\bar{\boldsymbol{t}}_{\boldsymbol{0}} = \mathbf{1}$).

4.4 Conclusions

A linear multimodal method coupled with the BEM was developed for analysis of transient liquid slosh in a laterally excited partly-filled cylindrical container with different

designs of baffles located in the mid-longitudinal plane. The analyses of slosh frequencies and modes required relatively few numbers of elements on the half length of the free-surface suggesting significantly greater computational efficiency of the method for baffled tanks compared to the BEM employing all the elements for solving the spectral problem. Considerations of only 4 to 5 modes resulted in accurate estimations of the hydrodynamic loads due to negligible contributions of the higher modes. The model could thus permit efficient analyses of transient fluid slosh and its effect on directional responses of a baffled tank vehicle, when integrated with the multi-body vehicle dynamics models. The results suggested that addition of a baffle could yield substantially lower antisymmetric slosh frequencies when the baffle pierced the free-surface, while the baffle had no effect on the symmetric frequencies and modes. The results also illustrated contributions of the higher modes to the hydrodynamic responses only when the baffle pierced the free-surface, while the first antisymmetric mode was the dominant one when the baffle was completely submerged. Lower fundamental frequency of slosh was also obtained when the baffle tip was close to the free surface but fully immersed in the fluid domain. A higher damping effect of the baffle was also observed for all the modes studied, when it pierced the free surface.

The anti-slosh effectiveness of the baffle was strongly affected by the baffle length relative to the free surface height. The results demonstrated greater effectiveness of the top-mounted baffle in suppressing the slosh force and overturning moment for relatively high fill levels, well above 50%, when subjected to a lateral acceleration excitation, while the bottom-mounted baffle was effective only under very low fill levels. The center-mounted baffle, on the other hand, could reduce the magnitude of slosh force moment only for intermediate fill levels. Taking these into consideration, an optimal baffle length could be obtained for a range of commonly encountered fill heights in tank vehicles.

CHAPTER 5

THREE-DIMENSIONAL DYNAMIC LIQUID SLOSH IN PARTIALLY-FILLED HORIZONTAL TANKS SUBJECT TO SIMULTANEOUS LONGITUDINAL AND LATERAL EXCITATIONS

5.1 Introduction

Liquid oscillations in partially filled tank vehicles under multiple excitations are known to adversely affect the directional dynamics and safety performance of such vehicles. The slosh forces and moments arising from liquid movements during a braking-in-a-turn maneuver may yield considerable dynamic load shifts in both the roll and pitch planes of the road tankers, which may cause lock-up of the rear wheels and thus the loss of vehicle stability. Directional response and safety performance of partially filled tank trucks during braking and steering maneuvers, however, have been mostly evaluated using quasi-static analysis, which only accounts for the steady-state load shifts due to change in position of liquid cargo center of mass. Ranganathan and Yang (1996) studied the effect of steady state liquid load shift occurring within a partially filled cylindrical clean-bore tank on the braking characteristics of a tank vehicle. Zhanqi *et al.* (1995) proposed optimal compartment sizing of a tank-trailer combination with an elliptical tank subject to a constant deceleration maneuver, using quasi-static fluid slosh along the longitudinal axis. Kang *et al.* (2000a) developed a three-dimensional quasi-static fluid slosh model considering simultaneous application of longitudinal and lateral accelerations to study the effect of liquid cargo load shift in the roll and pitch planes on dynamics of an articulated road tanker subject to braking-in-a-turn maneuvers.

Alternatively, a number of studies have investigated dynamic fluid slosh within partly filled clean-bore and baffled tanks using CFD methods (e.g., Modaressi-Tehrani *et al.*, 2006, 2007; Yan *et al.*, 2008). Applications of the dynamic slosh to the vehicle models, however, have met limited success due to high computational demands of the CFD methods and the need for elaborate data transfers for coupled fluid-vehicle simulations. Thomassy *et al.* (2003) coupled the CFD software, FLOW-3D, to a multi-body vehicle dynamic model through a master program to

perform coupled fluid-vehicle simulations. Yan and Rakheja (2009) investigated straight line braking performance of a partially filled tank truck by coupling the multi-body vehicle model with the FLUENT software. Alternatively, a number of mechanical analogous models have been proposed to describe liquid oscillations in moving containers, which can be directly integrated to the vehicle models to perform coupled fluid-vehicle dynamics analyses in an efficient manner. Identification of the mechanical model parameters, however, requires prior CFD simulations (Salem *et al.*, 2009), experimental measurements (Ibrahim, 1999) or analytical solutions (Ranganathan *et al.*, 1994).

Computationally efficient models for predicting dynamic fluid slosh loads in moving containers with sufficient accuracy and ease of integration to the multi-body vehicle models are thus vital for directional dynamic analyses of partly-filled tank vehicles and for designs of anti-slosh mechanisms. Analytical models based on the linear slosh theory are known to be most efficient (Hasheminejad and Aghabeigi, 2011, 2012; Kolaei *et al.*, 2014), while their limitations and ranges of applicability need to be considered when applied to tank vehicles (Kolaei *et al.*, 2014). These studies employed conformal transformation of the fluid domain to a domain in which the Laplace equation becomes separable. The aforementioned analytical studies are limited to the two-dimensional slosh under a lateral excitation. An analytical solution for free liquid slosh in horizontal cylinders of finite length was developed by Evans and Linton (Evans and Linton, 1993). Papaspyrou *et al.* (2004b) extended the eigenvalue formulation of Evans and Linton (1993) to study liquid slosh under a longitudinal excitation. These studies, however, were limited to only half-full condition. The linear liquid slosh in horizontal cylinders subject to a longitudinal excitation was also performed by Karamanos *et al.* (2009) using finite element method (FEM).

Faltinsen and Timokha (2009, 2010) formulated a computationally efficient linear multimodal model based on the linear slosh theory, which required prior estimations of the natural slosh modes/frequencies and hydrodynamic coefficients. The fluid slosh modes may be obtained using numerical methods such as boundary element method (BEM), which permits far more efficient computations of the influence matrices than the finite element method, where the entire fluid domain needs to be discretized (Katsikadelis, 2002). The application of the BEM for the modal analysis of three-dimensional liquid slosh, however, has been attempted in only a few studies generally focuses on upright tanks. Dutta and Laha (2000) reported natural frequencies

and modes of liquid slosh in upright cylindrical, spherical and conical tanks using a three-dimensional BEM. Firouz-Abadi *et al.* (2008, 2009) also developed a three-dimensional BEM for analysis of natural slosh frequencies and modes in various clean-bore and baffled tanks such as upright rectangular and cylindrical, and spherical tanks. The effect of ring baffles on the natural slosh frequencies and seismic responses of upright cylindrical tanks was studied by Gedikli and Erguven (1999, 2003) using BEM and superposition of modes.

In the present study, a linear multimodal model is presented for analyses of fluid slosh in horizontal cylindrical tanks subject to simultaneous application of longitudinal and lateral accelerations, idealizing a braking-in-a turn maneuver. Higher order BEM method is employed to obtain the slosh modes and hydrodynamic coefficients. Using the separation of variables, the BEM is applied in a two-dimensional domain so as to reduce the computational demand. The resulting generalized eigenvalue equation is further reduced to two standard eigenvalue problems considering only the velocity potential on the half free-surface length. Slosh forces and moments are subsequently obtained from the slosh modes and the hydrodynamic coefficients. An estimate of the viscous damping in the boundary layer is also obtained and implemented into the multimodal analysis. The validity of the model is illustrated using available analytical benchmarks and experimental data. The limitations of the linear slosh theory for predicting slosh forces and moments in moving containers are further presented.

5.2 Formulations

5.2.1 Natural sloshing modes and frequencies

Consider a horizontal container of length L with an arbitrary but symmetrical cross-section, as shown in Fig. 5.1a. The Cartesian coordinate system *Oxyz*, located at the geometric center of the tank, is used with the z-axis directed upward and the x-axis in the longitudinal direction of the container. The liquid fill-level h is measured with respect to the tank bottom, while the z_0 and y_0 denote the coordinates of the free-surface at the intersection of the tank wall (Fig. 5.1b). The free-surface slosh modes can be obtained using the boundary element method (BEM). Assuming inviscid, incompressible and irrotational flows, the problem of free linear slosh in a partly-filled tank can be expressed in the following form (Abramson, 1966; Ibrahim, 2005):

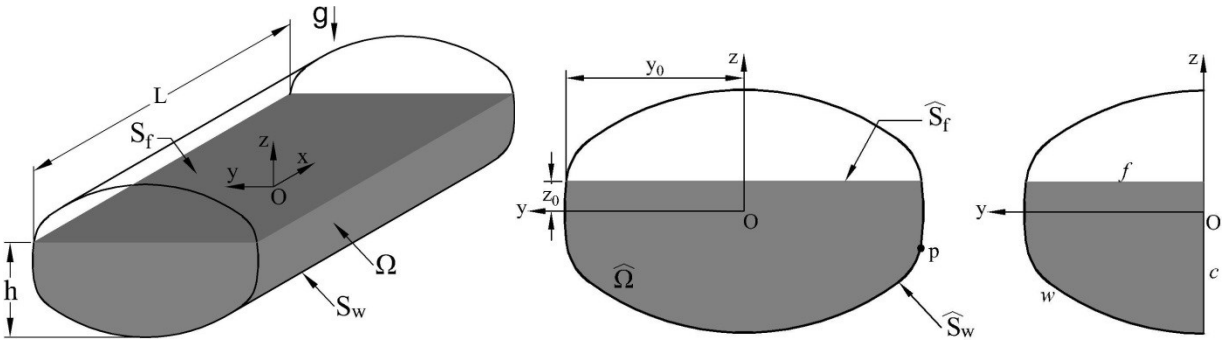

(a) (b) (c)

Fig. 5.1. (a) Three-dimensional fluid free-surface in a partially filled cylindrical tank of arbitrary but symmetrical cross-section; (b) two-dimensional tank cross-section; and (c) the fluid domain considered.

$$\nabla^2 \Phi_{i,j}(x,y,z) = 0 \qquad \text{in } \Omega \tag{5.1}$$

$$\frac{\partial \Phi_{i,j}}{\partial n} = 0 \qquad \text{on } S_w \tag{5.2}$$

$$\frac{\partial \Phi_{i,j}}{\partial z} = \kappa_{i,j} \Phi_{i,j} \qquad \text{on } S_f, \quad i + j \neq 0 \tag{5.3}$$

where i and j are non-negative integers, which refer to longitudinal and lateral mode number, respectively, $\Phi_{i,j}$ is the velocity potential corresponding to i^{th} longitudinal and j^{th} transverse mode and $\frac{\partial}{\partial n}$ denotes the derivative along the normal to the surface. In the above equations, $\kappa_{i,j} = \frac{\sigma_{i,j}^2}{g}$ is related to the circular frequency $\sigma_{i,j}$ of the liquid oscillations, and Ω, S_w and S_f represent the fluid domain, the wetted surface area of the tank and the liquid free-surface, respectively (Fig. 5.1a). The solution of the above eigenvalue problem satisfying the zero-Neumann boundary conditions at the tank end-walls, $x = \pm\frac{L}{2}$, can be sought as (McIver and McIver, 1993):

$$\Phi_{i,j}(x,y,z) = \varphi_{i,j}(y,z) \cos \omega_i \left(x + \frac{L}{2} \right) \tag{5.4}$$

where $\omega_i = \frac{\pi i}{L}$ is the wave number along the longitudinal axis, *Ox*. Introducing Eq. (5.4) into the above eigenvalue problem, Eqs. (5.1-5.3), gives the following series of two-dimensional problems:

$$\nabla^2 \varphi_{i,j}(y,z) - \omega_i^2 \varphi_{i,j}(y,z) = 0 \qquad \text{in } \hat{\Omega} \tag{5.5}$$

$$\frac{\partial \varphi_{i,j}}{\partial n} = 0 \qquad \text{on } \hat{S}_w \tag{5.6}$$

$$\frac{\partial \varphi_{i,j}}{\partial z} = \kappa_{i,j} \varphi_{i,j} \qquad \text{on } \hat{S}_f \tag{5.7}$$

where $\hat{\Omega}$, $\hat{S}_w$ and $\hat{S}_f$ denote two-dimensional fluid domain, tank wall and free-surface, respectively, as shown in Fig. 5.1b. Using Green's second identity, it can be shown that the boundary integral representation of the solution for the Helmholtz equation, Eq. (5.5), at a boundary point *"p"* is obtained as:

$$\frac{\alpha_p}{2\pi} \varphi_{i,j}(p) = -\int_{\hat{\Gamma}} \left(\psi_i \frac{\partial \varphi_{i,j}}{\partial n} - \varphi_{i,j} \frac{\partial \psi_i}{\partial n} \right) dS \tag{5.8}$$

where $\hat{\Gamma} = \hat{S}_w + \hat{S}_f$ is the boundary enclosing the fluid domain, and α_p is π when point p is located on a smooth boundary, or the angle between the tangents of the boundary at p when p is a corner point. In the above equation, ψ is the fundamental solution of the Helmholtz equation ($i \neq 0$), given by (Brebbia *et al.*, 1984):

$$\psi_i(y,z;y_p,z_p) = \frac{1}{2\pi} K_0 \left(\omega_i \sqrt{(y-y_p)^2 + (z-z_p)^2} \right), \qquad i \geq 1 \tag{5.9}$$

where K_0 is the modified Bessel function of the second kind and zero order. When $i = 0$, Helmholtz equation, Eq. (5.5), reduces to a Laplace equation, whose fundamental solution takes the form (Brebbia *et al.,* 1984):

$$\psi_0(y,z;y_p,z_p) = \frac{1}{2\pi} \ln \sqrt{(y-y_p)^2 + (z-z_p)^2} \tag{5.10}$$

Dividing the fluid boundaries into three-node quadratic elements, one can obtain a matrix equation from Eq. (5.8) for each free liquid oscillation mode in the form:

$$[\mathbf{H}]\{\boldsymbol{\varphi}\} = [\mathbf{G}]\{\mathbf{q}\} \tag{5.11}$$

Here $\{\boldsymbol{\varphi}\}$ and $\{\mathbf{q}\}$ are the unknown vectors of velocity potential $\varphi_{i,j}$ and normal velocity $q_{i,j} = \frac{\partial \varphi_{i,j}}{\partial n}$ on each node; and $[\mathbf{H}]$ and $[\mathbf{G}]$ are influence matrices, which are obtained from Eq. (5.8) using quadratic interpolating functions to evaluate $\varphi_{i,j}$ and $q_{i,j}$ on each element. The conditions of continuous velocity potential φ_i and discontinuous normal velocity q_i are considered at points where the type of boundary conditions change. Since the two-dimensional fluid domain is symmetric with respect to $y = 0$, one may consider only half of the fluid domain (Fig. 5.1c) in order to enhance the computational efficiency. The matrix Eq. (5.11) can thus be expressed as:

$$\begin{bmatrix} \mathbf{H}_{ff} & \mathbf{H}_{fw} & \mathbf{H}_{fc} \\ \mathbf{H}_{wf} & \mathbf{H}_{ww} & \mathbf{H}_{wc} \\ \mathbf{H}_{cf} & \mathbf{H}_{cw} & \mathbf{H}_{cc} \end{bmatrix} \begin{Bmatrix} \boldsymbol{\varphi}_f \\ \boldsymbol{\varphi}_w \\ \boldsymbol{\varphi}_c \end{Bmatrix} = \begin{bmatrix} \mathbf{G}_{ff} & \mathbf{G}_{fw} & \mathbf{G}_{fc} \\ \mathbf{G}_{wf} & \mathbf{G}_{ww} & \mathbf{G}_{wc} \\ \mathbf{G}_{cf} & \mathbf{G}_{cw} & \mathbf{G}_{cc} \end{bmatrix} \begin{Bmatrix} \mathbf{q}_f \\ \mathbf{q}_w \\ \mathbf{q}_c \end{Bmatrix} \tag{5.12}$$

where subscripts f, w and c refer to free-surface, wall and symmetry boundaries in Fig. 5.1c, respectively. The first subscript of submatrices $\mathbf{H}$ and $\mathbf{G}$ denotes the location of the source point (point *"p"* in Eq. (5.8)) and the second subscript refers to the element location on which the boundary integration is performed. The zero-Neumann boundary condition on the tank wall implies that $\mathbf{q}_w = 0$. The free-surface boundary condition (Eq. 5.7) also implies that $\mathbf{q}_f = \kappa_{i,j}\boldsymbol{\varphi}_f$ for each mode. Noting $\mathbf{q}_c = 0$ for the symmetric modes, and $\boldsymbol{\varphi}_c = 0$ for the antisymmetric modes, Eq. (5.12) can be reduced to the following matrix equations for the symmetric and antisymmetric modes as:

$$\mathbf{A}\boldsymbol{\varphi}_f = \kappa_{i,2j}\boldsymbol{\varphi}_f\,, \qquad \mathbf{B}\boldsymbol{\varphi}_f = \kappa_{i,2j+1}\boldsymbol{\varphi}_f \tag{5.13}$$

where $\mathbf{A}$ and $\mathbf{B}$ are square matrices with size of $2N_f+1$ and $2N_f$, respectively (where N_f is number of elements on half of the free-surface), which depend on submatrices $\mathbf{H}$ and $\mathbf{G}$. The above eigenvalue problems are solved to determine the natural slosh frequencies and modes.

5.2.2. Multimodal solution

The proposed BEM is used for multimodal analysis of the three-dimensional liquid slosh in a horizontal cylindrical tank of circular cross-section. The linearized form of the kinematic and dynamic boundary conditions on the free-surface for an ideal fluid in a rigid container (Fig. 5.1a) can be written as (Abramson, 1966):

$$\frac{\partial \delta}{\partial t} = \frac{\partial \Phi}{\partial z}, \qquad \frac{\partial \Phi}{\partial t} = -g\delta \qquad \text{on } S_f \tag{5.14}$$

where δ is the free-surface elevation. One may decompose the velocity potential Φ in the above equation into two parts; the potential Φ_R representing the rigid body motion of the fluid, which is the same as the potential of the container motion, and the potential Φ_S representing the liquid motion relative to the container, which is the potential of the sloshing fluid. Under simultaneous longitudinal and lateral motions of the tank arising during a braking-in-a-turn maneuver of the tank vehicle, the rigid body potential is given by $\Phi_R = \dot{X}x + \dot{Y}y$, where $\dot{X}$ and $\dot{Y}$ are the longitudinal and lateral velocity components of the container, respectively. Based on the multimodal approach (Faltinsen and Timokha, 2009), the sloshing potential, $\Phi_S(x, y, z, t)$, and free-surface elevation, $\delta(x, y, t)$, can be expressed as a summation of the natural slosh modes and generalized functions $\gamma_{i,j}$ and $\beta_{i,j}$ as:

$$\Phi_S(x, y, z, t) = \sum_{i=0}^{\infty}\sum_{j=0}^{\infty} \gamma_{i,j}(t)\Phi_{i,j}(x, y, z),$$

$$\delta(x, y, t) = z_0 + \sum_{i=0}^{\infty}\sum_{j=0}^{\infty} \beta_{i,j}(t)\Phi_{i,j}(x, y, z_0), \qquad i + j \neq 0 \tag{5.15}$$

In the above, the rigid body mode ($i = j = 0$) has been excluded. Substituting for $\Phi = \Phi_R + \Phi_S$ and δ into the free-surface boundary conditions (Eq. 5.14) together with orthogonality of the sloshing modes on the free-surface and considering Eq. (5.3) results in the following ordinary differential equations in terms of the generalized functions $\beta_{i,j}$:

$$\ddot{\beta}_{i,j} + \sigma_{i,j}^2\beta_{i,j} = -\frac{\mu}{L}\kappa_{i,j}\left(\lambda_{x_{i,j}}\ddot{X} + \lambda_{y_{i,j}}\ddot{Y}\right) \tag{5.16}$$

where $\mu = 1$ for $i = 0$ and $\mu = 2$ for $i \geq 1$, while the generalized functions $\gamma_{i,j}$ and $\beta_{i,j}$ are related as $\dot{\beta}_{i,j} = \kappa_{i,j}\gamma_{i,j}$. In the above equation, $\ddot{X}$ and $\ddot{Y}$ denote the longitudinal and lateral acceleration excitations imposed on the container, and $\lambda_{x_{i,j}}$ and $\lambda_{y_{i,j}}$may be regarded as hydrodynamic coefficients given by:

$$\lambda_{x_{i,j}} = \int_{S_f} x\Phi_{i,j}(x, y, z_0)dS \tag{5.17}$$

$$\lambda_{y_{i,j}} = \int_{S_f} y\Phi_{i,j}(x, y, z_0)dS \tag{5.18}$$

where the natural slosh modes $\varphi_{i,j}$, obtained from the BEM, are normalized such that $\int_{\hat{S}_f} |\varphi_{i,j}|^2 \, dS = 1$. It can be shown that $\lambda_{x_{i,j}} = 0$ when $i = 0,2,4, \ldots 2N$ for any j. Also, $\lambda_{y_{i,j}} = 0$ when $i \geq 1$. Therefore, the hydrodynamic coefficients for the remaining indices can be expressed as:

$$\lambda_{x_{i,j}} = -\frac{2}{\omega_i^2} \int_{\hat{S}_f} \varphi_{i,j}(y, z_0) dS \,, \quad i = 1,3,5, \ldots 2N-1; j \geq 0 \tag{5.19}$$

$$\lambda_{y_{0,j}} = L \int_{\hat{S}_f} y \varphi_{0,j}(y, z_0) dS \,, \quad j \geq 1 \tag{5.20}$$

It is obvious that $\lambda_{x_{i,j}} = 0$ for the antisymmetric lateral modes ($j = 1,3,5, \ldots 2N-1$). Moreover, $\lambda_{y_{0,j}} = 0$ for the symmetric lateral modes ($j = 2,4,6, \ldots 2N$); Both the symmetric and antisymmetric lateral modes are thus excited for a tank subjected to a combined longitudinal and lateral excitations, while only symmetric lateral modes contribute to the response in a longitudinal motion of the tank. The above hydrodynamic coefficients can be efficiently calculated using quadratic interpolating functions employed in the present boundary element model.

Since the multimodal method based on the potential flow assumption does not consider energy dissipation, an artificial damping term needs to be introduced in Eq. (5.16) to account for the damping effect due to the liquid viscosity (Faltinsen and Timokha, 2009). Equation (5.16) is thus expressed as:

$$\ddot{\beta}_{i,j} + 2\xi_{i,j}\sigma_{i,j}\dot{\beta}_{i,j} + \sigma_{i,j}^2 \beta_{i,j} = -\frac{\mu}{L} \kappa_{i,j} \left(\lambda_{x_{i,j}} \ddot{X} + \lambda_{y_{i,j}} \ddot{Y} \right) \tag{5.21}$$

where $\xi_{i,j}$ represents the damping ratio, which is estimated from the mean rate of energy dissipation (Abramson, 1966):

$$\xi_{i,j} = \frac{\overline{\frac{dE}{dt}}}{2\sigma_{i,j}E} \tag{5.22}$$

where $\overline{\frac{dE}{dt}}$ is the mean rate of energy dissipation over the oscillation period $T_{i,j} = \frac{2\pi}{\sigma_{i,j}}$ and E is the total energy of the liquid motion. The total energy E of the free liquid oscillations in a clean-bore

tank in addition to the mean dissipation rate $\overline{\frac{dE}{dt}}$ due to the liquid viscosity are calculated and implemented in Eq. (5.22) to evaluate the damping ratio. Under free oscillations of the liquid, the generalized functions $\beta_{i,j}(t)$ and $\gamma_{i,j}(t)$ may be expressed by harmonic functions as:

$$\beta_{i,j}(t) = \beta_{0_{i,j}} \sin(\sigma_{i,j} t) \ , \quad \gamma_{i,j}(t) = \frac{\beta_{0_{i,j}} g}{\sigma_{i,j}} \cos(\sigma_{i,j} t) \tag{5.23}$$

The velocity potential and the free-surface elevation corresponding to each mode can thus be expressed in the following forms:

$$\Phi_{S_{i,j}}(x, y, z, t) = \frac{\beta_{0_{i,j}} g}{\sigma_{i,j}} \Phi_{i,j}(x, y, z) \cos(\sigma_{i,j} t),$$
$$\delta_{i,j}(y, t) = z_0 + \beta_{0_{i,j}} \Phi_{i,j}(x, y, z_0) \sin(\sigma_{i,j} t) \tag{5.24}$$

Further, the potential and kinetic flow energies are given by (Ibrahim, 2005):

$$E_p = \frac{1}{2} \rho g \int_{S_f} (\delta_{i,j} - z_0)^2 dS \ , \qquad E_k = \frac{1}{2} \rho \int_{\Omega} \left| \nabla \Phi_{S_{i,j}} \right|^2 d\Omega \tag{5.25}$$

where ρ is the fluid density. Substituting for $\Phi_{S_{i,j}}$ and $\delta_{i,j}$ from Eq. (5.24) into Eq. (5.25) leads to the following expression for the potential energy:

$$E_p = \frac{L}{2\mu} \rho g \beta_{0_{i,j}}^2 \sin^2(\sigma_{i,j} t) \tag{5.26}$$

The kinetic energy is obtained by transforming the integral in Eq. (5.25) to an integral over the free-surface using the Divergence theorem and by letting $\Phi_{S_{i,j}} \nabla \Phi_{S_{i,j}}$ as the differentiable vector, such that:

$$E_k = \frac{1}{2} \rho \int_{S_f} \Phi_{S_{i,j}} \left(\nabla \Phi_{S_{i,j}} \cdot \boldsymbol{n} \right) dS = \frac{L}{2\mu} \rho g \beta_{0_{i,j}}^2 \cos^2(\sigma_{i,j} t) \tag{5.27}$$

The total energy can be subsequently derived as:

$$E = E_p + E_k = \frac{L}{2\mu} \rho g \beta_{0_{i,j}}^2 \tag{5.28}$$

The energy dissipation of liquid oscillations in the tank is considered as the viscous dissipation in the boundary-layer flow, which can be calculated from the velocity gradient and viscous stress developed in the laminar boundary-layer. The mean rate of viscous dissipation per unit area of the tank wall may thus be estimated as (Faltinsen and Timokha, 2009):

$$\overline{\frac{dE}{dt}} = \frac{1}{2\sqrt{2}}\rho\sqrt{\upsilon\sigma_{i,j}}u_0^2 \tag{5.29}$$

where υ is the dynamic viscosity of the liquid and u_0 is the amplitude of the tangential velocity at the tank wall, which is obtained from the derivatives of the sloshing potential from Eq. (5.24). Considering the boundary-layer along the cylindrical shell wall, the mean rate of the viscous dissipation can be expressed as:

$$\left.\overline{\frac{dE}{dt}}\right|_{shell} = \frac{\beta_{0\,i,j}^2 g^2 L}{2\sqrt{2}\sigma_{i,j}^{3/2}\mu}\rho\sqrt{\upsilon}\int_{\hat{S}_w}\left[\left(\frac{\partial\varphi_{i,j}}{\partial s}\right)^2 + (\mu-1)\omega_i^2\varphi_{i,j}^2\right]dS \tag{5.30}$$

In the above equation, $\varphi_{i,j}$ is obtained from the vectors $\boldsymbol{\varphi}_w$ for each mode using back substitution of the eigenvectors $\boldsymbol{\varphi}_f$ in Eq. (5.12) and eliminating the other unknowns in the velocity and potential vectors. When $i = 0$, contribution of the two end-walls to the viscous energy dissipation can be obtained using the divergence theorem in the form:

$$\left.\overline{\frac{dE}{dt}}\right|_{endwalls} = \frac{\beta_{0\,0,j}^2 g}{\sqrt{2}}\rho\sqrt{\upsilon\sigma_{0,j}} \tag{5.31}$$

The mean rate of the viscous dissipation on the end-walls for the higher modes corresponding to $i \geq 1$, however, cannot be calculated since the distribution of the velocity potential on the tank end-walls cannot be obtained from the present BEM. The effect of the end-walls on the viscous dissipation, however, may be considered negligible for large tanks used in liquid transport vehicles due to their relatively smaller area compared to the tank shell area. The damping ratio due to the liquid viscosity can thus be obtained by substituting for E and $\overline{\frac{dE}{dt}}$ from Eqs. (5.28), (5.30) and (5.31) into Eq. (5.22), as:

$$\xi_{i,j} = \frac{1}{2}\sqrt{\frac{\upsilon}{2\sigma_{i,j}}}\left(\frac{\chi_{i,j}}{\kappa_{i,j}} + \frac{2(2-\mu)}{L}\right) \tag{5.32}$$

where $\chi_{i,j}$ can be regarded as a hydrodynamic coefficient of the form:

$$\chi_{i,j} = \int_{\hat{S}_w}\left[\left(\frac{\partial\varphi_{i,j}}{\partial s}\right)^2 + (\mu-1)\omega_i^2\varphi_{i,j}^2\right]dS \tag{5.33}$$

The above integral can be numerically evaluated using the quadratic interpolating functions (and their derivatives) employed in the boundary element analysis of the free liquid sloshing.

5.2.3 Hydrodynamic pressure, slosh force and moment

The solutions of the ordinary differential equations, Eq. (5.21), yields other quantities of practical interest such as hydrodynamic pressure, slosh forces and moments in terms of time as well as spatial coordinates. The hydrodynamic pressure distribution, $P(x,y,z,t)$, on the container wall is derived using the linearized Bernoulli's equation (Abramson, 1966), such that:

$$P(y,z,t) = -\rho\frac{\partial(\Phi_R + \Phi_S)}{\partial t} = -\rho\left\{\ddot{X}x + \ddot{Y}y + \sum_{i=0}^{\infty}\sum_{j=0}^{\infty}\frac{\ddot{\beta}_{i,j}(t)}{\kappa_{i,j}}\Phi_{i,j}(x,y,z)\right\}, \qquad i+j \neq 0, \text{ on } S_w \tag{5.34}$$

The total hydrodynamic force acting on the container wall due to simultaneous applications of the lateral and longitudinal accelerations is obtained from integration of the hydrodynamic pressure over the wetted areas of the tank walls, such that:

$$\boldsymbol{F}(t) = F_x(t)\boldsymbol{e}_x + F_y(t)\boldsymbol{e}_y + F_z(t)\boldsymbol{e}_z \tag{5.35}$$

where

$$F_x(t) = \int_{S_w} P(\boldsymbol{e}_x\cdot\boldsymbol{n})dS, \quad F_y(t) = \int_{S_w} P(\boldsymbol{e}_y\cdot\boldsymbol{n})dS, \quad F_z = -mg \tag{5.36}$$

In the above equations, F_x, F_y and F_z are the longitudinal, lateral and vertical components of the hydrodynamic force, respectively, $\boldsymbol{e}_x$, $\boldsymbol{e}_y$ and $\boldsymbol{e}_z$ are the unit vectors in the *x*-, *y*- and *z*-directions, $\boldsymbol{n}$ is outer unit vector normal to the wetted surface area and m is the fluid mass. It should be noted that since the vertical component of the net slosh force is zero due to geometric symmetry, the magnitude of the vertical force is the weight of the liquid. The longitudinal component of the

hydrodynamic force, F_x, acting on the container end-walls ($x = \pm\frac{L}{2}$) may be considered as a summation of forces associated with the rigid body and the sloshing motion of the liquid, denoted as F_{x_R} and F_{x_S}, respectively, such that:

$$F_x(t) = F_{x_R}(t) + F_{x_S}(t) \tag{5.37}$$

where

$$F_{x_R}(t) = -\rho \ddot{X} L \int_{\hat{\Omega}} d\hat{\Omega} = -m\ddot{X} \tag{5.38}$$

$$F_{x_S}(t) = -\rho \sum_{i=0}^{\infty}\sum_{j=0}^{\infty} \frac{\ddot{\beta}_{i,j}(\mathrm{t})}{\kappa_{i,j}} \int_{S_w} \Phi_{i,j}(\boldsymbol{e}_x \cdot \boldsymbol{n}) dS \tag{5.39}$$

Using Green's second identity and Eqs. (5.2), (5.3) and (5.17), the dynamic slosh force $F_{x_S}(t)$ is obtained from the hydrodynamic coefficient $\lambda_{x_{i,j}}$, as:

$$F_{x_S}(t) = -\rho \sum_{i=0}^{\infty}\sum_{j=0}^{\infty} \ddot{\beta}_{i,j}(\mathrm{t}) \lambda_{x_{i,j}} \tag{5.40}$$

In a similar manner, the lateral component of the hydrodynamic force, F_y, acting on the tank shell is obtained as a summation of the rigid body and sloshing forces in the form:

$$F_y(t) = F_{y_R}(t) + F_{y_S}(t) \tag{5.41}$$

where

$$F_{y_R}(t) = -\rho \ddot{Y} L \int_{\hat{S}_w} y dz = -m\ddot{Y} \tag{5.42}$$

$$F_{y_S}(t) = -\rho \sum_{i=0}^{\infty}\sum_{j=0}^{\infty} \frac{\ddot{\beta}_{i,j}(\mathrm{t})}{\kappa_{i,j}} \int_{S_w} \Phi_{i,j}\big(\boldsymbol{e}_y \cdot \boldsymbol{n}\big) dS = -\rho \sum_{j=1}^{\infty} \ddot{\beta}_{0,j}(\mathrm{t}) \lambda_{y_{0,j}} \tag{5.43}$$

The total hydrodynamic moment about the tank base beneath the geometric center can be regarded as the resultant of the roll and pitch moments, $M_x(t)$ and $M_y(t)$, respectively, in the form:

$$\boldsymbol{M}(t) = M_x(t)\boldsymbol{e}_x + M_y(t)\boldsymbol{e}_y \tag{5.44}$$

The roll moment can be determined by integrating the moments resulting from the lateral and vertical components of the hydrodynamic force, as:

$$M_x(t) = \int_{S_w} P\big[y(\boldsymbol{e}_z \cdot \boldsymbol{n}) - (R+z)\big(\boldsymbol{e}_y \cdot \boldsymbol{n}\big)\big]dS \tag{5.45}$$

Substituting for the pressure from Eq. (34) into the above equation yields the total roll moment that may be decomposed into three components attributed to: (i) the rigid body moment (M_{x_R}); (ii) the moment due to the vertical forces (M_{x_V}); and (iii) the moment resulting from the dynamic fluid slosh effect (M_{x_S}), i.e.:

$$M_x(t) = M_{x_R}(t) + M_{x_V}(t) + M_{x_S}(t) \tag{5.46}$$

Considering a circular cross-section tank, one can express the above moment components as:

$$M_{x_R}(t) = \rho\ddot{Y}\int_{\hat{\Omega}} y(R+z)dz = mR\left(1 - \frac{2(1-\tau^2)^{3/2}}{3\left(\cos^{-1}\tau - \tau\sqrt{1-\tau^2}\right)}\right)\ddot{Y} \tag{5.47}$$

$$M_{x_V}(t) = -\rho\ddot{Y}L\int_{\hat{S}_w} y^2 dy = \frac{2}{3}\rho L y_0^3\ddot{Y} \tag{5.48}$$

$$M_{x_S}(t) = -\rho\sum_{i=0}^{\infty}\sum_{j=0}^{\infty}\frac{\ddot{\beta}_{i,j}(\mathrm{t})}{\kappa_{i,j}}\int_{S_w}\Phi_{i,j}\big[y(\boldsymbol{e}_z \cdot \boldsymbol{n}) - (R+z)\big(\boldsymbol{e}_y \cdot \boldsymbol{n}\big)\big]dS$$

$$= \rho R\sum_{j=1}^{\infty}\ddot{\beta}_{0,j}(\mathrm{t})\lambda_{y_{0,j}} \tag{5.49}$$

The expression within the parenthesis in Eq. (5.47) denotes the vertical distance between the liquid mass center and the container base for a tank with unit circle cross-section, where $\tau = 1 - \frac{h}{R}$. Equation (5.49) indicates that the sloshing component of the roll moment can be directly obtained from multiplication of F_{y_S} and the tank radius.

The pitch moment about the tank base is obtained by integrating the moments resulting from the longitudinal and vertical forces, as:

$$M_y(t) = \int_{S_w} P[(R+z)(\boldsymbol{e}_x \cdot \boldsymbol{n}) - x(\boldsymbol{e}_z \cdot \boldsymbol{n})]dS \tag{5.50}$$

Similar to the roll moment, components of the pitch moment, $M_y(t) = M_{y_R}(t) + M_{y_V}(t) + M_{y_S}(t)$, attributed to the rigid body moment (M_{y_R}), moment of vertical forces (M_{x_V}) and dynamic sloshing moment (M_{x_S}) can be formulated using Green's second identity, as:

$$M_{y_R}(t) = -\rho\ddot{X}L\int_{\hat{\Omega}}(R+z)d\hat{\Omega} = -m\left(R - \frac{2(1-\tau^2)^{3/2}}{3\left(\cos^{-1}\tau - \tau\sqrt{1-\tau^2}\right)}\right)\ddot{X} \tag{5.51}$$

$$M_{y_V}(t) = -\rho\ddot{X}\int_{S_w} x^2(\boldsymbol{e}_z \cdot \boldsymbol{n})dS = -\frac{1}{6}\rho y_0 L^3\ddot{X} \tag{5.52}$$

$$M_{y_S}(t) = -\rho\sum_{i=0}^{\infty}\sum_{j=0}^{\infty}\frac{\ddot{\beta}_{i,j}(\mathrm{t})}{\kappa_{i,j}}\int_{S_w}\Phi_{i,j}[(R+z)(\boldsymbol{e}_x \cdot \boldsymbol{n}) - x(\boldsymbol{e}_z \cdot \boldsymbol{n})]dS$$

$$= -\rho\sum_{i=0}^{\infty}\sum_{j=0}^{\infty}\frac{\ddot{\beta}_{i,j}(\mathrm{t})}{\kappa_{i,j}}\left[(h\kappa_{i,j}-1)\lambda_{x_{i,j}} + \frac{4}{\omega_i^2}\int_{\hat{S}_w}\varphi_{i,j}dy\right] \tag{5.53}$$

5.3 Results and discussion

The spectral problem of three-dimensional liquid slosh in a horizontal cylindrical tank is solved using the boundary element method presented in section 5.2.1. The fluid enclosed boundaries (Fig. 5.1c) are discretized using quadratic elements with equal node spacing. The results are presented for a tank of circular cross-section in the form of normalized slosh frequencies, free-surface profiles and hydrodynamic coefficients. The validity of the model is examined by comparing the results with reported analytical solutions and experimental data. Slosh forces and moments responses under an idealized braking-in-a-turn maneuver are also evaluated using the multimodal method presented in section 5.2.2. Moreover, a series of CFD simulations are conducted using the FLUENT software in order to identify the limitations of the present linear slosh model.

5.3.1 Natural slosh frequencies and modes

The convergence of the boundary element method was initially investigated by evaluating the normalized slosh frequencies, $\bar{\kappa}_{i,j} = \kappa_{i,j}R$, considering different number of elements on the half length of the free-surface, N_f. Table 5.1 summarizes the antisymmetric and symmetric modes normalized frequencies for a half-full tank of normalized length $L/R = \pi$ considering different number of elements, ranging from 10 to 60. The table shows normalized frequencies of the first five symmetric and antisymmetric lateral modes $(j = 0,1,2,\ldots,9)$ corresponding to the first three longitudinal modes $(i = 0,1,2)$, including the rigid body mode $(i = j = 0)$. The convergence was ensured after stabilizing the fourth decimal place using several values of N_f, up to a maximum of 60. The results revealed that only a maximum of 20 elements were needed for calculating the normalized slosh frequencies of the first five lateral

Table 5.1. Convergence of the normalized slosh frequencies, $\bar{\kappa}_{i,j} = \kappa_{i,j}R$, for different number of elements on the half length of the free-surface for a half-full (h/R=1.0) cylindrical tank of length $L/R = \pi$.

		Antisymmetric modes					Symmetric modes				
	N_f	$\bar{\kappa}_{i,1}$	$\bar{\kappa}_{i,3}$	$\bar{\kappa}_{i,5}$	$\bar{\kappa}_{i,7}$	$\bar{\kappa}_{i,9}$	$\bar{\kappa}_{i,0}$	$\bar{\kappa}_{i,2}$	$\bar{\kappa}_{i,4}$	$\bar{\kappa}_{i,6}$	$\bar{\kappa}_{i,8}$
	10	1.3557	4.6513	7.8225	10.9854	14.1637	0.0000	3.0331	6.2398	9.4023	12.5693
	20	1.3557	4.6511	7.8200	10.9727	14.1220	0.0000	3.0331	6.2392	9.3970	12.5472
$i = 0$	40	1.3557	4.6511	7.8199	10.9718	14.1191	0.0000	3.0331	6.2392	9.3967	12.5457
	50	1.3557	4.6511	7.8199	10.9718	14.1189	0.0000	3.0331	6.2392	9.3967	12.5457
	60	1.3557	4.6511	7.8199	10.9718	14.1189	0.0000	3.0331	6.2392	9.3967	12.5457
Faltinsen and Timokha (2010)		1.3557	4.6511	7.8199	10.9718	14.1189		3.0331	6.2392	9.3967	12.5457
Karamanos *et al.* (2009)		1.3558	4.6640	7.8669							
	10	1.6393	4.7564	7.8859	11.0308	14.1991	0.6441	3.1923	6.3190	9.4552	12.6091
	20	1.6393	4.7562	7.8834	11.0180	14.1574	0.6441	3.1923	6.3184	9.4499	12.5869
$i = 1$	40	1.6393	4.7562	7.8832	11.0172	14.1544	0.6441	3.1923	6.3184	9.4496	12.5855
	50	1.6393	4.7562	7.8832	11.0171	14.1543	0.6441	3.1923	6.3184	9.4496	12.5854
	60	1.6393	4.7562	7.8832	11.0171	14.1542	0.6441	3.1923	6.3184	9.4496	12.5854
Evans and Linton (1993)		1.6393	4.7562	7.8832	11.0171		0.6441	3.1923	6.3184	9.4496	
Karamanos *et al.* (2009)		1.6394	4.7618	7.9087	11.0855		0.6441	3.1938	6.3316	9.4931	
	10	2.3374	5.0587	8.0730	11.1658	14.3047	1.7784	3.6260	6.5505	9.6120	12.7276
	20	2.3374	5.0585	8.0705	11.1530	14.2627	1.7784	3.6260	6.5499	9.6067	12.7052
$i = 2$	40	2.3374	5.0585	8.0703	11.1521	14.2598	1.7784	3.6260	6.5499	9.6064	12.7038
	50	2.3374	5.0585	8.0703	11.1521	14.2596	1.7784	3.6260	6.5499	9.6064	12.7038
	60	2.3374	5.0585	8.0703	11.1521	14.2596	1.7784	3.6260	6.5499	9.6064	12.7037
Evans and Linton (1993)		2.3374	5.0585	8.0703	11.1520		1.7784	3.6260	6.5499	9.6064	
Karamanos *et al.* (2009)		2.3375	5.0644	8.0963	11.221		1.7784	3.6278	6.5635	9.6506	

modes corresponding to the first three longitudinal modes ($i = 0,1,2;\ j = 0,1,\ldots,5$). These suggest a very rapid convergence for all the longitudinal modes considered. The results are also compared with the reported analytical solutions (Evans and Linton, 1993; Faltinsen and Timokha, 2010) and those obtained from a finite element analysis (Karamanos *et al.*, 2009), although these have reported the frequencies for fewer modes. As seen from the table, the results are in full agreement with those reported in Evans and Linton (1993) and Faltinsen and Timokha (2010). The normalized frequencies reported in Karamanos *et al.* (2009), however, are slightly different from those obtained in this study and the benchmark solutions presented in Evans and

Linton (1993) and Faltinsen and Timokha (2010). This suggests that the finite element analysis may yield slight errors, apart from requiring discretization of the whole fluid domain and a higher computational time.

The normalized slosh frequencies ($i = 0,1,2; j = 0,1,2, \ldots 9$) of liquid in a tank of length $L/R = \pi$ are presented in Table 5.2 for different fill ratios ($\frac{h}{R} = 0.4, 0.8, 1.2, 1.6, 1.8$). The table also compares slosh frequencies corresponding to the purely lateral motion ($i = 0$) with those reported in Faltinsen and Timokha (2010). The results are in total agreement with the reported values for all the fill ratios. The results suggest that the normalized frequencies corresponding to the lateral modes increase with increase in the longitudinal mode number i. The greatest increase is observed in the first symmetric and antisymmetric frequencies, while the higher lateral mode frequencies increase slightly with the longitudinal mode number i.

The normalized slosh frequencies are also compared with the experimental data reported by McCarty and Stephens (1960) in Fig. 5.2. The figure shows variations in the normalized frequencies corresponding to $i = 1,3,5,7$ and $j = 0$ with respect to the fill ratio in a tank of length *L/R*=2, 3.5, 4 and 5.8. The results are in very good agreement with the reported values, irrespective of the fill level considered, except for some deviations in the higher mode frequencies of the tank with length *L/R*=2 for low fill levels. The results suggest that the lateral mode normalized frequencies corresponding to $j = 0$ increase with the fill ratio, irrespective of the tank aspect ratio. While the lowest normalized frequency, $\bar{\kappa}_{1,0}$, increases monotonically with the fill ratio, higher mode frequencies increase more rapidly for lower fill ratios. Comparisons of the results in Fig. 5.2 also suggest that the normalized slosh frequencies decrease with increase in the tank aspect ratio.

The three-dimensional natural sloshing modes are obtained from the two-dimensional eigenvalue problems described in Eq. (5.13) and Eq. (5.4). Figure 5.3 illustrates the free-surface profiles associated with mode numbers $i = 0,1,2$ and $j = 0,1,2,3$ excluding the zero-frequency mode, $i = j = 0$, for fill ratio *h/R*=1.5. The results show that free-surface profiles occur in the lateral plane independent of the longitudinal coordinate for $i = 0$ and $j = 1,2,3$, which describe the two-dimensional lateral slosh modes. The pure lateral sloshing free-surface profiles associated with the first symmetric ($j = 2$) and antisymmetric modes ($j = 1$) were also observed to be in complete agreement with those depicted in Faltinsen and Timokha (2010). The free-

Table 5.2. Normalized slosh frequencies, $\bar{\kappa}_{i,j} = \kappa_{i,j}R$, for a cylindrical tank with different liquid fill ratios ($L/R = \pi$).

	Antisymmetric modes					Symmetric modes				
	$\bar{\kappa}_{i,1}$	$\bar{\kappa}_{i,3}$	$\bar{\kappa}_{i,5}$	$\bar{\kappa}_{i,7}$	$\bar{\kappa}_{i,9}$	$\bar{\kappa}_{i,0}$	$\bar{\kappa}_{i,2}$	$\bar{\kappa}_{i,4}$	$\bar{\kappa}_{i,6}$	$\bar{\kappa}_{i,8}$
$h/R = 0.4$										
$i = 0$	1.0970	4.9370	9.0075	12.9835	16.9320	0.0000	2.8905	6.9906	11.0013	14.9595
Faltinsen and Timokha (2010)	1.0970	4.9370	9.0075	12.9835	16.9320		2.8905	6.9906	11.0013	14.9595
$i = 1$	1.2397	5.0259	9.0599	13.0205	16.9607	0.2680	3.0121	7.0569	11.0447	14.9918
$i = 2$	1.6388	5.2863	9.2154	13.1308	17.0463	0.9560	3.3690	7.2527	11.1737	15.0882
$h/R = 0.8$										
$i = 0$	1.2461	4.6067	7.8537	11.0741	14.2877	0.0000	2.9325	6.2361	9.4650	12.6812
Faltinsen and Timokha (2010)	1.2461	4.6067	7.8537	11.0741	14.2877		2.9325	6.2361	9.4650	12.6812
$i = 1$	1.4932	4.7095	7.9155	11.1183	14.3221	0.5241	3.0882	6.3135	9.5166	12.7200
$i = 2$	2.1283	5.0049	8.0978	11.2499	14.4250	1.5781	3.5147	6.5393	9.6696	12.8356
$h/R = 1.2$										
$i = 0$	1.5075	4.8509	8.0783	11.2932	14.5041	0.0000	3.2164	6.4675	9.6864	12.8988
Faltinsen and Timokha (2010)	1.5075	4.8509	8.0783	11.2932	14.5041		3.2164	6.4675	9.6864	12.8988
$i = 1$	1.8159	4.9572	8.1420	11.3385	14.5393	0.7603	3.3761	6.5471	9.7394	12.9385
$i = 2$	2.5455	5.2628	8.3299	11.4734	14.6444	1.9287	3.8142	6.7803	9.8966	13.0567
$h/R = 1.6$										
$i = 0$	2.1237	6.1393	10.0807	14.0138	17.9442	0.0000	4.1433	8.1031	12.0419	15.9749
Faltinsen and Timokha (2010)	2.1237	6.1393	10.0807	14.0138	17.9442		4.1433	8.1031	12.0419	15.9749
$i = 1$	2.4385	6.2411	10.1404	14.0557	17.9764	1.0148	4.3066	8.1839	12.0948	16.0141
$i = 2$	3.1432	6.5276	10.3126	14.1778	18.0707	2.1764	4.7284	8.4025	12.2397	16.1218
$h/R = 1.8$										
$i = 0$	3.0214	8.3139	13.5596	18.7997	24.0381	0.0000	5.6269	10.9061	16.1586	21.4032
Faltinsen and Timokha (2010)	3.0214	8.3139	13.5596	18.7997	24.0381		5.6269	10.9061	16.1586	21.4033
$i = 1$	3.3031	8.4045	13.6122	18.8365	24.0662	1.2340	5.8038	10.9941	16.2161	21.4456
$i = 2$	3.9325	8.6509	13.7587	18.9398	24.1456	2.3873	6.1827	11.1872	16.3432	21.5397

surface profiles associated with mode numbers $j = 0$ and $i = 1,2$, however, are not entirely planar and show slightly dependence on the lateral coordinate. Variation in the free-surface profile with respect to the lateral coordinate is more evident for the symmetric mode ($j = 0$; $i = 2$) than for the antisymmetric mode ($j = 0$; $i = 1$). It is also apparent from the figure that the free-surface profiles associated with mode numbers $i, j \geq 1$ vary substantially with both the longitudinal and the lateral coordinates.

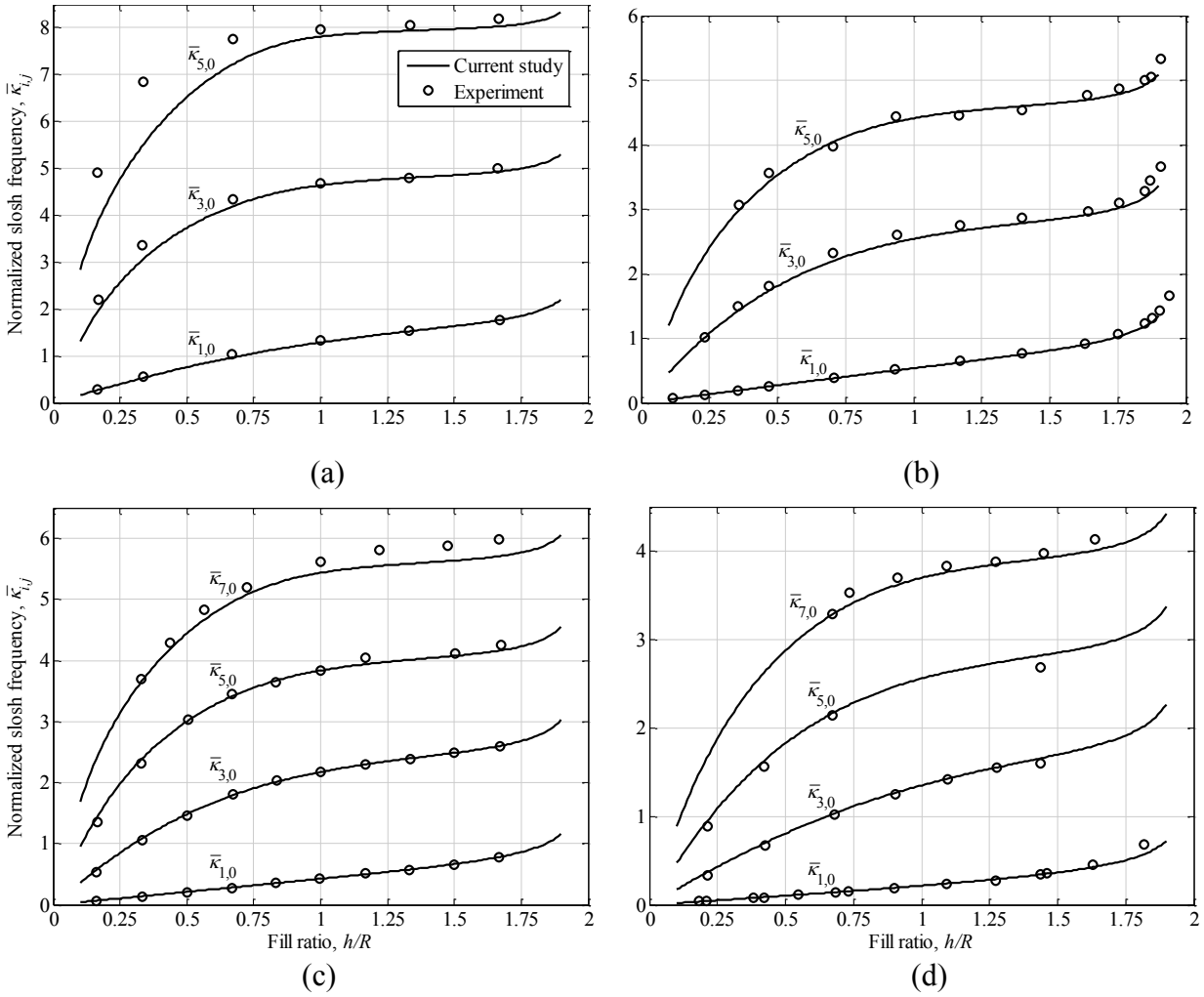

Fig. 5.2. Comparisons of normalized slosh frequencies, $\bar{\boldsymbol{\kappa}}_{\boldsymbol{i,j}} = \boldsymbol{\kappa}_{\boldsymbol{i,j}}\boldsymbol{R}$, with the experimental data reported in McCarty and Stephens (1960) for tanks of different lengths: (a) *L/R*=2; (b) *L/R*=3.5; (c) *L/R*=4; and (d) *L/R*=5.8.

5.3.2 Hydrodynamic coefficients

Normalized hydrodynamic coefficients $\bar{\lambda}_{y_{0,j}} = \frac{\lambda_{y_{0,j}}\sqrt{y_0}}{LR^2}$ $(j = 1,3,5,7,9)$ corresponding to the two-dimensional lateral slosh are initially calculated for fill ratios ranging from *h/R*=0.4 to *h/R*=1.8 and compared with those reported by Faltinsen and Timokha (2010) in Table 5.3. The results were obtained with the accuracy of five decimal places using a maximum number of 35 elements on the half-length of the free-surface. The results in Table 5.3 are identical with those reported. The hydrodynamic coefficients associated with the first antisymmetric lateral mode are substantially higher than those of the higher lateral modes. This suggests the dominance of the

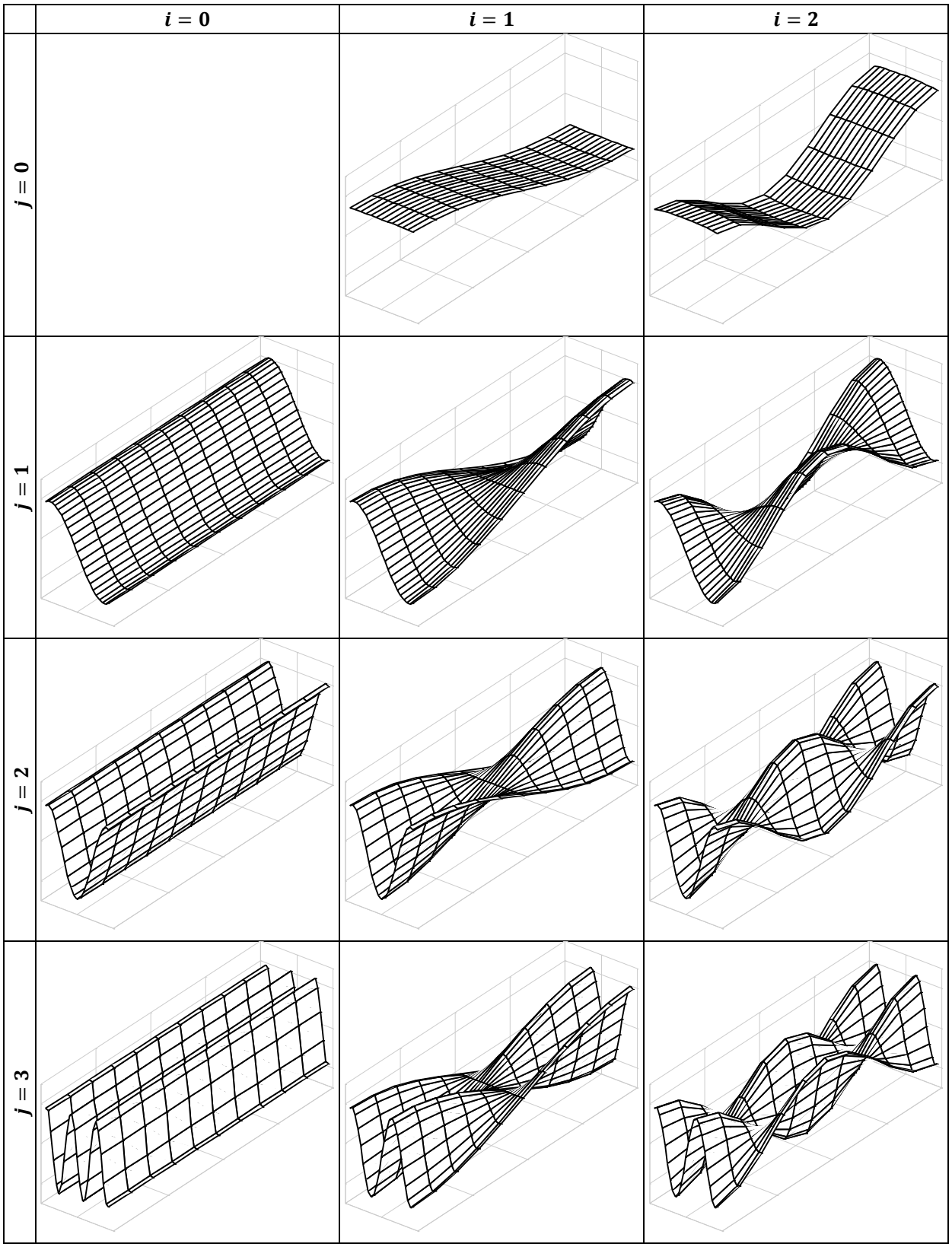

Fig. 5.3. Three-dimensional free-surface profiles ($\boldsymbol{i = 0, 1, 2}$; $\boldsymbol{j = 0, 1, 2, 3}$; $\boldsymbol{i + j \neq 0}$) for fill ratio *h/R*=1.5.

Table 5.3. Comparison of normalized hydrodynamic coefficients, $\bar{\lambda}_{y_{0,j}} = \frac{\lambda_{y_{0,j}}\sqrt{y_0}}{LR^2}$, with those reported in Faltinsen and Timokha (2010) corresponding to different fill ratios.

	$h/R = 0.4$					$h/R = 0.8$				
	$\bar{\lambda}_{y_{0,1}}$	$\bar{\lambda}_{y_{0,3}}$	$\bar{\lambda}_{y_{0,5}}$	$\bar{\lambda}_{y_{0,7}}$	$\bar{\lambda}_{y_{0,9}}$	$\bar{\lambda}_{y_{0,1}}$	$\bar{\lambda}_{y_{0,3}}$	$\bar{\lambda}_{y_{0,5}}$	$\bar{\lambda}_{y_{0,7}}$	$\bar{\lambda}_{y_{0,9}}$
	0.52211	0.02105	0.00495	0.00201	0.00104	0.78112	0.06044	0.02044	0.01013	0.00600
Faltinsen and Timokha (2010)	0.52211	0.02105	0.00495	0.00201	0.00104	0.78112	0.06044	0.02044	0.01013	0.00600
	$h/R = 1.0$					$h/R = 1.2$				
	0.81206	0.07753	0.02854	0.01484	0.00911	0.77765	0.08842	0.03455	0.01863	0.01173
Faltinsen and Timokha (2010)	0.81206	0.07753	0.02854	0.01484	0.00911	0.77765	0.08842	0.03455	0.01863	0.01173
	$h/R = 1.6$					$h/R = 1.8$				
	0.51483	0.07847	0.03339	0.01899	0.01245	0.28808	0.05048	0.02231	0.01299	0.00867
Faltinsen and Timokha (2010)	0.51483	0.07847	0.03339	0.01899	0.01245	0.28808	0.05048	0.02231	0.01299	0.00867

Table 5.4. Normalized hydrodynamic coefficients, $\bar{\lambda}_{x_{i,j}} = \frac{\lambda_{x_{i,j}}\sqrt{y_0}}{LR^2}$, for a cylindrical tank with different liquid fill ratios ($L/R = \pi$).

	$h/R = 0.4$					$h/R = 0.8$				
i	$\bar{\lambda}_{x_{i,0}}$	$\bar{\lambda}_{x_{i,2}}$	$\bar{\lambda}_{x_{i,4}}$	$\bar{\lambda}_{x_{i,6}}$	$\bar{\lambda}_{x_{i,8}}$	$\bar{\lambda}_{x_{i,0}}$	$\bar{\lambda}_{x_{i,2}}$	$\bar{\lambda}_{x_{i,4}}$	$\bar{\lambda}_{x_{i,6}}$	$\bar{\lambda}_{x_{i,8}}$
1	0.71999	-0.01941	-0.00212	-0.00066	-0.00030	0.88182	-0.02307	-0.00370	-0.00138	-0.00070
3	0.07786	-0.01837	-0.00200	-0.00064	-0.00029	0.09679	-0.01522	-0.00252	-0.00094	-0.00047
	$h/R = 1.0$					$h/R = 1.2$				
1	0.90020	-0.01454	-0.00200	-0.00063	-0.00028	0.88212	-0.00106	0.00138	0.00096	0.00067
3	0.09983	-0.00639	-0.00098	-0.00032	-0.00014	0.09798	0.00215	0.00094	0.00053	0.00034
	$h/R = 1.6$					$h/R = 1.8$				
1	0.71970	0.02581	0.00928	0.00494	0.00313	0.53931	0.02809	0.01013	0.00545	0.00349
3	0.07928	0.01009	0.00345	0.00177	0.00109	0.05929	0.00851	0.00306	0.00162	0.00102

first antisymmetric mode in the slosh force and moment responses under the lateral motion of the container. Normalized hydrodynamic coefficients $\bar{\lambda}_{x_{i,j}} = \frac{\lambda_{x_{i,j}}\sqrt{y_0}}{LR^2}$ $(i = 1,3; j = 0,2,4,6,8)$ for a tank with $L/R = \pi$ and same fill ratios were also evaluated considering a maximum number of 35 elements on the half-length of the free-surface, which are presented in Table 5.4. As can be seen from the table, numerical values of $\bar{\lambda}_{x_{1,0}}$ are substantially greater than the other normalized hydrodynamic coefficients, suggesting the dominance of the lowest symmetric mode in the longitudinal slosh force and pitch moment responses when the container is subjected to a

longitudinal excitation. Moreover, the normalized hydrodynamic coefficients associated with the first symmetric lateral mode ($j = 0$) decrease considerably as mode number i increases, while those associated with the higher lateral modes change only slightly with mode number i. These changes in the hydrodynamic coefficients corresponding to symmetric lateral modes with increasing mode number i are lower for lower fill ratios and higher lateral modes.

Table 5.5 presents the normalized hydrodynamic coefficients, $\bar{\chi}_{i,j} = \chi_{i,j} y_0 R$ ($i = 0,1,3; j = 0,1,2 \ldots 9$), due to fluid slosh in the tank of length $L/R = \pi$ for fill ratios *h/R*=0.4, 0.8, 1.2, 1.6 and 1.8. The results were obtained considering a maximum of 150 elements with two-decimal-place accuracy. The results obtained with 60 elements revealed only slight errors in the hydrodynamic coefficients. The maximum discrepancy of 0.4% was observed corresponding to $\bar{\chi}_{0,9}$ for fill ratio *h/R*=1.8. Faltinsen and Timokha (2010) reported the hydrodynamic coefficients for the lateral slosh mode ($i = 0$) alone, which are also presented in the Table. The results obtained in the present study are in agreement with those reported for the lateral slosh mode, except for slight deviations in the higher modes for fill ratios *h/R*>1. The peak discrepancy is observed in $\bar{\chi}_{0,8}$ in the order of 0.6% for fill ratio *h/R*=1.8. As can be seen from the results, the normalized hydrodynamic coefficients increase substantially as the lateral mode number j increases for each longitudinal mode number i, irrespective of the fill ratio. The hydrodynamic coefficients corresponding to the higher antisymmetric and symmetric lateral modes, however, increase slightly as the longitudinal mode number increases. It is further seen that the lowest non-zero values of the normalized hydrodynamic coefficients occur for $i = 1$ and $j = 0$, irrespective of the each fill ratio.

5.3.3 Slosh force and moment

Hydrodynamic forces and moments due to liquid slosh are evaluated under simultaneous applications of lateral and longitudinal accelerations, idealizing a braking-in-a-turn maneuver. The accelerations acting on the container are idealized by ramp-step functions, as shown in Fig. 5.4, where A_{0x} and A_{0y} represent the steady-state lateral and longitudinal accelerations, respectively, and t_{0x} and t_{0y} are the respective rise times. Furthermore, the range of applicability of the linear theory for predicting transient liquid slosh are examined by comparing the slosh force and moment responses with those obtained from nonlinear simulations. For this purpose, a

Table 5.5. Normalized hydrodynamic coefficients, $\bar{\chi}_{i,j} = \chi_{i,j}/y_0 R$, for a cylindrical tank with different liquid fill ratios ($L/R = \pi$).

	Antisymmetric modes					Symmetric modes				
	$\bar{\chi}_{i,1}$	$\bar{\chi}_{i,3}$	$\bar{\chi}_{i,5}$	$\bar{\chi}_{i,7}$	$\bar{\chi}_{i,9}$	$\bar{\chi}_{i,0}$	$\bar{\chi}_{i,2}$	$\bar{\chi}_{i,4}$	$\bar{\chi}_{i,6}$	$\bar{\chi}_{i,8}$
$h/R = 0.4$										
$i = 0$	2.86	17.31	28.94	40.36	51.98	0.00	10.01	23.31	34.61	46.16
Faltinsen and Timokha (2010)	2.86	17.31	28.94	40.36	51.98		10.01	23.31	34.61	46.16
$i = 1$	3.75	17.53	29.02	40.42	52.02	0.89	10.52	23.42	34.68	46.20
$i = 3$	10.70	18.65	29.56	40.81	52.33	7.37	12.65	24.11	35.14	46.55
$h/R = 0.8$										
$i = 0$	1.76	6.51	10.63	14.84	19.06	0.00	4.52	8.57	12.74	16.96
Faltinsen and Timokha (2010)	1.76	6.51	10.63	14.84	19.06		4.52	8.57	12.74	16.96
$i = 1$	2.69	6.71	10.75	14.93	19.13	1.10	4.86	8.72	12.84	17.03
$i = 3$	8.29	8.20	11.73	15.63	19.68	5.49	6.77	9.89	13.66	17.65
$h/R = 1.2$										
$i = 0$	1.30	3.84	6.35	8.87	11.39	0.00	2.64	5.08	7.59	10.11
Faltinsen and Timokha (2010)	1.30	3.84	6.35	8.87	11.40		2.64	5.08	7.60	10.15
$i = 1$	2.10	4.14	6.55	9.02	11.52	1.06	3.03	5.32	7.77	10.26
$i = 3$	5.24	6.21	8.02	10.17	12.46	2.63	5.57	7.05	9.07	11.30
$h/R = 1.6$										
$i = 0$	1.18	3.17	5.21	7.25	9.30	0.00	1.98	4.01	6.06	8.12
Faltinsen and Timokha (2010)	1.18	3.17	5.21	7.27	9.32		1.98	4.01	6.07	8.13
$i = 1$	1.77	3.50	5.46	7.47	9.49	0.88	2.50	4.41	6.40	8.42
$i = 3$	3.42	5.29	6.94	8.72	10.59	1.39	4.50	6.09	7.81	9.65
$h/R = 1.8$										
$i = 0$	1.35	3.55	5.78	8.02	10.25	0.00	2.06	4.29	6.53	8.77
Faltinsen and Timokha (2010)	1.35	3.56	5.79	8.04	10.29		2.07	4.30	6.56	8.82
$i = 1$	1.82	3.86	6.03	8.24	10.45	0.79	2.69	4.82	7.01	9.22
$i = 3$	3.12	5.36	7.35	9.41	11.52	1.22	4.35	6.34	8.36	10.46

series of CFD simulations were performed using ANSYS FLUENT 14.5.7 software. The meshing of the flow domains was conducted using ANSYS GAMBIT 2.4.6. The CFD simulations were performed for a 26 m^3 cylindrical tank (R=1.2 m and L=5.75 m) for two fill ratios: h/R=1 and 1.5, while subject to two different magnitudes of longitudinal and lateral accelerations: $A_{0x} = 0.1g$, $A_{0y} = 0.2g$; and $A_{0x} = 0.2g$, $A_{0y} = 0.3g$. The rise times for the longitudinal and lateral acceleration excitations were considered as 2.0 s and 0.5 s, respectively. The CFD simulations were performed for water (density $\rho = 998.2\ \frac{kg}{m^3}$ and kinematic viscosity

$\upsilon = 1.0048 \times 10^{-6} \frac{m^2}{s}$). The governing three-dimensional momentum (Navier-Stoke's) and continuity equations for the two-phase flow domains (water and air) in the tank were solved using a transient pressure-based solver considering volume-of-fluid (VOF) as the multiphase model assuming laminar flows. Non-Iterative Time Advancement scheme with variable time stepping method was used for the unsteady solver. Several trial simulations were performed to select appropriate mesh size and integration time step to achieve a stable and efficient convergence. Moreover, the effects of the mesh size and time step on the model responses were investigated to ensure independence of the results from the mesh size and the time step. A mesh size of 120,000 hexahedron elements was considered adequate for the simulations, with the integration time step ranging from minimum of 1×10^{-5} s to maximum of 0.0025 s.

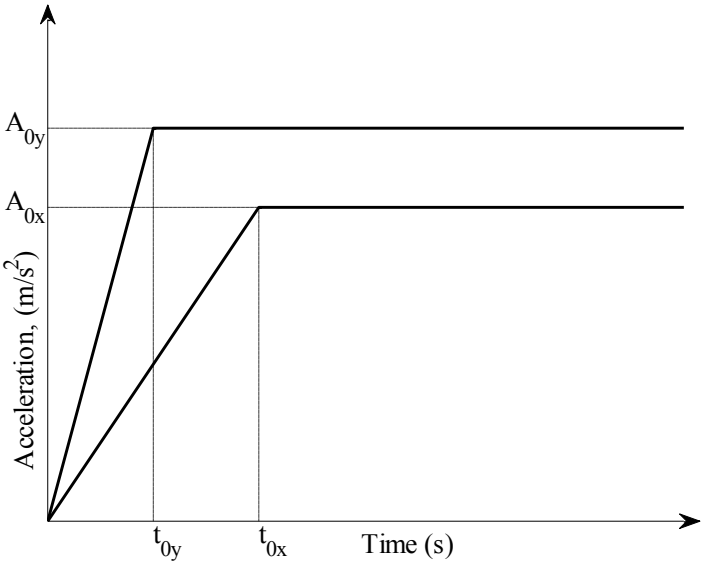

Fig. 5.4. Ramp-step lateral ($\boldsymbol{A_{0y}}$) and longitudinal ($\boldsymbol{A_{0x}}$) acceleration inputs applied to the tank.

Figures 5.5 and 5.6 illustrate time histories of the normalized slosh forces and moments obtained from the present linear model together with those obtained from the CFD simulations for the two fill ratios considered. Longitudinal and lateral slosh forces, and pitch and roll moments are normalized with respect to the rigid body forces and moments, as $\bar{F}_x = \frac{F_x}{F_{x_R}}$, $\bar{F}_y = \frac{F_y}{F_{y_R}}$, $\bar{M}_y = \frac{M_y}{M_{y_R}}$, $\bar{M}_x = \frac{M_x}{M_{x_R}}$. The normalized longitudinal force and pitch moment are presented

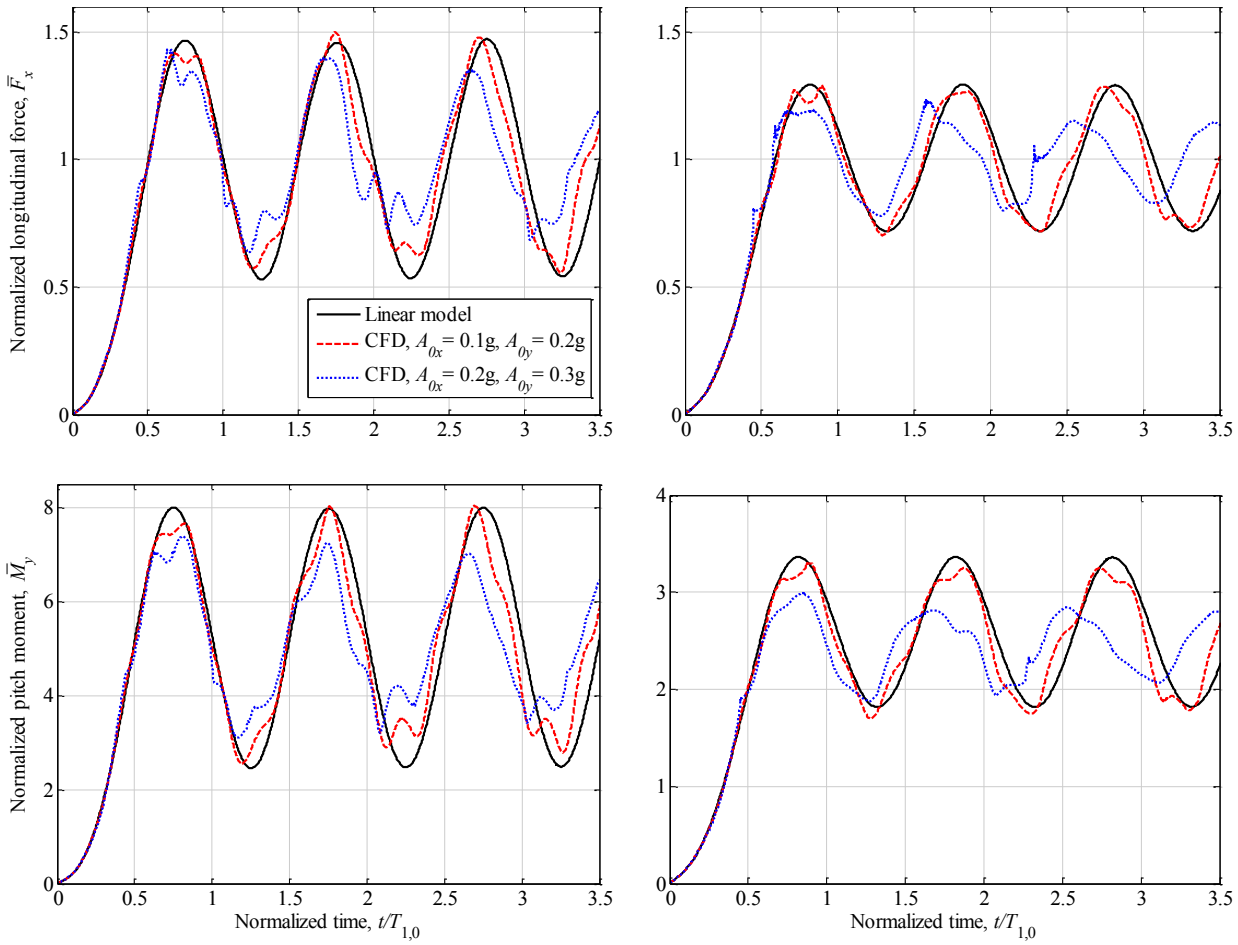

Fig. 5.5. Comparisons of normalized longitudinal force and pitch moment responses obtained from the proposed method with those from CFD simulations: (a) *h/R*=1; and (b) *h/R*=1.5.

against time normalized with respect to the slosh period $T_{1,0}$ (Fig. 5.5), while the lateral force and roll moment are illustrated against time normalized with respect to period $T_{0,1}$ (Fig. 5.6). It was judged that first 4 to 5 antisymmetric lateral modes were required to obtained lateral force and roll moment responses with an accuracy of 0.1 percent. Only the lowest 3 to 4 contributing longitudinal modes ($i = 1,3,5,7$) corresponding to lateral mode number $j = 0$, however, were sufficient to obtain the longitudinal force and pitch moment responses with the same accuracy. The results presented in the Figs. 5.5 and 5.6 suggest that the proposed linear analysis can yield reasonable good estimates of slosh force and moment responses under lower acceleration excitations (A_{0x}= $0.1g$ and $A_{0y} = 0.2\,g$) when compared to those obtained from the CFD simulations, for the two fill ratios considered. Notable discrepancies between the results from the

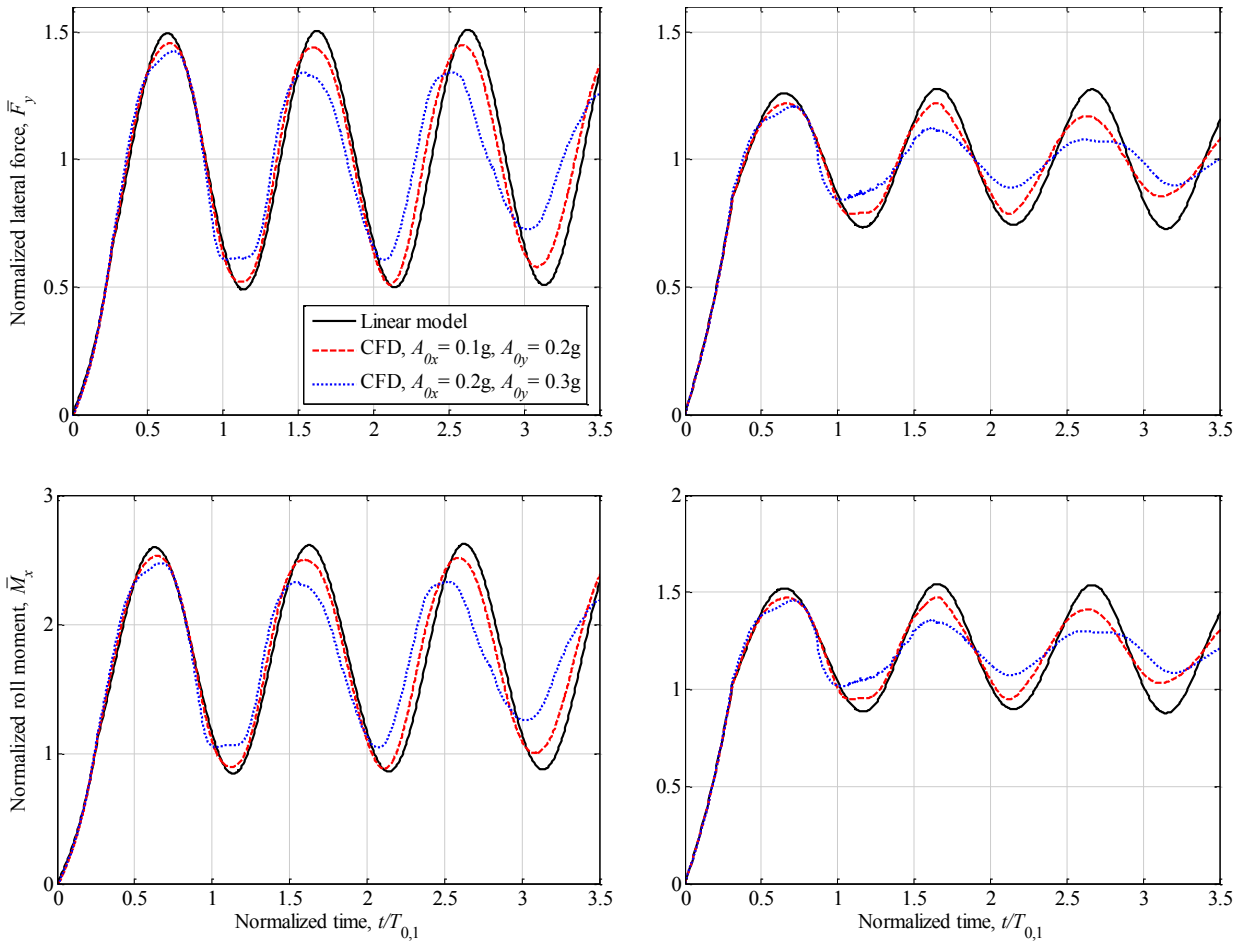

(a) (b)

Fig. 5.6. Comparisons of normalized lateral force and roll moment responses obtained from the proposed method with those from CFD simulations: (a) *h/R*=1; and (b) *h/R*=1.5.

proposed model and the CFD simulations, however, are evident under the higher acceleration excitations ($A_{0x} = 0.2g$, $A_{0y} = 0.3g$). The discrepancies between the two are even greater for the higher fill ratio, *h/R*=1.5. These are attributed to the effect of nonlinearities in the free-surface, which cannot be predicted by the linear model. The discrepancies in the peak normalized longitudinal force predicted by the linear and nonlinear analyses during the first oscillation period are in the order of 3% and 8% for the fill ratios *h/R*=1 and 1.5, respectively, under $A_{0x} = 0.2g$ and $A_{0y} = 0.3g$. The corresponding discrepancies in the peak normalized lateral forces are about 5% and 4%. The linear theory also overestimates the peak values of the normalized pitch and roll moments under $A_{0x} = 0.2g$ and $A_{0y} = 0.3g$. The first peak values of the normalized pitch moments are 8% and 12% greater than those obtained from the CFD simulations for the fill

ratios h/R=1 and 1.5, respectively. The discrepancy in the peak normalized roll moments is also similar to that observed in the peak normalized lateral forces.

The results in Figs. 5.5 and 5.6 also show relatively higher deviations of the longitudinal force and pitch moment responses compared to those in the lateral force and roll moment responses, even though the magnitudes of the longitudinal accelerations are considerably lower than those of the lateral accelerations. Furthermore, a relatively higher rise time was considered for the longitudinal acceleration compared to the lateral excitation. The greater deviations in the longitudinal force and pitch moment response can be attributed to substantially higher free-surface length in the longitudinal plane of the container compared to that in the lateral plane. The longer free surface in the longitudinal plane would cause greater variations in the free-surface elevation exceeding the critical value, and thus larger errors (Kolaei *et al.*, 2014). It is further seen that slosh modes corresponding to frequencies $\sigma_{1,0}$ and $\sigma_{0,1}$ are the dominant modes in the longitudinal force/pitch moment and lateral force/roll moment responses, respectively, as it was observed from the hydrodynamic coefficients (Tables 5.3 and 5.4). Contributions of the higher modes, however, can be observed from the nonlinear CFD simulations under the higher fill ratio and acceleration excitation.

5.4 Conclusions

A coupled multimodal and boundary-element method, based on the linear slosh theory, was developed for analysis of three-dimensional liquid slosh in a partially-filled cylindrical tank under simultaneous longitudinal and lateral acceleration excitations. The spectral problem of liquid slosh was solved using the boundary integral equations associated with two-dimensional Helmholtz equation, which resulted in greater computational efficiency of the method compared to the boundary element solution of the three-dimensional Laplace equation using two-dimensional boundary elements. The computational efficiency was further improved by reducing the generalized eigenvalue problem to a standard one considering only the velocity potential on the half free-surface length. The hydrodynamic loads could be predicted with high accuracy using only 4 to 5 modes, while the contribution of the higher modes was relatively negligible. Since the hydrodynamic loads are functions of generalized coordinates and hydrodynamic

coefficients, the multimodal model could be easily integrated into the multi-body vehicle dynamics models for efficient analyses of liquid cargo-vehicle interactions.

The results suggested more accurate prediction of the natural slosh frequencies compared to the finite element solution, which is inherently less efficient than the boundary element solution. It was also shown that antisymmetric lateral modes corresponding to the zero longitudinal mode number are only excited in the pure lateral motion of the container, while the symmetric lateral modes of odd longitudinal mode numbers contribute to the slosh responses under a longitudinal excitation. Comparisons of the results with those obtained from the CFD simulations revealed that the linear slosh theory would yield less accurate estimations of the longitudinal force and pitch moment responses compared to the lateral force and roll moment responses for the road tankers. This was attributed to the longer free-surface of the road tankers in the longitudinal direction, which would cause relatively higher amplitudes of the free-surface motion and thereby a stronger effect of nonlinearity in the free-surface. Furthermore, the free-surface motion under a high magnitude longitudinal acceleration is generally constrained by the top part of the container leading to a substantially less liquid load shift in the longitudinal plane than the one predicted by the linear theory. Higher discrepancies between the results from the linear and nonlinear slosh analyses were evident for a higher fill ratio, which were attributable to stronger effect of nonlinearities and relatively less liquid load shift under the higher fill ratios.

CHAPTER 6

CONCLUSIONS AND RECOMMENDATIONS

6.1 Major Contributions and Highlights of the Dissertation Research

This dissertation research presented analytical-based models of transient liquid slosh in moving containers using the linear slosh theory. A thorough literature review was conducted to illustrate the crucial importance of considering the effect of liquid slosh in tank vehicles, while only a few studies reported coupled fluid-vehicle system due to complexities associated with the coupled CFD fluid slosh and vehicle models. A comprehensive study has thus been carried out to develop computationally efficient models of fluid slosh which can be easily integrated with the vehicle dynamics models. The limitations and range of applicability of the linear slosh theory for predicting transient two- and three-dimensional liquid slosh were particularly highlighted. The major contributions of the dissertation research are summarized below:

- Proposed a mathematical model, based on bipolar coordinate transformation, for predicting transient two-dimensional liquid slosh in horizontal cylindrical containers filled to an arbitrary depth under a lateral excitation.
- Proposed a variational Ritz method for estimation of natural slosh frequencies and modes in partially-filled two-dimensional containers of arbitrary cross-section.
- Proposed a boundary element method for estimation of natural slosh frequencies/modes in two-dimensional circular cross-section containers with partial longitudinal baffles. The proposed method reduced the resulting generalized eigenvalue problem to a standard one involving only the velocity potentials of the half free-surface length in order to significantly reduce the computational time.
- Formulated the spectral problem of three-dimensional liquid oscillations in horizontal containers of finite length and arbitrary cross-section using higher order boundary integral solution of a two-dimensional Helmholtz equation.
- Formulated multimodal models of liquid slosh for different tank configurations including: two-dimensional slosh in partially filled clean-bore containers of an arbitrary cross-

section under a lateral excitation; two-dimensional slosh in partially filled circular cross-section containers with a longitudinal baffle under a lateral excitation; and three-dimensional slosh in partially filled horizontal cylindrical containers under simultaneous application of lateral and longitudinal accelerations. The models involved estimations of slosh force and moment in terms of the free-surface generalized coordinates and hydrodynamic coefficients, which permits an efficient integration of the fluid slosh models into vehicle dynamics models.

- Proposed a method for estimating the damping ratios due to liquid viscosity and baffles using empirical relations and mean energy dissipation rate.
- Identified the limitations and ranges of applicability of the linear slosh theory in the context of the liquid motions within partly-filled moving containers.

6.2 Major Conclusions

The major conclusions drawn from the study are summarized below:

- It was shown that the linear slosh models could yield more accurate prediction of dynamic slosh than the pendulum models and it was significantly more computationally efficient than the nonlinear CFD model.
- The linear slosh models yielded substantial errors when the excitation frequency was in the vicinity of the fundamental slosh frequency due to the effects of nonlinearities in the free-surface, which could not be predicted by the linear theory.
- The deviations between the hydrodynamic load responses obtained from the linear and CFD analyses increased with increase in the fill level, suggesting greater influence of nonlinearities under higher fill levels.
- The results obtained from the two-dimensional slosh analyses suggested that the linear theory could yield reasonably accurate predictions of lateral sloshing in liquid transporting vehicles, when the lateral acceleration is less than 0.4g, which is the highest level of lateral acceleration sustained by most tank vehicles prior to rollover.

- It was shown that only a few modes were required to obtain the hydrodynamic loads with sufficient accuracy for all the tank configurations studied, since the higher modes are strongly damped and their contributions are negligible. The linear slosh models could thus be easily integrated into multi-body vehicle dynamics models, unlike the direct numerical methods that require the boundary-value problem to be solved at each time step.
- The results suggested that the roll moment arising from the dynamic fluid slosh could yield considerably lower roll stability limit of a partly-filled tank vehicle compared to that predicted from the widely reported quasi-static fluid slosh model.
- Investigation of the effect of tank cross-section on transient lateral slosh revealed the overall effectiveness of the Reuleaux-triangle tank in suppressing the liquid slosh under intermediate and high fill volumes. It was also shown that a vehicle with Reuleaux-triangle tank had the highest level of the rollover threshold limit.
- The results obtained from the analysis of free liquid slosh in a tank with partial longitudinal baffles suggested that antisymmetric slosh frequencies were substantially reduced when the baffle pierced the free-surface, while it had no effect on the symmetric frequencies and modes. The lowest antisymmetric frequency was also substantially reduced when the baffle was fully immersed in the fluid domain but its tip was close to free-surface.
- The damping effect due to a free-surface-piercing baffle was observed to be greater than that of the slosh in a tank with a fully submerged baffle.
- The baffle length relative to the fill height strongly influenced the anti-slosh effectiveness of the baffle. The top-mounted baffle were most effective in suppressing the fluid slosh under more likely fill height conditions in road tankers (well above 50% of the diameter), when the baffle was partly submerged in the liquid domain. The center-mounted baffle was effective under intermediate fill levels in the vicinity of 50%, while the bottom-mounted baffle was effective only under very low fill heights.
- Comparison of the results obtained from the present three-dimensional slosh model for a half-full cylindrical tank with an analytical benchmark and a finite element solution

suggested that the present BEM could yield more accurate prediction of the natural slosh frequencies than those reported from the finite element method, which required discretization of the whole fluid domain and thereby significantly higher computational time.

- It was shown that only antisymmetric modes were excited under a pure lateral motion of the container, while symmetric modes corresponding to the odd longitudinal mode numbers were excited under a longitudinal excitation.
- The results suggested that linear slosh theory could yield less accurate prediction of the transient liquid slosh in a tank under a longitudinal excitation than that in a tank under a lateral excitation. The linear theory could predict the slosh force and moment due to simultaneous application of lateral and longitudinal accelerations with reasonably good accuracy when the steady-magnitudes of the lateral and longitudinal accelerations were less than 0.3g and 0.2g, respectively, for a tank with aspect ratio of 2.4.

6.3 Recommendations for Future Works

The present linear slosh models can serve as efficient tools for evaluating forces and moments arising from transient liquid slosh in moving containers, and thereby can be directly integrated into the multi-body vehicle dynamics models for the coupled fluid-vehicle simulations, which have not been addressed in this study. Furthermore, analysis of anti-slosh effectiveness of baffles in the present study are limited to the partial longitudinal baffles, while transverse baffles play significant role in suppressing the longitudinal slosh. The present study should thus be continued to include different maneuver-induced disturbances, carry out baffle design analysis, obtain an optimal tank geometry, and investigate the dynamic performance and controllability of tank vehicles in the presence of transient liquid slosh. Some recommendations for future studies are summarized below:

- The present analytical-based models can be extended to include the effect of roll, pitch and yaw motions of the container on slosh forces and moments derived from the two- and three-dimensional slosh analysis. The equivalent mass moment of inertia of the liquid cargo, which is used in the multi-body vehicle equations, can also be estimated using the linear slosh theory.

- Anti-slosh performance of different designs of longitudinal partial baffles including slat screen baffles can be analyzed in order to obtain an optimal deign in terms of the total baffle length and suppression effect of baffle on transient lateral sloshing. The effect of longitudinal baffles on the roll stability limits of tank vehicles can also be studied by integrating the fluid slosh models of the baffled tank with the roll plane vehicle model presented in chapters 2 and 3.
- The three-dimensional model presented in chapter 5 can be employed to obtain the slosh frequencies/modes as well as slosh force and moment for a tank of different cross-sections to investigate the effect of tank cross-section on transient longitudinal sloshing.
- It would be desirable to develop a three-dimensional model of linear slosh in tank with transverse baffles. For this purpose, a three-dimensional BEM needs to be developed and coupled with the multimodal method to investigate the suppression effect of transverse baffles on transient longitudinal slosh.
- Two-dimensional slosh models for clean-bore and baffled tanks can be coupled with a constant speed yaw/roll plane model of an articulated tank vehicle to compute dynamic responses of the vehicle due to time-varying steer inputs. The dynamic rollover threshold of the articulated tank vehicle can also be evaluated in presence of transient slosh.
- A pitch-plane model of a tank truck in the presence of a straight-line braking maneuver can be integrated with the three-dimensional slosh model to perform simulations of the coupled system. The effect of transient slosh on stopping distance and dynamic load transfer between the vehicle axles can be studied from the coupled simulation.

REFERENCES

Abramowitz, M. and Stegun, I. A. (1972), Handbook of Mathematical Functions, National Bureau of Standards,Washington, DC, USA.

Abramson, H. N. (1966), The Dynamic Behaviour of Liquids in Moving Containers, NASA SP-106, Publisher: Washington, Scientific and Technical Information Division, National Aeronautics and Space Administration.

Acarman, T. and Özgüner, Ü. (2006), Rollover prevention for heavy trucks using frequency shaped sliding mode control, *Vehicle System Dynamics*, Vol. 44, No. 10, pp. 737–762.

ADR (2011), Economic Commission for Europe Committee on Inland Transport, European Agreement Concerning the International Carriage of Dangerous Goods by Road, Vol. I and II.

Aliabadi, S., Johnson, A. and Abedi, J. (2003), Comparison of finite element and pendulum models for simulation of sloshing, *Computers & Fluids,* Vol. 32, pp. 535–545.

Aquaro, M., Mucino, V. H., Gautam, M. and Salem, M. (1999), A finite elemnt modeling approach for stability analysis of partially filled tanker trucks, SAE technical paper no. 1999-01-3708.

Aquelet, N. and Souli, M. (2003), A new ALE formulation for sloshing analysis, *Structural Engineering and Mechanics*, Vol. 16, No. 4, pp. 423-440.

Arafa, M. (2007), Finite Element Analysis of Sloshing in Rectangular Liquid-filled Tanks, *Journal of Vibration and Control*, Vol. 13, No. 7, pp. 883–903.

Aslam, M. (1981), Finite Element Analysis of Earthquake-Induced Sloshing in Axisymmetric Tanks, *International Journal for Numerical Methods in Engineering*, Vol. 17, pp. 159-170.

BaoZeng, Y. (2008), Large-scale amplitude liquid sloshing in container under pitching excitation, *Chinese Science Bulletin*, Vol. 53, No. 24, pp. 3816-3823.

Bastian, P., Birken, K., Johannsen, K., Lang, S., Neuß, N., Rentz-Reichert, H., Wieners, C. (1997), UG – A flexible software toolbox for solving partial differential equations, *Computing and Visualization in Science,* Vol. 1, pp. 27–40.

Bauer, H. F. (1964), Fluid oscillations in the containers of a space vehicle and their influence upon stability, NASA TR R-187.

Bauer, H. F. (1967), Nonlinear propellant sloshing in a rectangular container of infinite length, *Developments in Theoretical and Applied Mechanics: proceedings of the Southeastern Conference on Theoretical and Applied Mechanics*, Vol. 3, pp. 725–759.

Bauer, H. F. (1972), On the destabilizing effect of liquids in various vehicles (part 1), *Vehicle System Dynamics*, Vol. 1, No. 3, pp. 227-260.

Bauer, H. F. (1973), On the destabilizing effect of liquids in various vehicles (part 2), *Vehicle System Dynamics*, Vol. 2, No. 1, pp. 33-48.

Brebbia, C. A., Telles, J. C. F. and Wrobel, L. C. (1984), Boundary element techniques: theory and applications in engineering, Berlin; New York : Springer-Verlag.

Biglarbegian, M. and Zu, J. (2006), Tractor–semitrailer model for vehicles carrying liquids, *Vehicle System Dynamic,* Vol. 44, No. 11, pp. 871–885.

Billing, J. R. and Patten, J. D. (2005), An assessment of tank truck roll stability, Report TP 14237 E, Centre for Surface Transportation Technology, National Research Council for Transport Canada, Transport Dangerous Goods Directorate, Ottawa.

Bogomaz, G. I. and Sirota, S. A. (2002), Oscillations of a Liquid in Containers: Methods and Results of Experimental Studies (in Russian), National Space Agency of Ukraine.

Braess, H. and Wriggers, P. 2000, Arbitrary Lagrangian Eulerian finite element analysis of free surface flow, *Computer Methods in Applied Mechanics and Engineering,* Vol. 190, pp. 95-109.

Budiansky, B. (1960), Sloshing of liquids In Circular Canals and Spherical Tanks, *Journal of the Aerospace Sciences*, Vol. 27, March 1960, pp. 161-173.

CAN/CSA B620 (1987), Highway tanks and portable tanks for the transportation of dangerous goods, Canadian Standards Association, 1987.

CFR 49, part 178 (2011), Code of Federal Regulation, Title 49: Transportation, part 178–specifications for packaging, available online at: http://ecfr.gpoaccess.gov/cgi/t/text/text-idx?c=ecfr&sid=d1eadf7861790e0a8e6c705bb7e13b25&rgn=div5&view=text&node=49:3.1.1.1.1&idno=49

Chen, B. F. and Nokes, R. (2005), Time-independent finite difference analysis of fully non-linear and viscous fluid sloshing in a rectangular tank, Journal of Computational Physics, Vol. 209, pp. 47–81.

Chen, Y. H., Hwang, W. S. and Ko, C. H. (2007), Sloshing behaviours of rectangular and cylindrical liquid tanks subjected to harmonic and seismic excitations, *Earthquake Engineering and Structural Dynamics*, Vol. 36, pp. 1701–1717.

Cho, J. R. and Lee, H. W. (2004), Numerical study on liquid sloshing in baffled tank by nonlinear finite element method, *Computer Methods in Applied Mechanics and Engineering*, Vol. 193, pp. 2581–2598.

Cho, J. R., Lee, H. W. and Ha, S. Y. (2005), Finite element analysis of resonant sloshing response in 2-D baffled tank, *Journal of Sound and Vibration*, Vol. 288, pp. 829–845.

Colagrossi, A., Colicchio, G., Lugni, C. and Brocchini, M. (2010), A study of violent sloshing wave impacts using an improved SPH method, *Journal of Hydraulic Research*, Vol. 48, pp. 94–104.

Cremonesi, M., Frangi, A. and Perego, U. (2010), A Lagrangian finite element approach for the analysis of fluid–structure interaction problems, *International Journal for Numerical Methods in Engineering*, Vol. 84, pp. 610-630.

Crump, K. S. (1976), Numerical inversion of Laplace transforms using a Fourier series approximation, *Journal of the Association for Computing Machinery,* Vol. 23, No. 1, pp. 89-96.

Dahlberg, E. (2000), A method determining the dynamic rollover threshold of commercial vehicles, SAE technical paper no. 2000.01.3492.

Dahlberg, E. and Stensson, A. (2006), The dynamic rollover threshold - a heavy truck sensitivity study, *International Journal of Vehicle Design*, Vol. 40, Nos. 1/2/3, 2006.

Dai, L. and Xu, L. (2006), A numerical scheme for dynamic liquid sloshing in horizontal cylindrical containers, *Proceedings of the Institution of Mechanical Engineers, Part D: Journal of Automobile Engineering,* Vol. 220, pp. 901-918.

Delorme, L., Colagrossi, A., Souto-Iglesias, A., Zamora-Rodriguez, R. and Botia-Vera, E. (2009), A set of canonical problems in sloshing, Part I: Pressure field in forced roll—comparison between experimental results and SPH, *Ocean Engineering*, Vol. 36, pp.168–178.

DIS (2007), Dynamic Interactions Simulator, http://www.ascience.com, Advanced Science and Automation Corp.

Dodge, F. T. (2000), The new dynamic behavior of liquids in moving containers, Southwest Research Institute San Antonio, Texas.

Dogangun, A., Durmus, A. and Ayvaz, Y. (1996), Static and dynamic analysis of rectangular tanks by using the Lagrangian fluid finite element, Computers and Structures, Vol. 59, No. 3, pp. 547–552.

Dutta, S. and Laha, M. K. (2000), Analysis of the small amplitude sloshing of a liquid in a rigid container of arbitrary shape using a low-order boundary element method, *International Journal for Numerical Methods in Engineering*, Vol. 47, pp. 1633-1648.

Ervin, R. D. and Mathew, A. (1988), Reducing the risk of spillage in transportation of chemical wastes by tuck, UMITRI-88-28.

Evans, D. V. and Linton, C. M. (1993), Sloshing frequencies, Quarterly Journal of Mechanics and Applied Mathematics, Vol. 46, pp. 71-87.

Evans, D. V. and McIver, P. (1987), Resonant frequencies in a container with a vertical baffle, *Journal of Fluid Mechanics*, Vol. 175, pp. 295-307.

Faltinsen, O. M., Firoozkoohi R. and Timokha A. N. (2010), Analytical modeling of liquid sloshing in a two-dimensional rectangular tank with a slat screen, *Journal of Engineering Mathematics*, Vol. 9, pp. 93-109.

Faltinsen, O. M., Rognebakke, O. F., Lukovskii, I. A. and Timokha, A. N. (2000), Multidimensional modal analysis of nonlinear sloshing in a rectangular tank with finite water depth, *Journal of Fluid Mechanics,* Vol. 407, pp. 201–234.

Faltinsen, O. M., Rognebakke, O. F. and Timokha, A. N. (2003), Resonant three-dimensional nonlinear sloshing in a square base basin, *Journal of Fluid Mechanics,* Vol. 487, pp. 1–42.

Faltinsen O. M., Rognebakke, O. F. and Timokha, A. N. (2005a), Classification of three-dimensional nonlinear sloshing in a square-base tank with finite depth, *Journal of Fluids and Structures,* Vol. 20, pp. 81–103.

Faltinsen O. M., Rognebakke, O. F. and Timokha, A. N. (2005b), Resonant three-dimensional nonlinear sloshing in a square base basin Part2. Effect of higher modes, *Journal of Fluid Mechanics,* Vol. 523, pp. 199–218.

Faltinsen O. M., Rognebakke, O. F. and Timokha, A. N. (2006), Resonant three-dimensional nonlinear sloshing in a square base basin Part3. Base ratio perturbations, *Journal of Fluid Mechanics,* Vol. 551, pp. 93–116.

Faltinsen, O. M. and Timokha, A. N. (2001), An adaptive multimodal approach to nonlinear sloshing in a rectangular tank, *Journal of Fluid Mechanics*, Vol. 432, pp. 167–200.

Faltinsen, O. M. and Timokha, A. N. (2002), Asymptotic modal approximation of nonlinear resonant sloshing in a rectangular tank with small fluid depth, *Journal of Fluid Mechanics*, Vol. 470, pp. 319–357.

Faltinsen, O. M. and Timokha, A. N. (2009), Sloshing, Cambridge University Press.

Faltinsen, O. M. and Timokha, A. N. (2010), A multimodal method for liquid sloshing in a two-dimensional circular tank, *Journal of Fluid Mechanics,* Vol. 665, pp. 457-479.

Faltinsen, O. M. and Timokha, A. N. (2011), Natural sloshing frequencies and modes in a rectangular tank with a slat-type screen, *Journal of Sound and Vibration*, Vol. 330, pp. 1490–1503.

Firouz-Abadi, R. D., Haddadpour, H. and Ghasemi, M. (2009), Reduced order modeling of liquid sloshing in 3D tanks using boundary element method, *Engineering Analysis with Boundary Elements*, Vol. 33, pp. 750–761.

Firouz-Abadi, R. D., Haddadpour, H., Noorian, M. A. and Ghasemi, M. (2008), A 3D BEM model for liquid sloshing in baffled tanks, *International Journal for Numerical Methods in Engineering*, Vol. 76, pp. 1419-1433.

Fischer, F. D. and Rammerstorfer, F. G. (1999), A refined analysis of sloshing effects in seismically excited tanks, *International Journal of Pressure Vessels and Piping,* Vol. 76, pp. 693-709.

Fleissner, F., D´Alessandro, V., Schiehlen, W. and Eberhard, P. (2009), Sloshing cargo in silo vehicles, *Journal of Mechanical Science and Technology*, Vol. 23, pp. 968-973.

Fleissner, F., Lehnart, A. and Eberhard, P. (2010), Dynamic simulation of sloshing fluid and granular cargo in transport vehicles, *Vehicle System Dynamic,* Vol. 48, No. 1, pp. 3–15.

Forbes, L. K. (2010), Sloshing of an ideal fluid in a horizontally forced rectangular tank, *Journal of Engineering Mathematics*, Vol. 66, pp. 395–412.

Fox, D. W. and Kuttler, J. R. (1981), Upper and lower bounds for sloshing frequencies by intermediate problems, *Journal of Applied Mathematics and Physics (ZAMP)*, Vol. 32, pp. 667-682.

Fox, D. W. and Kuttler, J. R. (1983), Sloshing frequencies, *Journal of Applied Mathematics and Physics (ZAMP)*, Vol. 34, pp. 668-696.

Franck, R. M. and Lazarus, R. B., Mixed Eulerian-Lagrangian method. In Methods in Computational Physics, Vol. 3: Fundamental methods in Hydrodynamics Alder B, Fernbach S, Rotenberg M (eds). Academic Press: New York, 1964.

Frandsen, J. B. (2004), Sloshing motions in excited tanks, *Journal of Computational Physics*, Vol. 196, pp. 53-87.

Frandsen, J. B. and Borthwick, A. G. L. (2003), Simulation of sloshing motions in fixed and vertically excited containers using a 2-D inviscid σ-transformed finite difference solver, *Journal of Fluids and Structures*, Vol. 18, pp. 197-214.

Gedikli, A. and Erguven, M. E. (1999), Seismic analysis of a liquid storage tank with a baffle, *Journal of Sound and Vibration*, Vol. 223, No. 1, pp. 141-155.

Gedikli, A. and Erguven, M. E. (2003), Evaluation of sloshing problem by variational boundary element method, *Engineering Analysis with Boundary Elements*, Vol. 27, pp. 935–943.

Gertsch, J. and Eichelhard, O. (2003), Simulation of Dynamic Rollover Threshold for Heavy Trucks, SAE technical paper no. 2003-01-3385.

Goudarzi, M. A. and Sabbagh-Yazdi, S. R. (2012), Analytical and experimental evaluation on the effectiveness of upper mounted baffles with respect to commonly used baffles, *Ocean Engineering,* Vol. 42, pp. 205–217.

Harvie, D. J. E. and Fletcher, D. F. (2000), A New Volume of Fluid Advection Algorithm: The Stream Scheme, *Journal of Computational Physics*, Vol. 162, pp. 1–32.

Hasheminejad, S. M. and Aghabeigi, M. (2009), Liquid sloshing in half-full horizontal elliptical tanks, *Journal of Sound and Vibration*, Vol. 324, pp. 332-349.

Hasheminejad, S. M. and Aghabeigi, M. (2011), Transient sloshing in half-full horizontal elliptical tanks under lateral excitation, *Journal of Sound and Vibration*, Vol. 330, pp. 3507–3525.

Hasheminejad, S. M. and Aghabeigi, M. (2012), Sloshing characteristics in half-full horizontal elliptical tanks with vertical baffles, *Applied Mathematical Modelling,* Vol. 36, pp. 57-71.

Hasheminejad, S. M. and Mohammadi, M. M. (2011), Effect of anti-slosh baffles on free liquid oscillations in partially filled horizontal circular tanks, *Ocean Engineering*, Vol. 38, pp. 49–62.

Hayashi, M., Hatanaka, K. and Kawahara, M. (1991), Lagrangian finite element method for free surface Navier-Stokes flow using fractional step methods, *International Journal for Numerical Methods in Fluids*, Vol. 13, pp. 805-840.

Hill, D. and Frandsen, J. (2005), Transient evolution of weakly nonlinear sloshing waves: an analytical and numerical comparison, *Journal of Engineering Mathematics*, Vol. 53, pp. 187–198.

Hirt, C. W., Amsden, A. A. and Cook, J. L. (1974), An arbitrary Lagrangian–Eulerian computing method for all flow speeds, *Journal of Computational Physics*, Vol. 14, No. 3, pp. 227–253.

Hirt, C. W. and Nichols, B. D. (1981), Volume of fluid (VOF) method for the dynamics of free boundaries, *Journal of Computational Physics*, Vol. 39, pp. 201–225.

Hughes, T. J. R., Liu, W. K. and Zimmermann, T. K. (1981), Lagrangian-Eulerian finite element formulation for incompressible viscous flows, *Computer Methods in Applied Mechanics and Engineering*, Vol. 29, pp. 329–349.

Hutton, R. E. (1963), An investigation of resonance, nonlinear and nonplanar free surface oscillations of a fluid, NASA TN D-1870.

Ibrahim, I. M. (1999), Anti-Slosh Damper Design for Improving the Roll Dynamic Behavior of Cylindrical Tank Trucks, SAE technical paper no.1999-01-3729.

Ibrahim, R. A. (2005), Liquid Sloshing Dynamics Theory and Applications, © Cambridge University Press 2005.

Ibrahim, R. A., Pilipchuk, V. N. and Ikeda, T. (2001), Recent advances in liquid sloshing dynamics, *Applied Mechanics Reviews*, Vol. 54, No. 2, pp. 133-198.

Kandasamy, T., Rakheja, S. and Ahmed, A. K. W. (2010), An Analysis of Baffles Designs for Limiting Fluid Slosh in Partly Filled Tank Trucks, *The Open Transportation Journal,* 2010, Vol. 4, pp. 23-32.

Kang, X. (2001), Optimal Tank Design and Directional dynamics Analysis of Liquid cargo Vehicles under steering and braking, PhD Thesis, Concordia University, Montreal, Quebec, Canada, 2001.

Kang, X., Rakheja, S. and Stiharu, I. (1999), Optimal tank geometry to enhance static roll stability of partially filled tank vehicles, SAE technical paper no.1999-01-3730.

Kang, X., Rakheja, S. and Stiharu, I. (2000a), Directional dynamics of a partly-filled tank vehicle under braking and steering, SAE technical paper no.2000-01-3477.

Kang, X., Rakheja, S. and Stiharu, I. (2000b), Effects of tank shape on the roll dynamic response of a partly filled tank vehicle, *Vehicle System Dynamics*, Vol. 35, pp. 75-102

Karamanos, S. A., Papaprokopiou, D. and Platyrrachos, M. A. (2009), Finite Element Analysis of Externally-Induced Sloshing in Horizontal-Cylindrical and Axisymmetric Liquid Vessels, *Journal of Pressure Vessel Technology*, Vol. 131, pp. 051301:1-11.

Katsikadelis, J. T. (2002), Boundary Elements: Theory and Applications, Elsevier Science Ltd.

Keulegan, G. H. and Carpenter, L. H. (1958), Forces on cylinders and plates in an oscillating fluid. *Journal of Research of the National Bureau Standard*, Vol. 60, pp. 423–440.

Khandelwal, R.S. and Nigam, N.C. (1982), Digital simulation of the dynamic response of a vehicle carrying liquid cargo on a random uneven surface, *Vehicle System Dynamics*, Vol. 11, No. 4, pp. 195-214.

Kim, M. S. and Lee, W. I. (2003), A new VOF-based numerical scheme for the simulation of fluid flow with free surface. Part I: New free surface-tracking algorithm and its verification, *International Journal for Numerical Methods in Fluids*, Vol. 42, pp. 765-790.

Kim, M. S., Park, J. S. and Lee, W. I. (2003), A new VOF-based numerical scheme for the simulation of fluid flow with free surface. Part II: application to the cavity filling and sloshing problems, *International Journal for Numerical Methods in Fluids*, Vol. 42, pp. 791-812.

Kim, Y. (2001), Numerical simulation of sloshing flows with impact load, *Applied Ocean Research*, Vol. 23, pp. 53–62.

Kim, Y., Shinb, Y. S. and Lee, K. H. (2004), Numerical study on slosh-induced impact pressures on three-dimensional prismatic tanks, *Applied Ocean Research*, Vol. 26, pp. 213–226.

Kit, E., Shemer, L. and Miloh, T. (1987), Experimental and theoretical investigation of nonlinear sloshing waves in a rectangular channel, *Journal of Fluid Mechanics*, Vol. 181, pp. 265–291.

Kolaei, A., Rakheja, S. and Richard, M. J. (2014), Range of applicability of the linear fluid slosh theory for predicting transient lateral slosh and roll stability of tank vehicles, *Journal of Sound and Vibration*, Vol. 333, pp. 263-282.

Komatsu, K. (1987), Nonlinear sloshing analysis of liquid in tanks with arbitrary geometries, *International Journal of Nonlinear Mechanics*, Vol. 22, No. 3, pp. 193–207.

Kuttler, J. R. and Sigillito, V. G. (1984), Sloshing of liquids in cylindrical tanks, *AIAA Journal,* Vol. 22, No. 2, pp. 309-311.

Luab, A. J. (2005), Matrix analysis for scientists and engineers, Society for Industrial and Applied Mathematics.

Lepelletier, T. G. and Raichlen, F. (1988), Nonlinear oscillation in rectangular tanks, *Journal of Engineering Mechanics*, Vol. 114, No. 1, pp. 1–23.

Liu, D. and Lin, P. (2008), A numerical study of three-dimensional liquid sloshing in tanks, *Journal of Computational Physics,* Vol. 227, pp. 3921–3939.

Liu, G. R. and Liu, M. B. (2003), Smoothed Particle Hydrodynamics, World Scientific Publishing Co. Pte. Ltd.

Liu, P. J., Rakheja, S. and Ahmed, A. K. W. (1997), Detection of dynamic roll instability of heavy vehicles for open-loop rollover control, SAE Technical Paper 973263.

Liu, Z. and Huang, Y. (1994), A new method for large amplitude sloshing problems, *Journal of sound and Vibration*, Vol. 175, No. 2, pp.185-195.

McCarty, J. L. and Stephens, D. G. (1960), Investigation of the natural frequencies of fluids in spherical and cylindrical tanks, NASA TN D-252, May 1960.

McIver, P. (1989), Sloshing frequencies for cylindrical and spherical containers filled to an arbitrary depth, *Journal of Fluid Mechanics*, vol. 201, pp.243-257.

McIver, P. and McIver, M. (1993), Sloshing frequencies of longitudinal modes for a liquid contained in a trough, *Journal Fluid Mechanics*, Vol. 252, pp. 525-541.

Mitra, S., Upadhyay, P. P. and Sinhamahapatra, K. P. (2008), Slosh dynamics of inviscid fluids in two-dimensional tanks of various geometry using finite element method, *International Journal for Numerical Methods in Fluids*, Vol. 56, pp. 1625-1651.

Miles, J. W. (1984), Resonantly forced surface waves in a circular cylinder, *Journal of Fluid Mechanics,* Vol. 149, pp. 15–31.

Ming, P. and Duan, W. (2010), Numerical simulation of sloshing in rectangular tank with VOF based on unstructured grids, *Journal of Hydrodynamics*, Vol. 22, No. 6, pp. 856-864.

Modaressi-Tehrani, K. (2004), Analysis of Transient Liquid slosh inside a Partly Filled Tank Subjected to Lateral and Longitudinal Acceleration Fields, M.S. Thesis, Concordia University, Montreal, Quebec, Canada, 2004.

Modaressi-Tehrani, K., Rakheja, S. and Sedaghati, R. (2006), Analysis of the overturning moment caused by transient liquid slosh inside a partly filled moving tank, *Proceedings of the Institution of Mechanical Engineers, Part D: Journal of Automobile Engineering,* Vol. 220, No.3, pp. 289-301.

Modaressi-Tehrani, K., Rakheja, S. and Stiharu, I. (2007), Three-dimensional analysis of transient slosh within a partly-filled tank equipped with baffles, Vehicle System Dynamics, Vol. 45, pp. 525–548.

Moiseev, N. N. (1958), On the theory of nonlinear vibration of a liquid of finite volume, *Journal of Applied Mathematics and Mechanics*, Vol. 22, No.5, pp. 860-872.

Moiseev, N. N. (1964), Introduction to the Theory of Oscillations of Liquid-Containing Bodies, *Advances in Applied Mechanics*, Vol. 8, pp. 233-289.

Moiseev N. N. and Petrov, A. A. (1966), The Calculation of Free Oscillations of a Liquid in a Motionless Container, *Advances in Applied Mechanics*, Vol. 9, pp. 91-154.

Nakayama, T. and Washizu, W. (1980), Nonlinear analysis of liquid motion in a container subjected to forced pitching oscillation, *International Journal for Numerical Methods in Engineering*, Vol. 15, pp. 1207-1220.

Nakayama, T. and Washizu, K. (1981), The boundary element method applied to nonlinear sloshing problems the analysis of two-dimensional, *International Journal for Numerical Methods in Engineering*, Vol. 17, pp. 1631-1646.

Noh, W. F. (1964), CEL:A time-dependent two-space dimensional coupled Eulerian-Lagrangian code. *Methods in Computational Physics*, Vol. 3, pp. 117-179.

Okamoto, K. and Kawahara, M. (1990), Two-dimensional sloshing analysis by Lagrangian finite element method, *International Journal for Numerical Methods in Fluids,* Vol. 11, pp. 453–477.

Okamoto, T. and Kawahara, M. (1997), 3-D Sloshing Analysis by an Arbitrary Lagrangian-Eulerian Finite Element Method, *International Journal of Computational Fluid Dynamics*, Vol. 8, No. 2, pp. 129 — 146.

Ortiz, J. L. and Barhorst, A. A. (1998), Large-displacement non-linear sloshing in 2-D circular rigid containers - prescribed motion of the container, *International Journal for Numerical Methods in Engineering*, Vol. 41, pp. 195-210.

Pacejkaa, H. B. and Bakker, E. (1992), The Magic Formula Tyre Model, *Vehicle System Dynamics*, Vol. 21, No. 1, pp. 1-18.

Papaspyrou, S., Karamanos, S. A. and Valougeorgis, D. (2004a), Response of half-full horizontal cylinders under transverse excitation, *Journal of Fluids and Structures*, Vol. 19, pp. 985-1003.

Papaspyrou, S., Valougeorgis, D. and Karamanos, S. A. (2003), Refined Solutions of Externally Induced Sloshing in Half-Full Spherical Containers, *Journal of Engineering Mechanics*, Vol. 129, No. 12, pp. 1369-1379.

Papaspyrou, S., Valougeorgis, D. and Karamanos, S. A. (2004b), Sloshing effects in half-full horizontal cylindrical vessels under longitudinal excitation, *Journal of Applied Mechanics*, Vol. 71, pp. 255-265.

Pape, D. B., Harback, K., McMillan, N., Greenberg, A., Mayfield, H. and Chitwood, J. C. (2007), Cargo tank roll stability study, U.S. Department of Transportation, Federal Motor Carrier Safety Administration, Contract No. GS23-F-0011L.

Patkas, L. A. and Karamanos, S. A. (2007), Variational Solutions for Externally Induced Sloshing in Horizontal-Cylindrical and Spherical Vessels, *Journal of Engineering Mechanics*, Vol. 133, No.6, pp. 641-655.

Penney, W. G. and Price, A. T. (1952), Finite periodic stationary gravity waves in a perfect liquid, part II, *Philosophical Transactions of the Royal Society of London. Series A, Mathematical and Physical Sciences*, Vol. 244, No. 882, pp. 254-284.

Popov, G. (1991), Dynamics of liquid sloshing in road containers, PhD Thesis, Concordia University, Montreal, Quebec, Canada, 1991.

Popov, G., Sankar, S. and Sankar, T. S. (1993c), Optimal Shape of a Rectangular Road Container, *Journal of Fluids and Structures,* Vol. 7, No. 1, pp. 75-86.

Popov, G., Sankar, S. and Sankar, T. S. (1996), Shape Optimization of Elliptical Road Containers Due to Liquid Load in Steady-State Turning, *Vehicle System Dynamics*, Vol. 25, No. 3, pp. 203- 221.

Popov, G., Sankar, S., Sankar, T. S. and Vatistas, G. H. (1992), Liquid Sloshing in Rectangular Road Containers, *Computers and Fluids*, Vol. 21, No. 4, pp. 551-569.

Popov, G., Sankar, S., Sankar, T. S. and Vatistas, G. H. (1993a), Dynamics of liquid sloshing in horizontal cylindrical road containers, *Proceedings of the Institution of Mechanical Engineers. Part C: Mechanical engineering science*, Vol. 207, pp. 399-406.

Popov, G., Vatistas, G. H., Sankar, S. and Sankar, T. S. (1993b), Numerical simulation of viscous liquid sloshing in arbitrary shaped reservoirs, AIAA Journal, Vol. 31, No. 1, pp. 10-11.

Radovitzky, R. and Ortiz, M. (1998), Lagrangian finite element analysis of Newtonian fluid flows, *International Journal for Numerical Methods in Engineering*, Vol. 43, pp. 607-619.

Rafiee, A., Pistani, F. and Thiagarajan, K. (2011), Study of liquid sloshing: numerical and experimental approach, *Computational Mechanics*, Vol. 47, pp. 65-75.

Rakheja, S., Sankar, S. and Ranganathan, R. (1988), Roll Plane Analysis of Articulated Tank Vehicles During Steady Turning, *Vehicle System Dynamics*, Vol. 17, No. 1, pp. 81-104.

Rakheja, S., Sankar, S. and Ranganathan, R. (1989), Influence of tank design factors on the rollover threshold of partially filled tank vehicles, SAE technical paper no.892480.

Rakheja, S., Stiaharu, G. and Richard, M., (2003), Évaluation de la problématique reliée à l'instabilité en roulement des véhicules routiers de type citerne, transportant des produits liquids, Rapport Final, Le Ministe`re des Transport du Que`bec, Aout 2003.

Ramaswamy, B. and Kawahara, M. (1987), Lagrangian finite element analysis applied to viscous free surface fluid flow, *International Journal for Numerical Methods in Engineering*, Vol. 7, pp. 953-984.

Ramaswamy, B., Kawahara, M. and Nakayama, T. (1986), Lagrangian finite element for the analysis of two-dimensional sloshing problems, *International Journal for Numerical Methods in Engineering*, Vol. 6, pp. 659-670.

Ranganathan, R. (1990), Stability Analysis and Directional Response Characteristics of Heavy vehicles Carrying Liquid Cargo, PhD Thesis, Concordia University, Montreal, Quebec, Canada, 1990.

Ranganathan, R., Rakheja, S., Sankar, S. (1989), Kineto-static roll plane analysis of articulated tank vehicles with arbitrary tank geometry, *International Journal of Vehicle Design*, vol. 10, no.1, 1989.

Ranganathan, R., Rakheja, S. and Sankar, S. (1990), Influence of Liquid Load Shift on the Dynamic Response of Articulated Tank Vehicles, *Vehicle System Dynamics*, 19: 4, 177-200.

Ranganathan, R., Rakheja, S., Sankar, S. (1993a), Directional Response of a B-Train Vehicle Combination Carrying Liquid Cargo, *Journal of Dynamics Systems, Measurement, and Control*, March 1993, Vol. 115.

Ranganathan, R. and Yang, Y.S. (1996), Impact of Liquid Load Shift on the Braking Characteristics of Partially Filled Tank Vehicles, *Vehicle System Dynamics*, Vol. 26, No. 3, pp. 223-240.

Ranganathan, R., Ying, Y. and Miles, J. B. (1993b), Analysis of fluid slosh in partially filled tanks and their impact on the directional response of tank vehicles, SAE technical paper no.932942.

Ranganathan, R., Ying, Y. and Miles, J. B. (1994), Development of a mechanical analogy model to predict the dynamic behavior of liquids in partially filled tank vehicles, SAE technical paper no.942307.

Rebouillat, S. and Liksonov, D. (2010), Fluid–structure interaction in partially filled liquid containers: A comparative review of numerical approaches, *Computers & Fluids*, Vol. 39, pp. 739–746.

Romero, V. J. and Ingber, M. S. (1995), A Numerical Model for 2-D Sloshing of Pseudo-Viscous Liquids in Horizontally Accelerated Rectangular Containers, *Proceedings of 17th International Conference on Boundary Elements*, Madison, Wisconsin, July 17-19.

Ru-De, F. (1993), Finite element analysis of lateral sloshing response in axisymmetric tanks with triangular elements, *Computational Mechanics*, Vol. 12, pp. 51-58.

Rudman, M. (1997), Volume-tracking methods for interfacial flow calculations, *International Journal for Numerical Methods in Fluids*, Vol. 24, pp. 671-691.

Rumold, W. (2001), Modeling and Simulation of Vehicles Carrying Liquid Cargo, *Multibody System Dynamics,* Vol. 5, pp. 351–374.

Salem, M. I. (2000), Rollover Stability of Partially Filled Heavy-Duty Elliptical Tankers Using Trammel Pendulums to Simulate Fluid Sloshing, PhD Thesis, West Virginia University, Morgantown, West Virginia.

Salem, M. I., Mucino, V. H., Gautam, M. and Aquaro, M. (1999), Review of parameters affecting stability of partially filled heavy-duty tankers, SAE technical paper no.1999-01-3709.

Salem, M. I., Mucino, V. H., Saunders, E. and Gautam, M. (2009), Lateral sloshing in partially filled elliptical tanker trucks using a trammel pendulum, *International Journal of Heavy Vehicle systems*, Vol. 16, Nos. 1/2, pp. 207-224.

Sankar, S., Rakheja, S. and Ranganathan, R. (1989), Directional Response of Partially Filled Tank Vehicles, SAE technical paper no.892481.

Sankar, S., Rakheja, S. and Sabounghi, R. N. (1986), Stability Analysis of liquid tank vehicle, *International Symposium on Heavy Vehicle Weights and Dimensions*, June 8-13, 1986, Kelowna, British Columbia.

Sankar, S., Ranganathan, R. and Rakheja, S. (1992), Impact of Dynamic Fluid Slosh Loads on the Directional Response of Tank Vehicles, *Vehicle System Dynamics*, Vol. 21, pp. 385-404.

Shankar, P. N. and Kidambi, R. (2002), A modal method for finite amplitude nonlinear sloshing, *Pramana-Journal of Physics*, Vol. 59, No. 4, pp. 631–651.

Slibar, A. and Troger, H. (1975), Dynamic Steady State Behavior of a Tractor-Semitrailer-System Carrying Liquid Load, *Vehicle System Dynamics*, 4: 2, 110-114.

Slibar, A. and Troger, H. (1977), The Steady-State-Behavior of a Truck-Trailer-System Carrying Rigid or Liquid Load, *Vehicle System Dynamics*, 6: 2, 167-169.

Souli, M. and Zolesio, J. P., (2001), Arbitrary Lagrangian-Eulerian and free surface methods in fluid mechanics, *Computer Methods in Applied Mechanics and Engineering,* Vol. 191, pp. 451-466.

Southcombe, E., Ruhl, R. L. and Kuznetsov, E. (2000), Fluid load analysis within the static roll model, SAE technical paper no. 2000-01-3476.

Souto-Iglesias, A., Delorme, L., Perez-Rojas, L. and Abril-Perez, S. (2006), Liquid moment amplitude assessment in sloshing type problems with smooth particle hydrodynamics, Ocean Engineering, Vol. 33, pp. 1462–1484.

Staroszczyk, R. (2009), A Lagrangian Finite Element Analysis of Gravity Waves in Water of Variable Depth, *Archives of Hydro-Engineering and Environmental Mechanics,* Vol. 56, No. 1–2, pp. 43–61.

Strandberg, L. (1978), Lateral stability of road tankers, VTI Report No. 138A, National Road and Traffic Research Institute, Linkoping, Sweden.

Sumner, I. E. (1965), Experimentally determined pendulum analogy of the liquid sloshing in spherical and oblate-spherical tanks, NASA TN D-2737.

Sygulski, R. (2011), Boundary element analysis of liquid sloshing in baffled tanks, *Engineering Analysis with Boundary Elements*, Vol. 35, pp. 978–983.

Tang, B., Li, J. and Wang, T. (2008), The least square particle finite element method for simulating large amplitude sloshing flows, *Acta Mechanica Sinica*, Vol. 24, pp. 317–323.

Teng, B., Zhao, M. and He, G. H. (2006), Scaled boundary finite element analysis of the water sloshing in 2D containers, *International Journal for Numerical Methods in Fluids*, Vol. 52, pp. 659–678.

Thomassy, F. A., Wendel, G. R., Green, S. T. and Jank, A. C. (2003), Coupled Simulation of Vehicle Dynamics and Tank Slosh: Phase 2, Interim Report, TFLRF No. 368, U.S. Army TARDEC Fuels and Lubricants Research Facility (SwRI), Southwest Research Institute, San Antonio, TX.

Timokha, A. and Hermann, M. (2006), A Finite-Dimensional Modal Modelling of Nonlinear Fluid Sloshing, *Mathematics in Industry*, Vol. 8: Progress in Industrial Mathematics at ECMI 2004, Part VIII, pp. 528-532.

Toumi, M., Bouazara, M. and Richard, M. J. (2009), Impact of liquid sloshing on the behaviour of vehicles carrying liquid cargo, *European Journal of Mechanics A/Solids*, Vol. 28, pp. 1026–1034.

Turnbull, M. S., Borthwick, A. G. L. and Taylor, R. E. (2003), Numerical wave tank based on a σ-transformed finite element inviscid flow solver, *International Journal for Numerical Methods in Fluids,* Vol. 42, pp. 641–663.

UN-ECE No. 111 (2000), Uniform Provision Concerning the Approval of Tank vehicles of Category N and O with regard to the roll stability, United Nation Economic Commission for Europe.

Unruh, J. F., Kana, D. D., Dodge, F. T. and Fey, T. A. (1986), Digital data analysis techniques for extraction of slosh model parameters, *Journal of Spacecraft and Rockets*, Vol. 23, No. 2, pp. 171–177.

U.S. DOT (2002), Hazardous Materials Risk Assessment, U.S. Department of Transportation, Federal Motor Carrier Safety Administration, Publication No. FMCSA-RT-02-090, July 2002.

U.S. DOT (2008), Safety news rollover, U.S. Department of Transportation, Federal Motor Carrier Safety Administration, May 2008.

Ushijima, S. (1998), Three-dimensional arbitrary lagrangian–eulerian numerical prediction method for non-linear free surface oscillation, *International Journal for Numerical Methods in Fluids*, Vol. 26, pp. 605–623.

Ushijima, S. (2000), Numerical Visualization of Free Surface Oscillation Predicted with Arbitrary Lagrangian-Eulerian Method, *Journal of Visualization*, Vol. 3, No. 3, pp. 237-244.

Wang, C. Z. and Khoo, B. C. (2005), Finite element analysis of two-dimensional nonlinear sloshing problems in random excitations, *Ocean Engineering*, Vol. 32, pp. 107–133.

Wasfy, T. M., O'Kins, J. and Smith, S. (2007), Experimental Validation of a Time-Accurate Finite Element Model for Coupled Multibody Dynamics and Liquid Sloshing, SAE Paper No. 2007-01-0139.

Wasfy, T. M., O'Kins, J. and Smith, S. (2008), Experimental Validation of a Coupled Fluid-Multibody Dynamics Model for Tanker Trucks, SAE Paper No. 2008-01-0777.

Winkler, C. B., (2009), Full-scale Rollover Testing of commercial Cargo-Tank Vehicles, Proceedings of 1st Joint ITAI-EVU conference, Hinckely, Leicestershire, UK, September 2009, pp. 159-169.

Winkler, C. B., Blower, D. F., Ervin R. D. and Chalasani R. M. (2000), Rollover of Heavy Commercial Vehicles, Heavy Vehicle Systems, Research report RR-04, Society of Automotive Engineering.

Winkler, C. B. and Ervin, R. D. (1999), Rollover of Heavy Commercial Vehicles, UMTRI-99-19, The University of Michigan, Transportation Research Institute.

Woodrooffe, J. (2000), Evaluation of Dangerous Goods Vehicle Safety Performance, Final report, Transport Dangerous Goods, Safety and Security, Transport Canada, March 2000.

Wu, C. H. and Chen, B. F. (2009), Sloshing waves and resonance modes of fluid in a 3D tank by a time-independent finite difference method, *Ocean Engineering*, Vol. 36, pp. 500–510.

Wu, C. H., Faltinsen, O. M. and Chen, B. (2012), Numerical study of sloshing liquid in tanks with baffles by time-independent finite difference and fictitious cell method, *Computers & Fluids*, Vol. 63, pp. 9–26.

Wu, G. X., Ma, Q. W. and Taylor, R. E. (1998), Numerical simulation of sloshing waves in a 3D tank based on a finite element method, *Applied Ocean Research*, Vol. 20, pp. 337–355.

Xu, L., Dai, L., Dong, M. and Setiawan, B. (2004), Influence of liquid slosh on ride quality of liquid cargo tank vehicles, *Proceedings of the Institution of Mechanical Engineers, Part D: Journal of Automobile Engineering,* Vol. 218, pp. 675-684.

Yan, G. R. (2008), Liquid slosh and its influence on braking and roll responses of partly filled tank vehicles, PhD Thesis, Concordia University, Montreal, Quebec, Canada.

Yan, G. and Rakheja, S. (2009), Straight-line braking dynamic analysis of a partly filled baffled and unbaffled tank truck, *Proceedings of the Institution of Mechanical Engineers, Part D: Journal of Automobile Engineering*, Vol. 223, No.1, pp. 11-26.

Yan, G. R., Rakheja, S. and Siddiqui, K. (2008), Baffle Design Analysis for a Road Tanker: Transient Fluid Slosh Approach, SAE paper No. 2008-01-2670.

Yan, G., Rakheja, S. and Siddiqui, K. (2009), Experimental study of liquid slosh dynamics in a partially-filled tank, *Journal of Fluids Engineering*, Vol. 131, pp. 071303: 1-14.

Yan, G. R., Rakheja, S. and Siddiqui, K. (2010), Analysis of transient fluid slosh in partly filled tanks with and without baffles: Part 1 – model validation, *International Journal of Heavy Vehicle Systems*, No. 17, pp. 359-379.

Yan, G. R., Rakheja, S. and Siddiqui, K. (2010), Analysis of transient fluid slosh in partly filled tanks with and without baffles: Part 2 – role of baffles, *International Journal of Heavy Vehicle Systems*, No. 17, pp. 380-406.

Yan, G., Siddiqui, K., Rakheja, S. and Modaressi, K. (2005), Transient fluid slosh and its effect on the rollover-threshold analysis of partially filled conical and circular tank trucks, *International Journal of Heavy Vehicle Systems*, Vol. 12, No. 4, pp. 323-343.

Yin, L., Wang, B., Ma, X. and Zou, J. (1999), The nonlinear sloshing of liquid in tank with pitching, *Journal of Applied Mechanics*, Vol. 66, pp. 1032–1034.

Zhanqi, W., Rakheja, S., Cunzhen, S. (1995), Influence of Partition Location on the Braking Performance of a Prtially-Filled Tank Truck, SAE technical paper no.952639.

Zhou, H., Li, J. F. and Wang, T. S. (2007), Simulation of liquid sloshing in curved-wall containers with arbitrary Lagrangian–Eulerian method, *International Journal for Numerical Methods in Fluids*, Vol. 57, pp. 437–452.

Ziarani, M. M., Richard, M. J. and Rakheja, S. (2004), Optimisation of liquid tank geometry for enhancement of static roll stability of partially-filled tank vehicles, *Heavy Vehicle Systems, International Journal of Vehicle Design*, Vol. 11, No. 2, 2004.